

Investigating Triggering Events in T and B Lymphocytes

Caitlin Marie O'Brien-Ball

Balliol College

Supervisors: Prof. Simon J. Davis, Dr. Ana Mafalda Santos

Thesis submitted for the degree of Doctor of Philosophy

Trinity Term 2022



Approximate word count: 50,000

Declarations

The work in this thesis was supported by funding from the Medical Research Council, Balliol College's Dervorguilla Scholarship, and the John Radcliffe Hospital.

I hereby declare that, except where specific reference is made, the contents of this thesis are original and have not been submitted in whole or in part for consideration for any other degree or qualification in this, or any other, university. This thesis is my own work and contains nothing which is the outcome of work done in collaboration with others, except as specified in the text and in the following:

- Purification of CD43-H6-linker-H6 and CD45RABC-H6-linker-H6 was performed by Heather Brouwer (Davis group)
- Purification of CD58-H6-linker-H6 was performed by Jemma McBride and Francis Riddell (Davis group)
- Purification of ICAM-1-H6-linker-H6 was performed by Veronica Chang (Davis group)
- Purification of 9V-pMHC H6-linker-H6 was performed by Edward Jenkins (Davis group)
- Purification of gp100-pMHC H6-linker-H6 was performed with assistance from Mai Vuong (Davis group) and purification of gp100 pMHC (no tags) was performed by Mai Vuong
- Purification of UCHT1 Fab-Halo was assisted by João Ferreira Fernandes (Davis group)
- Quantitative analysis of TIRFM data was performed using code written by Markus Körbel (see section 4.2.7)
- Calcium flux and adhesion data was analysed using a MATLAB code written by Jane Humphrey (Klenerman group, section 2.6, www.github.com/janehumphrey/calcium)

Images were analysed using Fiji¹(Version 2.3.0) and flow cytometry data was analysed using FlowJo (fLowjo.com, version 10.8.1). Schematics produced with BioRender. Graphs produced with GraphPad Prism (graphpad.com, version 9).

Acknowledgements

I originally planned to write the acknowledgements as the very last part of my write-up, but I realised after a while that, much like the rest of this thesis, I was going to need a lot more time to write something that I was actually happy with and that did justice to everyone mentioned.

Firstly, I would like to thank my supervisor Simon for bringing me into his lab and giving me the confidence boost I needed as a very nervous interviewee 5 years (!) ago. To Mafalda, I have much to thank you for, from your exceptional scientific guidance as my supervisor to your never-ending patience, leadership, and innate ability to solve any problem. I am also grateful to David Klenerman and Steven Lee for the opportunity to collaborate on some exciting projects, even if it does mean going to "the other place".

The Davis lab has certainly been my home away from home for the past few years, and I would like to thank members of the scientific family we have built there. A lab atmosphere like this is probably a once-in-a-lifetime find! Thank you to Heather for helping me feel settled in my first year in the lab. Thank you to Oliver and Mai for your lab wisdom and impromptu cakes (whether bought or homemade like a pro), and to Sumana for your generosity and hilarious stories. To Francis and Toby, I have really enjoyed your company so far and I'm looking forward to working together more in the future. Thank you also to Rob, with your calming presence, and lab alumnus Vicky for many fun memories in Oxford and abroad.

More widely in the WIMM, I would like to thank Craig, Sally and Kevin in the flow facility, and Chris for his imaging expertise. Thank you to Mukta and Tanya from Richard Cornall's group for providing many mouse spleens and teaching me the ways of primary cell work. I extend my gratitude also to collaborators in Cambridge: Markus, James, Greg, Anna, Kevin, Jane, Ed and Sam, for sharing your cool analysis codes and putting up with my complaints about how cold the microscope rooms are.

A big thank you to my friends from home who have been a wonderful source of stability and good times over the (scary number of) years, especially Alice and Helen for our monthly video chats, Ellie for always reminding me what a weird child I was (still am?), and Elliot for your funny stories and immaculate vibes. I next have to thank Lizzie for putting up with me not only through puberty, but also through numerous questionable life decisions (many of which we made together). Thank you for having the absolute best sense of humour and ability for chaotic fun, while also being able to support me through tough times. I hope I have done the same for you.

Now onto another long-term bestie - Chloe, I couldn't forget you girl! Travel buddy, back-of-the-hall music companion and wonderful host, I am very lucky to have you as a friend and I wouldn't want to share near-death experiences with anyone else (shot bar and Scafell Pike I'm looking at you!). I'm really excited to see you living your best life with Harry!

Next, I extend my thanks to friends made during my time in Oxford: Inna, for providing me with a dose of dog when I need it; Mati, for exceptional party fashion; Ryan, for keeping me company with my many extracurricular projects in first year, and for being so effortlessly thoughtful; and Alex, for always listening without judgement (I think I finally know how to use coloco2 now). Kamal, I think the best thing that came out of lockdown was getting to know you better. I'm sorry for ruining glowsticks for both of us. Shoutout to Surya, Lois, Stefi, Matty, Maggie, Kate, Will, and all the others I've had plenty of good times with over the years and for stopping me going completely off the rails during write-up. More recently I

have been lucky to reignite my love of live music so a heartfelt thank you to rest of The Bankside Blues Band for making weekday evenings so much more 'fire-y'.

Onto my Balliol day ones. Ida, I think you're probably the coolest person I've ever met and I'm so grateful for the number of times we've ended up in some bizarre situation which has left us with some hilarious memories (even if they left us feeling shocking!). Stephanie, what can I really say except for you are absolute goals. I loved all of our time together at Balliol and I don't think I could've done social sec without you. I miss you both all the time and I'm so excited for when we next get to hang out. Chelsea, from Creamfields to Bucharest we've already had so much fun, but honestly, the silent disco parties top it all off - I'll make a rum and pineapple juice toast to that!

Somehow, I have been lucky enough to find myself in a lab full of extraordinary people, and I know that my DPhil would have been nowhere near as enjoyable without you all. To Martin, I want to thank you for always providing a helping hand, spreadsheet, or Scooter playlist when I need it, even if I don't ask. I won't be asking you for cranberry juice again though. Ed, thank you for many hilarious memories of Greece, Prague and that bathtub in the Manor. You're going to make a great PI one day but please remember not to bend down too quickly when wearing suit trousers. Nicole, I'm so glad you didn't stick to your strict work/life separation policy because I would've really missed out if we hadn't become friends. I've always felt comfortable talking to you about anything, and the huge worrier that I am, that is a rare occurrence. I hope we always live close enough for visits, and if not, I guess we'll just have to try another holiday- I'll make sure we book a cabin for any future overnight ferries though! João, I am grateful for your ruthless support through all the troubles we've talked about, and our many long runs together (sorry again about that 13k!). Your commitment to the scientific method is exceptional and I really admire that you give your absolute best to everything you do - except maybe checking into flights.

Merve, Lucy and Janina, my WIMM girls- thank you for countless coffees, dinners, and most importantly, laughs. The only bad thing about our friendship is that it didn't happen sooner! Merve, I'm glad I found someone who is as keen as I am to get out and about exploring (3 villages in one day, or was it 4?!). Lucy, your stories always make me laugh so hard and I honestly can't thank you enough for being there to help with my thesis when I was stressed out, even when you were ill! Janina, although I may be slightly jealous of your inability to take a bad photo, I'm so glad we've become almost-neighbours and know I can always rely on you if I need a chat, food delivery, or company to a formal.

Of course, my longest-running support team has been my family. Button, I wish you could read because you simply must know how much of a good girl you are (yes you are). Mum, Dad and Rhian, it was always so comforting to know that you absolutely never questioned my abilities, even when I did. I'm so lucky to have parents who allow me to really be myself. While Grandpa isn't here to see me finish this PhD, I know he always believed in me too. Rhian, you are already making more of a difference to people's lives than I ever will, and I hope you are *at least* as proud of yourself as I know you are of me.

Now I'm stuck with trying to wrap this up in a satisfying way with only a couple of sentences left. In typical 'me' fashion, I'm sure I'll think of something right after I submit. So, for now I will just try to take in the relief that I'm almost done, mixed with sadness that this part of my life is coming to an end. It's a strange feeling. Or maybe that's just my spine finally straightening out after months of sitting at my laptop with the 'second-gen hunch'. Finally, I would like to use the last bit of space I have to curse Mendeley cite for losing me many hours of important write-up time and brain cells.

Right then, who's joining me for a pint?!

Abstract

T cells have an important role in the resolution of infections and cancer. The mechanisms underlying early contact formation of T cells with antigen-presenting cells, and the contribution of T-cell receptor (TCR) microclusters (MCs) to T-cell activation, are still not well understood, especially given recent evidence demonstrating the importance of membrane topography in T-cell signalling. Furthermore, it is unclear what features of the TCR triggering mechanism are shared with other receptors, such as the B-cell receptor (BCR). For experiments presented in this thesis, cell lines were created that express TCRs with different affinities and surface densities, along with an inhibitable mutant of ZAP-70, which were used to probe the effects of TCR density and signalling in early T-cell contacts and antigen reactivity. TCR density did not affect the spreading or close contact formation of T cells with supported lipid bilayers (SLB) presenting agonist pMHC, suggesting that very few TCRs are needed to trigger these events. MC distribution was uncorrelated with close contacts, implying that these structures are real, and not imaging artefacts. However, T cells with low TCR expression levels signalled robustly, suggesting that MC formation might not be a pre-requisite of TCR signalling. Nevertheless, signalling triggered under these conditions did not result in full T-cell activation. ZAP-70 inhibited cells displayed reduced cell spreading, formed fewer but larger close contacts, and recruited more ZAP-70 at MCs. This data suggests that ZAP-70 is a strong regulator of T-cell contact formation, and that it also contributes to antigen discrimination, alongside its key role in signal amplification at the TCR. Finally, key requirements of the kinetic segregation (KS) model were confirmed in T and B cells, including the induction of TCR triggering by slowing the receptor's diffusion within a close contact, and the demonstration that the BCR is unclustered on resting cells, similarly to the TCR, thereby ruling out a popular model of BCR triggering. Work carried out in this thesis provides insight into the mechanisms regulating early contact formation by T cells, and by demonstrating key predictions of the KS model in both T and B cells, raises the possibility that a unified mechanism for immune receptor triggering could exist.

COVID-19 Statement

Due to the emergence of Sars-CoV-2, experimental work for this thesis was heavily disrupted. University building closures meant that experimental work could not be carried out from March to June 2020 inclusive, and from July 2020 until the end of 2021 measures placed on the number of people permitted in our lab necessitated a reduction in the number of hours available to conduct experiments. In total, I estimate that ~7 months of bench time was lost due to the pandemic. In addition, I was not able to access other buildings in Oxford from March 2020-November 2021, where I had been using a TIRF microscope for data collection in numerous experiments. Finally, from March 2020 to September 2021 I was not able to travel to Cambridge to work with collaborators who provide specialised equipment, analysis tools, and expertise. Usually, I would do this every two to four months.

Below, I will briefly describe key experiments that I expect would have been included in this thesis, had I been able to use the full amount of time expected at the beginning of my DPhil:

- Single-molecule tracking of pMHC and TCR on gp100^{lo} cells simultaneously with calcium flux or ZAP-70 recruitment, to observe whether single, long-lived pMHC/TCR interactions lead to ZAP-70 recruitment or calcium flux and therefore whether TCR microclusters are necessary for signal induction. This would form part of Chapter 6.
- Calcium flux assays for 1G4^{lo} cell lines on 2nd generation SLBs presenting a very low concentration of agonist pMHC. This would be compared to experiments conducted with gp100^{lo} cells to determine whether serial binding of pMHC/TCR is necessary to induce signalling at presumed 1:1 receptor/ligand stoichiometry. Additionally, a titration of agonist pMHC density to find the minimal density required to induce signalling under these conditions. This would be added onto experiments described in section 6.3.3.
- TCR and ZAP-70 microcluster analysis by TIRFM on cells fixed on 2nd generation SLBs, including a titration of agonist pMHC densities. This would provide additional evidence for or against the argument that microclusters may be a result of TCR/pMHC binding. This would be incorporated into experiments described in section 5.3.5.

0 Table of Contents

0	Table of Contents.....	7
1	Introduction	18
1.1	Immune System Overview.....	18
1.1.1	Introduction	18
1.1.2	Innate Immunity.....	19
1.1.3	Adaptive Immunity	21
1.2	Interplay between Innate and Adaptive Immunity.....	23
1.3	T Cell Overview	23
1.3.1	Development and Selection	23
1.3.2	Subtypes and Their Function	26
1.3.3	Antigen Presentation to T Cells.....	28
1.4	The T-Cell Surface	32
1.4.1	T-Cell Receptor	32
1.4.2	Adhesion molecules	33
1.4.3	The Glycocalyx	34
1.4.4	Co-Stimulatory and Co-Inhibitory Molecules.....	35
1.5	T-Cell Triggering Apparatus	36
1.5.1	T-Cell Receptor Complex	36
1.5.2	Coreceptors	37
1.5.3	CD45.....	38
1.5.4	Lck.....	38
1.5.5	ZAP-70	40
1.6	Models of Triggering.....	41
1.6.1	Conformational Change.....	41
1.6.2	Mechanotransduction	42
1.6.3	Receptor Aggregation	43
1.6.4	Kinetic Segregation	44
1.6.5	Lipid Rafts	45
1.6.6	Kinetic Proofreading.....	47
1.6.7	Serial Triggering Model.....	48
1.7	TCR Microclusters	49
1.8	Downstream Signalling and Activation of T Cells	53
1.9	T-Cell Topography.....	56
1.10	B Lymphocyte Overview.....	60
1.10.1	Development.....	60
1.10.2	Subtypes and Their Function	61
1.10.3	Antigen Presentation to B cells	62
1.10.4	BCR Structure and Function.....	63

1.10.5	B Cell Triggering Apparatus	64
1.11	Models of Triggering	66
1.11.1	Receptor Aggregation	66
1.11.2	Conformation-Induced Oligomerisation	67
1.11.3	Dissociation-Activation	68
1.11.4	Kinetic Segregation	69
1.11.5	Collision-Coupling/Dissociation.....	69
1.11.6	Lipid Rafts	70
1.12	Downstream Signalling and Activation of B Cells	71
1.13	Comparison of Triggering Models Across T and B Lymphocytes.....	73
1.14	Surfaces for Imaging T Cells.....	74
1.14.1	Coated Glass Surfaces.....	75
1.14.2	Glass-Supported Lipid Bilayers.....	76
1.14.3	Free-Standing 3D Membrane Surfaces	80
1.14.4	Cells as Substrates for Imaging	81
1.15	Techniques for Imaging Lymphocytes.....	82
1.15.1	Epifluorescence	82
1.15.2	Confocal Microscopy.....	82
1.15.3	Total Internal Reflection Fluorescence Microscopy	83
1.15.4	Light Sheet Microscopy	84
1.15.5	Super-Resolution Microscopy	85
1.15.6	Intravital Microscopy	86
1.16	Aims of Thesis	87
2	General Materials and Methods	88
2.1	Cell Lines and General Cell Culture Methods	88
2.1.1	Jurkat E6-1.....	89
2.1.2	HEK 293T	89
2.1.3	CHO-K1.....	90
2.1.4	U-2 OS.....	90
2.1.5	A20 HyHEL10 B Cells	90
2.1.6	MD4 Primary B Cells.....	91
2.2	DNA Methods	91
2.2.1	Vectors Used	91
2.2.2	Cloning Method Overview.....	92
2.2.3	CRISPR knockouts	96
2.2.4	DNA Sequencing.....	97
2.3	Protein Methods.....	98
2.3.1	Sodium Dodecyl Sulphate Polyacrylamide Gel Electrophoresis (SDS-PAGE)	98

2.3.2	Size Exclusion Chromatography.....	98
2.3.3	Spectrophotometry.....	99
2.3.4	Coomassie Staining.....	99
2.3.5	Western Blot.....	99
2.3.6	Expression of Soluble His-Tagged Proteins.....	100
2.3.7	Purification of His-Tagged Proteins.....	101
2.3.8	pMHC Production - Refolding.....	101
2.3.9	UCHT1 Fab-Halo Production.....	103
2.3.10	Protein Thawing and Storage.....	104
2.3.11	Protein Labelling.....	104
2.4	Flow Cytometry.....	105
2.4.1	Surface Staining.....	105
2.4.2	Intracellular Staining.....	105
2.5	Microscopy Methods.....	106
2.5.1	Glass-Supported Lipid Bilayer (SLB) Preparation.....	106
2.5.2	1 st and 2 nd Generation SLBs.....	107
2.5.3	Glass Surface Preparation.....	108
2.5.4	Total Internal Reflection Fluorescence Microscopy (TIRFM).....	108
2.5.5	Confocal Microscopy.....	109
2.5.6	Intracellular HaloTag protein labelling.....	110
2.5.7	Surface protein labelling with Fabs.....	110
2.6	Image Analysis with Custom Tools – Calcium Flux.....	111
3	Creation of Cell Lines to Study TCR Signalling and T-Cell Contact Formation.....	112
3.1	Introduction.....	112
3.2	Materials and Methods.....	115
3.2.1	DNA Cloning and Transduction.....	115
3.2.2	CRISPR/Cas9 Knockouts.....	115
3.2.3	Cell Sorting.....	116
3.2.4	Western Blot of Cell Lysates.....	116
3.2.5	Plate-bound Calcium Flux Assay.....	117
3.2.6	SLB Calcium Flux Assay.....	117
3.2.7	Plate-bound Activation Assays.....	118
3.2.8	Cell-cell Activation Assays.....	119
3.3	Results.....	120
3.3.1	Creation of 1G4 and gp100 TCR-Expressing Cell Lines.....	120
3.3.2	Novel Cell Lines Retain Expression of Important Surface and Intracellular Proteins	126
3.3.3	1G4 and gp100 TCR-Expressing Cells Signal in Response to OKT3.....	127

3.3.4	1G4 and gp100 TCR-Expressing Cells Signal in Response to Cognate pMHC 130	
3.3.5	1G4 and gp100 TCR-Expressing Cells Signal on 1 st Generation SLBs	130
3.3.6	1G4 and gp100 TCR-Expressing Cell Lines Form Immune Synapses on 1 st Generation SLBs.....	132
3.3.7	Creation of Analogue-Sensitive ZAP-70-Expressing Cell Lines	134
3.3.8	ZAP-70(AS) Cell Lines Retain Expression of Important Surface and Intracellular Proteins	139
3.3.9	ZAP-70(AS) Cell Lines Signal in Response to Cognate pMHC.....	139
3.3.10	ZAP-70(AS) Cells Form Immune Synapses on 1 st Generation SLBs.....	140
3.3.11	Effect of ZAP-70(AS) Inhibition by 3-MB-PP1	141
3.3.12	ZAP-70(AS) Cells Activate on Protein-Coated Surfaces and APCs.....	144
3.4	Discussion.....	147
3.4.1	1G4 and gp100 TCR-Expressing Cell Lines as a Model T-Cell System	147
3.4.2	ZAP-70(AS) As a Tool to Regulate TCR Signalling.....	148
3.4.3	SLBs as a Model of Antigen Presenting Cells.....	149
4	The Relationship between Early T-Cell Contacts and TCR Signalling	151
4.1	Introduction.....	151
4.2	Materials and Methods.....	154
4.2.1	Confocal Z-Stack Imaging	154
4.2.2	2 nd Generation SLB-Bound Protein Production.....	155
4.2.3	Initial Adhesion to SLBs	155
4.2.4	Protein accumulation on SLBs – Imaging and Analysis	156
4.2.5	Confocal IRM-based Cell Area Imaging and Analysis.....	156
4.2.6	Microvillar Contact Imaging.....	157
4.2.7	Close Contact Analysis	158
4.3	Results.....	160
4.3.1	Cell Morphology is not Affected by TCR or ZAP-70 at Rest.....	160
4.3.2	The TCR is Slightly Enriched on Microvilli Tips	162
4.3.3	The Adhesion Proteins CD2 and LFA-1 have Broadly Homogeneous Distribution Across Microvilli.....	165
4.3.4	T-Cell Interactions with 1 st Generation SLBs: Dependence on TCR expression and Signalling.....	166
4.3.4.3	ZAP-70 Activity, but not TCR Density, Regulates Cell Spreading on 1 st Generation SLBs	170
4.3.5	T-Cell Interactions with 2 nd Generation SLBs: Dependence on TCR expression and Signalling.....	173
4.4	Discussion.....	181
4.4.1	Differential Protein Localisation on the T-Cell Surface.....	182
4.4.2	The Role of TCR and ZAP-70 in T-Cell Interaction with SLBs	182

4.4.3	Regulation of T-Cell Contacts on 1 st and 2 nd Generation SLBs by TCR and ZAP-70	183
5	Microclusters and their Relationship with Microvilli	185
5.1	Introduction	185
5.2	Materials and Methods	189
5.2.1	TCR and ZAP-70 Microcluster Assays	189
5.2.2	Cell Topography in Relation to Microclusters	190
5.2.3	Early Signalling and Contact Area with Actin Inhibition	190
5.3	Results	192
5.3.1	Early TCR Signalling Microclusters are not Affected by TCR Expression	192
5.3.2	Early TCR Signalling Microclusters are not Substantially Affected by ZAP-70 Inhibition	195
5.3.3	Appearance of ZAP-70 Signalling Microclusters is Independent of TCR Expression	197
5.3.4	ZAP-70 Microcluster Intensity, but not Size or Number is Affected by ZAP-70 Inhibition	198
5.3.5	TCR and ZAP-70 Microclusters do not Appear Exclusively at Close Contacts	201
5.3.6	Actin Inhibition Disrupts Close Contact Formation	204
5.3.7	Actin Inhibition Does Not Prevent TCR Triggering	206
5.4	Discussion	208
5.4.1	The Effect of TCR Expression and ZAP-70 Activity on Early Signalling Microclusters	208
5.4.2	The Relationship between Microclusters and T-Cell Topography	211
6	Lymphocyte Receptors as Individual Functional Entities	213
6.1	Introduction	213
6.2	Materials and Methods	216
6.2.1	TCR Triggering in Solution	216
6.2.2	H2Kb mutant pMHC production	217
6.2.3	Serial Triggering Experiments	217
6.2.4	Single Molecule TIRFM for BCR Tracking (DySCO)	218
6.2.5	dSTORM Imaging	218
6.2.6	dSTORM Analysis	219
6.3	Results	221
6.3.1	Early Signalling Response is Similar Between 1G4 ^{lo} and 1G4 ^{hi} Cells	221
6.3.2	Slowing TCR Diffusion Increases the Probability of Receptor Triggering	224
6.3.3	High Affinity pMHC does not Induce Significant TCR Triggering at Very Low Densities on 2 nd Generation SLBs	227
6.3.4	MHC Affinity for CD8 does not Substantially Affect TCR Triggering Induced by High-Affinity Ligands	229
6.3.5	The BCR Behaves as a Monomer on Live B Cells	232

6.3.6	The BCR is Unclustered on Naïve Primary B Cells	235
6.4	Discussion.....	239
6.4.1	Robust Signalling by 1G4 ^{lo} Cells.....	239
6.4.2	Slowing TCR Diffusion Using His-Tagged pMHC on Ni-NTA-containing SLBs 240	
6.4.3	Gp100 TCR Triggering on Low Density Agonist-Presenting 2 nd Generation SLBs	241
6.4.4	The Effect of MHC Affinity for CD8	242
6.4.5	The BCR is Monomeric on Resting or Naïve B Cells	242
7	General Discussion	246
7.1	The Transition from TCR Triggering to T-Cell Activation	248
7.1.1	Early Signalling is Unimpeded in T Cells with Low TCR Densities.....	248
7.1.2	Cells with Low TCR Density do not Fully Activate	249
7.2	Regulation of Early T-Cell Contact Formation by TCR Density and ZAP-70 Activity 250	
7.2.1	Differential Protein Organisation on the Resting T-Cell Surface.....	250
7.2.2	T-Cell Spreading on Activating SLBs is Regulated by ZAP-70 Activity, but not TCR Density	251
7.2.3	T-Cell Close Contacts with Activating SLBs are Regulated by ZAP-70 Activity but not TCR Density	252
7.3	Regulation of Signalling Microclusters by TCR Density and ZAP-70 Activity	254
7.3.1	Signalling Microclusters Appear in Cells with Low TCR Density.....	254
7.3.2	ZAP-70 Activity Regulates the Density of Signalling Microclusters.....	255
7.4	The Relationship between T-Cell Topography and Early Signalling.....	256
7.4.1	The Actin Cytoskeleton is Required to Facilitate T-Cell Signalling in the Presence of a Glycocalyx	256
7.4.2	TCR and ZAP-70 Microclusters do not Correlate with Areas of Close Contact 257	
7.5	Kinetic Segregation-Based Signalling of Lymphocyte Receptors	258
7.5.1	Slowing TCR Diffusion Increases TCR Triggering	258
7.5.2	The BCR is Unclustered in Resting, Naïve B Cells.....	259
7.6	Concluding Remarks	260
8	Appendix.....	261
8.1	Creation of a UCHT1 Fab-Halo for Imaging TCRs on T-cells Interacting with SLBs 261	
8.2	Overcoming the Effect of 'Free' Nickel-Chelating Sites on SLBs	263
8.3	LFA-1 Boosting is Required to Facilitate Immune Synapse Formation in Jurkat- Derived T Cells	265
8.4	Cell Lines do not Signal Significantly on Non-Cognate pMHC.....	267
8.5	Further Analysis of T-Cell Close Contact Formation.....	268
8.6	Calculating the Surface Area of Cell Lines	269

8.7	Characterisation of Early TCR and ZAP-70 Microclusters.....	269
9	References.....	271

Table of Figures

Figure 1	Mechanisms of antigen presentation to T cells	31
Figure 2	Important components of the resting T-cell surface	40
Figure 3	Main models of TCR triggering	47
Figure 4	TCR and ZAP70 microclusters appear on T cells interacting with activating surfaces	53
Figure 5	Signalling networks downstream of the TCR	56
Figure 6	T cells are covered in microvilli which make initial contact with APCs or target cells	59
Figure 7	Models of BCR triggering	71
Figure 8	Schematic depiction of 1st and 2nd generation SLBs	80
Figure 9	Overview of major fluorescence microscopy methods	84
Figure 10	Creation of 1G4 and gp100 TCR-expressing cell lines	121
Figure 11	Expression and specificity of 1G4 and gp100 TCRs	122
Figure 12	Quantification of TCR expression on 1G4 and gp100 TCR-expressing cells	123
Figure 13	Comparison of extracellular and intracellular staining methods for the 1G4 TCR	125
Figure 14	1G4 and gp100-TCR expressing cell lines retain comparable expression of key proteins to Jurkats	127
Figure 15	Calcium flux assays for 1G4 and gp100 TCR-expressing cells	129
Figure 16	1G4 and gp100 TCR-expressing cells trigger in response to their cognate pMHC	131
Figure 17	1G4 and gp100 TCR-expressing cell lines accumulate pMHC and ICAM-1 and form immune synapses on 1st generation agonist-presenting SLBs	133
Figure 18	Creation of ZAP-70(AS)-expressing cell lines	135
Figure 19	Characterisation of ZAP-70(AS)-expressing cell lines	137
Figure 20	ZAP-70(AS) can be labelled via HaloTag and used to visualise ZAP-70 recruitment	138
Figure 21	ZAP-70(AS)-expressing cells express important proteins at a comparable level to Jurkats	139
Figure 22	ZAP-70(AS) and ZAP-70 wildtype cell lines trigger comparably on 1st generation agonist-presenting SLBs	140
Figure 23	ZAP-70(AS)-expressing cell lines accumulate pMHC and ICAM-1 and form immune synapses on 1st generation agonist pMHC-presenting SLBs	141
Figure 24	3-MB-PP1 abolishes TCR signalling in ZAP-70(AS)-expressing cells	143
Figure 25	Comparison of activation markers between ZAP-70(AS) and ZAP-70 wildtype cells	146
Figure 26	T-cell morphology at rest is not affected by TCR or ZAP-70	161
Figure 27	The TCR displays a slight preference for microvillar tips	164
Figure 28	CD11a and CD2 have broadly homogeneous distribution on the cell membrane	166

Figure 29	Initial adhesion to 1st generation SLBs is independent of TCR expression and ZAP-70 activity	168
Figure 30	TCR expression and signalling capacity modulate pMHC and ICAM-1 binding on 1st generation SLBs	170
Figure 31	ZAP-70 controls cell spreading on 1st generation SLBs	172
Figure 32	Initial adhesion to 2nd generation SLBs is independent of TCR expression and ZAP-70 activity	174
Figure 33	TCR expression and signalling capacity modulate pMHC and ICAM-1 binding on 2nd generation SLBs	175
Figure 34	ZAP-70 controls cell spreading on 2nd generation SLBs	177
Figure 35	TCR expression and ZAP-70 activity affect some metrics of T cell close contacts	180
Figure 36	Strategy for analysing TCR and ZAP-70 microclusters	194
Figure 37	Characteristics of early TCR microclusters in cells with different TCR expression and signalling capacity	196
Figure 38	Characteristics of early ZAP-70 microclusters in cells with different TCR expression and signalling capacity	200
Figure 39	TCR and ZAP-70 microclusters do not appear exclusively at close contacts	203
Figure 40	Dynamic microvilli are required to form normal close contacts on 2nd generation SLBs	205
Figure 41	Actin inhibition reduces TCR signalling when a glycocalyx is present	207
Figure 42	1G4^{hi} and 1G4^{lo} cells do not have significantly different calcium flux characteristics	223
Figure 43	Slowing TCR diffusion increases the probability of triggering	227
Figure 44	Agonist pMHC at a very low concentration does not induce significant triggering on 2nd generation SLBs	229
Figure 45	MHC affinity for CD8 does not affect TCR triggering induced by high-affinity ligands	231
Figure 46	Two-colour coincidence analysis suggests a monomeric BCR on live B cells	234
Figure 47	The BCR appears unclustered in primary murine B cells using dSTORM	238
Figure 48	Creation of a UCHT1 Fab-Halo for T-cell labelling and imaging	262
Figure 49	Exposed nickel-chelating lipids on SLBs cause T cell adhesion and triggering through the TCR	264
Figure 50	LFA-1 boosting in cells is required to facilitate immune synapse formation	266
Figure 51	Cell lines do not signal significantly on non-cognate pMHC	267
Figure 52	Close contact density and time to the formation of the first close contact does not change with TCR expression or ZAP-70 inhibition	268
Figure 53	Approximating the surface area of cell lines	269
Figure 54	Characterisation of early TCR and ZAP-70 microclusters under different signalling conditions	270

Abbreviations

ANOVA Analysis of variance

AP-1 Activator protein 1

APC Antigen-presenting cell

B2M Beta-2 microglobulin

BCR B-cell receptor

CD Cluster of differentiation

CDR Complementarity-determining region

CLIP Class-II associated invariant chain peptide

CRISPR clustered randomly interspaced short palindromic repeats

CTLA-4 Cytotoxic T-lymphocyte-associated protein 4

d/p/c SMAC Distal/peripheral/central supramolecular activation cluster

DAG Diacylglycerol

DC Dendritic cell

DTT Dithiothreitol

EDTA Ethylenediaminetetraacetic acid

FACS Fluorescence-activated cell sorting

FCS Foetal calf serum

FPLC Fast protein liquid chromatography

GPI Glycosyl-phosphatidyl-inositol

HLA Human leukocyte antigen

ICAM Intercellular adhesion molecule

IL Interleukin

IRM Interference reflection microscopy

ITAM Immunoreceptor tyrosine-based activation motif

ITIM Immunoreceptor tyrosine-based inhibitory motif

Kd Dissociation constant

KS Kinetic segregation

LAT Linker for activation of T cells

Lck Lymphocyte-specific protein tyrosine kinase

LFA-1 Lymphocyte function-associated antigen 1

MHC Major histocompatibility complex

NFAT Nuclear factor of activated T cells

NF- κ B Nuclear factor kappa-light-chain-enhancer of activated B cells

PBS Phosphate-buffered saline

PD-1 Programmed cell death protein 1

PDMS Polydimethylsiloxane

PKC Protein kinase C

PLC- γ 1 Phospholipase C, gamma 1

PLL Poly-L-lysine

pMHC Peptide: major histocompatibility complex

POPC 1-palmitoyl-2-oleoyl-glycero-3-phosphocholine

PRR Pattern recognition receptor

RAG Recombination-activating gene

RPMI Roswell Park Memorial Institute medium

SH Src-homology

SLB Supported lipid bilayer

SMLM Single-molecule localization microscopy

STORM Stochastic Optical Reconstruction Microscopy

SUV Small unilamellar vesicle

TCR T-cell receptor

TIRFM Total internal reflection fluorescence microscopy

TLR Toll-like receptor

ZAP-70 Zeta-chain associated protein of 70 kDa

1 Introduction

1.1 Immune System Overview

1.1.1 Introduction

The immune system protects the body from perpetual dangers coming from both the outside world (e.g., bacteria, viruses and parasites) and within (i.e., cancerous cells). The innate immune system reacts rapidly to generic signs of danger and the more complex adaptive immune system recognises and reacts to danger signals with incredible specificity while also creating a memory response.

Since the appearance of multicellular organisms 600 million years ago², the immune system has been continually refined. Innate immunity is present in every multicellular organism, and many features of our adaptive immune system are shared by all jawed vertebrates and some more distant ancestors. Interestingly, genetic recombination of immune receptors evolved independently more than once, in agnathans (jawless vertebrates) and gnathostomes (vertebrates with jaws)², indicating the evolutionary advantage of this complex mechanism. Agnathans evolved a system of variable lymphocyte receptors created by differential rearrangement of genes encoding protein segments rich in leucine and with variable amino acid sequences, which are attached to the lymphocyte membrane via a GPI anchor². Gnathostomes similarly rearrange a series of adjacent gene segments to create their lymphocyte receptors, albeit using a different mechanism (described in section 1.3.1). The end result in either case is an adaptive immune system with a comparably high level of lymphocyte receptor diversity².

The immune system relies on organs within the circulatory and lymphatic systems: firstly, for transport of cells, but also for cell development and the interaction between different cell types. Primary lymphoid tissue – the thymus and bone marrow – is where

lymphopoiesis, development, and central selection take place. Once cells leave the primary lymphoid organs, for the most part, they do not return. Secondary lymphoid organs (SLOs) include the spleen and lymph nodes and are the sites of adaptive immune cell activation and differentiation. SLOs are especially abundant in areas with high exposure to foreign antigen, such as the gut and throat, but exist throughout the body³. At rest, adaptive cells spend most of their time cycling through these structures, whereas many innate cells are tissue resident⁴. Formation of tertiary lymphoid organs (TLOs), transient structures that resemble SLOs, has been observed in almost every tissue in response to inflammation caused by infection, autoimmunity or cancer⁵. TLOs facilitate antigen scanning, activation, and differentiation of lymphocytes. The anatomy of lymphoid tissues allows T and B lymphocytes discrete areas in the body to develop and systematically screen for antigen, while the plasticity of TLOs ensures activation and control of the immune response wherever it is needed.

1.1.2 Innate Immunity

The innate immune system, which is present in some form in all multicellular organisms, relies on physical and biochemical mechanisms (for example barriers such as skin, antimicrobial peptides such as defensins and protein pathways such as the complement system) as well as cells which act to rapidly protect the body from infection. Activation of the cellular innate immune system occurs within minutes⁶.

The major cell types of the innate immune system are phagocytes (macrophages and neutrophils) natural killer (NK) cells, granulocytes (eosinophils and basophils), mast cells and dendritic cells (DCs)^{6,7}. Innate cells become activated after sensing pathogen- or danger-associated molecular patterns through pattern recognition receptors (PRRs), located on the cell surface or in the cytoplasm^{7,8}, or by other invariant receptors which bind antigen or other ligands expressed on cells^{9,10}. A variety of rapid cellular responses are initiated downstream of these receptors.

Phagocytes directly engulf and destroy a broad range of pathogens, while granulocytes and mast cells release numerous toxic and inflammatory proteins, as well as chemical mediators such as histamine which are involved in inflammation^{6,11}. NK cells detect and kill virally infected and cancerous cells after recognising cellular stress ligands or the downregulation of major histocompatibility protein class I (MHC I) proteins on the target cell surface¹². All nucleated cells express MHC I proteins on their surface, which are loaded with endogenous peptides in the cytoplasm. These molecules mark a healthy cell as 'self'. Professional antigen presenting cells (APCs) such as DCs and macrophages also express MHC class II which presents exogenously acquired peptides^{6,13}. DCs have the unique ability to present exogenous peptides on MHC class I allowing adaptive cells in the SLOs to respond to exogenous and endogenously derived peptides from the periphery (see also section 1.3.3). DCs constantly sample and process antigens from the extracellular environment. Upon sensing danger signals, they activate and mature, undergoing morphological and behavioural changes which allow them to efficiently activate T cells¹³.

A subset of unconventional T cells called $\gamma\delta$ T cells, which are mainly found in epithelial and mucosal tissues, are generally considered to be innate. Their major role is in the maintenance of barrier immune function and immune homeostasis. Their TCRs are not always MHC restricted, unlike $\alpha\beta$ TCRs, so despite being semi-invariant they can recognise a wider variety of antigens including lipids^{9,14}.

Despite the lack of recombined antigen receptors, the innate immune response is not completely generic. Many PRRs have evolved to detect a variety of antigens, which activate different signalling pathways. Furthermore, innate cells employ a variety of pathogen-specific responses, for example producing type I interferons in response to detecting viral DNA^{7,8}. Thus, the innate immune system can respond with some specificity while activation of the adaptive immune system begins.

1.1.3 Adaptive Immunity

1.1.3.1 Cellular Immunity

The adaptive immune system evolved more recently than the innate immune system and is incredibly complex in function. Two major cell types, B and T lymphocytes, control humoral and cellular immunity, respectively. Within each of these groups, there are multiple cell subsets with specialist roles.

DCs present antigen to two major subsets of T cells – CD4+ and CD8+ – which are named for the MHC coreceptor they bear on their surface^{15,16}. In line with this, $\alpha\beta$ T-cell receptors (TCRs) bind only one of two MHC types– class I for CD8-expressing cells, and class II for CD4-expressing cells. CD8+ T cells are also known as ‘killer’ T cells, or cytotoxic lymphocytes (CTLs). After their initial activation in SLOs by APCs, CTLs travel to the site of infection or cancer through the lymphatic and cardiovascular system, following chemokine signals released from innate immune cells^{7,17}. Once they detect a target cell bearing the same antigen as they were primed with, they carry out their cytotoxic function by the release of cytotoxic granules, anti-tumour and anti-viral cytokines such as IFN- α and IFN- γ , or through Fas-FasL interactions¹⁸.

The CD4+ T-cell subset, also known as T ‘helper’ cells, modulate the response of other immune cells, including B cells, via secretion of various cytokines. Depending on the environment in which CD4+ T cells are activated, they can differentiate into several subtypes¹⁹. Major effector subtypes include Th1, Th2, and Th17 which coordinate responses to intracellular pathogens, extracellular parasites, and extracellular pathogens, respectively. Naïve CD4+ T cells can also differentiate into an immune dampening phenotype called induced regulatory T cells (iT_{regs}). These act in a similar manner to natural regulatory T cells (nT_{regs}), which are produced in the primary lymphoid organs during central selection²⁰. These cells maintain immune tolerance under resting conditions and

resolve inflammation by secreting anti-inflammatory cytokines such as TGF- β and IL-10²⁰. T follicular helper (Tfh) cells are responsible for coordinating the B cell response in germinal centres by promoting differentiation and selection of B cells with the same antigen reactivity.

1.1.3.2 Humoral Immunity

The main function of B cells is to produce antibodies, Y-shaped proteins containing domains which bind antigen as well as Fc receptors on other (mainly innate) cells. Binding of antibody to antigen and to Fc receptors leads to toxin neutralisation, pathogen opsonisation for phagocytosis, and complement activation⁶. B cells are also considered professional APCs as they express co-stimulatory molecules and can present antigen to T cells on MHC class II²¹.

There are two main classes of B cells, with most being designated type B2. Immature B cells develop into several mature subsets, generally defined by their microanatomical location^{22,23}. Marginal zone B cells are non-circulating B cells, residing in the area around B cell follicles and the periarteriolar sheath in the spleen. They provide a rapid response to antigens, particularly those that are blood-borne. Follicular B cells mature in the spleen, then continuously patrol SLOs. Once activated, they transform either into short-lived plasma cells producing IgM antibodies or proceed to the germinal centre where they undergo somatic hypermutation, affinity maturation, and class switching, resulting in a refined antibody response²⁴. Some B cells become long-lived memory cells which reside in the bone marrow and produce antibodies rapidly in response to reinfection. Conversely, regulatory B cells can quench T-cell responses by secreting anti-inflammatory cytokines such as IL-10²³.

B1 cells are a small subset in humans which may have unique developmental origins. Despite being ill-defined in humans, they produce much of the circulating antibody pool, including 'natural' antibodies which are constitutively expressed IgM and IgA isotypes²⁵.

1.2 Interplay between Innate and Adaptive Immunity

The two arms of immunity are tightly interlinked. Generally, an inflammatory response by the innate immune system induces a secondary response by the adaptive immune system. Some innate cells such as basophils and NK cells can directly modulate CD4⁺ T cell differentiation with polarising cytokines. Additionally, a small subset of innate cells called innate lymphoid cells have been shown to phenotypically mirror some CD4⁺ T cell subsets, and by doing so, provide an early source of important cytokines²⁶. Equally, adaptive cells, especially CD4⁺ T cells, secrete cytokines which can modulate the innate response¹⁹.

Arguably, the most crucial link between the innate and adaptive immune system is the dendritic cell. By processing and presenting antigens derived from pathogens or cancerous cells, they are responsible for specifically activating and expanding the adaptive cells²⁷. DCs polarise naïve CD4⁺ T cells using cytokines to one of many effector subtypes depending on the local environment and type of antigen, thus directly influencing the nature of the adaptive immune response. For example, activated neutrophils drive CD4⁺ Th1 cell induction through ligation of the integrin Mac-1 to the C-type lectin DC-SIGN on DCs²⁸. Additionally, DCs can polarise T cells to a T_{reg} phenotype by presenting antigen whilst in an immature or partially mature state, where they lack adequate co-stimulatory molecules^{27,29}.

1.3 T Cell Overview

1.3.1 Development and Selection

T cells develop from haematopoietic stem cells in the bone marrow. These stem cells transition to lymphoid progenitors, which travel to the thymus (the organ for which T cells

are named) to carry out the rest of their development. The cells, now called thymocytes, travel through the thymus, interacting with thymic stromal cells in discrete microanatomical locations³⁰.

The stages of development are subdivided into several phases, characterised by the surface molecules CD34, CD38 and CD1a. Thymocytes express CD34 at earlier stages, and acquire CD38, then CD1a expression as they develop³¹. As cells gain CD1a expression, they rearrange their δ , then γ and β chain genes³². Two DJC β gene clusters³³ increase the chances of successful β chain rearrangement – indeed, 90% of these cells will eventually express $\alpha\beta$ TCR – although developing thymocytes seem to retain $\gamma\delta$ potential for some time³¹.

The TCR β locus contains variable (V), diversity (D) and joining (J) segments which are recombined under control of the recombination-activating genes RAG-1 and RAG-2³⁴. Further diversity is generated by the introduction of P- and N-nucleotides in the junctions between the V, D, and J gene segments of the TCR β gene and the V and J segments of the TCR α gene³⁵. β chain genes are allelically excluded, preventing simultaneous expression of multiple β chains³⁵.

After γ , δ and β chain rearrangement, cells express the coreceptor CD4 but not CD8, making them immature single-positive cells³⁰. They then become early double-positive cells, expressing CD4 and CD8 α chain only, which appears to be the final stage where β -selection and potential to form $\gamma\delta$ T cells can occur³¹.

Thymocytes undergo β -selection to determine whether TCR chain rearrangement has been productive, although the exact developmental stage at which this occurs in humans is unclear³⁰. Cells express their rearranged β chain with the invariant pre-T α chain and the CD3 complex, forming the pre-TCR which is capable of signalling if rearrangement is successful³². If signalling occurs, cells stop rearranging β chain genes, expand rapidly, and rearrange their TCR α chain. If the rearrangement is non-productive, cells die as they cannot

express a pre-TCR and therefore do not obtain survival signals^{30,32}. The TCR α locus, containing only V and J segments, is then rearranged and replaces the pre-T α chain in the TCR complex³⁰. After α chain rearrangement, cells progress to a double-positive phenotype expressing both CD4 and CD8³⁰.

At this stage, double-positive thymocytes interact with thymic cortical epithelial cells, APCs that express a high density of MHC class I and II loaded with self peptides. Here, cells with a weakly self-reactive TCR are positively selected and go onto the CD4/CD8 lineage choice stage, while the rest die by neglect (i.e., lack of mitogenic cytokines)^{30,36}. Negative selection occurs mainly in the thymic medulla where thymocyte TCRs are tested for strong recognition of self-peptides on DCs. Here, TCR signalling leads to thymocyte apoptosis^{30,36}. This process, called central tolerance, prevents self-reactive T cells exiting into the periphery.

An important exception to this process is the natural T regulatory cell (nT_{reg}) population, which derive from CD4⁺ cells with a moderate to high TCR affinity for self peptide that appear to escape this selection process by a currently unknown mechanism²⁰. Their development is driven by the master regulator Forkhead box P3 (FoxP3) and their function is to suppress the effector response of other T cells, maintaining homeostasis and resolving inflammation²⁰.

The final process in the thymus is the CD4/CD8 lineage decision - another area that is still not fully understood. Several competing models exist to explain this process³⁷. The so-called 'classical models' are the instruction model, which states that qualitatively different signals from the coreceptors determine CD4 or CD8 terminal differentiation; and the selection model, which suggests that cells are randomly assigned to CD4 or CD8 and subsequently selected for function. A newer model, called kinetic signalling, suggests that a combination of signal persistence through the TCR as CD4 and CD8 expression changes, and cytokines

such as IL-7, drive development into the single positive phenotype³⁷. Once the CD4/CD8 lineage choice has been made, cells leave the thymus for the periphery.

1.3.2 Subtypes and Their Function

The T-cell population is divided into two major groups: $\alpha\beta$ and $\gamma\delta$. Further divisions of $\alpha\beta$ T cells are separated by coreceptor expression. Most CD8+ T cells become cytotoxic upon activation. CD4+ T cells differentiate into several subtypes, the most well-studied of which are Th1, Th2, Th17, T_{reg} and Tfh. Other smaller subsets include natural killer T cells and CD8 $\alpha\alpha$ T cells. $\gamma\delta$ T cells, expressing neither CD4 nor CD8, are largely involved with barrier and mucosal immunity and can influence both the early and late immune response³⁸.

The role of CD8+, or cytotoxic T cells (CTLs) is to kill cells that are cancerous or infected with intracellular pathogens. CTLs cause apoptosis in target cells, preventing infectious material from spreading into the surrounding area³⁹. Their TCR recognises endogenously-derived peptides presented on MHC class I, which is expressed by all nucleated cells. They also rely on the MHC cross-presenting ability of DCs to react to antigen derived from cells located in the periphery⁴⁰.

Upon activation in the SLOs, CTLs proliferate in an IL-2-dependent manner over several days, then alter their surface molecule expression to facilitate travel to the site of infection by following a gradient of chemokines and cytokines^{41,42}. Local inflammation of tissues causes blood vessels to become permissive to immune cell extravasation,⁴³ allowing effector cells to migrate from the circulation to the site of infection or cancer. CTLs move through the tissue, searching for the activating peptide encountered in the SLO⁴¹. Upon engagement of TCR with the cognate pMHC on a target cell, the CTL forms an immune synapse with the target cell⁴⁴. The synapse allows for full activation of the CTL and forms a tight contact between the CTL and its target cell, facilitating controlled and targeted killing which can occur through several mechanisms.

CTLs primarily kill target cells by the release of cytotoxic granules containing perforin, granzymes, and other components^{45,46}. These are released in modified lysosomes which are directed towards the membrane area in contact with the target cell by the centrosome^{39,47}. Although the specific mechanisms are unknown, perforin forms pores in the membrane, disrupting osmotic balance^{48,49}, while granzymes cleave DNA, initiating apoptosis⁵⁰. Another mechanism employed by CTLs is Fas/Fas ligand signalling. Target cells express the death receptor Fas, which is bound by Fas ligand on the T cell^{45,51}. Ligation of this receptor induces cell death by activation of caspases⁵². Additionally, the release of cytokines such as IFN- γ and TNF- α from CTLs have several effects on intracellular pathogens and diseased cells, including blocking viral replication and increasing endogenous peptide presentation on MHC-I⁵³. After elimination of one target cell, the CTL continues to kill other cells displaying the activating pMHC in a process called 'serial killing'^{39,49}.

As the immune response is curtailed, approximately 95% of the effector cell population dies by apoptosis, driven by the ratio of anti-apoptotic and pro-apoptotic factors^{54,55}. The remaining cells form the hyper-responsive memory cell population, which remain distributed in the body indefinitely with maintenance from cytokines such as IL-7 and IL-15⁵⁶. Memory cells are more sensitive and faster to respond than naïve cells upon stimulation, decreasing the severity of repeated infection in most cases⁵⁶.

As with CD8+ T cells, CD4+ cells are largely activated in SLOs by DCs bearing agonist peptide on MHC¹⁹. Depending on the environment in which the DCs were activated, they become primed to polarise CD4+ cells to different effector subsets^{19,57}.

The development of Th1 cells is critically dependent on IFN γ and IL-12 and the master transcription factor T-bet¹⁹. They specifically eliminate intracellular pathogens by secretion of IFN γ , lymphotoxin α , and IL-2 which have effects on mononuclear phagocytes, CD8+ T cells and nT_{regs}^{58,59}. Th2 cells are specialised to remove extracellular parasites such as helminths⁶⁰. Their development depends on the master transcription factor GATA3,

mediated by IL-4 and IL-12¹⁹. They secrete cytokines including IL-4 and IL-5, which control B cell class switching to IgE and stimulate eosinophils¹⁹. Th2 cells also have immune dampening functions through secretion of IL-10⁶¹. Th17 development is stimulated by IL-21, IL-6, IL-23 and TGF- β and mediated by the transcription factor ROR γ t¹⁹. They mount an immune response against extracellular bacteria and fungi largely by secretion of IL-17, which induces secretion of pro-inflammatory cytokines and IL-21 from a variety of immune and non-immune cells. These in turn activate T cells and NK cells and induce plasma cell differentiation^{19,62}.

Tfh cells are polarised by IL-6 and IL-21, driving STAT3 signalling^{19,63}. These cells are localised to the follicles of SLOs where they drive antigen-dependent B cell-mediated immunity by several mechanisms. Firstly, by providing survival signals to the B cells with the highest affinity BCRs; secondly, by inducing differentiation of B cells into plasma and memory cells; and finally, by directing B cells to re-enter the cell cycle and undergo somatic hypermutation^{64,65}.

Natural T_{regs}, which develop during central selection, are reliant on the master transcription factor FoxP3²⁰. Inducible T_{regs} are produced from conventional naïve CD4+ cells in the periphery under the control of TGF- β and IL-10^{19,20}. Both subtypes control the immune response to self antigens and help resolve inflammation. They directly modulate DC function, effector cell metabolism and behaviour, through cytokines such as IL-10, IL-35 and TGF- β . T_{regs} can also induce cytotoxicity of effector cells through the perforin/granzyme mechanism⁶⁶.

1.3.3 Antigen Presentation to T Cells

Most TCRs (i.e., $\alpha\beta$ TCRs) can only bind an antigen when it is presented in a complex with the MHC molecule. As previously described, there are two major types of T cells, CD4+ and CD8+, named for their coreceptor expression and therefore which MHC type they bind.

MHCs are both polygenic (i.e., every individual expresses a combination of several MHC genes) and polymorphic (i.e., numerous variants exist of each gene within a population)⁶⁷, which likely evolved to avoid pathogens escaping presentation to T cells. MHC molecules are further divided into classical (HLA-A, B and C for class I and HLA-DR, DP, DQ and DR α for class II)⁶⁷ and non-classical groups (including HLA-E, CD1 and FcRn)⁶⁸. Classical molecules present peptides only and are responsible for antigen presentation to $\alpha\beta$ TCR-expressing cells, while non-classical MHC molecules present a greater variety of ligands including lipids, vitamin metabolites and fatty acids to other types of T cell⁶⁸.

Both MHC classes are composed of two chains, α and β . For MHC I, the α chain (also known as heavy chain) contains three segments, which pairs non-covalently to the invariant beta-2 microglobulin (β_2m ; light chain). MHC class II contains two more similarly-sized chains which form one immunoglobulin domain each. MHC molecules are anchored in the cell membrane by either one (MHC I) or two (MHC II) transmembrane stalks, and do not contain a significant intracellular domain. The most critical part of the MHC structure, the peptide binding groove, is formed with only the heavy chain in MHC I and both chains in MHC II molecules. The groove itself is formed by two α -helices, which lie far enough apart to accommodate a short peptide chain between them, supported by a β -sheet base^{69,70}. Due to structural differences in the peptide binding groove, MHC class I presents peptides of typically around 8-10 residues⁷¹⁻⁷⁶, whereas MHC II molecules accommodate peptides between 13-25 residues in length⁷⁶.

MHC I molecules present endogenous self and viral peptides which are derived from proteins cleaved in the cytosol by proteases and fed into the endoplasmic reticulum (ER) by the protein transporter associated with antigen processing (TAP). TAP forms a peptide loading complex in the ER with tapasin, calreticulin, ERp57 and an empty class I MHC molecule^{77,78}. Once a stable peptide/MHC complex has been formed, it exits the ER and is transported to the cell surface for presentation to T cells⁷⁸. MHC II molecules present

peptides derived from exogenous proteins which are transported into the cell by endocytosis and subsequently degraded via the endo-lysosomal pathway⁷⁹. MHC II chains are first assembled in the ER in a complex with an invariant protein (Ii) which fills the peptide binding groove and targets its location to the late endosomal MHC class II compartment (MIIC). Next, the invariant protein is cleaved by cathepsins leaving only a short protein fragment called CLIP (Ii-associated invariant chain peptide) in the binding groove. This is then switched for an exogenously-derived peptide fragment by the chaperone HLA-DM and the peptide/MHC complex is then transported to the plasma membrane (Figure 1⁸⁰)⁷⁷.

Additionally, presentation of exogenously-derived peptides on MHC class I can occur, particularly in dendritic cells, and is important for mounting an adaptive immune response against viruses that do not infect dendritic cells, as well as tumours. This is called cross-presentation and occurs through two main mechanisms: the vacuolar pathway and the endosome-to-cytosol pathway. In the vacuolar pathway, exogenously derived peptides are loaded into class I molecules in the endo-lysosomal compartment, and in the endosome-to-cytosol pathway, endocytosed proteins are transported to the cytosol and degraded by proteases, where they are then transported into the ER by TAP⁸¹.

MHC class I molecules can theoretically bind 7.7×10^9 peptides and MHC class II up to 1.2×10^{14} , and the number of unique peptides presented on a single cell may be up to 10,000 by some estimates⁷⁷. The large peptide binding capacity of MHC molecules, in combination with cross-presentation, and the ability of TCRs to respond to multiple peptide/MHC complexes, means that specific antigen detection by T cells is extremely efficient.

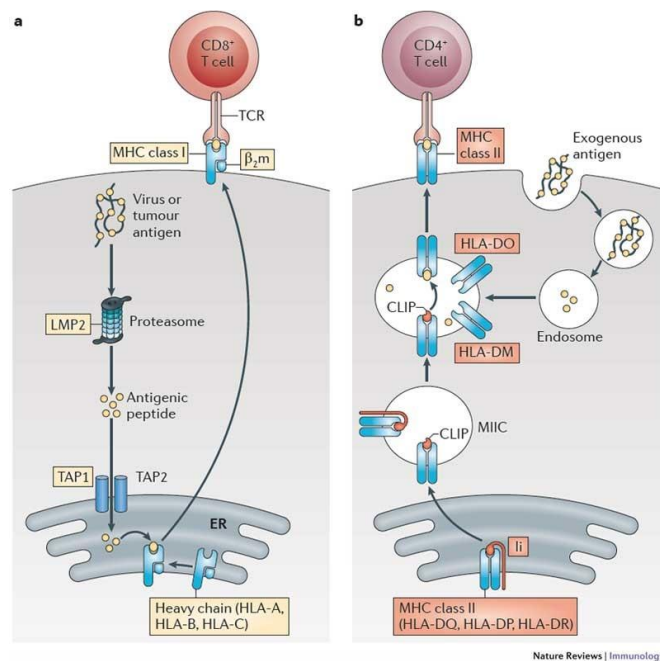


Figure 1 Mechanisms of antigen presentation to T cells (A) Endogenously-derived proteins (either self or viral proteins) are cleaved into peptides by the proteasome and brought into the ER by TAP. A variety of proteins in the ER, including tapasin, calreticulin and ERp57, load the empty MHC class I molecule with a peptide and it is subsequently transported to the cell surface where it can be bound by CD8+ T cells. In some circumstances, exogenous proteins can be transported to the cytoplasm and processed via this pathway, leading to presentation of exogenous proteins on class I molecules. Dendritic cells are specialised for this function. (B) Exogenous proteins are endocytosed and subsequently cleaved in the endosomal compartment. Meanwhile, MHC class II molecules are assembled with an invariant protein (Ii) in the ER, which is cleaved in the MIIC to form the shorter peptide CLIP. This peptide can then be exchanged for a higher affinity antigenic peptide with the assistance of HLA-DM and the peptide/MHC complex is subsequently expressed on the cell surface for binding by CD4+ T cells. From ref⁸⁰

1.4 The T-Cell Surface

1.4.1 T-Cell Receptor

The TCR is a highly sensitive receptor, present at a high density ($\sim 1 \times 10^5/\text{cell}$)⁸² on the T cell surface. It is made up of two chains which form the ligand binding portion (either α and β , or γ and δ)⁸³. These chains have no functional intracellular regions, thus are incapable of signalling. The functional TCR complex therefore is comprised of these two chains and a hexamer of invariant CD3 proteins which provide the ITAM motifs required for signal transduction⁸³. The CD3 chains all associate with each other and the TCR chains via non-covalent binding, with the CD3 $\epsilon\delta$ dimer associated with TCR α chain and the CD3 $\epsilon\gamma$ dimer contacting the TCR β chain^{84,85}.

The ligand-binding α and β chains are type I transmembrane proteins, formed of an extracellular domain (ECD) with variable (V) and constant (C) regions, a membrane-proximal connecting peptide (CP), single-pass transmembrane (TM) domain and a short cytoplasmic tail⁸⁶. The V and C domains of the TCR β , and the TCR α V domain contain immunoglobulin-like folds, whereas the C α domain has a more unique structure⁸⁶. The TCR α and TCR β chains are linked via several disulfide bonds in the C and V regions⁸⁷ as well as other interactions between their CPs and TM domains⁸⁴. The N-terminal variable domains contain 3 complementarity-determining regions (CDRs) which are the most variable portions of the receptor. The hypervariable loops CDR1 and CDR3 interact with the peptide and MHC molecule, while CDR2 interacts only with MHC⁸⁸. CDR3 is the most variable loop as it is encoded by the D and J gene segments which undergo additional modifications, including N- and P-nucleotide addition, during genetic recombination. The FG loop on the TCR β chain constant region is said to play a role in pMHC binding duration as well as contacting the CD3 $\gamma\epsilon$ heterodimer⁸⁹.

1.4.2 Adhesion molecules

To facilitate the TCR finding cognate pMHC, T cells also express a variety of adhesion molecules on their surface, which differ in their size and degree of interaction with TCR signalling.

The $\alpha_L\beta_2$ integrin LFA-1 (also known as CD11a/CD18), which binds ICAM-1-5 (mainly ICAM-1), is a glycoprotein expressed on all T cell subtypes⁹⁰. Its two chains, α and β , are non-covalently associated and have a molecular weight of 180 kDa and 96 kDa respectively⁹¹. The structure of each chain comprises 6-8 unique extracellular domains and an intracellular portion which interacts with the actin cytoskeleton and associated proteins⁹². The ligand-binding portion, domain I, is located on the α chain which forms part of the globular headpiece⁹³. The β chain (CD18) of LFA-1 is shared with other integrin types but the α chain (CD11a) is unique to this integrin⁹⁴.

LFA-1 can exist in several different activation states which are controlled by its structure. Low-affinity state LFA-1 is essentially unable to bind ICAM-1 due to its bent-closed conformation sequestering the ligand-binding α chain I domain. Inside-out signalling, where intracellular signalling molecules interact with the intracellular portions of LFA-1, causes a rapid (< 1 second) conformational change⁹³. This transforms LFA-1 to an extended conformation where the affinity for ICAM-1 is increased. The extended form comprises an intermediate (extended-closed) and high-affinity (extended-open) state of LFA-1 which are distinguished by the full opening of the ligand-binding site (caused by disruption of the salt bridge between the two chains) as well as the metal ion-dependent adhesion site (which coordinates Mg^{2+} ions to stabilise ICAM-1 binding⁹⁵). These changes in conformation increase the affinity for ICAM-1 approximately 9000-fold⁹³ and can be induced by chemokines secreted by, for example, endothelial cells. LFA-1 is also capable of outside-in signalling, where ligand binding generates intracellular signalling via molecules including VAV1, Lck, and ZAP-70⁹⁰.

The main role of LFA-1 is to facilitate cell-cell adhesion as well as being involved in cell migration and arrest at the site of inflammation⁹². Since TCR and LFA-1 signalling together are both necessary and sufficient to activate T cells⁹⁶, it has been widely assumed that LFA-1 contributes to early T-cell contact formation. However, since external signals are required to prime LFA-1 for efficient ligand binding, it seems that its role in migration and late contact formation may be more relevant.

Another adhesion protein, which may be more relevant to early T-cell contact formation, is CD2. This relatively small (between 40-50 kDa depending on glycosylation status⁹⁷) surface protein is part of the immunoglobulin superfamily (IgSF) and binds CD58 (3D K_d 9-22 μ M⁹⁸) which is expressed widely on both non-immune (e.g., endothelial and epithelial cells) and most haematopoietic cells⁹⁹. Its extracellular domain comprises a V-set IgSF domain, a C2-set IgSF domain, a linker, and a flexible stalk¹⁰⁰. Intracellularly, CD2 has a disordered proline-rich cytoplasmic tail which contains five SH3-binding domains that interact with several intracellular proteins. These include Lck, and others that link CD2 with the actin cytoskeleton⁹⁷.

The CD2/CD58 complex is likely to span a distance of \sim 15 nm (comparable to TCR/pMHC interaction) as suggested by CD2 crystal structures with other ligands^{100,101}. This means it is unlikely to be excluded from early close contacts formed by T cells and could even have a role in stabilising them. Indeed, CD2 has been shown to initially colocalise with the TCR on agonist-presenting SLBs¹⁰², be enriched in memory and activated T cells⁹⁷, and may be enriched in microvillar tips¹⁰³, again suggesting a role in early contact formation.

1.4.3 The Glycocalyx

Surface proteins that make up the glycocalyx essentially perform an opposing role to adhesion proteins, making it harder for cells to form close contacts which are required for activation. In immune cells, it is thought that the glycocalyx therefore prevents non-specific

cell activation. Most cells have a glycocalyx^{104,105} which hints at its importance. The glycocalyx contains proteins which are heavily sialylated, generating a strong negative charge around the cell. This is at least partially responsible for its anti-adhesive effect due to repulsion of like charges on other cells¹⁰⁶. T cells therefore must push through the glycocalyx 'barrier' of APCs and target cells in order to find cognate pMHC, help B cells, and kill infected or cancerous cells.

Two major protein components of the T cell glycocalyx are CD43 and CD45. CD43 is a highly glycosylated single-pass transmembrane protein expressed densely (about 1.5×10^5 molecules/cell) on most haematopoietic cells^{106,107}. It is estimated to protrude ~45 nm away from the T cell membrane¹⁰⁸ and has a molecular weight of 115 kDa or 130 kDa depending on the level of glycosylation¹⁰⁷. The biological function of CD43 has not been studied in great detail, and although several ligands have been suggested, including ICAM-1¹⁰⁷, it seems that its clearest function (at least with regard to immune cells) is to provide a physical barrier to cell/cell contact as part of the glycocalyx. Another crucial surface glycoprotein and component of the glycocalyx, CD45, is discussed in detail below (section 1.5.3).

1.4.4 Co-Stimulatory and Co-Inhibitory Molecules

Co-stimulatory/inhibitory molecules are crucial to the fine tuning of T cell function by modulating TCR signalling in either a positive or negative manner respectively. Furthermore, co-stimulatory receptors such as the prototypical molecule CD28 are required for generating the 'second signal' necessary for T-cell activation¹⁰⁹.

Ligands for these receptors (of which there are many) are found ubiquitously but change depending on the cell type and tissue environment. Professional APCs such as DCs change the variety of co-stimulatory/inhibitory receptors on their surface in response to environmental cues, thus modulating the T-cell response. For example, T cells interacting with an APC in an immunosuppressive environment are likely to become tolerised or exhausted, whereas under conditions of inflammation an effector response will be

generated^{110,111}. Co-stimulatory/inhibitory receptors mostly fall into two groups, designated the IgSF and the TNF receptor superfamily, which each contain subgroups based on amino acid composition, protein structure and function¹¹¹.

Well-studied co-stimulatory molecules include CD28, ICOS, 4-1BB and OX40 (the latter two are used in CAR T cell therapies). CD2 also belongs to this category in addition to its adhesive role. Stimulation of these receptors promotes T-cell proliferation, survival, and guides differentiation and effector function. Conversely, co-inhibitory receptors such as CTLA-4, LAG3 and TIGIT inhibit progress through the cell cycle as well as inducing tolerance, exhaustion and even apoptosis of T cells¹¹¹.

1.5 T-Cell Triggering Apparatus

The first step in signalling through the TCR is known as triggering, where the activating signal is relayed to the intracellular portion of the receptor complex allowing recruitment of proximal signalling molecules and ITAM phosphorylation¹¹². ITAM phosphorylation is necessary, but not sufficient, for full T-cell activation^{109,113}. Phosphorylation of ITAMs occurs within seconds of productive TCR/pMHC binding¹¹⁴, but even in this short period of time a number of molecules are involved.

1.5.1 T-Cell Receptor Complex

The CD3 γ , CD3 δ and CD3 ϵ chains are all type I transmembrane proteins, each comprised of an extracellular immunoglobulin domain, short CP, TM segment, and an intracellular ITAM sequence^{84,89}. ITAMs contain paired YxxL/I motifs separated by a spacer of 6-8 amino acids, creating the consensus sequence YxxL/I-X₆₋₈-YXXL/I. Many ITAMs also have a negatively charged aspartic or glutamic acid residue at position +2 relative to the first tyrosine^{115,116}. The sequence and spacing of the residues in the ITAM motifs permits binding by SH2-domain-containing proteins¹¹⁷. The CP of the CD3 chains contains a conserved CXXC motif

which may be important for TCR signalling¹¹⁸. These CD3 chains are found as heterodimers of either ϵ and δ , or ϵ and γ . One of each heterodimer is associated with the TCR complex¹¹⁹. Finally, each TCR complex has two CD3 ζ chains, providing six of the total ten ITAMs in the complex¹²⁰. The CD3 ζ chains have a short ECD, TM region, and a long cytoplasmic region containing the ITAMs¹²¹. Two CD3 ζ chains form a homodimer, interacting through a disulfide bridge and the coiled-coil structure in their TM domains^{84,120}. The structure of the intracellular sections remains poorly resolved⁸⁴, reflecting its flexible nature. Structural data published in 2019 suggests that the CD3 $\zeta\zeta$ homodimer is instrumental in the assembly of the TCR complex by forming hydrophobic interactions with the other CD3 chains in their TM regions⁸⁴.

1.5.2 Coreceptors

As early as the 1970s, T cells were subdivided into two groups based on their main functions: cytotoxicity or B cell help¹⁵. It was subsequently discovered that the surface molecules CD4 and CD8 could be used to distinguish between these two subtypes, or more accurately, the class of MHC molecule bound by the TCR¹⁶.

Both CD4 and CD8 are surface glycoproteins with molecular weights of 58 kDa¹²² and 32-34 kDa respectively^{123,124}. CD4 is a single chain made up of an extracellular region of four IgSF domains with a short stalk linking the extracellular portion to an intracellular tail containing the binding site for Lck which is facilitated by a zinc clasp^{16,125-127}. Its binding affinity for MHC is exceptionally low, measured recently at >2.5 mM ($3D K_D$ ¹²⁸). CD8 comprises a heterodimer of α and β chains (however CD8 $\alpha\alpha$ expression can occur) and binds MHC class I with an approximate affinity of 150 μ M¹²⁷. It comprises a single immunoglobulin-like domain connected by a long stalk to a transmembrane domain, with a similar cytoplasmic tail structure to CD4^{125,127}.

Coreceptors are recruited to the TCR/pMHC complex where they bind MHC and bring Lck into proximity with the TCR intracellular chains¹²⁹. While some studies have shown that

coreceptors can strengthen T-cell responses by many orders of magnitude^{130,131}, others have shown that neither CD4 nor CD8 are necessary to induce signalling, as high affinity ligands can trigger the TCR without coreceptor expression^{16,131}. Their purpose on T cells therefore may be to improve sensitivity to low affinity antigens.

1.5.3 CD45

Protein tyrosine phosphatases (PTPs) are equally important to T cell function. One of the most critical PTPs involved in TCR triggering is CD45, which is a large single-pass transmembrane protein expressed at high levels on the T-cell surface. CD45-deficient cells have severe signalling impairments¹³², and patients without CD45 develop severe combined immunodeficiency¹³³, illustrating its importance in T-cell signalling. The heavily glycosylated ECD has four fibronectin type II repeats, one of which is rich in cysteine^{134,135}. A 22-amino acid transmembrane domain links the ECD to the cytoplasmic region of 705 amino acids¹³⁴, comprising two phosphatase domains. Exons 4, 5 and 6 of the CD45 gene correspond to mucin-like protein domains A, B and C which are differentially spliced to create several isoforms. Cells express the different isoforms of CD45 depending on their subtype, stage of development, and activation status. Naïve T cells generally express CD45RA, whereas activated and memory T cells express CD45RO (a shorter form that includes neither A, B nor C mucin-like segments)¹³⁶. CD45 has a complex role in TCR triggering as it can positively regulate Lck, but also dephosphorylates CD3 ITAMs which directly opposes Lck function^{137,138}.

1.5.4 Lck

The main protein responsible for phosphorylation of TCR ITAMs is Lck, a 56 kDa Src family tyrosine kinase^{139,140}. Cell lines deficient in Lck cannot signal through the TCR¹⁴¹, and Lck-deficient mice have severe block in T cell development¹⁴¹, demonstrating the importance of this kinase. Lck contains myristoylated and palmitoylated residues in its N-terminal Src-

homology (SH) 4 domain which facilitate attachment to the cell membrane^{140,142}. It associates with the coreceptors CD4 and CD8 through a zinc clasp¹²⁵, although the fraction of total Lck bound to these receptors, and the importance of this in TCR triggering, is controversial^{129,143,144}. A single SH2 and SH3 domain bind phosphorylated tyrosines and proline-rich regions, respectively. The catalytic tyrosine kinase domain is followed by a short C-terminal tail which is important for the regulation of the kinase¹⁴².

Lck exists in one of four possible phosphorylation states with different activity levels. The main proteins responsible for driving change between these states are the PTP CD45 and the kinase Csk¹³⁹. Two tyrosine sites on Lck have critical importance – Y394 and Y505. When no sites are phosphorylated, Lck is in a 'primed' state with some kinase activity¹³⁹. Autophosphorylation at Y394, located in the activation loop of the tyrosine kinase domain, increases its catalytic activity by 2-4-fold^{139,145}. Conversely, Y505 phosphorylation in the C-terminal tail by Csk permits binding by Lck's SH2 domain, changing the conformation of Lck and blocking interactions with other signalling proteins¹⁴⁶⁻¹⁴⁸. If both sites are phosphorylated Lck is catalytically active, perhaps as much as Y394-monophosphorylated Lck^{140,149}. Although CD45 can dephosphorylate any of these regulatory sites, it seems to act as an overall suppressor of Lck activity at the expression levels observed on T cells^{150,151}.

Another Src kinase, Fyn, has also been found to associate with the CD3 chains¹⁵², and Fyn-deficient mice display some defects in TCR signalling¹⁵³. However, its comparative role in TCR triggering seems to be minimal, and instead it may play a more important role in T cell development¹³⁹.

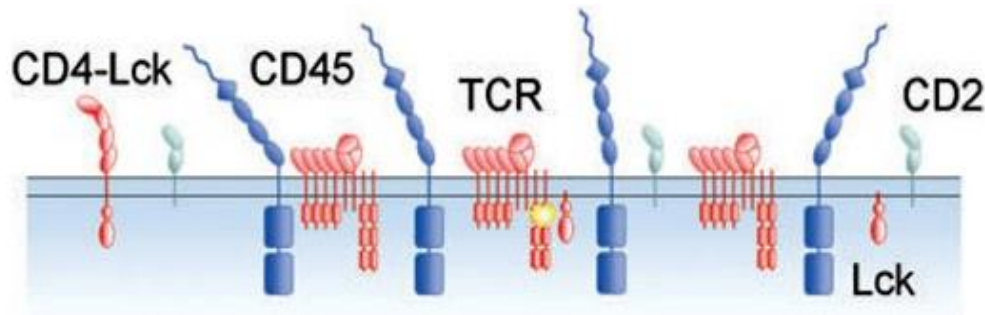


Figure 2 **Important components of the resting T-cell surface** The major surface components of the TCR triggering apparatus drawn roughly to scale on a resting T cell. The TCR can be phosphorylated randomly by Lck (yellow star) and just as frequently dephosphorylated by the phosphatase CD45. Coreceptors such as CD4 can be bound to Lck, and this may facilitate early ITAM phosphorylation during TCR triggering. CD2, a small adhesion protein, binds CD58 on APCs or target cells and brings their membranes into close apposition. Figure adapted from ref¹⁸⁵

1.5.5 ZAP-70

After ITAM phosphorylation, another protein tyrosine kinase, ZAP-70, is recruited to the TCR complex^{154,155}. ZAP-70 is a cytoplasmic protein vital for TCR triggering, demonstrated by the fact that ZAP-70-deficient patients exhibit severe immunodeficiency^{154,155}. It contains two SH2 domains separated by a linker sequence (interdomain A), and a kinase domain near the C terminus separated from the SH2 domains by another linker region (interdomain B)¹⁵⁵. Like Lck, ZAP-70 requires full activation through phosphorylation, as it exists in an autoinhibited state at rest¹⁵⁶. After binding the TCR ITAMs through its SH2 domains, the autoinhibited conformation of the protein is relaxed, and full activation occurs after upon phosphorylation of the kinase domain by Lck or other ZAP-70 molecules in *trans*¹⁵⁷⁻¹⁵⁹. ZAP-70 then facilitates further signalling through phosphorylation of scaffold and adaptor proteins such as linker of activated T cells (LAT), and SH2 domain containing leukocyte protein of 76kDa (SLP-76)¹⁶⁰. Syk, another kinase expressed by lymphocytes, has a similar role in TCR signalling, however, it is not vital for normal T cell function and is instead key for BCR signalling¹⁶¹.

1.6 Models of Triggering

Despite decades of research, the mechanism for TCR triggering, and indeed other immune receptors, is not agreed upon. The intriguing balance between TCR sensitivity (that is, the ability to react to very low frequency of agonist pMHC) and specificity (the ability to detect small changes in peptide sequence, without high-affinity ligand/receptor interactions) provides a difficult set of observations to reconcile.

1.6.1 Conformational Change

This model necessitates that a structural change in the extracellular portion of the TCR translates into the CD3 chains, thereby facilitating the phosphorylation of ITAMs, for example by exposing the ITAM sites for Lck binding. One structural study of the $\alpha\beta$ heterodimer noted a reversible conformational change in the A-B loop of the $C\alpha$ domain upon ligand binding and proposed that this could be involved in triggering¹⁶². The change was observed in $\alpha\beta$ heterodimers of different specificities and did not occur when binding antagonist pMHC. However, a more recent structural study of the complete TCR complex showed that this loop is partially buried, although the authors did not rule out the possibility of a role in higher-order oligomers⁸⁴. Other crystal studies of bound and unbound TCRs suggest that any conformational changes observed are unlikely to be translated to distal regions of the receptor¹⁶³, or are likely not large enough to have any effect⁸⁴.

Other studies have suggested that a conserved CXXC motif in the CP of the CD3 chains transmits a signal to the intracellular portions of the receptor, independently of clustering¹¹⁸. Indeed, mutations in this motif of the CD3 ϵ chain have been shown to quench TCR signalling and impair T cell development *in vivo*¹¹⁸. However, a mutagenesis study of the CD3 ϵ ECD did not find any effect on antibody-induced TCR triggering^{164,165}. Some studies suggest that CD3 ϵ cytoplasmic tails interact with the inner leaflet of the plasma membrane, and are released upon ligand binding, making the ITAMs available for binding¹⁶⁴. However,

when phosphatases are pharmacologically inhibited, ITAMs are readily phosphorylated in the absence of TCR binding, suggesting these sites are not sequestered¹⁶⁶. Another study suggests that a conformational change in CD3 ϵ facilitates binding of the adaptor protein NCK, which initiates signalling. Subsequent studies however found the role of NCK to be in regulating TCR expression, not triggering^{160,167}.

Conformational change-based models can explain TCR triggering by monovalent antigen and surface-bound antigens but are not well supported by structural or experimental data. Additionally, other models could also explain TCR triggering from monovalent antigen and ligands at surfaces.

1.6.2 Mechanotransduction

The notion of force inducing changes in the TCR came about from recognising that the interaction of pMHC and TCR in live cells was likely to exert a force on the TCR complex^{112,168}, and the fact that surface-tethered ligands are better at inducing signalling than soluble ligands¹⁶⁹. Most studies support the idea of a pulling force on the TCR, but others suggest pushing, shearing or twisting^{168,170}. One study showed that the CD3 $\gamma\epsilon$ heterodimer demonstrates some rigidity¹⁷¹, hinting at a possible role for force transmission. The authors of a complete TCR complex structure suggest the structure does not exclude the possibility of piston-like movement, although this would likely disrupt inter-chain interactions that may be important for structural integrity⁸⁴. Drugs that disrupt the actin cytoskeleton, a likely candidate for force generation, have been found to prevent formation of TCR microclusters¹⁷² and abrogate sustained TCR signalling¹⁷³, although triggering of TCRs by soluble (oligomeric) ligands suggests that force may not be required to initiate signalling¹⁷⁴. Moreover, binding of small adhesion molecules such as CD2/CD58 could insulate the TCR from many potential forces applied through pMHC in a physiological setting¹⁰⁰.

Force-based models could explain how variable ligands induce the same conformational change in the TCR, and studies which have applied force to the TCR demonstrate subsequent triggering^{168,175}. However, the ability of soluble antigen to induce triggering of the TCR suggests force is not necessary, and while force generation by T cells has been demonstrated¹⁷⁶⁻¹⁷⁸, a recent study shows that these forces are very weak¹⁷⁷. Furthermore, it is currently impossible to determine whether force directly causes TCR triggering in a physiological setting.

1.6.3 Receptor Aggregation

It is well established that TCR cross-linking results in triggering. Indeed, studies have demonstrated triggering through induced clustering by antibodies or multimeric pMHCs^{112,174}. One study suggested that CD3 chains are arranged away from important dimerisation motifs in the constant regions of both the $\alpha\beta$ and $\gamma\delta$ TCR, and that if these areas are mutated, signalling is impaired¹⁶². This asymmetry in the TCR complex structure was confirmed recently⁸⁴. It is unclear, however, how receptor clustering leads to ITAM phosphorylation and what the physiological relevance of this is, since T cells do not encounter multimeric pMHC *in vivo*, and a recent study showed that monomeric TCRs are responsible for ligand recognition¹⁷⁹. One idea is that CD4 or CD8, which are associated with Lck, bring the kinase into proximity with ITAMs as they bind MHC on the APC. However, soluble monomers of pMHC cannot trigger the TCR in solution¹⁷⁴, and studies suggest most Lck is not associated with coreceptors^{149,180}, making the role of Lck-bound coreceptors partial at most. The pseudodimer model suggests that unbound TCRs cluster around a pMHC-bound TCR through their coreceptors. This could explain triggering in response to low ligand concentrations, and some studies have provided evidence that self pMHCs can enhance TCR signalling¹⁸¹, although the data is not consistent across CD4+ and CD8+ T cells¹⁸² and signalling still occurs in the absence of coreceptors¹⁸³.

While receptor aggregation undoubtedly leads to triggering, single pMHCs can trigger the TCR under specific conditions suggesting aggregation may not be necessary^{169,184}. Furthermore, *in vivo*, ligand density will not likely be high enough to induce receptor cross-linking, suggesting a complementary or alternative mechanism.

1.6.4 Kinetic Segregation

The kinetic segregation (KS) model of TCR triggering¹⁸⁵ centres on the balance of signal-enhancing kinases and signal-quenching phosphatases with access to the TCR ITAMs. At rest, T-cell surface proteins diffuse freely. Proximal signalling kinases such as Lck therefore randomly collide with, and phosphorylate, TCR ITAMs. Phosphatases such as CD45 behave in a similar but opposing manner, leading to a resting equilibrium where net TCR phosphorylation is not enough to activate the cell, but may instead promote cell survival or other functions¹⁸⁵. When an APC interacts with a T cell using small adhesion molecule pairs such as CD58/CD2, the membranes of these cells are brought into close apposition – areas called ‘close contacts’^{101,135}. Proteins with large and rigid ECDs such as CD45 are passively excluded from close contacts, whereas Lck, with no ECD, is unaffected¹³⁵. Unbound TCRs continue to diffuse randomly regardless of their location, but pMHC-bound TCRs are retained in the close contact. The dimensions of TCR/pMHC are expected to be similar to CD58/CD2¹⁰¹, therefore are retained in close contacts. The local lack of phosphatase activity in close contacts shifts the equilibrium towards net TCR phosphorylation, which is sustained for long enough at agonist pMHC-bound TCRs to initiate intracellular signalling¹⁸⁵.

Evidence for this theory has been directly obtained using live cell imaging, where CD45 can be seen forming rings around close contacts, whereas Lck is homogeneously distributed within and around the contact¹³⁵. Furthermore, the extracellular domain size of phosphatases such as CD45 have been shown to directly influence triggering^{186,187}, as has altering the gap size between T cell and activating surface¹⁸⁸, and extending the pMHC ligand¹⁸⁹. An important prerequisite for this model is that all molecules in the TCR triggering

apparatus are freely diffusing and monomeric^{179,190,191}, which indeed has been observed through a variety of biophysical and biochemical methods, although is disputed by some studies¹⁹²⁻¹⁹⁴. An important prediction of KS, which is not explained by other models, is the occurrence of ligand-independent triggering. This states that triggering can occur without TCR binding a ligand if retained for sufficiently long enough in the close contact to allow ITAM phosphorylation and recruitment of downstream signalling proteins before the TCR diffuses out of the contact^{135,185}. Indeed, this has now been demonstrated in imaging studies, where either increasing the area of the close contacts without ligand present¹⁹⁵ or slowing TCR diffusion within close contacts¹⁹⁶ was shown to coincide with increased TCR triggering. Molecular redistribution theories such as KS are intuitive and backed by a variety of experimental data. However, they cannot explain the apparent need for such complex regulation of Lck¹³⁸ (see section 1.5.4) and do not necessarily exclude additional mechanisms of triggering such as conformational change.

1.6.5 Lipid Rafts

Another type of molecular reorganisation theory involves areas of lipid heterogeneity in the cell membrane called lipid rafts. This theory suggests that TCR binding to an agonist pMHC leads to its association with lipid rafts, which are enriched with certain proteins such as Lck and deficient in proteins such as CD45^{112,197}. Models involving lipid rafts are controversial as methods initially used to prove their existence were later dismissed as unreliable¹⁹⁸. Furthermore, a FRET-based study found no evidence of lipid raft probe enrichment at TCR microclusters²⁰². Nevertheless, there is still some support for this model, and newer imaging probes have allowed for more detailed visualisation of lipid heterogeneity in the membrane of model systems and living T cells^{199,200}. For example, a 2015 study observed aggregation of ordered lipid domains surrounding the TCR upon microcluster formation²⁰¹, and another study in 2021 showed that TCR crosslinking, or ligand binding, changes its preference to a more ordered lipid environment, although this was measured after cell

spreading¹⁹⁹. A more recent study²⁴⁶ used a combination of microscopy techniques to show CD45 pre-exclusion in microvilli tips of human and murine lymphocytes, which was reversed by depletion of cholesterol, suggesting a lipid-mediated partitioning of membrane proteins. However, they did not directly visualise cholesterol at microvilli tips.

Lipid-based models are an interesting prospect but remain to be supported fully by the literature. Although some studies have demonstrated differential lipid composition in the cell membrane, and in relation to the TCR and other relevant proteins, a direct link to the mechanism of TCR triggering remains to be demonstrated.

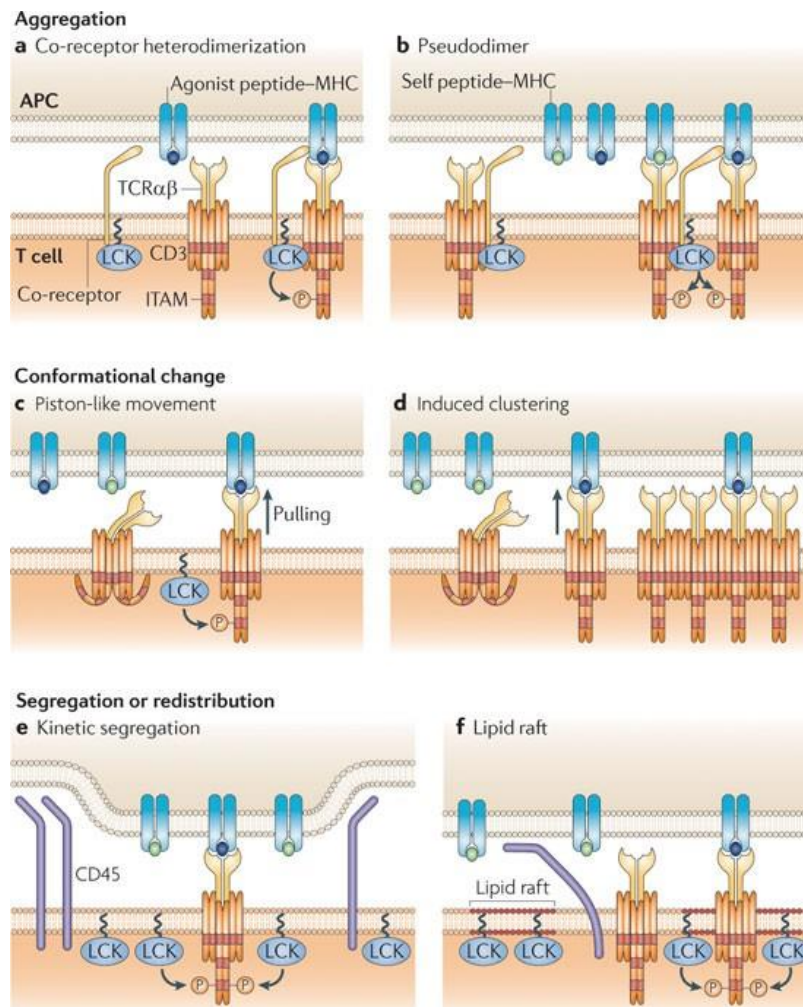


Figure 3 **Main models of TCR triggering** Models proposed to explain TCR triggering generally fall into three categories: receptor aggregation, conformational change, and molecular redistribution. TCR aggregation could be facilitated by coreceptors or binding self pMHC. Clustering of receptors leads to TCR triggering but the mechanism by which this occurs is unknown. Conformational change, possibly induced by force, could permit triggering by making ITAMs available for phosphorylation or by facilitating receptor clustering. Close contacts created by the apposition of T cell and APC/target cell membranes could physically exclude phosphatases with large extracellular domains, creating a local region permissive to sustained ITAM phosphorylation. Finally, preference of transmembrane proteins for certain lipid domains within the membrane could facilitate bringing TCR into proximity with Lck and induce triggering. Figure taken from ref¹¹²

1.6.6 Kinetic Proofreading

The kinetic proofreading model does not explain the TCR triggering mechanism *per se*, however it is important to consider in the context of TCR triggering as it could explain how ligand discrimination takes place.

First postulated in 1995²⁰³, the kinetic proofreading mechanism suggests that efficient discrimination by the TCR is achieved by the occurrence of numerous reversible biochemical steps in between ligand binding and signal transduction. These steps require

energy input and/or recruitment of other signalling molecules, for example tyrosine phosphorylation or recruitment of ZAP-70 to phosphorylated TCR ζ chains. This creates a time delay between TCR binding and *bona fide* signal generation. Furthermore, upon dissociation of TCR/pMHC binding, these steps must be reversible (e.g., by phosphatase activity), and this must happen at a sufficiently fast rate at which non-agonist pMHCs binding to TCR (mostly) do not cause signalling.

In support of the kinetic proofreading model, studies have shown that T-cell activation is dependent on TCR/pMHC half-life^{204,205}. However, other studies have shown that ligands with short dwell times can robustly activate T cells^{206,207} which seems to be at odds with this model. It is possible that pMHC rapidly and repeatedly binding the same TCR could artificially increase the dwell time on the TCR for long enough to induce signalling²⁰⁶, but the rapid diffusion of unbound membrane proteins on the cell surface makes this unlikely. Another apparent contradiction to this model was that the TCR was thought to display a sharp affinity threshold response which could not be reconciled with its extremely high sensitivity by the kinetic proofreading model³⁷⁸. Recently however, a thorough analysis of T-cell responses to ligands of different affinities showed that the TCR in fact does not display a sharp affinity threshold response³⁷⁸, therefore providing new support for the model.

1.6.7 Serial Triggering Model

The serial triggering model suggests that T cells are able to 'count' the number of TCRs triggered by a limited number of agonist pMHC and use this to make the decision for activation. This model was proposed to explain the observation that T cells downregulate a far larger (up to 200-fold) number of TCRs than the number of agonist pMHC molecules presented to them¹⁷³, noting that the binding affinity of agonist pMHC/TCR is low in comparison to other biological molecules such as antibodies²⁰⁹.

In support of this idea, one study showed that short-lived TCR/pMHC interactions could lead to T-cell activation when rebinding of pMHC was rapid and to TCRs within close

proximity²⁰⁵. Interestingly, simultaneous binding events did not increase the chance of activation. Another study which monitored the activation of T cells with different TCR expression found that a threshold number of TCRs (~8000 without, and ~1500 with costimulation) was required to induce T-cell activation, suggesting signal integration over TCRs which is 'counted' by the cell. However, at all TCR expression levels T cells produced calcium flux suggesting that there are additional mechanisms between TCR triggering and T-cell activation²¹⁰.

1.7 TCR Microclusters

Tightly linked with TCR triggering is the formation of TCR microclusters. These small clusters of TCRs are consistently observed on T cells interacting with ligand-presenting surfaces or cells^{172,211-214}. They can form on T cells interacting with mobile (i.e., SLBs, APC) or immobile (i.e., protein-coated glass) surfaces although only mobile surfaces allow for microcluster movement and eventual immune synapse formation (see section 1.8).

Clustering of TCR components was first noted in 2000 in T-cell/B-cell conjugates²¹⁵, and subsequent measurements have quantified the number of TCRs in microclusters to be between 40-200^{172,212,213}. Microclusters are detectable within seconds of T cells interacting with an activating surface^{172,213}. However, some studies argue that smaller TCR clusters (sometimes termed nanoclusters) already exist on resting cells^{192,193}, possibly with other molecules such as LAT²¹⁶, and that these clusters coalesce to form larger structures upon TCR triggering^{216,217}. One study found that denser TCR microclusters have a higher probability of containing phosphorylated signalling proteins, thus suggesting a role for cluster formation in signal initiation²¹⁷. Microclusters generally form before or simultaneously with calcium flux^{172,213,215}, a downstream marker of TCR triggering.

TCR microclusters have been observed to colocalise with important signalling and scaffolding molecules including ZAP-70 and LAT^{172,213,214}, and to exclude the phosphatase CD45^{211,218}. In one study, TCR microclusters were observed forming structures called

'micro-adhesion rings', with central TCR surrounded by a ring of LFA-1, similar to a small version of the immune synapse²¹². Furthermore, there is some evidence that TCR aggregation in microclusters also aggregates ordered lipid domains in the T-cell membrane²⁰¹, although the functional relevance is still unclear, and this result has been disputed by other studies²⁰².

Since the development of super-resolution microscopy techniques, the spatiotemporal resolution of TCR microclusters and other molecules involved in signalling has been studied extensively. It is generally accepted that ZAP-70 is highly colocalised with the TCR but that other proteins such as LAT are found in segregated domains surrounding the TCR, although they partially overlap with ZAP-70^{216,219,220}. Other molecules such as the adaptor SLP-76 have been observed on the periphery of LAT clusters²²⁰, and other studies demonstrated localisation of other signalling molecules, including NCK, PLC γ , and VAV1 around LAT and TCR microclusters²¹⁴. These imaging studies suggest the formation of highly structured signalling hubs nucleated by TCRs.

Once the cell has spread, new microclusters continuously form at the periphery of the cell where they initiate signalling by recruiting molecules such as ZAP-70 and SLP-76²¹³. As they move inwards, they lose association with these proteins, and upon reaching the cSMAC at the centre of the cell (described in section 1.8), their signalling is respectively terminated or propagated by a balance between receptor endocytosis and clearing of the phosphatase CD45, which occur in different temporal phases^{172,211,213,221}.

It is generally believed that TCR microclusters are the initiators and propagators of TCR signalling. However, there is some opposing evidence to this theory. Firstly, blocking pMHC binding has been shown only to prevent new microcluster formation and not disrupt established microclusters, a result recapitulated by disruption of the actin cytoskeleton²¹¹. Furthermore, cytoskeletal disruption was found to abolish TCR microclusters in a study where TCR microclusters were observed on resting cells¹⁹⁴, suggesting a role for active

processes in the formation of TCR microclusters. Finally, imaging data acquired by Yokosuka and colleagues²¹³ demonstrated ZAP-70 recruitment in the periphery of activated T cells to areas with no visible TCR clustering, suggesting that ZAP-70 may be recruited to a single TCR. If true, this would imply that TCR microclusters are not required to initiate signalling.

If TCRs are indeed randomly distributed on the T-cell surface, presumably some form of signalling would be required to form microclusters in the first place, especially if passive clustering can be ruled out (e.g., when ligand density is very low). In line with this, an imaging study on live T cells provided evidence that antigen recognition is carried out by monomeric TCRs¹⁷⁹. However, a study using a reductionist DNA model TCR system showed that ligand on-rate was increased in areas adjacent to ligand-bound receptors relative to other cell areas. Furthermore, larger receptor clusters more efficiently recruit and retain ZAP-70²²². Therefore, the question of exactly how TCR microclusters relate to initial TCR signalling remains open.

The importance of protein distribution within the 3D structure of the T cell is a topic of great interest. T-cell topography will be discussed in detail in sections 1.9 and Chapter 4, but it is increasingly clear that T cells likely do not form completely flat, homogenous contacts with other cells or model APC surfaces. Indeed, studies of contact formation by T cells have demonstrated small points called close contacts where the large phosphatase CD45 is passively excluded, presumably as the T-cell membrane comes into close apposition with the underlying surface¹³⁵. Therefore, these variations in structure could be expected to influence the apparent distribution of cell surface proteins, especially with methods such as TIRFM, which is very sensitive to changes in fluorophore distance from the interacting surface (see section 1.15.3). In agreement with this idea, a study observing microvillar close contacts made by T cells on quantum dot decorated-supported lipid bilayers noted that TCR intensity was often increased at areas of close contact formation²²³. This suggests that, at

least in part, observations of TCR microclusters might be due to fluctuations in T-cell membrane topography. However, this idea has not yet been thoroughly explored, which could be explained at least in part by the lack of appropriate surfaces on which to image T-cell topography and protein distribution simultaneously. Previous work from the Davis group (described in the thesis of Edward Jenkins) led to the creation of a more physiological SLB APC model (described in section 1.14.2.2), which includes (amongst other components) glycocalyx proteins which are excluded upon close contact formation. This APC model presents a method to investigate the relationship between T-cell topography and TCR microclusters.

While the existence and structure of TCR microclusters have been extensively examined, new observations have begun to cast doubt on the exact nature of these structures, in particular, their relationship to signalling and T-cell topography. The function and formation of signalling TCR microclusters will be addressed in Chapter 5.

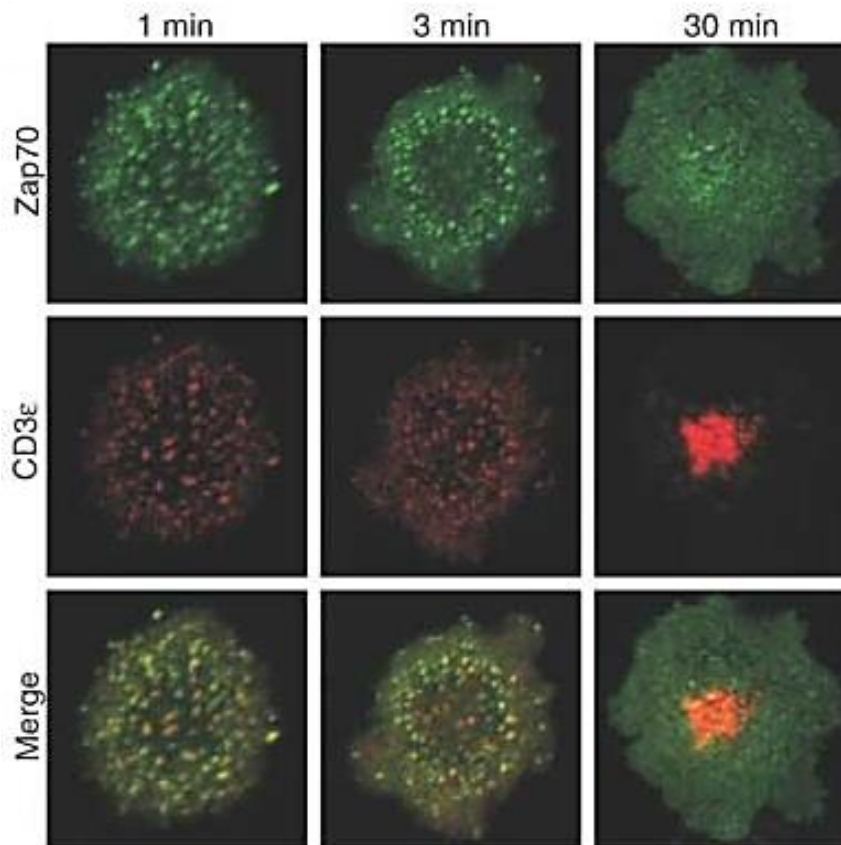


Figure 4 TCR and ZAP70 microclusters appear on T cells interacting with activating surfaces
 Primary murine T cells expressing EGFP-ZAP70 were placed on SLBs presenting agonist pMHC and ICAM-1 and fixed after different time points, then stained for CD3 ϵ . Throughout the time points small clusters of TCR and ZAP70 can be observed and these change over time as the immune synapse begins to form. TCR and ZAP70 strongly colocalise at early time points but ZAP70 is less abundant in the centre of the cell as time moves on, indicating that active signalling occurs mainly at the cell periphery as the immune synapse is established. Figure adapted from ref²¹³.

1.8 Downstream Signalling and Activation of T Cells

After triggering, numerous downstream signalling pathways become activated, ultimately resulting in a change in the T-cell behaviour to initiate effector function.

Phosphorylated ITAMs provide a docking site for ZAP-70, a key molecule in the initiation of further signalling (see section 1.5.5). Two important targets of ZAP-70 are the adaptors LAT and SLP-76^{224,225} which, along with ZAP-70, form a multimolecular signalosome which initiates signalling cascades controlling the cytoskeleton, integrin activation and gene transcription²²⁶.

The kinase IL-2-induced tyrosine kinase (Itk), activated at the proximal signalling complex, activates phospholipase C gamma 1 (PLC γ 1), which subsequently cleaves the membrane lipid phosphatidylinositol-4,5-bisphosphate (PIP $_2$) producing the second messengers inositol triphosphate (IP $_3$) and diacylglycerol (DAG). IP $_3$ activates the calcium channel IP $_3$ R on the endoplasmic reticulum membrane, releasing intracellular calcium stores²²⁷. This increase in calcium activates proteins such as calcineurin, which promotes nuclear localisation of the nuclear factor of activated T cells (NFAT), a transcription factor responsible for, among other things, IL-2 production²²⁶.

DAG initiates two major pathways involving mitogen-activated protein kinases (MAPK) and protein kinase C θ (PKC θ). The MAPK pathway begins with activation of the guanine nucleotide-binding protein Ras and culminates in translocation of transcription factors such as STAT3 and activation protein-1 (AP-1), leading to CD69 upregulation and cell survival^{228,229}. PKC θ induces nuclear translocation of NF- κ B, which initiates transcription of genes involved in cell survival, proliferation and effector functions²³⁰.

T cells become activated after receiving two extracellular signals – this is known as the two-signal hypothesis²³¹. The first is TCR binding with agonist pMHC and coreceptor support and the second is engagement of co-stimulatory receptors by ligands on the APC, which are upregulated after APC activation¹¹⁰. CD28 binding CD80 (also known as B7-1) on APCs are the prototypical costimulatory pair, but other important co-stimulatory molecules on T cells include 4-1BB and OX40^{111,232}. Without both signals, T cells cannot carry out their effector function and become anergic^{109,233}. On the other hand, co-inhibitory receptors such as PD-1 and CTLA-4 negatively regulate T cell activation by recruiting phosphatases through their immunoreceptor tyrosine inhibitory motif (ITIM) domains²³⁴, and also by competing for binding with ligands of co-stimulatory receptors²³⁵ (see also section 1.4.4). Cytokines released by APCs are generally considered a 'third signal', however this may be dispensable for T cell activation and instead play a main role in T helper cell polarisation²³⁶.

T cells contacting APCs or target cells often form a dynamic structure called the immune synapse or supra-molecular adhesion complex (SMAC), containing a distinct pattern of surface receptors. Small molecules such as TCR/pMHC and CD28 localise to the central-SMAC, adhesion molecules such as LFA-1/ICAM-1 form a ring around these in the peripheral-SMAC²³⁷ and other molecules such as CD43, CD44, and CD45 are found in the distal-SMAC²²¹. The spatio-temporal location of these molecules is likely to be important in facilitating full T cell activation through several mechanisms²³⁸. Moreover, differences in SMAC architecture and timing between T cell types hint at different functions depending on context^{238,239}. However, an immune synapse has not yet been directly observed in T cells interacting with DCs, suggesting this structure may not be necessary for T-cell activation, at least in some cases.

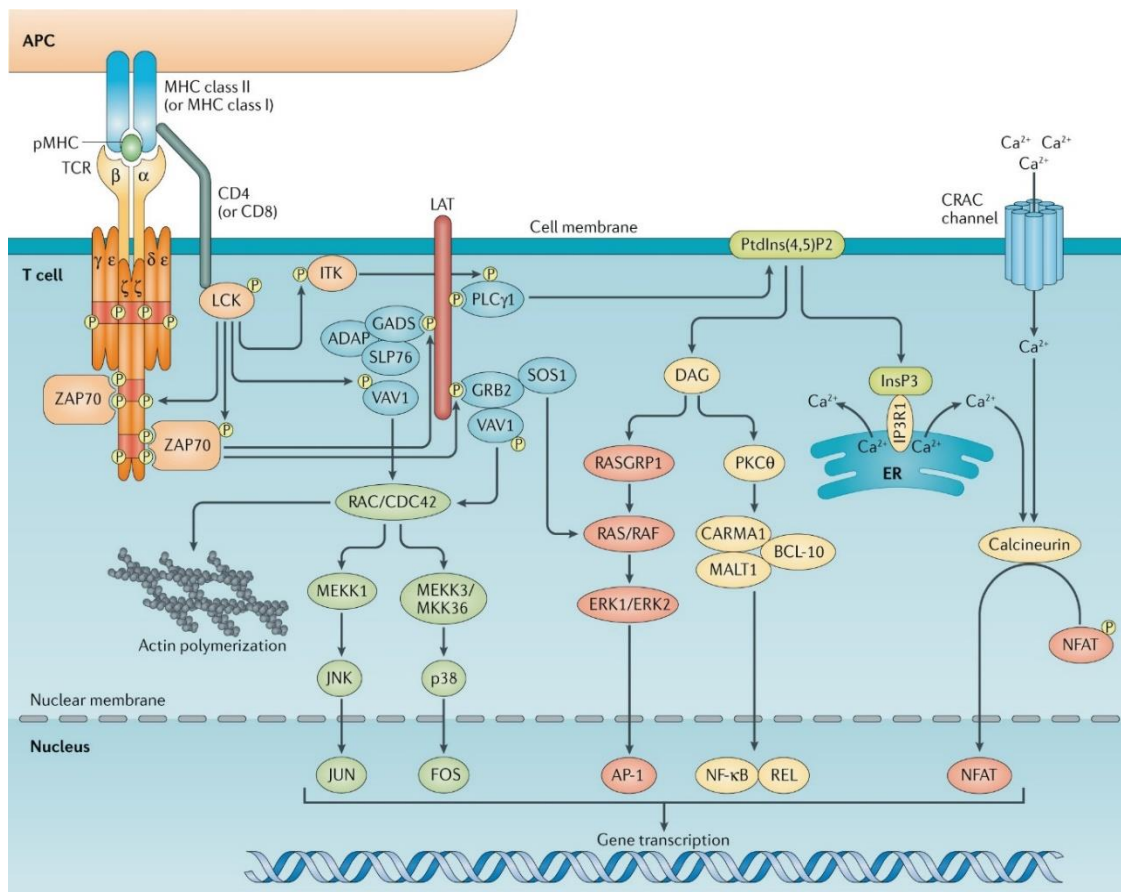


Figure 5 **Signalling networks downstream of the TCR** TCR ITAMs are phosphorylated predominantly by Lck, which is often anchored to a coreceptor. Phosphorylated ITAMs recruit ZAP70 which is responsible for phosphorylating numerous downstream targets including LAT. This scaffolding protein amplifies the signal to various pathways including the MAP kinase cascade, NF-κB, and NFAT pathways. Signalling through the membrane lipid PIP₂ causes calcium flux which can be easily measured as a proxy for TCR signalling. Figure taken from ref³⁸⁷

1.9 T-Cell Topography

The morphology of T cells, like many other cell types, is not a simple sphere but is instead covered in membrane protrusions called microvilli. These actin-rich structures are 70-500 nm in diameter, between 100 to several hundred nm in length^{103,194,223} and are highly dynamic, cumulatively sweeping across the entire T-cell surface in approximately 1 minute²²³. Microvilli are supported by filaments of F actin²⁴⁰ and there is evidence that the TCR is both directly and indirectly linked to the actin cytoskeleton, especially upon signalling and recruitment of various scaffold proteins such as SLP76 and Nck^{241,242}. Studies have shown that TCR microclusters do not form when actin nucleation is inhibited¹⁷², but established TCR microclusters seem to be resistant to the same treatment^{172,223}.

Furthermore, treating T cells with actin inhibitors such as Cytochalasin D abrogates calcium flux in T cell/APC conjugates²⁴³ suggesting a tight link between sustained TCR signalling and cytoskeletal function.

Since access to pMHC on other cells is hindered by glycocalyx proteins, and membrane protrusions in T cells have been implicated in the penetration of the glycocalyx²⁴⁴, it is reasonable to assume that these structures likely have an important role in TCR signal initiation and antigen discrimination. Indeed, several studies, including super-resolution techniques, have suggested enrichment of molecules such as TCR, CD2 and CD4 at microvillar tips^{103,194}. In contrast, other proteins such as LFA-1 may be concentrated on the cell body²⁴⁵. These data imply a deliberately constructed local environment for signal initiation on microvilli. Additionally, one study proposes the exclusion of the negative signal mediator, CD45, from microvillar tips²⁴⁶. This finding however is disputed by numerous studies^{103,195,223}.

While membrane protrusions made by CTLs with target cells were observed using electron microscopy as early as the 1970s⁴³⁸⁻⁴⁴⁰, an imaging-based study in 2017²²³ provided the first live images of T cell microvilli forming contacts with an APC. The number and speed of microvillar protrusions did not change during synapse development, nor between the side of the T cell forming a synapse with an APC and the opposite uncontacted side. The authors used quantum dot-decorated SLBs, which indicate areas of close contact formation between the cell and SLB surface by the exclusion of the quantum dots, to show that TCR-positive microvillar contacts are stabilised compared to TCR-negative contacts. Interestingly however, microvillar contacts were shown to be unaffected by abolishing TCR signalling and disrupting the cytoskeleton, suggesting a constitutive (certainly TCR signalling-independent) ligand-searching and synapse-forming process by T cells. As this is the first published study looking directly at microvilli in live early T-cell contacts, there remains

substantial room for further investigation into the role and regulation of microvilli in this process.

Despite different overall cell sizes, several other immune cell types have the same diameter of microvilli²⁴⁰, as do naïve and effector T cells¹⁹⁴, suggesting a deliberate and necessary size restriction imposed on these structures. In agreement with this, a recent modelling study demonstrated that T-cell contacts of ~200 nm radius provide optimal conditions for specific antigen detection¹⁹⁵. This size is comparable to that measured for T cell microvilli. The model predicts that contacts much smaller than this crucial size essentially abolish TCR signalling by not allowing the TCR to be in a phosphatase-depleted area for long enough to propagate downstream signalling pathways, whereas larger contacts result in non-specific TCR triggering by the converse mechanism. Based on a dwell time concept – that is, the length of time a TCR has to stay in a close contact to become triggered – of 2 seconds, the model predicts ligand-independent triggering of the TCR would occur with ~80% probability if the close contact radius was 0.4 μm (just twice the typical radius observed for microvilli). In contrast, for 0.2 μm -radius close contacts the probability was 0. Indeed, recent work in the Davis group showed that an increase in ligand-independent triggering of ~4-fold when the median area of T-cell close contacts was increased by ~4-fold by overexpressing the small adhesion molecule CD2. Furthermore, cells with increased CD2 expression, and therefore larger contacts, demonstrated comparable levels of calcium flux on agonist- vs null pMHC-presenting SLBs whereas T cells with wildtype CD2 expression showed a ~4-fold increase in calcium flux on agonist-presenting SLBs compared to null-presenting SLBs (thesis of Edward Jenkins, Davis group), therefore demonstrating the dependence of antigen discrimination on close contact size. This theoretical and experimental evidence provides a strong argument that the size of these initial contacts is essential in maintaining both TCR specificity and sensitivity. Therefore, their regulation by the cell is an important area for investigation.

It is clear that TCR signalling directly influences T-cell morphology, and morphology (i.e., microvilli) may regulate TCR signalling, especially at the earliest close contacts between a T cell and an APC or target cell. Given these new insights, proposed mechanisms for TCR triggering and activation can no longer be considered without this additional three-

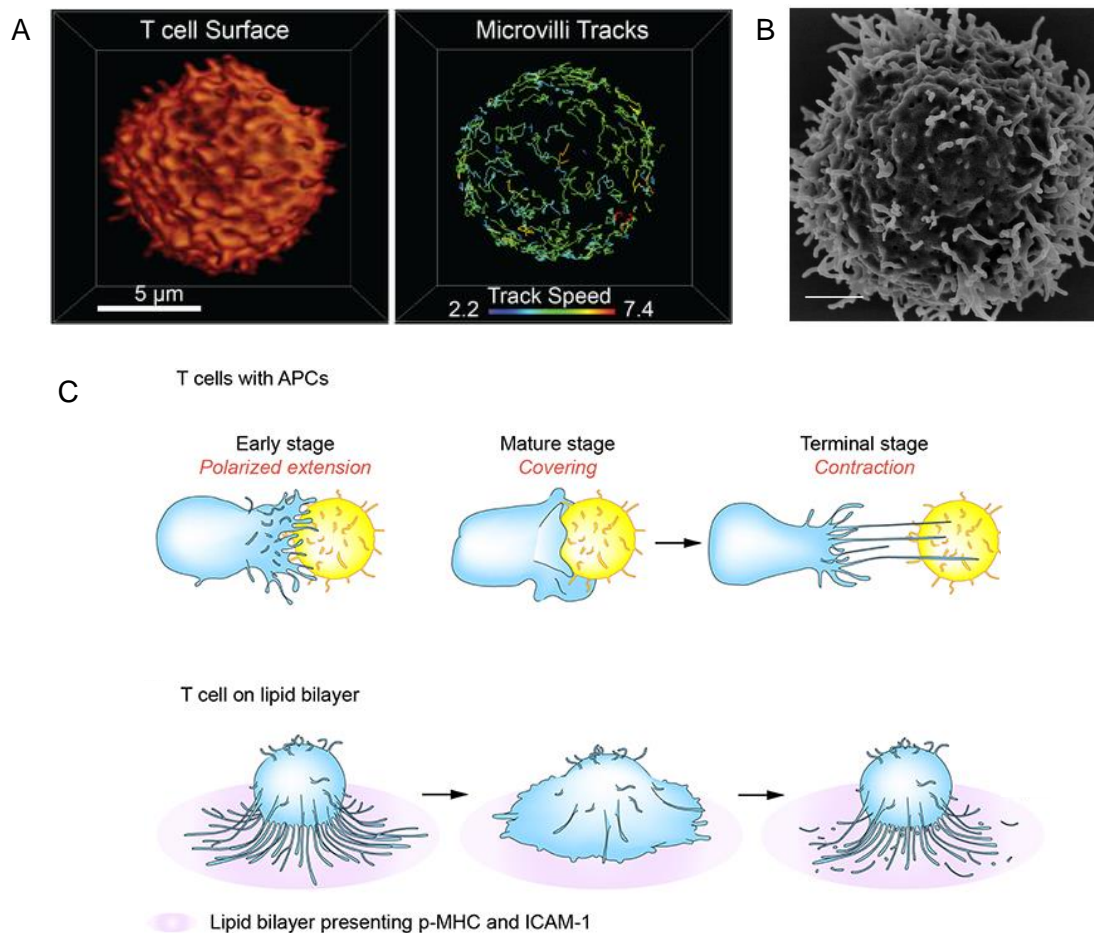


Figure 6 T cells are covered in microvilli which make initial contact with APCs or target cells (A) Light sheet microscopy image of a primary murine T cell with the movement of each individual microvillus labelled on the right. (B) Scanning electron micrograph image of a human effector T cell (scale bar 1 μm) showing the surface covered in microvilli. (C) Schematic representation of a T cell interacting with an APC (upper) and an SLB presenting agonist pMHC and ICAM-1 (lower). Initial interactions are mediated by small microvillar protrusions, followed by cell spreading, and retraction. Figures adapted from refs^{194,223,434}

dimensional context, where opposing cell membranes interact in space and time. The effect of TCR density and signalling on early T-cell contact formation will be addressed in Chapter 4.

1.10 B Lymphocyte Overview

1.10.1 Development

B cells were first identified as the antibody-producing cells in the chicken bursa of Fabricius, an organ equivalent to mammalian bone marrow²⁴⁷. Most B cells begin their development in the bone marrow from the haematopoietic stem cell compartment, where they divide asymmetrically producing B cell progenitors²³. Progenitors transition into Early Pro-B cells where Ig α and Ig β signalling chains are expressed and D-J joining occurs in the heavy chain genes, then Late Pro-B cells which undergo V-DJ joining. Like T cells, this process is mediated by the enzymes RAG-1 and RAG-2²⁴⁸ and heavy chains are allelically excluded²⁴⁹. During the next stage of development, Large Pre-B cells express a pre-BCR comprising Ig α and Ig β , as well as the BCR heavy μ chain with an invariant surrogate light chain. After rapid proliferation, cells transition to the Small Pre-B cell stage where V-J joining occurs in the light chain genes of one chromosome. V-J joining occurs first on the κ light chain and continues through several cycles if the initial rearrangement is not productive (known as light chain rescue). If no κ chains are successfully rearranged, the process is started on the λ light chain. If this also fails, the cell undergoes apoptosis^{250,251}. If successful, the light chain is expressed on the surface with the μ heavy chain forming a unique BCR on the now immature B cell. As with T cells, addition of N- and P-nucleotides in the junction between the V and J segment creates additional diversity in CDR3, part of the ligand-binding portion of the immunoglobulin³⁵. These cells travel to the spleen where they become transitional B cells, then subsequently express surface IgD and differentiate into long-lived mature FO or MZ B cells, residing in different areas of the spleen^{22,23,252}.

1.10.2 Subtypes and Their Function

The total B cell population is comprised of several subsets. Most B cell subsets share a developmental pathway and are described as B2 cells, while B1 cells make up the small but potentially significant remainder.

FO B cells are a mature but naïve population circulating through B cell follicles in SLOs, scanning for antigen²². CD4⁺ Tfh cells provide the 'help' needed for their full activation, in the form of co-stimulation through CD40/CD40-L and cytokines such as IL-21^{64,65}. Upon activation, some FO B cells undergo clonal expansion and form a GC within the B cell follicle²⁵³, and some differentiate into plasmablasts, which generate large quantities of low-affinity antibodies. Subsequent processes in the GC produce a higher affinity BCR and therefore, antibody. In the dark zone of the GC, B cells proliferate and undergo somatic hypermutation. During this process, the cells modify their genomic DNA using an enzyme called activation-induced cytidine deaminase (AID), which preferentially targets the gene sequences transcribing the antigen-binding portions of the BCR²⁵⁴. GC B cells with a mutated BCR proceed to the light zone where they compete for an ever-shrinking pool of antigen and undergo class switch recombination^{254,255}. In this process, mediated by cytokines from T cells, regions of DNA coding for the μ or δ constant regions are excised from the genome, therefore cells no longer express the IgD or IgM isotypes. The remaining DNA is joined back together, creating a new heavy chain gene of a different isotype (IgA, IgE or IgG) depending on the specific function required. Often cells must go through multiple rounds of proliferation to finish this process^{254,255}.

Cells with the highest affinity BCR/antigen interactions from the initial cycle either differentiate into plasma cells, or re-enter the dark zone for further affinity maturation, while cells with disadvantageous mutations die by neglect²⁵⁶. Affinity maturation takes many days, and results in a substantial increase in antibody affinity for the antigen^{257,258}. Plasma cells created by this process are long-lived, secreting antibodies for many days or

weeks before travelling to the bone marrow²⁵⁹. Some GC B cells become memory B cells, which remain circulating in the body in a resting state until they are reactivated through the BCR²⁶⁰.

MZ B cells largely remain in the spleen where they detect blood-borne antigens²⁶¹. MZ B cells are quick to respond to infection as they do not require T cell help²⁵². After encountering cognate antigen, they rapidly proliferate and differentiate into short-lived plasmablasts^{262,263}.

B1 cells make up a small proportion of the total B cell population and may have separate developmental origins. B1 cells have usually relatively unmutated BCRs and they produce most of the low affinity circulating IgM, IgA and natural antibodies, which can be autoreactive²⁵.

The most recently discovered functional subset of B cells are the regulatory B cells, which, like T_{regs}, are capable of suppressing the immune response^{264,265}. However, at present, it is uncertain whether they constitute a discrete subtype, as opposed to an induced phenotype²⁶⁶.

1.10.3 Antigen Presentation to B cells

B cells are much more versatile in their ability to recognise antigen than T cells. They can recognise the antigen in its native form, without additional processing or presentation by specific molecules on other cells. Additionally, B cells of all types can respond to non-peptide antigens^{267,268}.

B cells can bind antigen in solution, for example small molecules which are carried into lymph nodes or in the spleen, although this is not the most common method by which antigen recognition occurs. Antigens coated in complement can be captured by complement receptors on follicular dendritic cells, which can also directly bind immune complexes (several antigen and antibody proteins bound together) through Fc receptors. Macrophages

can also present antigen to B cells through receptors binding complement, Fc portions of antibodies, or carbohydrates. Finally, a population of dendritic cells in the splenic paracortex has also been identified that can present native antigen to B cells^{267,268}.

1.10.4 BCR Structure and Function

The BCR is a multifunctional surface protein with some structural and functional similarities to the TCR. It is essentially a membrane-bound antibody (also known as immunoglobulin), with only small differences between the signalling and soluble form of the receptor created in the C terminal portion by alternative gene splicing²⁶⁹. Hundreds of thousands of BCRs are expressed on the surface of a mature B cell²⁷⁰. The BCR heavy and light chains have no capacity to induce signalling on their own, as they lack ITAM domains. These are instead provided by the Ig α -Ig β heterodimer (also known as CD79a and CD79b)^{271,272}. These chains together make up the BCR complex, the functional unit of B cell signalling.

The overall immunoglobulin architecture consists of two heavy and two light chains, named for their relative sizes (50 and 25 kDa respectively). Disulfide bridges hold the two heavy chains together and attach one light chain to each heavy chain. The light chain is comprised of one variable and one constant domain and has two classes – kappa (κ) and lambda (λ)– which are mutually exclusive in their expression. In humans and mice, kappa chains are more common, but the kappa/lambda ratio is variable between species for currently unknown reasons. The heavy chain consists of one variable domain and several constant domains depending on the isotype. In both the heavy and light chains, domains are made up of two β -sheets held together by a disulfide bond^{269,273}.

Protease cleavage studies demonstrated two functionally important segments of the immunoglobulin – fragment of antigen binding (Fab) and fragment crystallisable (Fc). The antigen-binding portion of the immunoglobulin is comprised of the variable regions of the

heavy and light chains (giving each BCR/antibody two binding sites), and the Fc portion is made up of the C-terminal halves of the two heavy chains²⁷³.

The IgD and IgM BCR isotypes are expressed before SHM and class switching to either IgE, IgA or IgG. Each isotype has a slightly different functional role and therefore structure²⁷³. IgD, expressed on naïve B cells, is secreted only in small amounts and is rarely found on the surface of a class-switched B cell²⁵⁵, however its preservation through most jawed vertebrates²⁷⁴ suggests functional importance. Secreted IgM makes up most of the natural antibodies and first-wave immune response as class switching is not required for expression²⁵⁵. At 900 kDa, it is the largest antibody isotype, as it is expressed as a heavily glycosylated pentameric complex. IgA is secreted as a dimer with the main function of protecting mucous membranes. There are two subgroups of IgA termed IgA1 and IgA2. IgG antibodies belong to one of 4 sub-groups – IgG1, IgG2a, IgG2b and IgG3 – which each have differing functions and structures. IgG is the most abundant antibody type in the body and forms much of the secondary humoral response to antigen. Finally, IgE is utilised in the anti-parasite response, but also plays a role in hypersensitivity and allergy²⁷³.

1.10.5 B Cell Triggering Apparatus

Many aspects, both structural and functional, are shared between BCR and TCR triggering. BCR triggering, where ITAM motifs on Ig α and Ig β are phosphorylated, results in recruitment of proximal kinases. Shortly after this, a multimolecular complex forms with other intracellular proteins and signalling is initiated.

In B cells, the primary kinase responsible for phosphorylating the BCR ITAMs is Lyn¹¹⁵, functionally equivalent to Lck in T cells. Lyn is a Src-family kinase which is localised to the cell membrane via acylation of the SH4 domain²⁷⁵. It contains an SH3 and SH2 domain connected to the kinase domain by a hinge region, and a C terminal tail. The kinase domain contains a critical tyrosine residue in the activation loop at position 397^{142,276}, which must

be phosphorylated for activation. An opposing tyrosine in the C terminal tail, Y507, renders the protein inactive through inducing an auto-inhibitory conformation²⁷⁷. PTPs such as CD45 dephosphorylate both of these sites²⁷⁸ and Csk preferentially phosphorylates the inhibitory tyrosine (Y507)¹⁴⁸. Phosphorylation of the BCR complex ITAMs by Lyn recruits other Lyn molecules via their SH2 domains and numerous other signalling molecules, for example spleen tyrosine kinase (Syk)²⁷⁹.

Syk, a homologue of ZAP-70, binds phosphorylated ITAMs through its two SH2 domains. It also contains an SH3 domain and C-terminal catalytic domain¹¹⁵. After recruitment to the ITAMs, Syk is fully activated via phosphorylation by Lyn and by other Syk molecules in *trans*¹¹⁵. Through its SH3 domain, Syk acts as a molecular scaffold and propagates downstream signalling^{115,280} as well as phosphorylating nearby ITAMs to amplify the initial signal.

Like T cells, B cells express the phosphatase CD45 on their surface, but specifically its largest isoform, CD45RABC¹³⁶, which maintains low levels of basal BCR signalling through dephosphorylating BCR ITAMs. Deletion of CD45 in B cells does not cause severe functional problems but does lead to a developmental block at the transitional stage, leading to an accumulation of immature cells^{132,136,281}, suggesting its role in B cells is not as essential as in T cells. A lack of CD45 perturbs Lyn regulation by disturbing the balance of maintaining phosphorylation sites with Csk. However, the phenotype of Lyn deficient mice is not the same as CD45-deficient mice, suggesting its role here is not crucial^{278,282,283}.

Another important PTP expressed by B cells is CD148 which is a single-pass transmembrane protein with an ECD comprised of 8-9 fibronectin domains²⁸⁴ and an ICD with a single PTP domain²⁸⁵. While CD148 is expressed in T cells, and has an overall negative regulatory effect on TCR signalling^{286,287}, its function appears much more crucial in B cells. Total knockouts in mice cause embryonic lethality²⁸⁸, however models where surface CD148 function was abolished were similar to CD45-deficient mice, implying redundancy in the function of these

two phosphatases²⁸⁹. CD45/CD148 double-deficient mice show a severe block in B cell development as well as insufficiency in several signalling pathways. Additionally, this phenotype included hyperphosphorylation of Lyn at position Y507, indicating both phosphatases have a positive regulatory role in Lyn signalling²⁸⁹.

1.11 Models of Triggering

Several mechanisms to explain BCR triggering have been postulated. Like the TCR, they either involve receptor aggregation, rearrangement, or conformational change, which hints at potentially similar triggering mechanisms between these lymphocyte receptors.

1.11.1 Receptor Aggregation

The crosslinking model of triggering was initially conceived in the 1960s and has remained widely accepted ever since²⁹⁰. The model postulates that monomeric BCRs induce signalling when receptors are brought together in the membrane, for example by polyvalent antigen.

In favour of this model, experiments have shown that B cell signalling can be initiated by full antibody or F(ab')₂ fragments of IgG, which have 2 binding sites, but not by monovalent Fab fragments²⁹¹, similarly to monomeric and multimeric pMHCs interacting with T cells¹⁷⁴. Imaging studies have indicated the BCR as a resting monomer which forms microclusters after engaging cognate antigen^{292,293}. Additionally, this theory matches well with structural studies illustrating the flexibility of the immunoglobulin hinge region²⁹⁴, as conformational change is not necessarily required.

Whilst the capability of polyvalent over monovalent antigens to induce triggering in solution has been demonstrated, the applicability of this model to all antigens is uncertain. Unlike most T cell antigens which are processed and presented by MHC, B cell antigens are heterogenous, making it unlikely that they would all bind several BCRs in a similar manner^{267,268}. Furthermore, the majority of antigen encountered by B cells *in vivo* is not

soluble²¹, and it has been shown that monovalent antigen triggers robustly on a surface^{295,296}. Since the crosslinking model cannot explain triggering by monovalent antigen in any capacity, nor does it directly explain why crosslinking leads to receptor triggering, this suggests an alternative or complementary triggering mechanism.

1.11.2 Conformation-Induced Oligomerisation

Like receptor crosslinking, this model suggests that the resting BCR is monomeric. Binding of antigen causes a conformational change in the receptor, which is translated to the otherwise sequestered C μ 4 domain (in the constant region of the BCR heavy chains) and WTxxST motif in the transmembrane region, promoting receptor clustering. This clustering in turn drives signalling through making ITAMs available for intracellular protein binding²⁹⁶.

Evidence for this model comes largely from imaging studies and mutational analysis. In one study, Fab-labelled BCRs in live cells had diffusion profiles consistent with a monomeric protein, which then formed clusters upon binding monovalent or polyvalent antigen²⁹⁶. A FRET-based study attached donor and acceptor fluorescent proteins to the cytoplasmic region of Ig α molecules and tested FRET efficiency under different conditions. Resting cells showed no FRET signal, but upon binding surface-bound antigen the FRET signal peaked, followed by a drop which remained above background. These results were interpreted as monomeric BCRs clustering upon antigen engagement and a subsequent conformational change in the intracellular domains to promote signalling by making ITAMs available for binding²⁹³. A further study found that deletion of the C μ 4 domain prevented BCR oligomerisation and signalling, but the expression of the C μ 4 domains alone lead to their clustering and B cell activation²⁹⁶. This implies that the C μ 4 domain is essential for clustering and signalling, and that this activity is prevented by the conformation of the resting BCR complex.

As with conformational change-based models of TCR triggering, this idea is not robustly backed by experimental evidence. Although this model could explain how antigens of varying size, valency, and presentation can initiate triggering, it is still unclear how a conformational change would be translated from the antigen binding portions of the BCR into the C μ 4 and intracellular domain, which would be especially challenging through the flexible hinge region as determined by crystal structures of antibodies²⁹⁴.

1.11.3 Dissociation-Activation

The dissociation-activation model is very different from proposed models of TCR triggering as it theorises that resting BCRs exist in an autoinhibitory oligomerised state, where ITAMs are sequestered by the packing together of the BCR complex intracellular domains. In this model, antigen binding transforms the restrictive oligomer into a more dissociated island, freeing the ITAMs for binding by kinases and signalling proteins²⁹⁷. Evidence for this model initially came from biochemical techniques indicating the presence of BCRs in oligomers in resting cells²⁷¹. More recently, a bi-fluorescence complementation assay in a reconstituted *Drosophila* S2 cell system demonstrated the existence of BCR oligomers in a resting state. Furthermore, mutation of the BCR to force monomeric expression led to constitutive receptor internalisation²⁹⁸, suggesting that BCR oligomers are autoinhibitory. However, these findings have not been confirmed in B cells. Modern super-resolution imaging experiments have provided evidence for both monomeric and oligomeric BCRs on resting cells (with the majority of BCRs determined to be monomeric)^{270,299}, although these methods can be prone to overcounting errors^{300,301}. This matches well with data on the TCR which largely supports a (mainly) monomeric receptor distribution^{179,190,302,303}.

Dissociation-activation could explain how antigens with a range of sizes could trigger the BCR, since the requirement is only to spread out the oligomer island rather than bring the receptors into a certain specific proximity, but it does not explain how monovalent antigen can trigger the BCR at a surface²⁹⁵. Moreover, support for this model largely comes from

biochemical assays which are known to create clustering artefacts and are far removed from a physiological setting. Additionally, cells imaged on 'inert' surfaces may not be truly in a resting state³⁰⁴, and analysis of stoichiometry by super-resolution methods can be prone to error^{300,301}.

1.11.4 Kinetic Segregation

More recently, the role of KS-based signalling has been considered in B cells. As previously described (section 1.6.4), this model relies on the balance between inhibitory large phosphatases and activating small kinases, which is perturbed upon receptor binding a membrane-bound ligand at a close contact. Although this mechanism has been extensively studied in T cells, studies in B cells are in earlier stages. A key difference between B and T cells in terms of the KS model is that the BCR is substantially different in height from the TCR, its size varies with isotype, and it can bind differently sized ligands as they are not restricted by MHC presentation. Additionally, the BCR is bivalent and binds ligands with much higher affinity than those observed with TCR/pMHC³⁰⁵. Rather than being dependent on CD45 for most of the phosphatase activity in the cell as T cells are³⁰⁶, B cells express two large phosphatases, CD45 and CD148. Interestingly however, CD148 has dimensions even larger than CD45 (estimated at approximately 50nm)³⁰⁷, and B cells also express the largest isoform of CD45³⁰⁸, which suggests a possible requirement for a larger phosphatase. Moreover, cells deficient in both large phosphatases show impaired signalling and CD45 was found to be excluded from signalling BCR microclusters in imaging experiments³⁰⁹.

1.11.5 Collision-Coupling/Dissociation

The collision-coupling model focusses on the role of the actin cytoskeleton in BCR signalling and is quite different to any TCR triggering models. In this model, resting BCRs exist in nanoclusters which are confined by the cytoskeleton to areas rich in inhibitory coreceptors, and distant from activating coreceptors and kinases. Alterations to the cytoskeleton permit

BCRs to be released from association with negative coreceptors and/or to interact with molecules promoting signalling^{310,311}.

This model was derived from single-molecule imaging-based data. Single-particle TIRF imaging showed BCRs restricted in areas of the actin cytoskeleton at rest and when the cytoskeleton was disrupted, their diffusion and signalling increased^{270,311}. A dSTORM-based study additionally showed that small clusters of BCRs on resting cells clustered further, and with the BCR coreceptor CD19, upon antigen stimulation²⁷⁰. In keeping with this idea, disruption of the actin cytoskeleton has been shown to induce BCR signalling on B cell lines²⁷⁰ and primary B cells in line with increased BCR diffusion³¹¹. While some studies observe similar clustering behaviour with the TCR²¹⁶, receptor diffusion is generally accepted to become slower during/after triggering, and indeed slowing the TCR correlates with increased triggering¹⁹⁶.

While supported by several experimental methods, this model does not specify how antigen binding is able to stimulate such a rapid cytoskeletal change, and to what extent the BCR is linked to the actin cytoskeleton. Modern imaging technique such as dSTORM are powerful, however, artefacts in data analysis^{300,301} and selection of non-stimulating surfaces³⁰⁴ have called the validity of this type of data into question.

1.11.6 Lipid Rafts

Lipid rafts have been implicated in BCR as well as TCR signalling. Biochemical and microscopy-based studies have observed a preference of crosslinked or antigen-bound BCRs for membrane areas enriched in sphingolipids and cholesterol which contain Lyn but exclude CD45, therefore facilitating phosphorylation of Ig α and Lyn and initiating BCR signalling^{312,313}. However, as with T cells, whether protein reorganisation (and therefore

signalling) is caused by lipid reorganisation or vice versa remains unanswered, and no recent studies have confirmed these findings.

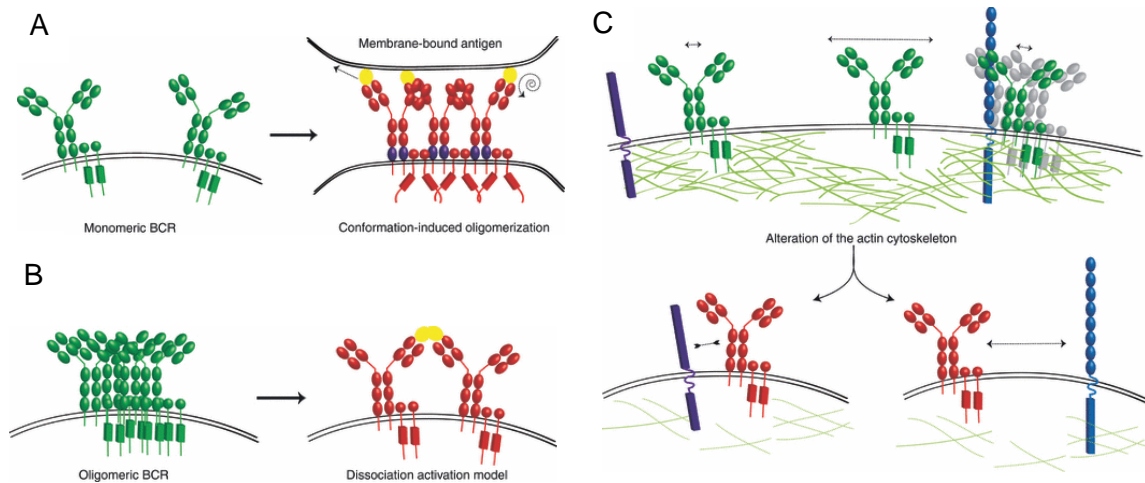


Figure 7 **Models of BCR triggering** (A) Conformation-induced oligomerisation model. Resting monomeric BCRs bind cognate antigen and translate a conformational change in the constant and transmembrane domains to the intracellular domains of the BCR, permitting receptor clustering and ITAM phosphorylation. (B) Dissociation-activation model. BCRs exist in an autoinhibitory oligomeric conformation at rest. Binding of cognate antigen releases the BCRs from this state, allowing ITAMs to become accessible to kinases. (C) Collision-coupling/dissociation model. At rest, BCRs exist largely in nanoclusters restricted by the actin cytoskeleton. They are confined to areas in proximity with inhibitory coreceptors and distant from activating coreceptors. Disruption of the cytoskeleton permits BCRs to interact with activating coreceptors and induce signalling. Adapted from ref³¹⁰

1.12 Downstream Signalling and Activation of B Cells

Signalling pathways activated downstream of the BCR also have similarities with the TCR. After its full activation, Syk phosphorylates downstream signalling proteins and neighbouring ITAMs, recruiting more Syk molecules and scaffold proteins such as B cell linker protein (BLNK), thus propagating and amplifying signalling from the BCR^{115,280} in a similar manner to how LAT functions for T cells. Key signalling pathways activated include the mitogen-activated protein kinase (MAPK) cascade, phosphoinositide-3-kinase (PI3K), NFAT and RAS pathways²⁸⁰. Together, these pathways result in a change in B cell behaviour including cytoskeletal reorganisation, BCR internalisation, and antigen presentation to T cells^{305,314}.

Activation of PLC γ 2 by Syk results in cleavage of the plasma membrane lipid PIP $_2$ into PIP $_3$ and DAG, which are involved in intracellular calcium release and PKC activation, respectively³¹⁵. Calcium release stimulates NFAT nuclear translocation³¹⁶, while PKC and intracellular calcium release leads to NF- κ B pathway activation³¹⁵ as in T cells. Downstream of DAG, the MAPK cascade results in activation of c-JUN NH2-terminal kinase (JNK), and extracellular-related kinase (ERK) which mediate cell survival and proliferation through AP-1³¹⁵. Through binding to the phosphorylated coreceptor CD19³¹⁷, Phosphoinositide-3-Kinases (PI3K) can activate AKT, localising it to the membrane. AKT in turn activates mTOR which is involved in cell division and survival³¹⁸.

During signalling, the BCR also forms microclusters which move into the cSMAC, while adhesion proteins move to the periphery, forming an immune synapse analogous to that in T cells²⁹². Interestingly, some studies suggest that BCR isotypes differentially activate downstream pathways – for example, the IgG cytoplasmic tail has been shown to resist CD22-mediated quenching of ERK activity in comparison to IgM and IgD isotypes³¹⁹ although this is disputed by other studies³²⁰.

In contrast to T cells, B cells can be activated via two mechanisms. T cell-dependent activation requires a T cell to recognise a peptide presented by MHC on the B cell surface, which is derived from antigen bound to the B cell receptor (BCR). Upon recognition of the peptide/MHC complex (pMHC), the T cell releases cytokines to induce B cell proliferation, while co-stimulation is provided by ligation of CD40 and CD40L. In turn, signals received through the TCR induces T cell clonal expansion³²¹. T cell help is also required for BCR class switching, a process where the BCR and antibodies expressed by a B cell changes from one isotype to another, thus changing its functional capabilities^{255,321}. T cell-independent activation can occur through binding of mitogenic antigens to toll-like receptors (TLRs) on the B cell, or through polyvalent antigens crosslinking the BCR³²². Therefore, B cells do not require two or more signals to become activated as T cells do.

1.13 Comparison of Triggering Models Across T and B Lymphocytes

As previously described, both the structure and proposed triggering mechanisms for the B and T cell receptors have striking similarities despite the functions of their respective cells being very different. This suggests a potential for conserved signalling mechanisms between these cell types, and potentially also other immune receptors.

The main structural similarity between the BCR and TCR is their (non-covalent) association with signalling chains that contain the ITAMs required for signal initiation. The main chains of the BCR (light and heavy) and TCR (α and β) both lack a substantial cytoplasmic tail therefore additional chains required for signalling are provided by Ig α and Ig β or the CD3 complex respectively^{84,273}. Furthermore, each are initially phosphorylated by small membrane-bound Src family kinases (Lck and Lyn)^{115,138} and negatively regulated by phosphatases with large extracellular domains (CD148 and/or CD45)^{136,284}. However, the BCR and TCR bind antigens in a very different affinity range²⁰⁹ and also of different valency, as the BCR comprises two binding sites compared to the TCR's single site. These differences are substantial and imply a need for different triggering requirements.

Both the TCR and BCR trigger when aggregated by oligomeric ligands or generic ligands such as antibodies^{290,323}, although exactly why this occurs is not yet known. Ligand binding could produce a conformational change in the receptors, which could induce triggering directly or by receptor aggregation, but this is tricky to reconcile with the fact that monomeric ligand does not trigger either receptor in solution³²³. To date no study has been able to demonstrate how a conformational change in the extracellular domains of the BCR or TCR could translate to intracellular ITAM phosphorylation.

The BCR is thought by some to exist in small clusters in a resting state^{270,271}. Because of this, it was proposed that these oligomers on the BCR surface are autoinhibitory and change when bound by ligand to induce signalling²⁹⁷. While this is an attractive model, other studies

have determined the BCR to be mainly monomeric at the surface^{299,324}. It is likely that the same distribution is true for the TCR^{179,190,303} although some studies point to nanoclusters of the receptor on resting cells^{192,193}, which could explain the high sensitivity of T cells to antigen¹⁹³. If the BCR and TCR were to be differently distributed on the cell surface it is likely that their triggering mechanisms would be different.

Kinetic segregation is a model which could apply to either receptor and has already been studied extensively in T cells^{112,135,185,186,189,325-327}. The phosphatase CD45 (and CD148 in unpublished data from the Davis group) has been shown to be excluded from clusters of BCR and TCR^{211,218,312,328}, and the fact that both cell types respond to monomeric antigen at a surface^{169,295} could be easily explained by this model. The BCR likely protrudes further from the cell membrane than the TCR, but interestingly B cells tend to express the largest isoform of CD45 and additionally express CD148 which is likely even larger than CD45²⁸⁴. This suggests adaptation to retain kinetic segregation across cell types.

Given the similarities in signalling behaviour between these receptors despite their structural and functional differences, it is possible that they could share a triggering mechanism(s), which presents an exciting area for further study. This question will be incorporated into the experiments in Chapter 6.

1.14 Surfaces for Imaging T Cells

Studies described in this thesis have used a variety of different surfaces to study T-cell behaviour, each with its own advantages and disadvantages. Several options are available for *in vitro* studies which are necessary to observe molecular-scale events in live cells, rather than using static fixed tissue samples or intravital imaging where this resolution is not yet possible. Studies of this nature generally involve APCs (for example B cells), or glass surfaces coated with proteins and/or phospholipids to provide a reductionist two-dimensional model of an APC. Other models include freestanding three-dimensional

spheres made from simple lipids and proteins (i.e., large or giant unilamellar vesicles; LUVs/GUVs), spheres of plasma membrane derived from cells (giant plasma membrane vesicles; GPMVs), or glass beads coated with proteins and/or phospholipids.

1.14.1 Coated Glass Surfaces

T-cells can easily be imaged interacting with coated glass slides using various microscopy methods (discussed in section 1.14). Glass surfaces are cheap, durable and withstand harsh chemicals used for cleaning, and do not contribute significantly to background noise during imaging. However, it has been shown that T cells can signal non-specifically when interacting with bare glass³⁰⁴ therefore if ligand-specific signalling is required the glass surface should be 'blocked' with an inert substance such as BSA which prevents cell adhesion and signalling.

Glass slides can be coated with a variety of molecules from proteins to lipids to present T cells with different surfaces for interaction. One commonly used molecule is the cationic polymer poly-L-lysine (PLL) which can be sourced in preparations of different molecular weights and simply adsorbs to the glass surface. While PLL has been widely used as an inert surface to study T-cell behaviour, recent evidence suggests that non-specific interactions with T-cell surface proteins can cause cell adhesion, molecular redistribution and robust signalling³⁰⁴. A more suitable alternative for an inert surface could be fibronectin, a large glycosylated glyocalyx protein which appears to have no effect on T cells unless in combination with an anti-TCR stimulus (³²⁹and previous work from Davis group).

The simplest two-dimensional surface for imaging ligand-specific interactions of T cells is with proteins adsorbed onto glass. Purified proteins can be produced as needed and will bind the glass surface without the need for specific tags or linkers. One or more proteins can be adsorbed on the surface simultaneously so the effects of multiple protein interactions can be studied. This reductionist system is relatively quick to prepare and can recapitulate many key behaviours of T cells observed in more complex systems such as microcluster

formation and cell migration^{330,331}. Its major disadvantage in terms of its physiological relevance is the lack of lateral protein mobility on the surface since there is no fluid component. This prevents behaviours such as centripetal microcluster movement and immune synapse formation^{214,332}, however deliberately preventing movement of T-cell proteins bound to the glass surface may be useful to simplify analysis, for example, of protein recruitment to the TCR.

1.14.2 Glass-Supported Lipid Bilayers

Phospholipids can be used to further functionalise glass surfaces by creating a fluid bilayer surface which can be decorated with proteins. Since the introduction of this technique in the 1980s³³³, it has become perhaps the most widely used model APC surface in T-cell imaging.

SLBs are typically made up of the phospholipid 1-palmitoyl-2-oleoyl-sn-glycero-3-phosphocholine (POPC) with small amounts of modified lipids such as 1,2-dioleoyl-sn-glycero-3-[(N-(5-amino-1-carboxypentyl) iminodiacetic acid) succinyl] (DGS-Ni-NTA) which provide a method for binding proteins to the bilayer surface. Other conjugation methods such as streptavidin-biotin and GPI anchors can also be used for this purpose³³². Generally, proteins purified for SLB production are truncated at the transmembrane portion which helps maintain their mobility in the SLB³³². Virtually any protein of interest can be incorporated onto SLBs if it can be produced as a truncated version with an appropriate tag. Lipids can be deposited onto clean glass surfaces by vesicle fusion, which occurs spontaneously over tens of minutes, or spin coating which is much faster. T-cells do not seem to interact with SLBs (see section 6.3.2) as long as they do not contain nickel-chelating lipids such as DGS-Ni-NTA. 'Exposed' nickel ions on SLBs have been shown to cause T cell signalling and adhesion (section 8.2 and ³³⁴). Therefore, as with uncoated glass, measures should be taken to block these sites with an inert substance such as casein or a non-binding tagged protein (see section 8.2 and ³³²).

The main advantage of this system is that it recapitulates lateral diffusion of cell surface proteins well (due to sitting on top of a very thin ($\sim 10 \text{ \AA}$) layer of water above the glass surface³³⁵) and precise control of diffusion can be achieved by incorporating other lipids such as 1,2-dipalmitoyl-sn-glycero-3-phosphocholine (DPPC) which decreases membrane fluidity³³⁶. Furthermore, multiple proteins can be bound to SLBs simultaneously to investigate cooperative or antagonistic effects, and protein densities can be measured easily and quickly using fluorescent microscopy methods. Its major disadvantage is in the rigidity of the underlying glass substrate, which is estimated to have a stiffness 10^7 - 10^8 times that of APCs³³⁷. T cells have previously been shown to activate more robustly and migrate faster on stiffer surfaces³³⁸ which suggests that behaviours observed on glass SLBs may be exaggerated compared to physiological settings. Furthermore, the surface available for interaction with T cells is relatively large compared to *in vivo* settings where cell topography of the APC or target cell may modulate protein-protein interactions on the cell surface^{240,339}.

However, many similarities have been observed between T-cell responses to SLBs and APCs, including clustering and exclusion of surface and intracellular proteins^{44,96,211,215}, indicating that their use as a model APC is valid. Recently, a method was developed for forming SLBs on surfaces coated first with the polymer polydimethylsiloxane, which can be made with variable stiffnesses³⁴⁰. This addition to SLBs could be used in future studies to increase their physiological similarity.

Finally, SLBs can also be created on surfaces other than glass slides which allows for different properties to be investigated. By coating glass beads with SLBs for example, the effect of surface area and curvature on different receptor/ligand interactions can be examined as the diameter of the beads can be easily modified. Additionally, SLB-coated beads can be used for bulk stimulation of T cells³⁴¹.

1.14.2.1 1st Generation Supported Lipid Bilayers

SLB-based experiments corroborated transplantation and *in vitro* studies with T cells in demonstrating that pMHC was the ligand for the TCR³⁴²⁻³⁴⁶. While SLBs presenting only agonist pMHC are sufficient to generate TCR triggering, by only providing T cells with one molecule to bind, this forces the TCR to act both as an adhesion molecule and signalling receptor. The role of force on TCR triggering, and its relevance *in vivo*, is debated^{84,112,168,175,347} (and section 1.6.2) but it is certain that there are many more molecular interactions occurring at the T cell/APC surface than simply the TCR and its ligand^{90,97,100,101,348-351}. Therefore, researchers rapidly began incorporating other proteins into SLBs for T cells to interact with, in the hope of creating a more physiologically relevant model.

The most popular of these models, used heavily in T cell research for the past few decades, provides two key elements required for assessing T cell behaviour: signal generation from an agonist pMHC and adhesion from ICAM-1, which binds LFA-1 on the T cell³⁵². This type of SLB was used in a seminal paper by Grakoui and colleagues to demonstrate in detail for the first time the dynamic nature of the immune synapse, a structure containing a concentric circle formation of TCR/pMHC and LFA-1/ICAM-1 that drives T cell activation⁹⁶. This complemented previous work carried out in cell-cell settings²³⁷, indicating that this reductionist approach is sufficient to induce biologically relevant T cell behaviours.

While SLBs containing other proteins have been used to study different aspects of T cell behaviour and the role of other adhesion³⁴⁹ and costimulatory or inhibitory molecules³⁵¹, the combination of agonist pMHC (or more generic TCR ligands such as OKT3 or UCHT1) and ICAM-1 presented on an SLB is probably the most widely used 2D APC model system to study T-cell behaviour. In this thesis, this SLB type is termed '1st generation' as it was the first SLB system used to study T-cell spreading and activation.

1.14.2.2 2nd Generation Supported Lipid Bilayers

Whilst 1st generation SLBs can induce important T cell behaviours, they overlook many important proteins that are present on an APC surface. Additionally, the role of ICAM-1/LFA-1 binding in the earliest contacts formed may not be the most relevant adhesion pair, given the weak nature of its interaction prior to signalling⁹³, and the fact that LFA-1 may be situated on the cell body rather than at putative initial contact sites on microvilli²⁴⁵. Thus, the concept of a '2nd generation' SLBs was introduced and is described extensively in the thesis of Edward Jenkins (Davis group). Both are schematically illustrated in Figure 8.

Simply, 2nd generation SLBs incorporate further protein elements to create a more physiologically accurate 2D APC model. These are the small adhesion protein CD58, which binds CD2 on the T cell and is known to stabilise early close contacts formed between the T cell and APC^{97-99,101,349}, and the proteins CD43 and CD45, to mimic the glycocalyx present on APCs which forms a steric barrier to close contacts and decreases cell adhesion¹⁰⁴. 2nd generation SLBs therefore provide a system to observe more physiologically relevant early T-cell contacts *in vitro*, and permit visualisation of small close contacts by labelling any of the proteins present which may accumulate at T-cell close contacts (CD58^{103,349}), or especially, be excluded by them (CD43 and CD45^{135,185}). SLB types used in this thesis are described in sections 2.5.2 and 8.2).

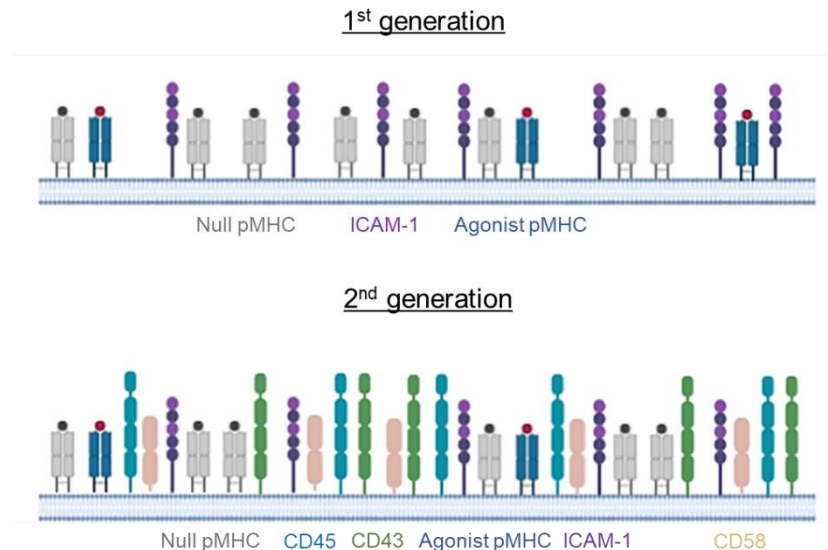


Figure 8 **Schematic depiction of 1st and 2nd generation SLBs** In this thesis, vesicle fusion was used to create a lipid bilayer supported on a clean glass coverslip containing 2% Ni-NTA lipids and 98% POPC lipids. Proteins containing dual histidine (His) tags were added to these lipid bilayers to provide ligands for interactions with T-cell surface proteins. 1st generation SLBs contain only agonist pMHC, ICAM-1 and a null (i.e., non-stimulatory) pMHC to function as a minimal SLB system that is sufficient for inducing T cell activation. 2nd generation SLBs also contain the small adhesion protein CD58 and large glycoalyx proteins CD43 and CD45 and therefore provide a more physiological SLB for T cells to interact with. 2nd generation SLBs are useful for imaging small close contacts made between T cells and SLBs.

1.14.3 Free-Standing 3D Membrane Models

As well as stiffness, glass-SLBs do not accurately recapitulate topography of an APC or target cell. One method to improve this aspect of glass-SLBs is free-standing membrane surfaces, which include large and giant unilamellar vesicles (named for their relative sizes) and GPMVs.

Unilamellar vesicles are spherical lipid bilayers without the support of an underlying substrate. LUVs typically range from 100 nm-1 μ m in diameter, whereas GUVs tend to be larger than 1 μ m and therefore most suitable for standard light microscopy³⁵³. Like SLBs, their protein and lipid composition can be finely tuned, and the diffusion of lipids and proteins is similar to a cell³⁵⁴. However, unlike SLBs, the lack of underlying substrate means they have the advantages of being able to incorporate full-length proteins rather than truncated versions and mimic the stiffness of a real APC or target cell more accurately. A

further extension to unilamellar vesicles is GPMVs, which are created by inducing plasma membrane blebbing of a cell of interest³⁵⁵. GPMVs therefore capture the full lipid and protein complexity of the cell of interest. However, since they are separated from the cell, GPMVs will only demonstrate passive events which do not require energy generation.

These lipid vesicle variants are useful for studying passive, large-scale protein and lipid events related to T cell-behaviour. The main disadvantage of unilamellar vesicles and GPMVs is that, because of their three-dimensional nature, only relatively large-scale protein reorganisation events can be imaged (i.e., accumulation or exclusion of proteins) as current 3D imaging techniques do not have appropriate resolution and/or speed for 3D imaging.

1.14.4 Cells as Substrates for Imaging

Finally, other cells such as B cells or cancer cells can be used directly to study T-cell behaviour *in vitro*. T cells form cell-cell conjugates relatively easily *in vitro* and using whole live cells is the most physiologically relevant system available outside of an *in vivo* setting. B cell lines are commonly used as model APCs^{44,215} and cancer cell lines such as P815 are frequently used as target cells in CTL-based studies^{39,47}.

The APC/target cell can be loaded with various peptides of interest and can be themselves labelled using probes or genetic markers, meaning that molecular events on both T cell and target cell can be imaged simultaneously³⁹. Furthermore, the stiffness, protein density, lipid composition and membrane topography will be suitably complex.

As with other free-standing systems, the main disadvantage of cell-cell experiments is the lack of resolution using current microscopy methods, especially with live cells, although this is improving (light sheet microscopy for example gives high temporal resolution, see section 1.15.4). Furthermore, it is hard (or impossible) to change protein and lipid composition of whole live cells so subtle effects of a specific protein may be lost in cell-cell systems.

1.15 Techniques for Imaging Lymphocytes

Directly visualising immune cells via microscopy is one of the most powerful tools available to understand their behaviour. By engineering cells to express fluorescent proteins or genetically encoded tags which can be labelled with inorganic dyes, proteins of interest can be observed. Many methods are widely available for use, and these are constantly evolving as technology enables higher spatial and temporal resolution of live cells. Different experimental set ups require different microscopy methods as each has its own strengths and weaknesses, which will be outlined here.

1.15.1 Epifluorescence

Epifluorescence is the simplest fluorescence microscopy method. Excitation and emission light are channelled through the same objective. Dichroic mirrors and filters are used to separate light into appropriate wavelengths³⁵⁶.

This technique provides a standard diffraction-limited lateral (x, y) resolution of 200-300 nm but very poor axial (z) resolution as the entire sample is illuminated, and emission collected simultaneously^{356,357}.

1.15.2 Confocal Microscopy

The optical basis for confocal microscopy was invented in the 1950s³⁵⁸ and is used widely for imaging studies. The main advantage of confocal microscopy is the rejection of out-of-focus light coming from a sample, which is achieved using two pinholes on the illumination and detection side of the setup. This dual-pinhole configuration ensures that only light emanating from the in-focus plane is projected onto the detector^{357,359}.

Building on the original design, filters and mirrors were added to achieve better control of laser wavelengths and detectors were modernised to become more sensitive. Now, two main types of confocal microscope exist: laser scanning and spinning disk, each with a different method to scan the illuminating laser over the sample. Laser scanning microscopes

employ mirrors to direct the single point of illuminating laser beam rapidly across the sample, building up an image frame. Spinning disk microscopes on the other hand use a disk containing small holes arranged in a pattern that scans the entire sample at once as it spins, resulting in faster image acquisition but more potential artefacts due to moving parts³⁵⁹.

Confocal microscopes can produce images in up to four dimensions simultaneously (x, y, z and time). Furthermore, images can be taken through the entire depth of the cell with equal signal-to-noise, and since only part of the sample is illuminated, phototoxicity is reduced. This makes it suitable for imaging cell-cell contacts in three dimensions. However, confocal microscopy is diffraction-limited and has a poor axial resolution ($\sim 0.6 \mu\text{m}$) compared to lateral resolution ($\sim 0.2 \mu\text{m}$)³⁵⁹. Depending on sample size and other parameters, acquisition can be slow meaning rapid cellular events may be missed.

1.15.3 Total Internal Reflection Fluorescence Microscopy

Total internal reflection fluorescence (TIRF) microscopy was introduced after the confocal method. This technique is suitable for imaging samples in an aqueous environment in close proximity to a solid material with a high refractive index (typically glass). This is achieved by orientating the illuminating laser to create a high incident angle at the solid surface, which will, at a critical angle, become reflected from the interface between the solid surface and aqueous buffer rather than passing through. This generates an evanescent field (i.e., an electromagnetic field) of the same frequency which penetrates a thin depth of the sample (100-200 nm). Prisms or the objective itself can be used to change the incident angle of the laser and using the objective-based system one can switch between epifluorescence and total internal reflection^{357,360}.

TIRF microscopy has many advantages and is especially suitable for imaging molecules either existing at the cell surface or being recruited to it. Indeed, it is frequently used in T-cell and B-cell imaging studies to observe phenomena such as protein clustering. The evanescent field generates a very high signal-to-noise ratio by illuminating only a small depth of the sample closest to the solid surface, which improves the axial resolution and means that the sample is not exposed to as much light (minimising phototoxicity) and minimal out-of-focus light is collected^{357,360}. However, it also means that TIRF cannot be used to image different planes within a sample.

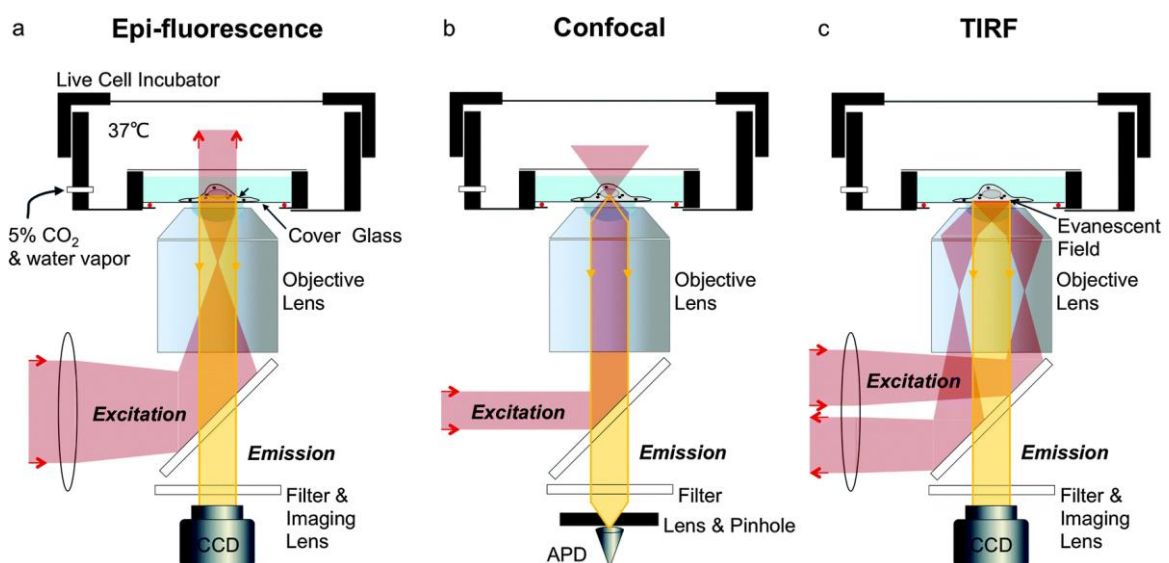


Figure 9 **Overview of major fluorescence microscopy methods** (A) Epifluorescence. The entire sample is illuminated, and all emitted light collected. (B) Confocal microscopy. Illuminating light is focused onto a single small point at the same focal plane as the emitted light is collected. Light is passed through a pinhole before reaching the detector. An image is built up either by scanning this point rapidly over the sample or by illuminating multiple points simultaneously which change over time using a rotating disk. (C) Total internal reflection fluorescence. Illuminating light is directed at a critical angle towards the interface between the sample and the surface it is resting on, creating a thin evanescent field which illuminates a few hundred nm into the sample. Adapted from ref⁴³⁷

1.15.4 Light Sheet Microscopy

Light sheet microscopy has produced some of the most visually appealing images of cells and works by 'optically sectioning' a sample using a relatively thin, but large plane of excitatory light sweeping across the sample. This technique can be used to image a wide range of sample sizes in four dimensions (x, y, z, and time) ranging from individual organelles to whole embryos. A typical set up for a light microscope involves a configuration

of lenses with the objective illumination lens most proximal to the sample, and perpendicular to this, the detection objective with filters and a camera³⁶¹. Lattice light sheet microscopy is a recent advancement to this technique which can permit super-resolution imaging (in one plane) by illuminating the sample with a lattice-patterned light sheet as opposed to a solid sheet³⁶².

The temporal resolution of light sheet microscopy is excellent and phototoxicity is minimised due to the thin nature of the exciting light beam, which also leads to minimal out-of-focus light being captured. However, the axial resolution is relatively poor compared to lateral resolution (as with confocal microscopy) and therefore the gap size between sections should be selected carefully³⁶¹.

1.15.5 Super-Resolution Microscopy

Super-resolution microscopy describes a set of optical and computational methods which permit an image resolution lower than the diffraction limit of standard light microscopy techniques (i.e., ≤ 200 nm)³⁶³.

Common super-resolution methods rely on fluorophore 'blinking' – that is, the selective illumination of a small proportion of available fluorophores at any one time in a sample. Methods which use this principle include photoactivation localization microscopy (PALM) and stochastic optical reconstruction microscopy (STORM), types of single molecule localisation microscopy (SMLM). By imaging a sample over time, all the fluorophores will eventually emit photons, but by only capturing a small number of fluorophores at any one time they are very unlikely to overlap within a diffraction-limited area^{363–365}. By estimating the true localisation for any given point spread function (i.e., light emitted by a fluorophore) as its exact centre, a 2D image can be reconstructed with extremely high resolution (as low as 20 nm)³⁶⁴.

Other common super-resolution methods involve patterning of excitation light across samples (structured illumination microscopy; SIM) and changing the effective scanning spot size to sub-diffraction scales by overlapping excitation and depletion lasers (stimulated emission depletion microscopy; STED)³⁶³.

Super-resolution methods have the obvious advantage of increased clarity in images, and depending on the method used, multiple fluorophores can be imaged simultaneously. However special fluorophores are often required, along with challenging sample preparation, and potentially costly equipment. Furthermore, imaging fixed cells can lead to artefacts as fixation may change the shape and distribution of molecules in the cell. Finally, reconstruction of super-resolution images is more complex and therefore open to artefacts which is particularly relevant for studies of molecular distribution, a property studied frequently with super-resolution methods^{300,301,363} (see also section 6.4.5).

1.15.6 Intravital Microscopy

Imaging immune cells interacting in their native environment is a very attractive prospect, but the technical challenges presented are likely the greatest of all imaging methods. Some type of intravital imaging has been available since the 19th century³⁶⁶ but the pairing of this technique with genetically encoded fluorescent proteins or tags in cells greatly expanded its uses. It is now regularly used to image immune cell interactions within living tissue.

A key principle used in this technique is multi-photon imaging. This method creates illumination of a single plane within relatively thick samples by sending multiple low-energy photons which meet at the desired plane and cause excitation of the fluorophore. Further expansions to intravital imaging include methods to perform *in vivo* cytometry across a circulatory vessel³⁶⁷ and direct imaging of lipid distributions within a tissue³⁶⁸.

Intravital imaging techniques yield low photobleaching and phototoxicity as well as reduced autofluorescence. Numerous fluorophores can be imaged simultaneously and over time,

meaning that several cell types of interest can be monitored as they move, interact, signal and divide. The main drawback of intravital imaging is the lack of resolution compared to a more controlled *in vitro* environment, and the complicated preparation of animal models involving surgery and anaesthesia³⁶⁶.

1.16 Aims of Thesis

The molecular mechanisms surrounding TCR triggering have been the subject of intense research for decades, and no single proposed model is widely accepted. Furthermore, the regulation and function of TCR microclusters is an exciting area that could help determine the mechanism by which T cells respond to antigen. Additionally, as the nature of cell topography, and particularly microvilli, on the T-cell surface become more easily observable with new techniques, their relationship to T-cell signalling needs now to be explored. Since receptor triggering is likely to be similar across different immune cells, confirming key predictions of triggering models on other immune cell receptors could lead to a 'unified theory' of immune receptor triggering.

The overall aims of this thesis are to better understand the initiation and propagation of TCR signalling by modulating TCR expression and ZAP-70 activity and observing how this affects functional aspects of the T-cell response, including early contact formation with model APCs, signalling microcluster formation and calcium signalling. It will also examine whether, and how, the TCR functions as a monomeric entity, and whether principles governing TCR triggering may also be true for the BCR.

2 General Materials and Methods

2.1 Cell Lines and General Cell Culture Methods

Tissue culture was carried out using sterile methods in a level 2 tissue culture facility. Cell lines were maintained at 37°C and 5% CO₂ in an IncuSafe CO₂ Incubator (Panasonic). Cell density and viability was regularly checked using a Countess II automatic cell counter (Thermo Fisher) by mixing cells in complete media in a 1:1 ratio with 0.4% Trypan Blue (Thermo Fisher). Cell lines were split regularly to maintain density within the recommended range for each cell line and used for a maximum of 3 months before earlier passage stocks were thawed. Newly generated cell lines were frozen for stocks at an early passage. Cell lines were checked for mycoplasma by the Human Immunology Unit facility at the WIMM.

Suspension cells were sub-cultured by counting followed by dilution in an appropriate volume of fresh complete media in a new flask. Adherent lines were passaged by removal of media, washing with PBS, then addition of 0.05% (w/v) EDTA-trypsin in PBS (Sigma-Aldrich) or 2 mM EDTA in PBS (Sigma-Aldrich). Cells were left to incubate in EDTA/EDTA-trypsin until they were visibly removed from the surface. At this point, the trypsin was neutralised with twice the volume of complete media. The cell suspension was removed and centrifuged at 395 x g for 3 minutes at room temperature. The supernatant was discarded, and cells were resuspended in complete media, counted, and diluted with complete media to achieve the desired cell density in a new flask.

Cells were frozen in a sterile freezing solution composed of 90% FCS (Sigma-Aldrich) and 10% DMSO (Sigma-Aldrich). 1 – 5 x 10⁶ cells were centrifuged at 395 x g for 3 minutes and resuspended in 1 ml of freezing media, transferred to a cryovial and placed in a Nalgene

freezing chamber (Thermo Fisher) at -80°C overnight. For long-term storage, cells were transferred to liquid nitrogen vapour storage containers.

Cryovials of cells to be thawed were placed directly into a water bath at 37°C for 1-2 minutes before the contents was removed, mixed with 5ml complete media at 37°C and then spun at $395 \times g$ for 3 minutes at room temperature. The supernatant was discarded, and the cell pellet resuspended in an appropriate volume of complete media and transferred to a flask. Cells were examined microscopically after 48 hours to check viability and split after reaching an appropriate density.

2.1.1 Jurkat E6-1

The Jurkat cell line is a human T lymphocyte line isolated from an acute T cell leukaemia^{159,160}. The line E6-1 is a clone from the original cell sample (ATCC TIB-152). Jurkats were maintained in RPMI medium (Sigma-Aldrich) supplemented with 10 % foetal calf serum (Sigma-Aldrich), 2 mM L-glutamine (Sigma-Aldrich), 10 mM HEPES (Sigma-Aldrich) and 1X penicillin/streptomycin/neomycin solution (final concentrations 50 $\mu\text{g}/\text{ml}$ penicillin, 50 $\mu\text{g}/\text{ml}$ streptomycin, 100 $\mu\text{g}/\text{ml}$ neomycin; Sigma-Aldrich). Cultures were maintained between 1×10^5 and 1×10^6 cells/ml.

2.1.2 HEK 293T

The 293T cell line is an adherent epithelial cell line, isolated from human embryonic kidney cells and containing the SV40 T-antigen, making them efficient at replicating vectors containing the SV40 region of replication (ATCC CRL-3216). This line was maintained in Dulbecco's Modified Eagle's Medium (DMEM; Sigma-Aldrich), supplemented with 10% FCS, 2 mM L-glutamine, and 1X penicillin/streptomycin/neomycin. Cultures were maintained between 30-90% confluency.

2.1.3 CHO-K1

CHO-K1 cells were isolated from the ovary of an adult Chinese hamster (ATCC CCL-61). They are an adherent cell line, grown in DMEM (Gibco, Invitrogen) supplemented with 10 % FCS, 2 mM L-glutamine, 1 mM sodium pyruvate (Invitrogen), 1X penicillin/streptomycin/neomycin and a 1X non-essential amino acid supplement (Gibco). Cultures were maintained between 30-90% confluency.

2.1.4 U-2 OS

Originally known as T2, the U-2 OS cell line is an adherent epithelial cell line derived from an osteosarcoma (ATCC HTB-96). U-2 OS cell lines were maintained in McCoy's 5a Medium Modified (Sigma-Aldrich), supplemented with 10 % FCS, 2 mM L-glutamine, 1 mM sodium pyruvate, 1X penicillin/streptomycin/neomycin. Cultures were maintained between 30-90% confluency.

2.1.5 A20 HyHEL10 B Cells

A cell line derived from A20 B cells (murine spontaneous reticulum cell sarcoma; ATCC TIB-208) previously created by Martin Wilcock (Davis group). CRISPR/Cas9 targeting the BCR heavy and light chains as well as Ig α was used to ablate expression of the A20 endogenous BCR which were replaced by heavy and light chains of the HyHEL10 BCR, whose ligand is hen egg lysozyme (HEL), using standard lentiviral transduction (see section 2.2.2.8). Ig α containing an intracellular HaloTag was also introduced for further labelling methods. Cells were created with the BCR expressed under either a strong or weak promoter in pHR and pHRi vectors respectively (described in section 2.2.1) and sorted to obtain homogenous expression across the cell population. Cultures were maintained in RPMI medium supplemented with 10 % foetal calf serum, 2 mM L-glutamine, 10 mM HEPES, 1X penicillin/streptomycin/neomycin and 50 μ M beta-mercaptoethanol (Gibco). Cultures were maintained between 1×10^5 and 1×10^6 cells/ml.

2.1.6 MD4 Primary B Cells

MD4 cells were acquired from mice transgenic for the B cell receptor HyHEL10, which binds the ligand hen egg lysozyme (HEL) with high affinity. Primary B cells were harvested from a recently sacrificed mouse by mashing the spleen through a 40 μ M cell strainer (Corning; Sigma-Aldrich), lysis of red blood cells with 1 ml ACK buffer (Thermo Fisher), centrifugation at 526 x g for 5 minutes and removal of supernatant before magnetic cell sorting using a MACS B cell isolation kit (Cat# 130-090-862; Miltenyi) as per manufacturer's instructions. Purity was checked through labelling of cells with fluorescent HEL and deducing the positively stained population. MD4 cells were used within the same day and kept in sterile PBS at 4°C.

2.2 DNA Methods

2.2.1 Vectors Used

pHR

The pHR-SIN-CSGW (pHR) vector is a lentiviral vector derived from the human immunodeficiency virus. The gene of interest is expressed under the control of the spleen focus forming virus (SFFV) promoter and includes an additional woodchuck hepatitis virus posttranscriptional regulatory element (WPRE) enhancer at the 3' end. The vector contains an ampicillin resistance gene for selection in bacterial cells. It is used in combination with the plasmids pMDG and pP8.91 to produce replication-incapable lentiviral particles for stable insertion of a gene of interest into target cell lines.

pHRi

The pHRi vector is identical to the pHR vector except for a change in promoter to the ecdysone inducible promoter, E/GRE. This promoter requires the activity of the nuclear factors RXR and FB-ERV (together with ponasterone) for optimal expression. As these are

not present in any of the cells used in this study, genes in this vector are expressed at very low levels.

LentiCRISPRv2

This lentiviral vector contains the *Streptococcus pyogenes* Cas9 nuclease together with restriction sites that allow insertion of a 20 bp single guide RNA and is used for CRISPR/Cas9 stable knockdowns in cell lines. The vector confers resistance to ampicillin in bacterial cells and puromycin in mammalian cells.

2.2.2 Cloning Method Overview

Genes of interest were amplified from plasmids or cDNA with 5' and 3' primers containing restriction sites and then run on agarose gels to check product size and purity. Vectors and PCR products were digested with restriction enzymes and then respectively purified by gel electrophoresis or PCR cleaning. Ligation was conducted by addition of DNA ligase before DNA transformation into chemically competent bacteria (Top10). Colonies were grown and screened by antibiotic resistance. Selected colonies were grown up in nutrient culture and used to prepare larger quantities of DNA. Newly generated plasmids were confirmed by DNA sequencing.

2.2.2.1 Primer Design

Primers were designed on Snapgene (GSL Biotech; available at snapgene.com) software using the following parameters where possible: (1) 15-60bp in length to reduce secondary structure formation and folding while binding (2) 3' end ending in a GC clamp to increase specificity of binding (3) melting temperature between 50-68°C (4) 3' and 5' primers not differing in melting temperature by more than 5°C.

2.2.2.2 PCR

PCR reactions were set up using the following mix.

Reagent	Concentration/mass
Template DNA	100 ng
Forward primer	0.5 μ M
Reverse primer	0.5 μ M
dNTPs	200 μ M
Phusion High-Fidelity DNA Polymerase (NEB)	1X final concentration
Phusion HF buffer	1X final concentration
De-ionised (Milli-Q) water	Up to 20 μ L total volume

Reactions were carried out in a Bio-Rad T100 Thermal Cycler using the following settings.

Step		Temperature/ $^{\circ}$ C	Time/s
1	Enzyme activation	98	60
2	DNA denaturation	98	10
3	Primer annealing	50-70 (depending on primers)	30
4	DNA extension	72	60 per kb
5	DNA amplification		X 29 cycles
6	Final extension	72	300
7	Cooling	10	<Infinite

In some instances, a two-step PCR was used to generate chimeric proteins. Each segment of DNA was first amplified with primers designed to generate overlapping ends of approximately 50-100 bp. These two products were then added in equimolar concentrations to a PCR mixture as above with the number of amplification cycles reduced to 15.

2.2.2.3 Restriction Enzyme Digestion

Vector DNA (up to 5 μ g) or PCR product (entire volume extracted) was digested for 60 minutes at 37 $^{\circ}$ C, with the following reaction mixture:

Reagent	Concentration/mass
DNA	Up to 5 μ g
Restriction enzyme (NEB)	10-20 U
Buffer (NEB)	1X final
De-ionised (Milli-Q) water	Up to 50 μ l

The optimal buffer was chosen according to the online tool Double Digest Finder (NEB). After digestion, vectors were purified by gel electrophoresis and PCR products were purified using a PCR purification kit (Qiagen).

2.2.2.4 Agarose Gel Electrophoresis

PCR products and digested vectors were separated by gel electrophoresis. Molecular grade agarose (Thermo Fisher) was mixed with TBE (Tris/Borate/EDTA buffer, Sigma-Aldrich) to a concentration of 1% w/v. Approximately 75ml of the mixture per gel was heated in a microwave in bursts of 90 s until the agarose dissolved. The mixture was left to cool, and ethidium bromide (Sigma-Aldrich) was added to a concentration of 0.5 µg/ml. Gels were cast in Flowgel Bioscience gel tanks and left to set at room temperature. Samples were diluted with loading DNA gel stain (NEB) and added to the wells, along with HyperLadder 1kb (Bioline). A Bio-Rad powerpack was used to apply current to the gel at 100 V for 30-60 minutes. DNA was then visualised with UV light using a GelDocXR+ (Bio-Rad) and analysed with Image Lab (Bio-Rad). Where needed, DNA was extracted using a scalpel by placing the gel on a low-UV lamp. DNA was then extracted from the gel using a PureLink® Quick Gel Extraction Kit (Invitrogen).

2.2.2.5 Ligation

Digested DNA was ligated into the appropriately digested plasmid using the following mixture:

Reagent	Concentration
Digested insert DNA	Variable
Digested vector	Approximately 100ng
DNA ligase buffer (NEB)	1X final
T4 DNA ligase (NEB)	400 U
De-ionised (Milli-Q) water	Up to 20 µl

The ratio of insert:vector was varied to increase ligation success. Ratios of 5:1, 10:1 and 1:1 insert:vector were most commonly used. Control reactions contained either no insert, or no

ligase and no insert to test for vector re-ligation and incomplete vector digestion respectively. Ligation reactions were undertaken at 16°C for 1 hour in a Bio-Rad T100 Thermal Cycler, or at room temperature overnight.

2.2.2.6 Transformation into Chemically Competent Bacteria

Ligation products were transformed into TOP10 *E. coli* by heat shock. TOP10 were thawed on ice and 10µl ligation mix was added to 50µl of bacteria. Samples were left on ice for 5-30 minutes, then heat shocked at 42°C for 45 seconds in a Bio-Rad T100 Thermal Cycler before returning to ice for a further minute. 150 µl of LB broth was added to each mixture followed by incubation for one hour at 37°C. Transformed bacteria were plated onto an LB agar plate containing the appropriate antibiotic and incubated at 37°C overnight.

2.2.2.7 Vector Extraction and Purification

Colonies were used to inoculate LB broth containing the appropriate antibiotic, which was incubated overnight at 37°C with 225 rpm agitation. After centrifugation at 3739 x g and removal of supernatant, plasmid DNA was purified using PureLink™ HiPure Plasmid Miniprep Kit (Invitrogen). DNA was eluted in TE buffer and the concentration was determined spectrophotometrically using a NanoDrop II (Thermo Fisher). Purity was determined by measuring the 260nm/280nm ratio, with a value > 1.8 indicating acceptable DNA purity.

2.2.2.8 Lentiviral Transduction of Suspension Cells

On day 1, 293 T cells were plated into 6-well plates (Thermo Fisher) at 3×10^5 cells/ml (2 ml per well). On day 2, the cells were checked by light microscopy and the media was swapped for 2 ml/well of the media used to grow the target cells. The following reaction mixture was prepared:

Reagent	Mass per well
Plasmid DNA with gene of interest	0.5 µg
pMDG	0.5 µg
p8.91	0.5 µg
De-ionised (Milli-Q) water	Up to 20ul

This mixture was then mixed with 100 µl DMEM (Lonza) and 3 µl Genejuice (Novagen) per well under sterile conditions and left to incubate at room temperature for 15-30 minutes. The mixture was then added dropwise to each well of 293T cells. After 48-72 hours, the supernatant was harvested and filtered through 0.22 µm filters to remove cell debris. Generally, 1×10^6 target cells were infected with up to 2 ml of viral supernatant and recovered 24 hours later with complete media up to 10 ml. The cells were cultured according to standard methods and tested for expression by flow cytometry 72 hours after infection. Cells with the desired expression level at the lowest volume of viral supernatant were kept, and subsequent cell sorting was undertaken to obtain a pure cell population if necessary.

2.2.3 CRISPR knockouts

CRISPR/Cas9 gene editing was used to permanently knock out expression of certain genes in cell lines. Cloned CRISPR/Cas9 guides used in this thesis were kindly provided by Edward Jenkins (Davis lab) and were created by the following process.

Guide sequences were identified by submitting target genes to the CRISPOR design tool¹⁶¹ and cross-referenced with CRISPR design feature in Benchling (hg38 reference genome). Targeted sequences were chosen beyond the ATG start codon and within the first few exons. Guides were selected based on low off-target predictions and sequences which were experimentally verified were preferred. Sequences for gRNAs used in this thesis are shown below.

Name	Exon target	Strand	Sequence (5'-3')
ZAP-70Ex3 gRNA top	3	Top	CACCGTCTACTCGCGGACCCCGAC
ZAP-70Ex3 gRNA bot	3	Bottom	AAACGTCGGGGTCGCGGAGTAGAC
ZAP-70Ex4 gRNA top	4	Top	CACCGTTGCTACGACGGCCACGAG
ZAP-70Ex4 gRNA bot	4	Bottom	AAACCTCGTGGGCCGTCGTAGCAAC

Oligos were annealed in the following mixture to create guides for cloning into the LentiCRISPRv2 plasmid:

Reagent	Concentration
Forward oligo	100 μ M
Reverse oligo	100 μ M
T4 DNA ligase buffer (NEB)	1 X
Milli-Q	Up to 20 μ L

The annealing reaction was carried out in a Bio-Rad T100 Thermal Cycler with the following program:

Step	Temperature ($^{\circ}$ C)	Time (min)
1	37	30
2	98	5
3	Reduce by 5 $^{\circ}$ C/minute until 25 $^{\circ}$ C	

Annealed oligos were ligated into the lentiviral CRISPRv2 vector via the BsmBI restriction site and transformed into chemically competent TOP10 bacteria as previously described (section 2.2.2.6). Colonies were picked, grown in LB broth and DNA was extracted and sequenced (section 2.2.2.7). Guides were transfected into cell lines using lentiviral transduction as previously described (section 2.2.2.8), with the addition of puromycin (1 μ g/ml) selection after 3 days, which was maintained for 3 days. Knockdown of proteins was confirmed by flow cytometry and/or Western blot. Where necessary and possible, cell sorting was used to obtain a pure population of cells negative for the protein of interest.

2.2.4 DNA Sequencing

Sequencing was carried out by Source BioScience. Alignment of sequencing reads was undertaken using SnapGene software (GSL Biotech; available at www.snapgene.com). When

required, further confirmation of sequences was carried out using the Basic Local Alignment Search Tool (NIH; available at www.blast.ncbi.nlm.nih.gov/Blast.cgi) and cross-referenced against known protein sequences within the UniProt database (UniProt Consortium; available at www.uniprot.org/).

2.3 Protein Methods

2.3.1 Sodium Dodecyl Sulphate Polyacrylamide Gel Electrophoresis (SDS-PAGE)

Proteins were analysed by sodium dodecyl sulphate polyacrylamide gel electrophoresis (SDS-PAGE) under reducing and non-reducing conditions by mixing the diluted (typically 1:10) protein solution 1:1 with either Laemmli Sample Buffer (Bio-Rad) alone or sample buffer with 5% v/v β -mercaptoethanol (Bio-Rad) and denaturing by heating to 95°C for 10 minutes. Precision markers (Bio-Rad) were run in parallel with experimental samples to determine approximate protein size. Samples were loaded into a NuPage 12% Bis-Tris gel (Thermo Fisher) for SDS-PAGE analysis. Gels were run in a Mini-PROTEAN® Tetra Cell (Bio-Rad) at 180V in Tris/glycine/SDS running buffer (Merck) for an hour.

2.3.2 Size Exclusion Chromatography

Size exclusion chromatography was used to analyse and purify proteins. The machine used to perform Fast Protein Liquid Chromatography (FPLC) was an AKTA pure FPLC system with a variety of columns available depending on optimum separation range and quantity of protein. The protein was first concentrated to an appropriate volume (between 0.5-1 ml) and centrifuged at 17,000 g at 4°C to pellet any large aggregates. Columns and pumps were flushed with 1.5 column volumes of 0.5M sodium hydroxide followed by filtered Milli-Q water. The system was then calibrated with 1.5 column volumes of appropriate buffer (filtered PBS or HBS either with or without sodium azide depending on the protein use), which was also used to flush the injection loop. A maximum of 10 mg of protein was used

per injection and protein was eluted into 0.5-1 ml fractions in the desired buffer. The concentration of each fraction was determined using a NanoDrop II. Selected fractions were analysed by SDS-PAGE to check purity, and the highest quality fractions were pooled. If the protein was not to be used immediately small aliquots were snap frozen using dry ice and isopropanol and stored at -80°C.

2.3.3 Spectrophotometry

Protein concentrations were assessed by spectrophotometry using a NanoDrop II (ThermoFisher Scientific). Absorption was measured at 280 nm and concentration was determined by dividing this value by the extinction coefficient of the protein.

2.3.4 Coomassie Staining

After SDS-PAGE, gels were then removed and stained with Coomassie Blue solution (0.1% (w/v) Coomassie Brilliant Blue, 50% (v/v) methanol, 10% (v/v) acetic acid), for 2 hours and subsequently incubated in de-stain solution (10% (v/v) acetic acid and 12% (v/v) methanol) overnight to visualise protein bands.

2.3.5 Western Blot

After SDS-PAGE with Amersham ECL Rainbow Molecular Weight Marker (GE Healthcare Life Sciences), samples were transferred to a nitrocellulose blotting membrane (0.45µm, GE Healthcare) by electroblotting using an XCell II Blot module (Invitrogen, UK) at 100V in ice-cold transfer buffer (1X tris-glycine buffer, 20% methanol, Milli-Q water). Membranes were blocked with PBS containing 0.1% (v/v) Tween 20 (Sigma Aldrich) and 3% (w/v) BSA (Sigma) on a rocker for either 1 hour at room temperature or 4°C overnight. For His tag detection, blocked membranes were stained with a 1:10000 dilution of HRP-conjugated anti-His tag antibody (Abcam clone ab1187) diluted in PBS with 3% BSA for 1 hour at 4°C on a rocker. For other stains, the appropriate primary antibody was diluted 1:100-1:1000

in PBS with 3% BSA, left to incubate for 1 hour at 4°C on a rocker, followed by 3 x 5-minute washes with PBS containing Tween 0.05% (v/v) before incubation with secondary HRP-conjugated antibody (usually Sigma Aldrich clone A0168) for 1 hour at 4°C on a rocker. Membranes were then washed three times with PBS containing Tween 0.05% (v/v) every 5 minutes. Immunoblots were developed using a Pierce ECL kit (Thermo Fisher) and captured digitally using an iBright FL1000 machine (Thermo Fisher) with adjustable exposure time.

2.3.6 Expression of Soluble His-Tagged Proteins

On day 1, CHO-K1 cells were plated out in 20 ml complete media in a T75 flask at a density of 4×10^6 cells/ml. On day 2, prior to transfection, the media was changed to DMEM (Gibco, Invitrogen) supplemented with 10 % FCS, 1 mM sodium pyruvate, 1X penicillin/streptomycin/neomycin and a 1X non-essential amino acid supplement. The transfection mixture was prepared as follows:

	Volume/mass
Plasmid DNA with gene of interest	10 μ g
Genejuice (Novagen)	30 μ l
DMEM (Gibco)	500 μ l

The mixture was incubated at room temperature for 15-30 minutes then added to the appropriate flask. An additional flask was set up as a control transfection, containing no DNA. After several days, an aliquot of the supernatant was removed to test for protein expression by Western blot. Cells were then expanded by trypsinisation, centrifugation, re-suspension and seeding as previously described (section 2.1), into flasks of increasing volume once confluency was reached, until occupying 10 x T175 flasks. During the first expansion, and after Western blot confirmation, aliquots were frozen for future use. After the final expansion, media was exchanged for complete media with only 1 % FCS. Supernatant was harvested after 1 week and media was replaced onto the cells, where the final harvest was carried out after a further week. For storage, supernatant was centrifuged

(935 x g, 10 minutes) to remove cell debris, sodium azide was added (0.05% w/v) and the supernatant was placed at 4°C until purification.

2.3.7 Purification of His-Tagged Proteins

Tissue culture supernatant was mixed with an equal volume of PBS + 0.5 M NaCl, adjusted to pH 8.0 and sodium azide added to a final concentration of 0.05%. The elution column was prepared by packing 5ml of Ni-NTA-Agarose beads (Qiagen) for every 1 L of supernatant. The supernatant was then run through the column by gravity flow. Pre-elution was undertaken with 50 ml of 10 mM imidazole in 5 ml fractions, which were then analysed by NanoDrop II to ensure a low optical density (OD) of below 0.03, indicating removal of non-specifically bound protein. A further 50 ml of 20 mM imidazole was used to pre-elute in 5 ml fractions and the optical density of each fraction was checked again. The protein was then eluted from the column with 250 mM imidazole in 1 ml fractions. The absorption at 280 nm of each fraction was measured and selected fractions were analysed by SDS-PAGE with Coomassie staining to check protein size and purity. Desired fractions were selected, pooled, and concentrated using Amicon filters with an appropriate size cut off before being purified by FPLC on an AKTA pure Protein Purification System. Desired fractions from the FPLC were analysed by Western blot before final pooling, aliquoting and storage at -80°C.

2.3.8 pMHC Production - Refolding

cDNA encoding the extracellular domain of HLA-A2 (residues 25-304, UniProtKB P79603) and β -2-microglobulin (β 2M, residues 21-119, UniProtKB P61769) were ligated into the pET28a+ vector (kanamycin resistant) for expression in Rosetta 2 (DE3)pLysS competent *E.coli* (Merck). A double His tag (6xHis-linker-6xHis) was added to the C terminus of the HLA-A2 gene to facilitate adhesion to supported lipid bilayers containing Ni-NTA-chelating lipids.

Rosetta 2 cells were transformed with 250 ng of vector DNA by heat shock (described in section 2.2.2.6) and plated on LB agar plates containing kanamycin (final concentration 50 $\mu\text{g/ml}$) and chloramphenicol (final concentration 34 $\mu\text{g/ml}$). Single colonies for each vector were selected and grown overnight in high salt LB (1L de-ionised water contains 10 g tryptone, 5 g yeast extract, 10 g NaCl) with kanamycin (50 $\mu\text{g/ml}$) and chloramphenicol (34 $\mu\text{g/ml}$), at 37°C with 200 rpm shaking. The overnight culture was diluted to 0.05 OD600 (measured by NanoDrop II) in 1 L LB high salt with kanamycin (50 $\mu\text{g/ml}$) and chloramphenicol (34 $\mu\text{g/ml}$) and incubated in the same conditions until the OD600 reached 0.6 (approximately 2 hours), at which point a final concentration of 1 μM IPTG was added to induce expression of T7 RNA polymerase under the lacUV5 promoter, thus expressing the MHC heavy chain and $\beta 2\text{M}$ genes. The culture was incubated for 4 hours at 37°C and 200rpm then centrifuged 3739 x g for 12 minutes at 4°C, and finally resuspended in chilled (4°C) Milli-Q water with 0.9% NaCl. Pellets were stored at -80°C until use.

Pellets were resuspended in 100 ml of resuspension buffer (1 L MQ water with 50 mM Tris-HCl pH 8.0, 100 mM NaCl, and 12.5 $\mu\text{g/ml}$ DNase I) and mixed with a magnetic stirrer at 4°C for 30 minutes. The resuspended cells were lysed in a 1.1-kW cell disruptor (Constant Systems), which was prepared by washing with Milli-Q water, then resuspension buffer, and cooled to 10 °C with a Frigomix R (Sartorius-Stedim). The resuspension mix was passed through the disruptor twice at a pressure of 28 kPSI. The disrupted cells were centrifuged at 15,000 x g at 4°C for 10 minutes, resuspended in 3 ml resuspension buffer and homogenised using a glass tissue grinder (Sigma Aldrich). This process was repeated, then the pellets were resuspended in 11 ml EDTA/urea denaturation buffer (taken from a mix of 250 ml Milli-Q water with 120.12 g urea, 50 mM Tris-HCL, 10 mM EDTA pH 8.0) and left to incubate at room temperature overnight. This suspension was centrifuged at 15,000 x g at 4°C for 10 minutes and the resulting supernatant (containing inclusion bodies) was 0.22 μm -filtered and concentrated using an Amicon 10kDa Ultracel-10 membrane (Millipore) to either 15 mg/ml (HLA-A2/heavy chain) or 10 mg/ml ($\beta 2\text{M}$ /light chain).

For refolding of the complete pMHC complex, 1 mg of relevant peptide (gp100), 15 mg of HLA-A2- H6-linker-H6 and 6 mg of β 2M inclusion bodies were separately resuspended in 50ml falcon tubes containing 15 ml EDTA/urea denaturation buffer with 1 % (v/v) 1M DTT. The proteins were incubated at 37-42°C for 30 minutes to denature, then were added into 200 ml of pre-chilled (4°C) refold buffer (1 L Milli-Q water with 100 mM Tris-HCL, 1.2 M L-Arginine, 2 mM EDTA, and 1.14 g cysteamine hydrochloride and 0.23 g cystamine dihydrochloride (last two added 30 minutes before use)). This solution was incubated for 20 minutes at 4°C with a magnetic stirring bar, then placed into 12 kDa cellulose membranes (Sigma) for dialysis, which were previously prepared by boiling in 2% (w/v) sodium bicarbonate and 1 mM EDTA pH 8.0 and pre-washed in de-ionised water. Dialysis was performed over four days (with replacement of de-ionised water after day three) in chilled (4°C) de-ionised water with magnetic bar stirring. After four days the dialysis buffer was exchanged for de-ionised water with 10 mM Tris-HCL pH 8.0 and left at 4°C overnight, then the contents of the dialysis tubes was collected and centrifuged at 3739 x g at 4°C for 20 minutes to remove aggregate before concentrating to 20-40 OD A280 using Amicon 10kDa Ultracel-10 membrane filters (Millipore). Concentrated protein was analysed by FPLC and Coomassie staining and fractions indicating complex formation were chosen and used.

2.3.9 UCHT1 Fab-Halo Production

The plasmids containing the UCHT1 Fab light and heavy chains were a kind gift from Nicole Ashman (Davis group). The UCHT1 Fab heavy chain was amplified by PCR and ligated into a plasmid with a C-terminal linker and Strep-tag II provided by João Ferreira Fernandes (Davis group). Both plasmids were co-transfected into CHO-K1 cells, which were grown as per the soluble protein purification method previously described (section 2.3.6) and the supernatant was harvested for purification, which was based on an established method³⁷². An Econo-column (Bio-Rad) containing Strep-tactin purification resin was fixed in an upright position and the 20% ethanol solution used for storage was removed. The resin was

then washed in 5 column volumes of Milli-Q water and equilibrated by passing over 5 column volumes of buffer W (100 mM Tris-HCl pH8, 150 mM NaCl, 1 mM EDTA, adjusted to pH8). The cell supernatant was concentrated using a Vivaflow 200, 10-kDa MWCO PES concentrator to 50 ml and applied to the column, which was then sealed and attached to a rotator to bind in batch for 90 minutes at room temperature. After this, the column was fixed upright, and the supernatant was allowed to flow through by gravity flow. The column was then washed in 25 column volumes of buffer W before elution in 5 column volumes of elution buffer (buffer W with 2.5 mM d-Desthiobiotin) in 1 ml fractions. Column washes, and elution fractions were analysed for protein concentration by A280 readings on a NanoDrop II (ThermoFisher). Fractions containing high concentrations of protein were analysed by Coomassie stain, and selected fractions containing the protein at the correct size were pooled, concentrated and purified using gel filtration as previously described (section 2.3.2).

2.3.10 Protein Thawing and Storage

After initial freezing, proteins were thawed at 4°C and centrifuged at 17,000 x g for 5 minutes at 4°C to remove potential aggregate. The supernatant was transferred to a fresh Eppendorf tube and concentration was determined by A280 measured using a NanoDrop II (ThermoFisher). If being thawed for labelling, the protein was subsequently aliquoted into small volumes and snap frozen, or if being used for other means, was kept at 4°C for two weeks before being discarded.

2.3.11 Protein Labelling

Proteins were labelled non-specifically using Alexa Fluor 488, 555 or 647 Antibody Labelling Kit (ThermoFisher) according to the manufacturer's instructions, which resulted in a labelling efficiency of ≥ 1 dye per protein. For labelling of proteins via HaloTag, approximately 100 μ L of protein at 1 mg/mL was mixed at a 1:2 molar ratio with HaloTag

ligand dye and incubated at room temperature for 1 hour, with regular mixing. The protein solution was then passed over a Bio-Spin 6 Tris column (Bio Rad), (previously centrifuged at 1100 g for 3 minutes) and centrifuged at 1100 g for 5 minutes with a test tube below to collect labelled protein. Labelling efficiency and protein concentration were determined using a NanoDrop II (ThermoFisher).

2.4 Flow Cytometry

2.4.1 Surface Staining

Approximately 5×10^5 cells were harvested into round-bottomed 12 x 75 mm test tubes (Fisher Scientific), topped up with 3 ml of PBS containing 0.05% sodium azide, and centrifuged at 395 x g for 2 minutes at room temperature. The supernatant was removed, and cells were resuspended in 100 μ l of PBS-azide with the appropriate antibody and incubated in the dark at 4°C for 30-60 minutes. Antibody isotype, antigen-negative and unstained controls were prepared in parallel. If a conjugated primary antibody was not available, cells were labelled first with a primary antibody, washed twice with PBS-azide and then incubated with a conjugated secondary antibody in the dark at 4°C for 30-60 minutes. Cells were then washed twice with 3ml PBS-azide before final resuspension in 200-300 μ l of 2% paraformaldehyde diluted in PBS.

2.4.2 Intracellular Staining

For intracellular proteins, cells were first fixed in 300 μ l of 4% paraformaldehyde at room temperature for 15 minutes. Cells were washed in 3 ml PBS-azide and resuspended in 100 μ l of intracellular staining (ICS) buffer (0.5% Saponin, 5% FCS, PBS) with the appropriate concentration of antibody (typically 0.5 ng/ μ l). Cells were left to incubate in the dark at 4°C for 60 minutes, washed twice with 3 ml ICS buffer and resuspended in 200-300 μ l PBS-azide. If a conjugated primary antibody was not available, cells were labelled first with a primary

antibody, washed twice with ICS buffer and then incubated with a conjugated secondary antibody for a further hour in the dark at 4°C.

Staining for intracellular Halo or SNAP-Tags was carried out by harvesting 1×10^6 cells, centrifuging at $395 \times g$ for 2 minutes and resuspending in an appropriate amount of fluorescent label diluted in complete media. Cells were placed in the cell culture incubator for labelling, then washed as per the manufacturer's instructions and fixed in 200-300 μl of 2% paraformaldehyde diluted in PBS before flow cytometry analysis.

Cells were analysed using Attune NxT (Life Technologies) machines. At least 30,000 cells were collected per sample. Cell sorting was performed by the WIMM FACS facility. Data was analysed using FlowJo. Where necessary, quantification of surface proteins was undertaken using BD QuantiBrite-PE beads as per recommended instructions.

2.5 Microscopy Methods

2.5.1 Glass-Supported Lipid Bilayer (SLB) Preparation

Small unilamellar lipid vesicle (SUV) fusion was used to create SLBs. To prepare the SUV suspension, a total of 1 mg of lipids were mixed in the required molar ratio (either 98% POPC and 2% DGS-NTA-Ni²⁺ (Avanti Polar Lipids) or 100% POPC) in a glass vial rinsed with chloroform. The vial was rotated under nitrogen gas until the chloroform had evaporated. The lipid film was then hydrated with 1 ml of 0.22 μm -filtered PBS, vortexed for 30 seconds and incubated for 30 minutes on ice. The sample was then sonicated on ice using a tip sonicator for 30 minutes (cycles of 10 seconds on, 10 seconds off at 55 Hz) until clear.

Glass slides (25 mm, thickness no. 1.5; VWR) were cleaned in piranha solution (3:1 ratio of concentrated sulphuric acid:30% hydrogen peroxide solution) for at least 1 hour then washed liberally with Milli-Q water. Slides were dried rapidly with compressed air and then placed in a plasma cleaner (Plasma Surface Technology) for 1 minute. CultureWell 50-well

silicon covers (Grace Bio-Labs) were adhered to the slides and 10 μl of SUVs diluted 1:1 with 0.22 μm -filtered PBS were added to each well. After incubation for 30 mins, wells were washed three times with 10 μl 0.22 μm -filtered PBS, making sure the well did not dry out. If protein was required on the bilayer, after the final wash, all but 2 μl of liquid was removed from the wells and 5 μl of protein mix was added and left to incubate for 1 hour. A final wash with 10 μL of 0.22 μm -filtered PBS was carried out ten times before use.

2.5.2 1st and 2nd Generation SLBs

The final concentrations of proteins used, and the approximate density produced on the SLB (for 2nd generation SLBs), are shown below. Proteins were first mixed with 0.22 μm -filtered PBS to achieve the desired concentration before adding to the SLB. Concentrations of protein and densities quoted in this thesis are based on the work of Edward Jenkins (Davis group), who set up and optimised 2nd generation SLB conditions to match the density of proteins on primary human monocyte-derived dendritic cells. The concentration of null pMHC was determined by subtracting the concentration of agonist pMHC from the total pMHC density used, since both agonist and null have the same molecular weight. Density values were not measured on 1st generation SLBs.

1st generation SLBs

Protein	Final concentration (ng/μl)
Agonist pMHC	0-2
Null pMHC	8-10
ICAM-1	1.2

2nd generation SLBs

Protein	Final concentration (ng/μl)	Density on SLB (x/μm^2)
Agonist pMHC	0-0.5	0-100
Null pMHC	9.95-10	> 1700
ICAM-1	1.2	400-600
CD58	0.5	200-300
CD45RABC	2.5	250-350
CD43	1.5	300-400

2.5.3 Glass Surface Preparation

Sterile μ -Slide 8 well glass chambers (Ibidi) were incubated with antibody or Fab diluted in 0.22 μ m-filtered PBS at the desired concentration for 2 hours at room temperature, then washed 3 times with 400 μ l 0.22 μ m-filtered PBS immediately before use. When PLL coating was required, each well was incubated for at least 15 minutes with 300 μ l PLL solution (0.01% high molecular weight solution, Sigma Aldrich) and washed the same way. If being used for live cell imaging, chambers were allowed to equilibrate in the microscope incubator box for 5-10 minutes prior to the addition of cells.

2.5.4 Total Internal Reflection Fluorescence Microscopy (TIRFM)

Images were acquired on an Olympus IX83 inverted TIRF microscope with a 150X 1.5 NA oil objective, Photometrics Prime camera and cellTIRF-4Line system. Laser power was adjusted for optimal signal:noise ratio with minimal photobleaching. For live cell imaging, the incubator was maintained at a temperature of 37°C.

Some TIRFM experiments were carried out on a custom-built TIRF microscope, located with collaborators in the Department of Chemistry, University of Cambridge. The microscope uses a 100X 100 Plan Apo TIRF, NA 1.49 oil-immersion objective (Nikon) mounted on an inverted optical microscope (Ti2, Eclipse, Nikon). The lasers used were 488 nm (iBeam-SMART, Toptica), 561 nm (LaserBoxx, DPSS, Oxxius), and 641 nm (Obis, Coherent) and powers were adjusted for maximum signal:noise with minimal bleaching. Images were formed onto an electron-multiplying charge-coupled device (EMCCD, Evolve 512 Delta, Photometrics). Focus was controlled with the Nikon Perfect Focus System and image acquisition was automated using Micro Manager open-source software³⁷³. The microscope was fitted with an incubator (DigitalPixel) to maintain a temperature of 37°C for live cell imaging.

2.5.5 Confocal Microscopy

Confocal imaging data was acquired on an LSM 880 or 780 Inverted Confocal Microscope (Carl Zeiss) with an incubation box. Zen software was used to operate the microscope. Several objectives from 10-63X were used depending on experimental needs. The pinhole diameter was set to 1 airy unit.

2.5.5.1 Calcium Flux Imaging

Calcium flux experiments were conducted using the incubation box to maintain the sample temperature at 37°C, with 5% CO₂. A 10X air objective was used.

Cells were maintained at an optimal density for at least 2 days before use in triggering experiments to ensure reproducibility. Approximately 1×10^6 cells were harvested into a 1.5ml Eppendorf and spun in a MiniSpin (Eppendorf) at 2000rpm for 60 seconds. Cells were then resuspended in 100 µl RPMI (no supplements), 100 µl PBS and 1 µl Fluo-4 AM dye (Thermo Fisher; final concentration 2.5 µg/ml). Cells were incubated for 3-5 minutes at 37°C and 5% CO₂ in the dark before 2 washes in 500 µl 0.22 µm-filtered PBS with 2mM magnesium sulphate (hereafter PBS-MgSO₄). The final cell pellet was resuspended in 50-200 µl of 0.22 µm-filtered PBS-MgSO₄ depending on the density needed. Cells were allowed to equilibrate for 3 minutes in the microscope incubator prior to placing on surfaces for imaging. During this time, the correct focal plane was determined by focussing on the glass surface, then video acquisition was started and 1-20 µl of the cell mixture was added, depending on the density of cells required. Calcium triggering videos were acquired with the 488 laser with 1 frame taken per second for 600 frames/10 minutes.

2.5.5.2 Cell and SLB Imaging

SLBs were imaged using a 63X NA 1.4 oil objective either at 37°C or room temperature depending on the sample. To achieve the clearest images, the highest averaging possible

was used, typically 8-16x. For timelapse experiments, autofocus was used approximately every 10 seconds depending on frame length to keep illumination as even as possible throughout.

2.5.5.3 Interference Reflection Microscopy (IRM)

To analyse cell areas in close contact with the surface, an IRM path was used. This involves a light path set up with an emission filter that allows incident light reflected from the sample to be detected. Areas closer to the surface appear darker (i.e., less signal intensity).

2.5.6 Intracellular HaloTag protein labelling

Approximately 5×10^5 cells were harvested into a 1.5 ml eppendorf, centrifuged at 2000 rpm in a MiniSpin and resuspended in 200 μ l complete media containing the appropriate concentration of HaloTag ligand dye as per the manufacturer's instructions. Cells were left to incubate in a tissue culture incubator at 37°C and 5% CO₂ for 30 minutes before centrifugation and resuspension in 1 ml of complete media. Cells were incubated again in a tissue culture incubator for 30 minutes before a final round of centrifugation and resuspension in 1 ml of complete media, and incubation for 30 minutes. These steps are taken to wash away free dye in the cells. Cells were finally washed twice in 500 μ l warmed 0.22 μ m-filtered PBS-MgSO₄ and resuspended in the same buffer for imaging.

2.5.7 Surface protein labelling with Fabs

Approximately 5×10^5 cells were harvested into a 1.5 ml eppendorf, centrifuged at 2000 rpm in a MiniSpin and resuspended in 200 μ l complete media with an appropriate concentration of Fab (typically 20 μ g/ml). Cells were left to incubate in a tissue culture incubator at 37°C and 5% CO₂ for 10 minutes before centrifugation and washing twice in 500 μ l warmed 0.22 μ m-filtered PBS-MgSO₄ and finally resuspending in the same for imaging.

2.6 Image Analysis with Custom Tools – Calcium Flux

Bulk calcium flux analysis of hundreds to thousands of cells was carried out using custom MATLAB script written by Jane Humphrey (Klenerman group). The script automatically processes the video for analysis and then determines the position of each cell by local maxima of signal. Over the frames of the video, the nearest-neighbour method is used to combine the signal from each cell into a single continuous track. This allows first for the distance travelled and the speed of each cell to be calculated. Time to adhesion is determined when the cell speed drops, and stays, below $0.2 \mu\text{m/s}$ (value previously determined based on T cells interacting with highly adherent surfaces; carried out by Edward Jenkins, Davis group). The mean intensity of signal per cell is used to produce an intensity trace for each cell, from which user-set thresholds determine whether a cell is counted as 'triggered' or not. This is defined by the fold change in signal intensity from a baseline value, which is calculated per cell, so that discrepancies in cell size and dye loading are accounted for, and that calcium traces can be compared across conditions. For subsequent analysis, cells which were designated as 'triggered' but had a calcium trace which started off with a high value and then declined over time were excluded as this likely is caused by triggering from pipetting/charge interactions during sample preparation. Cells triggering earlier than 10 s into their tracks were excluded as these are also likely to be triggered through non-specific means before genuine interaction with the surface. The code also provides information about the number and amplitude of calcium spikes and time to triggering. Cells landing ≤ 300 seconds before the end of acquisition were automatically excluded from analysis to avoid artificially being counted as non-triggering or non-adherent.

3 Creation of Cell Lines to Study TCR Signalling and T-Cell Contact Formation

3.1 Introduction

Antigen-specific triggering of the TCR has been studied for decades, yet no single model explaining the triggering mechanism is agreed upon. While using primary human T cells would provide the most physiologically relevant system for studying these pathways, challenges arise in obtaining, propagating, and genetically editing these cells. Furthermore, since the experiments carried out in this thesis rely on model APCs (i.e., SLBs) for imaging purposes, the T cells being studied must express a TCR with known pMHC specificity as this must be made in advance for presentation on SLBs. This, along with the other genetic modifications required to manipulate signalling used in this thesis, is why immortalised cell lines were chosen for study.

The cell lines created all derive from the well-characterised Jurkat T cell line (E6-1 clone) which was isolated from the blood of a fourteen-year-old leukaemia patient in the 1970s^{369,370}. They are amenable to transduction and have an approximate doubling time of 20 hours³⁷⁴, making them a practical candidate for generating modified cell lines. Furthermore, they are the most frequently used cell line for studying T cell signalling³⁷⁰, so findings from this thesis can be readily discussed in the context of the literature.

The two TCRs used in this thesis are the 1G4³⁷⁵ and gp100 (also known as GPa3b17)³⁷⁶ TCRs, which are both MHC class I-restricted. These will each be introduced at two different expression levels (either physiological or very low density) to compare T-cell responses when TCR availability is substantially different. This not only presents an opportunity to investigate the role of TCR microclusters vs. single TCRs in signal initiation, but also provides different T cell models for microscopy experiments where low TCR expression

would facilitate single-molecule TCR/pMHC imaging of all receptors, rather than a subset as achieved by sub-stoichiometric labelling.

The 1G4 TCR is a useful model TCR as its binding kinetics and affinities to many peptides are well characterised^{377,378}. In this thesis, the selected agonist peptide was 9V (HLA-A2-restricted, NY-ESO-derived peptide; SLLMWITQV), which has a 3D K_d of $\sim 7 \mu\text{M}$ ³⁷⁸, lying within the physiological range of affinities (typically 1-100 μM) expected for a TCR^{378,379}. Therefore, the behaviour observed in 1G4 TCR-transduced cells is likely to reflect a physiological T-cell response, and so 1G4 TCR-expressing cell lines will be used for studying the effect of parameters such as TCR density and signalling capacity on various aspects of T cell behaviour.

The gp100/GPa3b17 TCR (hereafter gp100 TCR) is an affinity-matured TCR developed for immunotherapy purposes and is specific to a melanoma-derived peptide (HLA-A2 restricted peptide, derived from gp100₂₈₀₋₂₈₈; YLEPGPVTV)^{376,380}. Its incredibly high affinity (11 pM³⁷⁶) means that gp100 TCR-transduced cells make a good model for use in experiments where long-lived TCR/pMHC interactions (i.e., over minutes) are required, such as single-molecule TCR/pMHC imaging on live cells and pMHC binding in solution, as binding will last much longer than for the 1G4 TCR.

Furthermore, experiments in this thesis will investigate the impact of TCR signalling on T-cell behaviours such as contact formation, spreading and microcluster formation, by controlling the kinase activity of ZAP-70. ZAP-70 is a proximal kinase recruited to phosphorylated TCR ζ chains, responsible for propagating TCR signalling through phosphorylating the adapter protein LAT (among others)^{155,160,213,225,381}. Control of ZAP-70 activity, therefore, presents an opportunity to ablate TCR signalling at an early stage in the pathway and without affecting TCR/pMHC binding. Endogenous ZAP-70 will be knocked out by CRISPR/Cas9 and replaced by a mutated version known as ZAP-70(AS), which contains a mutation in the ATP-binding domain (methionine 414 to alanine), rendering it

reversibly sensitive to inhibition by the small-molecule drug 3-MB-PP1³⁸². While this ZAP-70 mutant has been used in the context of synapse formation, and effector and memory responses *in vivo*³⁸²⁻³⁸⁵, it has not yet been applied in the context of early signalling events.

To study the behaviour of T cells with different TCR expression levels, ligands, and signalling capacities, several cell lines were generated for use in this thesis. This chapter will describe the generation, sorting and validation of the cell lines and discuss the advantages and disadvantages of these model T cell lines.

3.2 Materials and Methods

3.2.1 DNA Cloning and Transduction

Sequences for the gp100 and 1G4 TCR were kindly provided by Mai Vuong and Edward Jenkins (Davis group) respectively. The α and β chains of the gp100 TCR were PCR amplified from existing plasmids created by Mai Vuong and cloned into a pHR and pHRi backbone, with the native signal peptide left in the sequence. The chains of the 1G4 TCR with a modified signal peptide (MGILPSPGMPALLSLVSLLSVLL) in separate pHR backbones were provided by Edward Jenkins. The 1G4 β chain was subsequently amplified without the stop codon and cloned into a pHR and pHRi backbone with a C-terminal SNAP-Tag present after a flexible linker sequence (GSGSGSG), to facilitate imaging through intracellular staining at a 1:1 label:receptor stoichiometry. The 1G4 α chain was PCR amplified and ligated directly into a pHRi vector. TCR α and β chains of each TCR specificity were co-transduced into a Jurkat-derived CD4⁻ CD8⁺ TCR α/β knockout cell line provided by Edward Jenkins by the standard lentiviral transduction method (see section 2.2.2.8) and sorted by FACS when necessary to ensure a homogenous population (see section 2.4.1). Vectors for transduction of LFA-1 (CD11a and CD18 in pHR) were also provided by Edward Jenkins.

The sequence for human ZAP-70(AS) was kindly provided by Mafalda Santos (Davis group). The sequence was amplified by PCR, removing the stop codon, and ligated into a pHR plasmid with a C-terminal flexible linker sequence (GSGSGSG) followed by a HaloTag and stop codon, to encode the chimeric protein ZAP-70(AS)-Halo.

3.2.2 CRISPR/Cas9 Knockouts

The TCR α/β CD4⁻ CD8⁺ starting cell line was created by Edward Jenkins (Davis group). Briefly, the endogenous TCR of the Jurkat T cell line was removed using a single guide in the LentiCRISPRv2 plasmid for each chain of the TCR targeting exon 2, which were introduced

simultaneously by lentiviral transduction. Cells were sorted for a CD3 ϵ negative population. CD4 was then removed using two CRISPR gRNAs targeting exon 2 and 4 of the gene, followed by sorting for a CD4 negative population. CD8 chains were then introduced and matched to expression levels of human PBMC-derived CD8⁺ T cells.

Two ZAP-70 knockout guides targeting exon 3 and 4 in the LentiCRISPRv2 plasmid were provided by Edward Jenkins (Davis group; see also section 2.2.3). These were transduced by the standard lentiviral method singly and in combination into the Jurkat-derived TCR α/β CD4⁻ CD8⁺ cell line and subjected to puromycin selection as previously described (section 2.2.3). Flow cytometry and Western blot were used to confirm knockout efficiency.

3.2.3 Cell Sorting

All procedures were carried out in a tissue culture cabinet to avoid contamination of cell lines. Approximately 1×10^7 cells were harvested into 50 ml falcon tubes (Fisher Scientific) and centrifuged at 395 x g for 3 minutes. The supernatant was discarded, and cells were washed in 5 ml of sterile PBS before centrifugation. After washing, 50 μ l of relevant antibody (a large excess) was added to the residual supernatant after resuspending cells. This was mixed and left to incubate on ice for 1 hour in the dark. Cells were washed twice in 5 ml of sterile PBS before final resuspension in 500 μ l of sterile PBS with 2% FCS and flowed through a 40 μ m cell strainer (Corning) into a sterile round-bottomed test tube (Fisher Scientific) for sorting. Cells were collected into complete media after sorting, then centrifuged at 395 x g for 5 minutes, supernatant discarded and resuspended in 5 ml of complete media. Cells were left to grow until the desired density was reached and aliquots were frozen down as soon as possible after sorting.

3.2.4 Western Blot of Cell Lysates

Western blot was used to confirm (lack of) expression of intracellular proteins. For each cell line to be probed, 5×10^7 cells were harvested and washed in 3 ml of ice-cold PBS. Cells were

then lysed by resuspending in 100 μ l of lysis buffer (10 mM Tris-HCl pH 7.4, 150 mM NaCl, 1mM EDTA, 1mM PMSF and 1% w/v NP-40) and incubating on ice for 30 minutes. The samples were then centrifuged at 11,000 x g for 10 minutes at 4°C to remove the nuclear fraction. The supernatant was transferred to a fresh 0.6 ml Eppendorf and prepared for SDS-PAGE and Western blot as previously described (section 2.3). After transfer, the nitrocellulose membrane was blocked with 3% BSA in PBS and probed with mouse anti-human ZAP-70 antibodies (Bio Legend), then secondary donkey anti-mouse HRP-conjugated antibodies (Sigma). ECL reagents were used to visualise the protein bands and digital images of blots were acquired on an iBright FL1000.

3.2.5 Plate-bound Calcium Flux Assay

For experiments described in this chapter, plates were incubated with OKT3 antibody (provided by unit purification services) at a concentration of 1 μ g/ml in PBS, incubated and washed as previously described (section 2.5.3), and a final volume of 300 μ l of PBS-MgSO₄ was added. Up to 20 μ l of the final cell suspension was added to each well as the volume and surface area is much larger than for SLBs and cells disperse more. Timelapse images were obtained in the 488 channel by taking one frame every second for 600 frames.

3.2.6 SLB Calcium Flux Assay

SLBs were created, washed, and incubated as previously described (section 2.5.1). The concentration of agonist pMHC used was 2 ng/ μ l unless otherwise specified. 1-10 μ l of labelled, washed and equilibrated cells were added to each bilayer by gently allowing a single drop to fall into the well from the tip of a micropipette. Timelapse images were obtained in the 488 channel by taking one frame every second for 600 frames.

3.2.7 Plate-bound Activation Assays

OKT3-coated 96-well plastic plates (Ibidi) were used. Freshly thawed OKT3 in PBS was centrifuged at 17,000 x g for 10 minutes to remove aggregate, the supernatant transferred to another Eppendorf and its concentration determined using a NanoDrop II. A solution of 10 µg/ml OKT3 was made up in sterile PBS in a tissue culture cabinet. This was serially diluted in sterile PBS a flat-bottomed 96-well plate (Sigma Aldrich) to produce triplicate concentrations for each cell line at each concentration, ranging from 10 µg/ml to 1 ng/ml. The total volume in each well was kept at 100 µl. Plates were left to incubate for 2 hours at 37°C before removing the solution and washing each well twice with 250 µl sterile PBS.

Cell lines were counted using a Countess II automatic cell counter and diluted to a concentration of 1×10^6 /ml in complete media (having been split the previous day to 5×10^5 /ml). PBS was removed from each well and replaced with 100 µl of media containing either a 2X dose of drug (PP2, 3-MB-PP1) or the control DMSO at the same volume. Drugs were prepared such that their final dilution in media would not be less than 1 in 1000, to avoid cells dying due to a high concentration of DMSO. Finally, 100 µl of cells were added to each well (5×10^4 /well final concentration) and plates were incubated in a tissue culture incubator (Panasonic) at 37°C and 5% CO₂ for 18 hours, enough time for the activation markers CD25 and CD69 to be expressed at detectable levels.

To obtain flow data about cell activation, cells in each well were recovered by gentle resuspension with a P200 multichannel micropipette and the total volume transferred to a round-bottomed 96-well plate (Sigma Aldrich). Plates were spun at 395 x g for 2 minutes to pellet cells. Supernatant was discarded and cells were washed in 200 µl/well PBS with 0.05% sodium azide. After centrifugation, cells were resuspended in residual liquid by gentle vortexing. Antibodies against CD3ε (clone UCHT1, BioLegend), CD8α (clone SK1, BioLegend), CD25 (clone BC96, BioLegend) and CD69 (clone FN50, BioLegend) were

together diluted 1:150 in PBS, and 50 μl of this solution was added to each well. Fluorophores were carefully selected to avoid significant spectral overlap.

Staining was carried out in the dark at 4°C for an hour, then 200 μl /well PBS-azide was used to wash the cells twice before final resuspension in 200 μl PFA diluted to 2% in PBS.

Samples were analysed on an Attune NxT with an automatic plate reader attachment. A small volume of control cells was aspirated and used to determine appropriate voltages and gates. The plate was then acquired automatically. Where an experiment required two 96-well plates, the acquisition was taken immediately after the first plate, acquisition settings were copied over, and the same machine was used.

3.2.8 Cell-cell Activation Assays

On day 1, U-2 OS cells were plated onto flat-bottomed 96-well plates at 2.5×10^4 cells/well in 200 μl of complete McCoy's 5A media (Sigma Aldrich) and T cells were split to 5×10^5 /ml. On day 2, the peptide to be used for activation was serially diluted in sterile complete McCoy media in a 96-well round-bottomed plate, with a total final volume of 100 μl /well. Media was removed from the cells in the plate and replaced with 90 μl of diluted peptide (stored in DMSO), ranging from 10^{-4} M to 10^{-8} M and a control with no peptide and DMSO only. These were incubated in a tissue culture incubator (Panasonic) at 37°C and 5% CO_2 for 2 hours before media was removed and replaced with 100 μl complete RPMI media with appropriate drug (PP2 or 3-MB-PP1) or control DMSO. This solution was 2X concentrated and never at a dilution lower than 1 in 500. T cells to be used for activation were diluted to a concentration of 1×10^6 /ml in complete media and 100 μl of this suspension was added to each well. Plates were incubated, stained and analysed as described above.

3.3 Results

Several cell lines were created to facilitate ligand-dependent interactions with model APCs across a variety of ligand/receptor affinities and TCR expression levels.

3.3.1 Creation of 1G4 and gp100 TCR-Expressing Cell Lines

The starting T cell line for this project was provided by Edward Jenkins (Davis group). These Jurkat-derived cells were previously modified using CRISPR/Cas9 gene editing to delete CD4 and the endogenous Jurkat TCR α (TRAV8-4*01) and TCR β (TRBV12-3*01) chains, while introducing the CD8 α and CD8 β chains, to produce a TCR negative, CD4 $^{-}$, CD8 $^{+}$ Jurkat hereafter referred to as 'TCR KO'.

Figure 10 summarises the creation of these cell lines in a flow chart. Viral supernatant for the TCR α and TCR β chains of the 1G4 and gp100 TCRs was produced and used to transduce 1×10^6 TCR KO cells either singly or in combination. To produce cell lines with different expression levels, each TCR chain was transduced in a pHR and pHRi vector framework, which contain promoters of different potency. TCR expression was checked by flow cytometry using labelled anti-CD3 ϵ antibody (UCHT1), showing a shift in staining only when both chains were transduced together. This indicates that both α and β chains must be present to successfully express TCR complex at the cell surface, and that no significant amount of endogenous α or β TCR chains remain in these Jurkats.

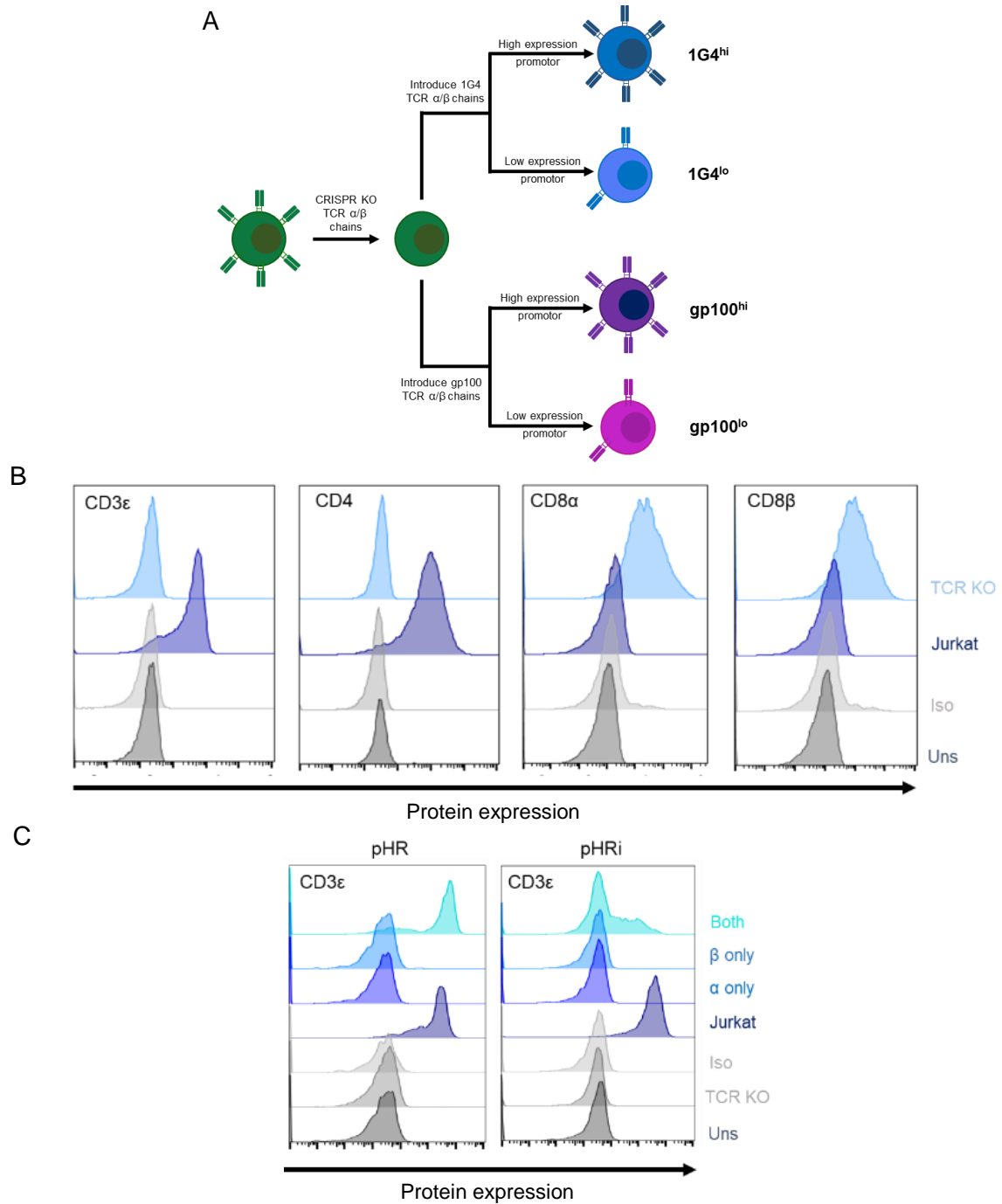


Figure 10 Creation of 1G4 and gp100 TCR-expressing cell lines (A) Schematic illustrating the workflow for creating 1G4^{hi}, 1G4^{lo}, gp100^{hi} and gp100^{lo} cells. (B) Approximately 5×10^5 cells were harvested, stained with the relevant antibody before fixation for flow cytometry analysis. Panels show characterisation of modifications in Jurkat-derived CD4⁻ CD8⁺ TCR KO cells by flow cytometry, which was used to create all subsequent cell lines. (C) Flow cytometry analysis indicating that the expression of TCR in cells requires the presence of both TCR α and TCR β chains in either high (pHR) or low (pHRi)-expressing vectors, and therefore that undetectable amounts of endogenous Jurkat TCR are expressed. TCR expressed in a pHR vector (left) produce similar TCR expression to Jurkat cells, whereas a pHRi vector (right) produce a much lower expression.

To achieve a more homogeneous population, cells were subsequently sorted for a TCR^{hi} and TCR^{lo} population depending on the vector used for transduction and re-analysed by flow cytometry to ensure expression level matching between TCR^{hi} and TCR^{lo} cell lines of each specificity. Subsequently, each cell line was stained with its cognate pMHC to demonstrate TCR/agonist pMHC binding. The gp100 TCR-expressing cells could be directly stained with labelled monomeric gp100 pMHC due to its high affinity, but for the 1G4 TCR-expressing cell lines, pMHC tetramers were used to increase staining efficiency. To produce these, a modified version of 9V-loaded pMHC with a C-terminus BirA tag was biotinylated and mixed in a 5:1 ratio with Alexa Fluor 647-labelled streptavidin (tetramers were made previously by Edward Jenkins, Davis group). The distributions of the stained populations matched well with the UCHT1 stain, seen in Figure 11.

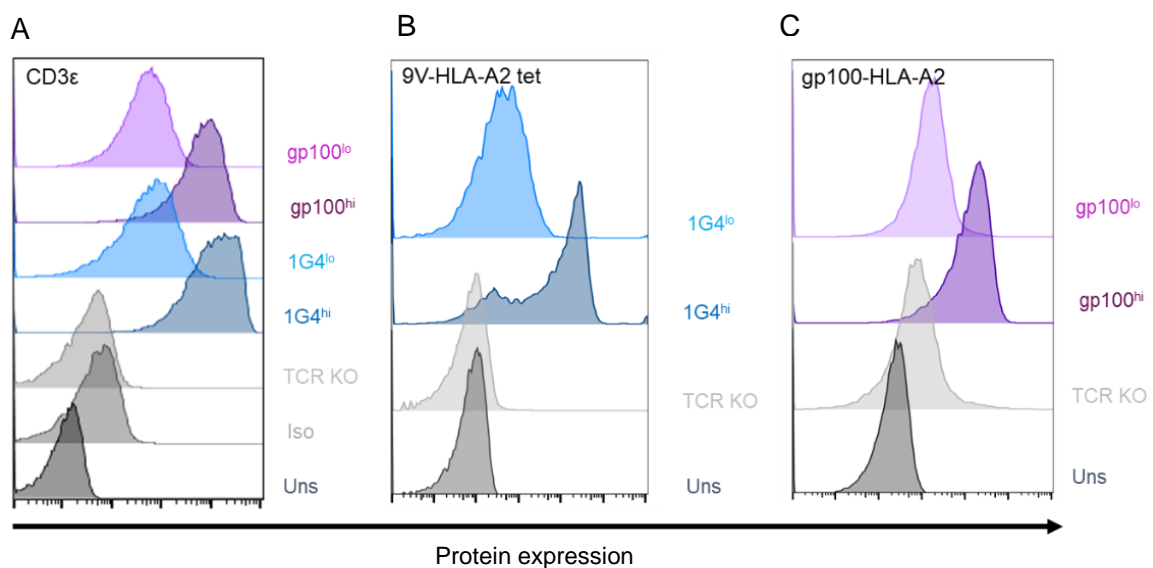


Figure 11 Expression and specificity of 1G4 and gp100 TCRs Approximately 5×10^5 cells were harvested and stained with the relevant antibody before fixation for flow cytometry analysis. (A) Surface TCR expression by flow cytometry on TCR^{hi} and TCR^{lo} cells after sorting. (B) Staining of the 1G4 TCR on high and low TCR-expressing cell lines with labelled HLA-A2-9V tetramer. (C) Staining of the gp100 TCR on high and low TCR-expressing cell lines by monomeric labelled HLA-A2-gp100.

Next, quantitative analysis of TCR expression was performed by flow cytometry using a QuantiBrite kit (BD Biosciences). Cells were stained with a saturating concentration of PE-labelled UCHT1 antibody for 1 hour at 4°C and analysed at the same time as standard PE-labelled beads (Figure 12A). Using the geometric mean of each bead population, a standard

curve was generated from which the average number of PE molecules per cell could be determined (Figure 12B). Based on an average labelling efficiency of one PE molecule per UCHT1 antibody (determined by NanoDrop II absorbance readings), and two UCHT1 antibodies binding per TCR at saturation, an approximate number of TCRs per cell was calculated (Figure 12C). 1G4^{hi} cells were found to express ~17,100 TCRs/cell and gp100^{hi} cells slightly lower at ~11,000 TCRs/cell, comparable to unmodified Jurkats (data not shown). Of the TCR^{lo} cells, the 1G4^{lo} cells had an average of ~240 TCRs/cell and the gp100^{lo} cells had an average of ~490 TCRs/cell.

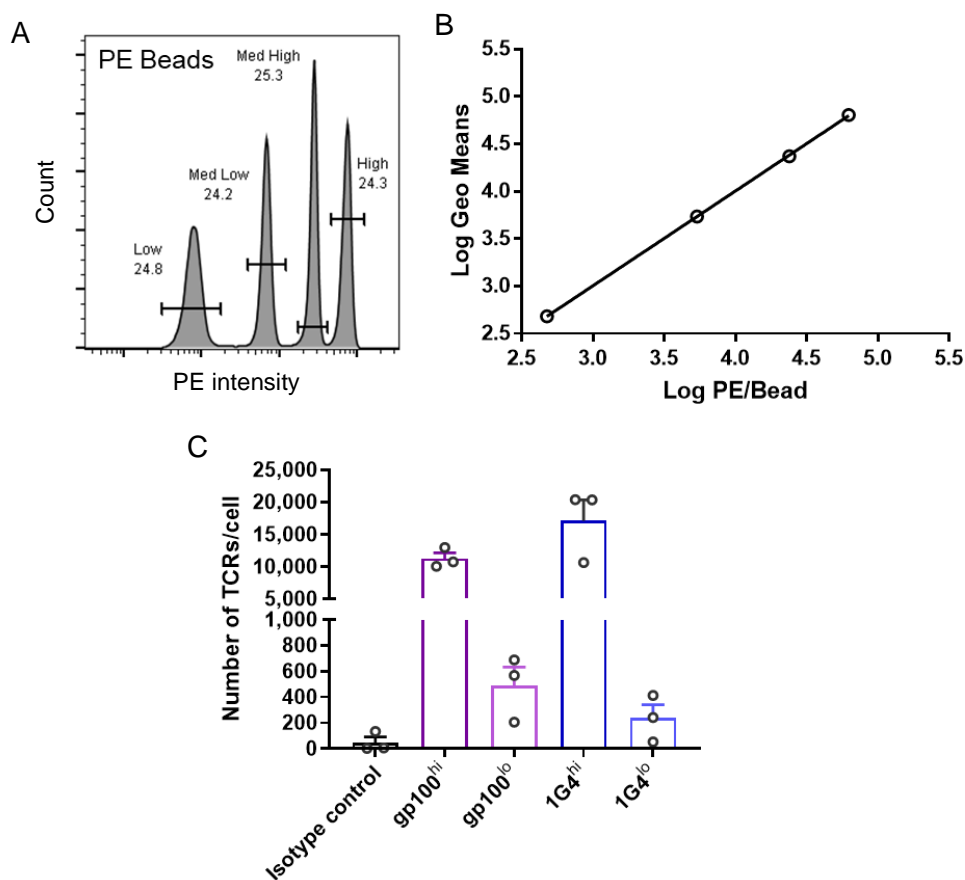


Figure 12 **Quantification of TCR expression on 1G4 and gp100 TCR-expressing cells** Cells and quantification beads were prepared and analysed as per the manufacturer's instructions. (A) Intensity distributions on Quantibrite beads, which have known densities of fluorophore, measured by flow cytometry (B) Representative standard curve generated from one replicate of beads, from which the number of PE molecules per cell can be derived. (C) Quantification of the number of TCRs per cell, based on taking the intensity of a saturating label of UCHT1 antibody per cell and using this to determine the number of CD3 ϵ molecules present. UCHT1 antibodies were labelled with ~1 PE molecule per antibody as determined by NanoDrop II readings. Mean \pm SD plotted. Data from 3 independent repeats using thousands of cells and beads per repeat.

In addition to labelled antibodies and Fabs, which label the TCR extracellularly, a fused SNAP-tag on the C terminus of the β chain of the 1G4 TCR allows for further labelling options. The main advantage of this method is that 1:1 labelling of the TCR complex can be achieved, and since the labelling reaction is irreversible, there is no significant loss of label over the time course of experiments, even at 37°C. Since most data acquired for this thesis would be imaging-based, it was important to test the characteristics of each labelling method during imaging. Cells were labelled sequentially with SNAP Cell 647-SiR and Alexa Fluor 488-labelled UCHT1 Fab (see sections 2.5.6 and 2.5.7), allowed to settle on 1st generation agonist-presenting bilayers for 20 minutes at room temperature and then fixed for immediate imaging on a TIRF microscope. Images were taken of several cells and line profiles were constructed at random points across the cell to compare the intensity and signal-to-noise ratio of each labelling method (Figure 13). From the images acquired, it appears that using the SNAP-Tag labelling method does not produce as high a signal-to-noise ratio as with the UCHT1 Fab, probably because of the increased difficulty of washing unbound intracellular dye (demonstrated by high background in Jurkat cells which are SNAP-Tag negative).

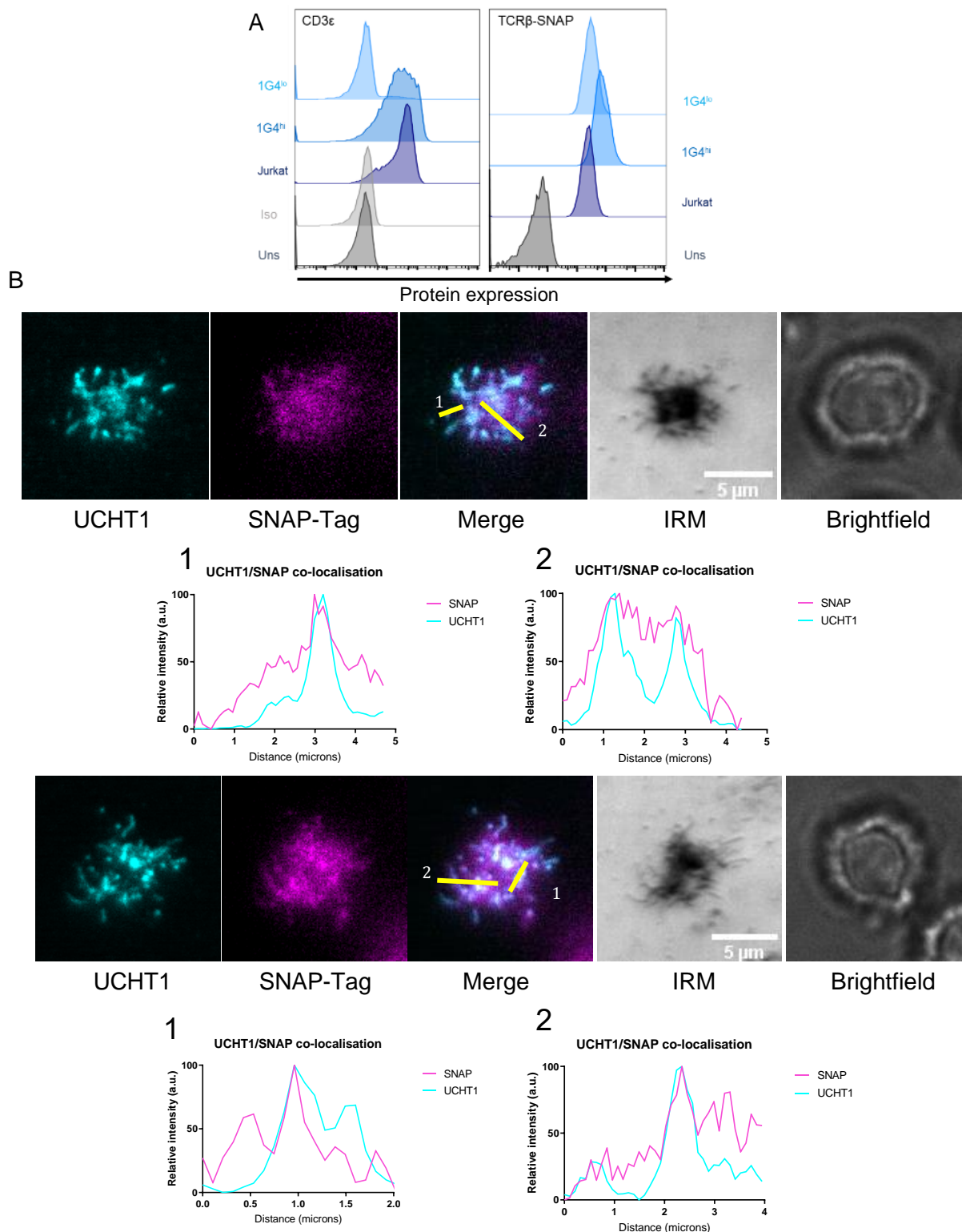


Figure 13 Comparison of extracellular and intracellular staining methods for the 1G4 TCR (A) Approximately 5×10^5 1G4^{hi} and 1G4^{lo} cells were harvested, stained with UCHT1 Fab (left panel) or via TCRβ-SNAP-Tag (right panel) before fixation for flow cytometry analysis. **(B)** Representative examples of 1G4^{hi} cells labelled in the same manner and placed on a 1st generation agonist-presenting SLB for 20 minutes before fixation. Images were acquired by TIRFM. Matching normalised intensity plots located below cell images compare signal-to-noise for each method. Healthy cells (selected from the brightfield image) forming contacts (shown by dark areas in the IRM channel) were selected for image acquisition.

3.3.2 Novel Cell Lines Retain Expression of Important Surface and Intracellular Proteins

To check whether the modifications made on the cell lines had changed other proteins that were likely to affect T-cell responses in experiments, the cell lines were stained for proteins known to affect T-cell signalling and adhesion. These included the coreceptors CD4 and CD8, the adhesion protein CD2, the phosphatase CD45, and the intracellular signalling proteins Lck and ZAP-70. Since cells would primarily be interacting with SLBs presenting agonist pMHC and ICAM-1 (hereafter referred to as 1st generation SLBs) in imaging experiments, LFA-1 expression was also analysed. All cell lines had a relatively low expression of CD11a and CD18 (the two subunits of LFA-1) and subsequent imaging confirmed that they did not readily form immune synapses (see Figure 50, section 8.3). Low expression of LFA-1, and subsequent difficulty forming immune synapses, has also been observed by another group³⁸⁶. Since primary T cells make readily observable immune synapses on ICAM-1-containing SLBs⁹⁶, lentiviral transduction of CD11a and CD18 (using standard techniques, see section 2.2.2.8) was performed on the cell lines to make them a more representative model (Figure 14A and Figure 50). All cell lines were then sorted to ensure matching of LFA-1 expression. For simplicity, cells with boosted LFA-1 expression will be referred to as TCR KO, 1G4/gp100^{hi} or 1G4/gp100^{lo} henceforth and LFA-1^{lo} cell lines will be specified if used.

Flow cytometry analysis on these cell lines showed that all proteins tested were expressed at similar levels to Jurkats, except for CD4, CD8 and LFA-1 as previously indicated. Intracellularly, Lck and ZAP-70 staining also showed comparable expression to the parental Jurkat line (Figure 14).

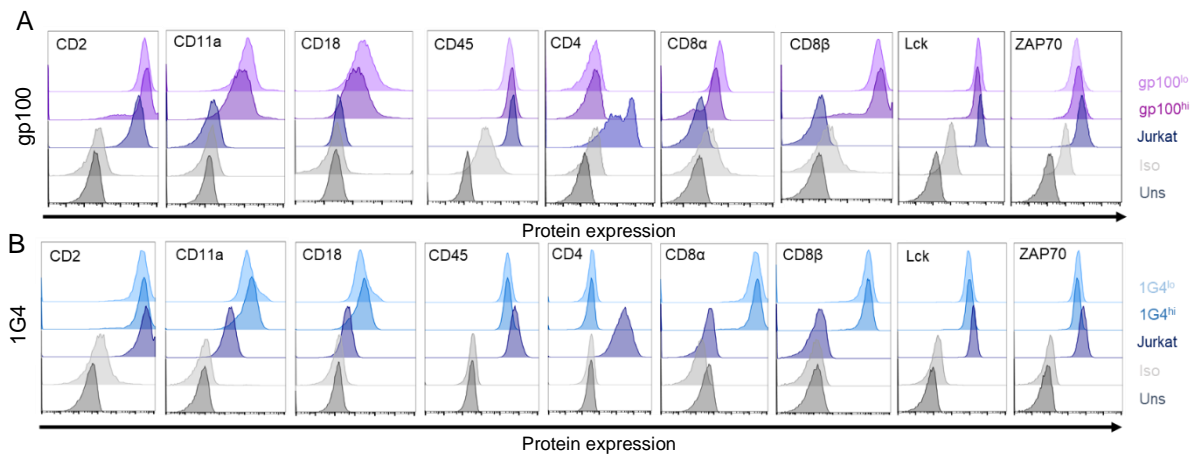


Figure 14 1G4 and gp100-TCR expressing cell lines retain comparable expression of key proteins to Jurkats Approximately 5×10^5 cells from each cell line were harvested and labelled with the appropriate antibody, washed and fixed for flow cytometry analysis. Analysis was directed towards surface and intracellular proteins which are known to affect early T-cell signalling and adhesion. (A) Comparison of expression of important surface and intracellular proteins on gp100 TCR-expressing cells with Jurkats. (B) Comparison of expression of important surface and intracellular proteins on 1G4 TCR-expressing cells with Jurkats.

3.3.3 1G4 and gp100 TCR-Expressing Cells Signal in Response to OKT3

To test the functionality of the newly transduced TCRs, calcium flux assays were carried out. Calcium flux from intracellular stores occurs shortly downstream of TCR triggering³⁸⁷, therefore it provides a rapid and easily measurable readout for T-cell responsiveness to agonist pMHC.

Fresh glass slides were coated with 1 $\mu\text{g/ml}$ of the anti-CD3 ϵ antibody OKT3 before thorough washing in filtered PBS and temperature equilibration (37°C) in the microscope incubator (see section 2.5.3 for details). Approximately 1×10^6 cells were harvested and labelled with Fluo-4 AM, a calcium indicator. Cells were then washed in prewarmed filtered PBS with 2 mM magnesium sulphate (hereafter PBS-MgSO₄, used to increase ICAM-1/LFA-1 binding affinity) and equilibrated in the microscope incubator before being placed onto the surfaces (see section 2.5.5.1 for full details). Timelapse images were taken over 10 minutes and videos were subsequently analysed with a custom MATLAB code written by Jane Humphrey (Klenerman group, described in section 2.6) to obtain metrics such as the

fraction of cells signalling, the time at which signalling occurs, the amplitude of the spike and the number of spikes per cell.

As expected, TCR KO cells did not signal at a significant level (<10%). The average fraction of Jurkat cells signalling was 66%, compared to 68% of gp100^{hi} cells, 60% of gp100^{lo} cells, and 71% and 42% of 1G4^{hi} and 1G4^{lo} cells respectively (Figure 15). This suggests that the cell lines created for this thesis are capable of signalling through the TCR. There was no significant difference between any of the TCR-expressing cell lines and Jurkat T cells, except for the 1G4^{lo} cells, which may be a result of their particularly low TCR expression (see Figure 12).

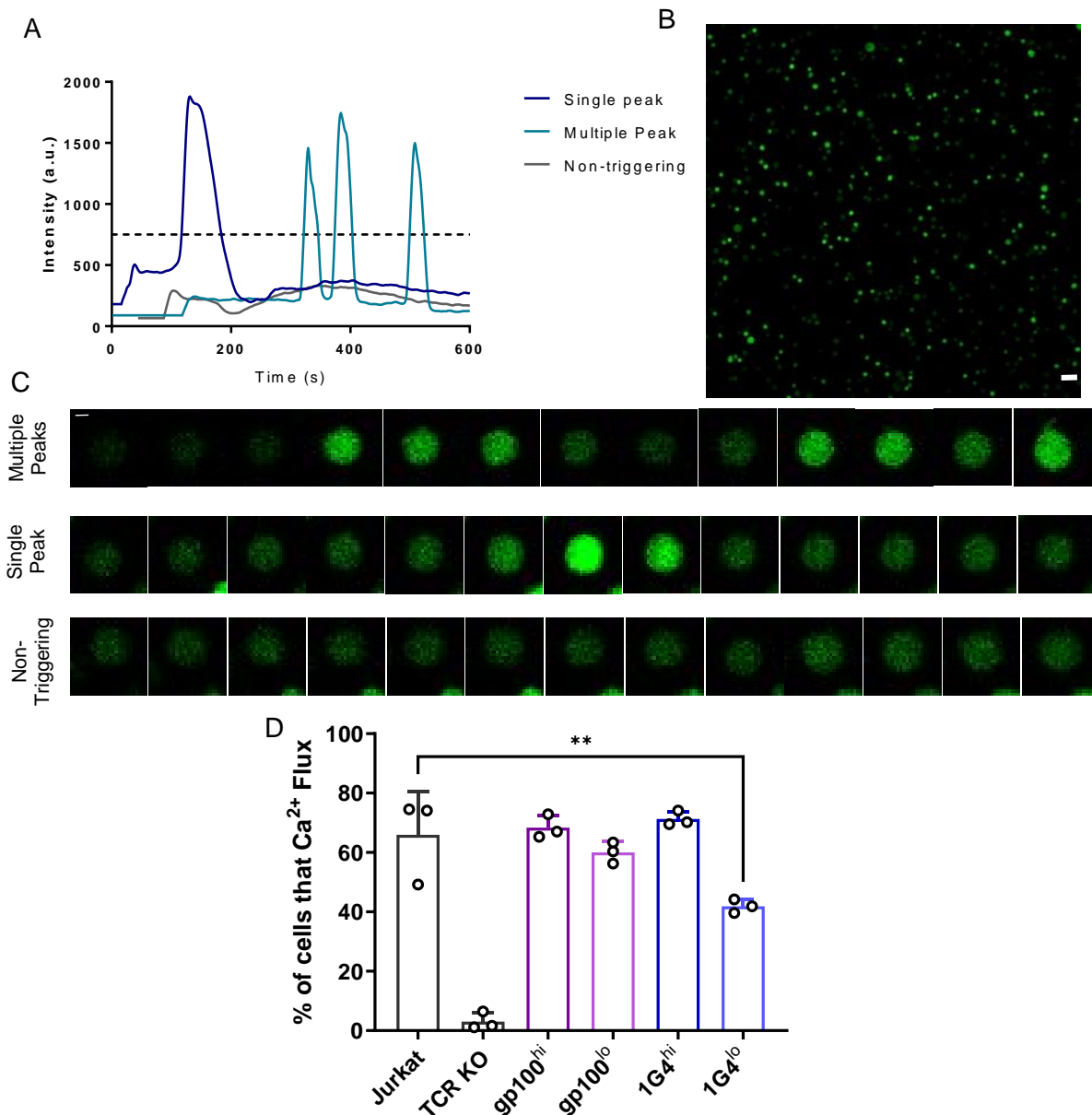


Figure 15 Calcium flux assays for 1G4 and gp100 TCR-expressing cells Approximately 5×10^5 cells from each cell line were harvested and labelled with Fluo-4 AM before being washed in PBS-MgSO₄, equilibrated to 37°C and placed on OKT3-coated surfaces. Timelapse images were acquired every second for 600 frames/10 minutes. (A) Example calcium flux traces for individual cells generated by the custom MATLAB code used to analyse calcium flux assay data (see section 2.6). Thresholds for each cell are set based on their average baseline intensity and the code can distinguish the number of peaks per cell, as well as peak amplitude and peak timing relative to the cell landing on a surface. (B) Example of one field of view containing hundreds of cells labelled with Fluo-4 AM from a calcium assay experiment. Scale bar 50 μ m. (C) Timelapse of representative individual Jurkat cells illustrating the different calcium flux behaviours observed: single peak, multiple peak or non-triggering. (D) Fraction of cells from each cell line triggering on an OKT3-coated surface compared to Jurkats. Mean \pm SD plotted. Data from 3 repeats of \sim 200-1000 cells per repeat. Statistical analysis was carried out by one-way ANOVA with Dunnett’s multiple comparisons, with Jurkat cells used at the control. ** = $p < 0.01$ There was a significant difference between the values obtained for Jurkat vs TCR KO cells ($p = <0.0001$) not shown in the graph. Non-significant values are not shown.

3.3.4 1G4 and gp100 TCR-Expressing Cells Signal in Response to Cognate pMHC

To test calcium flux response to agonist pMHC, SLBs were made (see sections 2.5.1 and 2.5.2) comprising a high concentration (2 ng/ μ l) of appropriate agonist pMHC and null pMHC (8 ng/ μ l), which is used to block unbound nickel-chelating sites created by Ni-NTA lipids in the SLB and prevent non-specific TCR signalling and adhesion (see section 8.2). When the SLBs were almost ready to use, cells were labelled as before with Fluo-4 AM (described in section 2.5.5.1). Both cells and SLBs were washed in warm PBS-MgSO₄ and allowed to equilibrate in the microscope incubator before the correct focal plane was found and cells added.

In both the 1G4^{hi} and gp100^{hi} cell lines, a strong calcium flux response could be observed (around 70% for 1G4 TCR and 63% for gp100 TCR) when measured on their respective agonist-presenting SLBs (Figure 16A). In both cases, this was TCR-specific signalling as neither TCR KO cells nor ZAP-70 KO cells signalled significantly ($\leq 4\%$ and $\leq 6\%$ respectively). The 1G4^{lo} and gp100^{lo} cells signalled on average 26% and 42% respectively. There were no significant differences in signalling between the 1G4 and gp100 TCR-expressing cell lines (with similar TCR expression), which is likely because the concentration of agonist pMHC was very high on these SLBs and therefore this is an observation of the maximal response. There was also no significant difference between the gp100^{hi} and gp100^{lo} cells, whereas there was for the 1G4 cell lines, suggesting that the very high affinity gp100 TCR makes the T cell more sensitive to pMHC.

3.3.5 1G4 and gp100 TCR-Expressing Cells Signal on 1st Generation SLBs

As previously described (section 1.14.2) the combination of pMHC and ICAM-1 presented on a glass-supported lipid bilayer (i.e. 1st generation SLBs) is used most frequently for early T-cell signalling studies and provides sufficient T-cell stimulation to induce robust

signalling, spreading and activation^{96,332}. Therefore, it is the main SLB type used in this thesis.

Cells were then checked for their ability to signal on agonist-presenting 1st generation SLBs (Figure 16B). SLBs were made as per section 2.5.1, and contain a high concentration (2 ng/ μ l) of agonist pMHC (to ensure maximal response), null pMHC (8 ng/ μ l) and ICAM-1 (1.2 ng/ μ l). 1G4^{hi} and 1G4^{lo} cells signalled 70% and 44% respectively, and signalling for gp100^{hi} cells was 66% while for gp100^{lo} this was 60%.

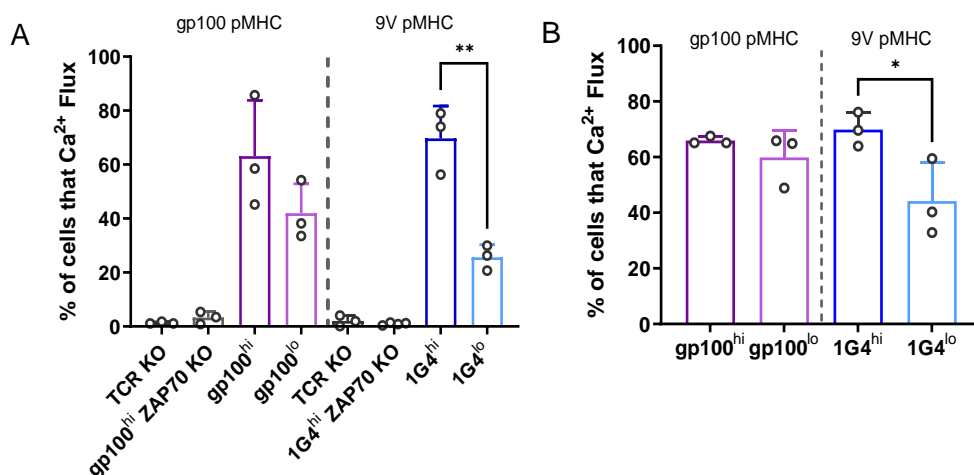


Figure 16 1G4 and gp100 TCR-expressing cells trigger in response to their cognate pMHC (A) Approximately 5×10^5 cells from each cell line were harvested and labelled with Fluo-4 AM before being washed in PBS-MgSO₄, equilibrated to 37°C and placed on agonist pMHC-presenting SLBs. Timelapse images were acquired every second for 600 frames/10 minutes. Graph shows the fraction of cells triggering on agonist pMHC-presenting SLBs. The agonist pMHC in each case is indicated above the bars and was added to a final concentration of 2 ng/ μ l. (B) Fraction of cells triggering on 1st generation agonist-presenting SLBs. Agonist pMHC was added to a final concentration of 2 ng/ μ l. Mean \pm SD plotted in both graphs. Data acquired from ~200-1000 cells per repeat, with 3 biological repeats per condition. Comparisons were made between TCR^{hi} and TCR^{lo} cell lines using a Student's t-test. ** = $p < 0.01$ * = $p < 0.05$.

3.3.6 1G4 and gp100 TCR-Expressing Cell Lines Form Immune Synapses on 1st Generation SLBs

The immune synapse forms after many minutes of stable contact and is induced by TCR signalling^{96,388}. Therefore, to confirm that signalling pathways downstream of the transduced TCRs were still (at least largely) functional, cells were imaged forming stable contacts on 1st generation agonist-presenting SLBs. Cells were harvested, washed in PBS-MgSO₄, and resuspended in the same. A small volume of this cell suspension was added to washed SLBs and allowed to incubate at room temperature for 10 minutes before the excess liquid was removed (leaving just enough to prevent the SLBs and cells from drying out) and replaced with a fixative solution of 4% PFA and 0.25% glutaraldehyde in PBS to capture all cells at a similar timepoint in immune synapse formation for imaging. Cells were fixed at room temperature for 30 minutes before being washed three times in PBS and imaged immediately.

On agonist-presenting SLBs, ICAM-1 was observed accumulating under all cells, but especially those expressing TCR, where a ring structure of ICAM-1 often formed around a central pMHC cluster (Figure 17). Accumulation of agonist pMHC under the cells was most readily observed under the TCR^{hi} cells, although it could occasionally be seen under TCR^{lo} cells, presumably for cells where TCR expression was relatively high. In contrast, no pMHC accumulation could be observed under TCR KO cells, again confirming the TCR specificities of each cell line (Figure 17). These images indicate that key signalling pathways downstream of the TCR were likely functional.

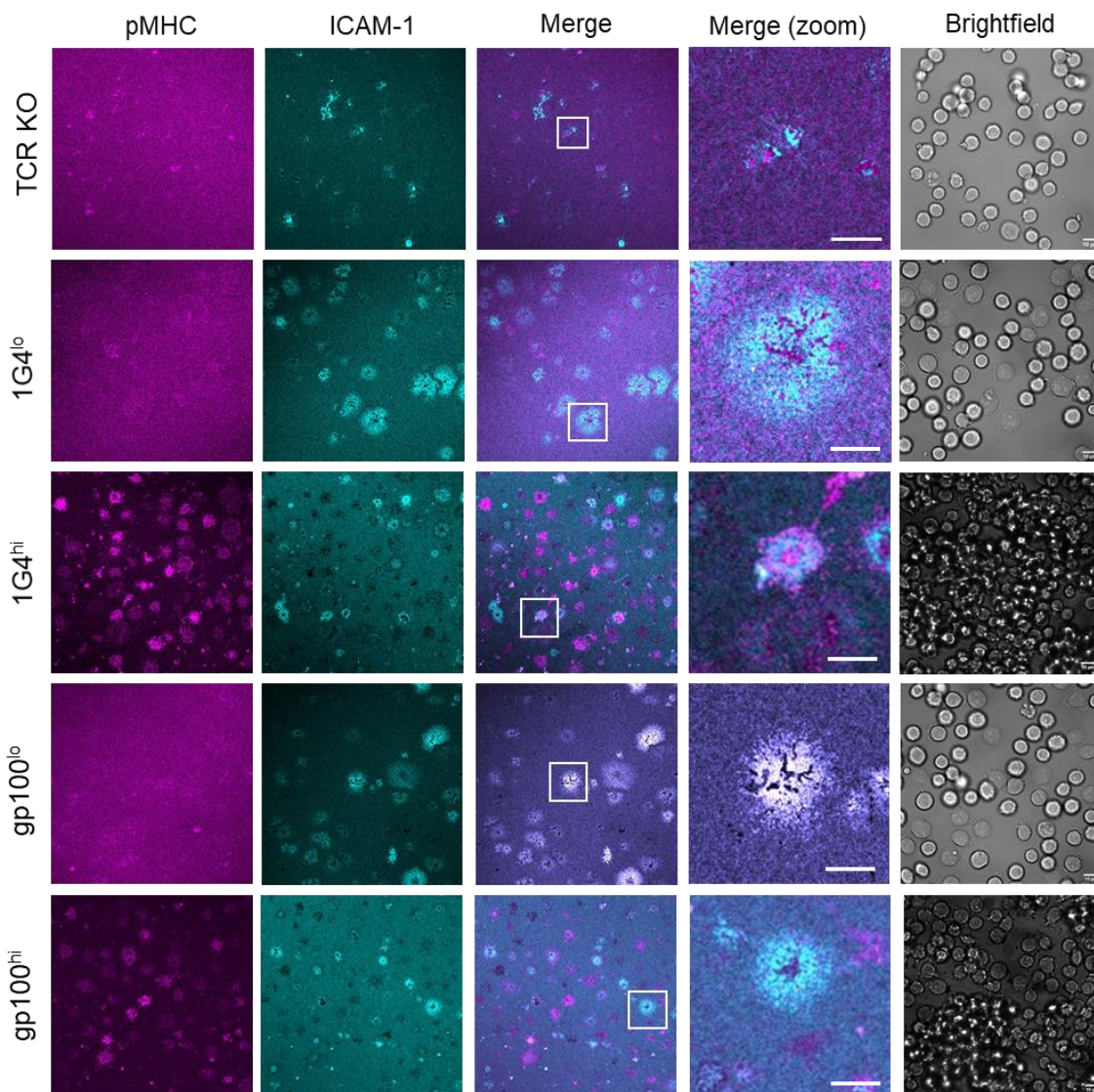


Figure 17 **1G4 and gp100 TCR-expressing cell lines accumulate pMHC and ICAM-1 and form immune synapses on 1st generation agonist-presenting SLBs** Approximately 5×10^5 cells of each cell line were harvested, washed in PBS-MgSO₄, and allowed to interact with 1st generation agonist-presenting SLBs with labelled pMHC and ICAM-1 for 10 minutes before fixation. Accumulation of pMHC and ICAM-1 can be observed to different degrees under each cell line. SLBs comprised proteins at the following concentrations: agonist pMHC 0.3 ng/ μ l, null pMHC 9.7 ng/ μ l, ICAM-1 1.2 ng/ μ l. Merge (zoom) panels are enlarged images of cells highlighted in white boxes. Scale bar for zoomed images is 5 μ m; otherwise 10 μ m.

3.3.7 Creation of Analogue-Sensitive ZAP-70-Expressing Cell Lines

Selective inhibition of a single protein within the signalling pathway, and subsequent observation of changes in cell behaviour, is a method widely used in cell signalling studies. One such protein of interest in T-cell signalling is ZAP-70, a kinase recruited very early in the TCR signalling cascade to phosphorylated ITAMs on the TCR ζ chains^{155,160,381}. In 2008, researchers in Arthur Weiss's group engineered a mutated version of ZAP-70, known as ZAP-70(AS), which is sensitive to inhibition by the small molecule 3-MB-PP1³⁸² (see section 3.1). Several studies have used T cells expressing the ZAP-70(AS) mutant to explore the role of this protein in T cell functions including contact formation with SLBs²²³, target cells³⁸⁴, and immune synapse formation³⁸³, however it has not yet been employed in the context of early T-cell signalling. Therefore, a variety ZAP-70(AS)-expressing cell lines were created (summary in Figure 18).

Starting with the TCR KO parental cell line, two CRISPR guides against different exons of ZAP-70 (see section 2.2.3 for further information) were transduced singly and in combination using the standard lentiviral transduction technique (section 2.2.2.8). ZAP-70 expression was checked by intracellular staining after 3 days, which indicated the increased efficiency of knockdown using both guides in combination (Figure 18B, left panel). Approximately 1×10^6 of these doubly-transduced cells were then subjected to puromycin selection for a further 3 days, after which ZAP-70 expression appeared completely lost according to intracellular staining (Figure 18B, right panel). A Western blot of cell lysates was then carried out, confirming the absence of ZAP-70 in these cells (Figure 18C).

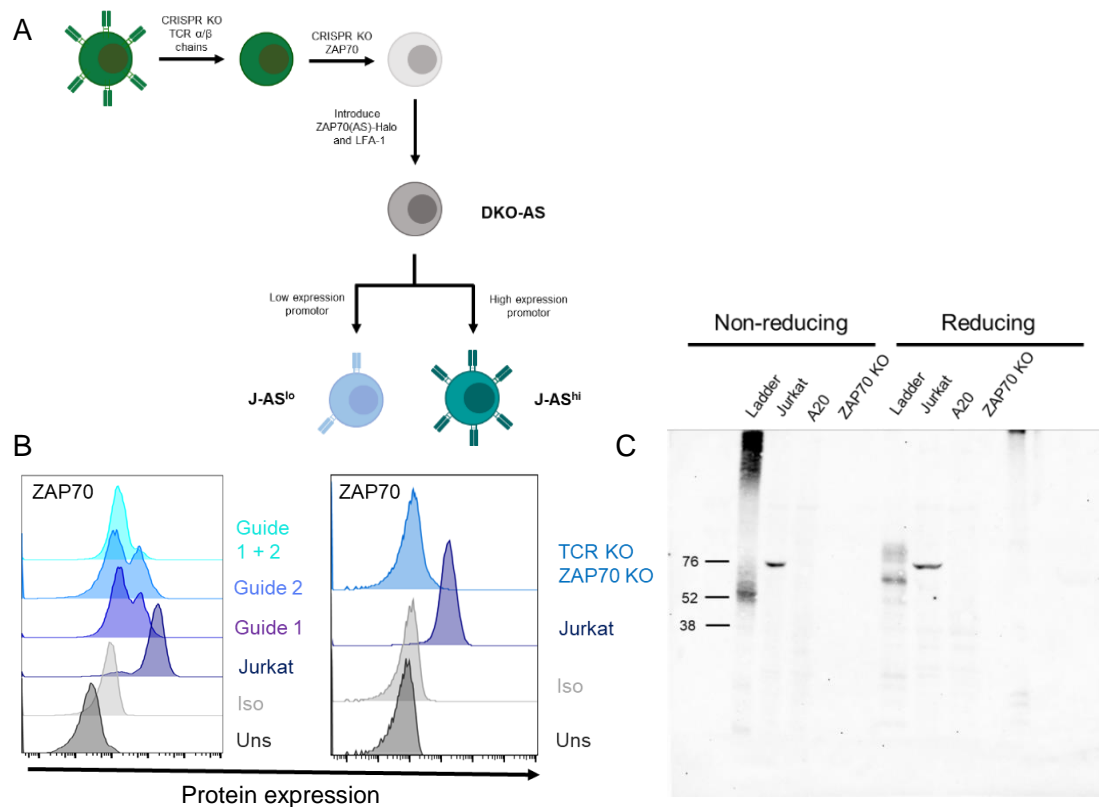


Figure 18 Creation of ZAP-70(AS)-expressing cell lines (A) Schematic showing the workflow of creation of ZAP-70(AS)-expressing cell lines. (B) Approximately 5×10^5 cells were harvested, stained intracellularly for ZAP-70, washed and fixed for flow cytometry. Panels show staining of ZAP-70 in TCR KO cells transduced with each CRISPR guide singly and in combination before puromycin selection (left panel) and with both guides after puromycin selection (right panel). (C) Approximately 1×10^7 cells from each sample were lysed, processed and analysed by Western blot. Anti-ZAP-70 antibodies were used to probe each sample. Jurkats were used as a positive control and the B cell line A20 as a negative control. A band appears in the Jurkat sample at the correct size (70 kDa), which is absent in both other cell lines, indicating an effective knockout.

To reconstitute the expression of ZAP-70 with the mutant ZAP-70(AS), the parental TCR/ZAP-70 double KO cells were transduced with viral supernatant as previously described (section 2.2.2.8). The addition of this construct presented an opportunity to create cell lines where every ZAP-70 protein was available for labelling. Therefore, a genetically encoded HaloTag on the C terminus of ZAP-70(AS) was used to create a flexible labelling system suitable for flow cytometry and microscopy. Using a HaloTag allows for variety of fluorophore usage within the same cell line, and HaloTag dyes are often brighter and more bleaching-resistant than fluorescent proteins^{389,390} making the ZAP-70(AS)-Halo ideal for microscopy experiments. After 4 days, the cells were tested for expression of chimeric ZAP-70(AS)-Halo by flow cytometry, which indicated strong and homogeneous

expression of the construct, as expected for the pHR vector which uses a strong promoter (Figure 19A).

It had already been established that the endogenous expression of LFA-1 in the parental TCR KO cell line was not high enough to allow substantial ICAM-1 accumulation and immune synapse formation (Figure 14 and Figure 50). Therefore, this TCR KO ZAP-70(AS) line was transduced with CD11a and CD18 as per the standard lentiviral protocol (section 2.2.2.8) and increased LFA-1 expression was confirmed by flow cytometry (Figure 21). The resulting cell line is henceforth called DKO-AS, as it has no TCR or endogenous ZAP-70, and instead expresses ZAP-70(AS).

Finally, to create the remaining cell lines with high and low TCR expression, 1G4 α and 1G4 β TCR chains were introduced to DKO-AS cells by the standard lentiviral transduction technique (section 2.2.2.8), either in the pHR high-expression or the pHRi low-expression vector, and cells were sorted where necessary to achieve a homogeneous population. These cell lines are henceforth called J-AS^{hi} and J-AS^{lo}. As with the ZAP-70 wildtype cell lines, quantification of TCR expression was carried out using the Quantibrite kit (BD Biosciences) (Figure 19B and C). J-AS^{hi} cells were found to express an average of ~18,000 TCRs per cell, whereas for the J-AS^{lo} cell line this was ~1,500 TCRs per cell. The DKO-AS cell line had staining comparable to the isotype control (i.e., negligible/no TCRs).

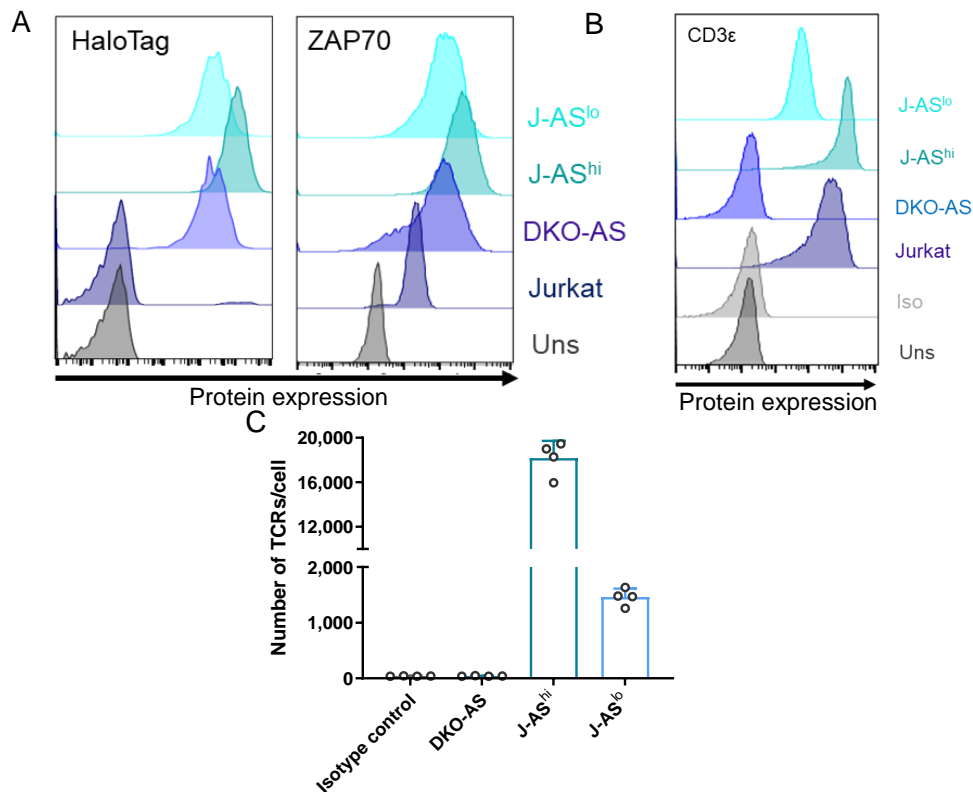


Figure 19 **Characterisation of ZAP-70(AS)-expressing cell lines** Approximately 5×10^5 cells were harvested, stained with either anti-ZAP-70 or anti-CD3ε antibodies or a HaloTag ligand, washed and fixed for flow cytometry analysis. (A) Staining of ZAP-70(AS) via intracellular antibody staining against ZAP-70 (right panel) and via HaloTag (left panel) in ZAP-70(AS) cell lines. (B) Staining of TCR on ZAP-70(AS) cell lines by UCHT1 antibody for TCR quantification. (C) Quantification of TCR expression on ZAP-70(AS)-expressing cell lines using Quantibrite kit analysis. 4 matched repeats were conducted for each condition with thousands of cells and beads per repeat.

Since the ZAP-70 expressed by these cell lines is readily observable by imaging, each cell line (DKO-AS, J-AS^{hi} and J-AS^{lo}) was stained with the HaloTag ligand Janelia Fluor 549 (see section 2.5.6) and allowed to settle on 1st generation agonist-presenting SLBs for 5 minutes at room temperature before being fixed. Images clearly show the presence of ZAP-70 microclusters in J-AS^{hi} and J-AS^{lo} cells, but not DKO-AS, which is expected since they have no TCR for the ZAP-70 to bind (Figure 20). These images, along with signalling data, indicate that ZAP-70(AS)-Halo is likely recruited to the TCR in a similar fashion to ZAP-70 wildtype cells and functions in a comparable way in TCR signalling.

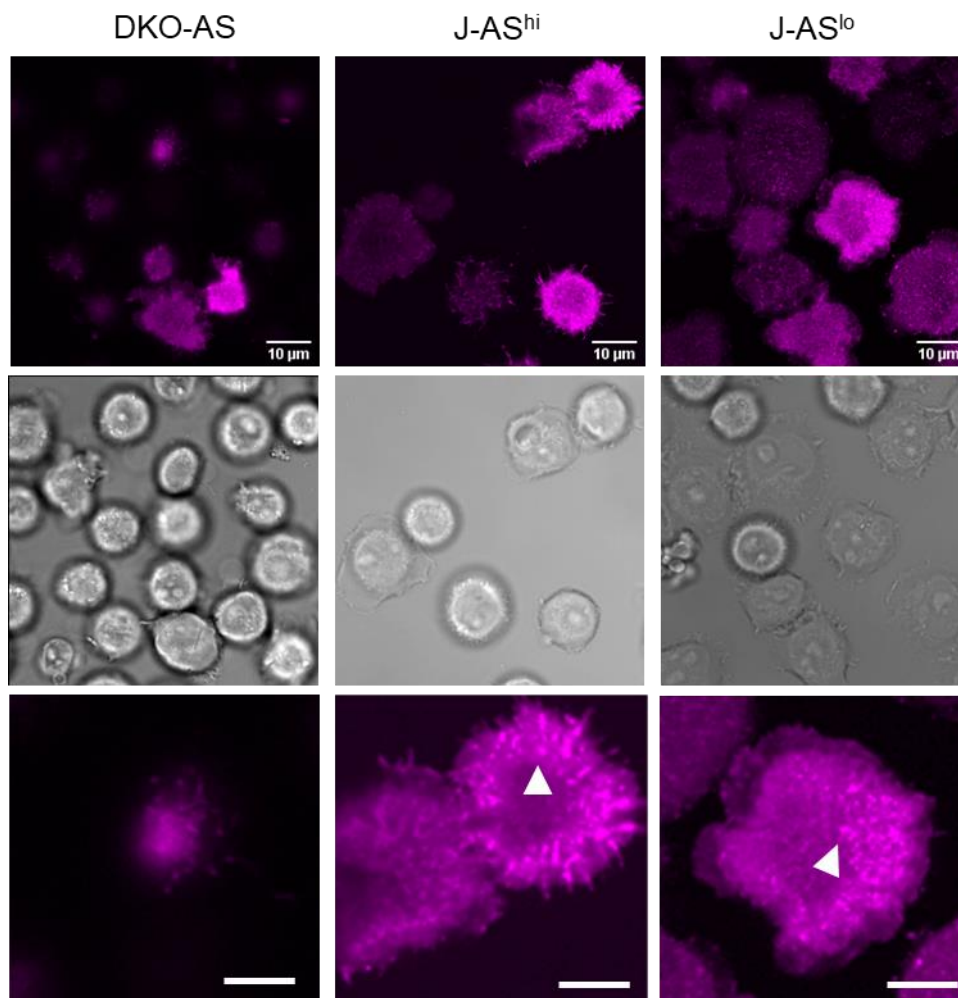


Figure 20 ZAP-70(AS) can be labelled via HaloTag and used to visualise ZAP-70 recruitment
Approximately 5×10^5 cells were harvested and labelled with the HaloTag ligand Janelia Fluor 549, washed in PBS-MgSO₄, allowed to settle on 1st generation agonist-presenting bilayers and fixed after 5 minutes. Brightfield images confirm TCR signalling through cell spreading for J-AS^{hi} and J-AS^{lo}, but not DKO-AS cells. In the bottom row, bright puncta, formed by ZAP-70 microclusters, can be readily observed on TCR-expressing cells but not on DKO-AS cells with no TCR. Examples of individual microclusters indicated by white arrowheads. Scale bar 5 μ m. Brightness and contrast of images adjusted for illustrative purposes.

3.3.8 ZAP-70(AS) Cell Lines Retain Expression of Important Surface and Intracellular Proteins

As with the ZAP-70 wildtype cell lines, a validation panel was carried out using flow cytometry to ensure matching expression of key surface and intracellular proteins (Figure 21), which were comparable to the parental Jurkat line (except for CD4/CD8 and CD11a/CD18). This analysis indeed showed that the ZAP-70(AS) cell lines still expressed CD8 but not CD4, and had comparable levels of CD45, CD2, and Lck to Jurkat cells, with relatively high LFA-1 due to the lentiviral boost.

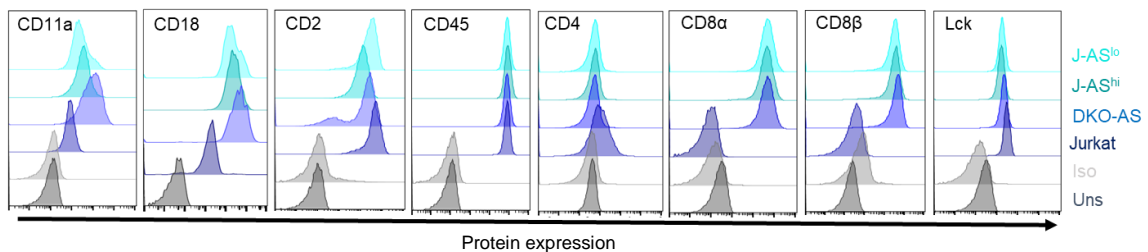


Figure 21 ZAP-70(AS)-expressing cells express important proteins at a comparable level to Jurkats Approximately 5×10^5 cells were harvested, stained with the relevant antibody and fixed for analysis by flow cytometry. Analysis was directed towards the surface and intracellular proteins which are known to affect early T-cell signalling and adhesion. No substantial differences were found between the ZAP-70(AS) cell lines and Jurkat cells except for CD4/CD8 and LFA-1 as expected.

3.3.9 ZAP-70(AS) Cell Lines Signal in Response to Cognate pMHC

The ZAP-70(AS) mutant was designed to retain wildtype function when the small molecule inhibitor 3-MB-PP1 is not present, as shown by previous studies^{223,382-385}. Nevertheless, it is important to check functionality in these cell lines as they were created using different methods to those used in previous studies. As with the ZAP-70 wildtype cell lines, several functional tests were carried out to check the functionality of the TCR and ZAP-70(AS).

Firstly, ZAP-70(AS) cell lines were placed onto agonist-presenting 1st generation SLBs and their calcium flux response was measured (Figure 22). J-AS^{hi} and J-AS^{lo} cell lines showed no statistically significant difference in the fraction of cells signalling when compared to 1G4^{hi} and 1G4^{lo} respectively. The average fraction of cells signalling was 66% vs 70% for J-AS^{hi}

and 1G4^{hi} cells respectively, and 19% vs 44% average signalling for J-AS^{lo} and 1G4^{lo}, although the standard deviations for the TCR^{lo} cell lines were higher – 11.3% and 11.2% for J-AS^{lo} and 1G4^{lo} compared to 9.9% and 5.0% for J-AS^{hi} and 1G4^{hi} respectively.

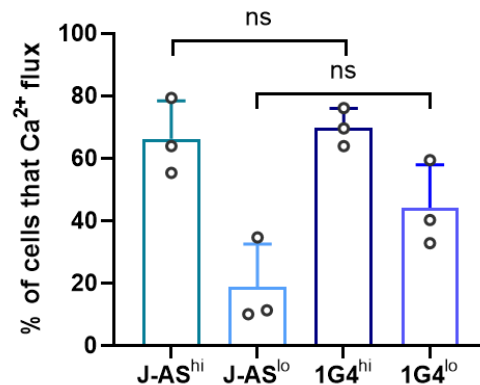


Figure 22 ZAP-70(AS) and ZAP-70 wildtype cell lines trigger comparably on 1st generation agonist-presenting SLBs Approximately 5×10^5 cells of each cell line were harvested and labelled with Fluo-4 AM before washing and placing on 1st generation agonist-presenting SLBs. The fraction of cells triggering between ZAP-70(AS) and ZAP-70 wildtype cell lines of comparable TCR expression was analysed by Student's t-test and no significant differences were found. Mean \pm SD plotted. \sim 200-1000 cells analysed per repeat over 3 repeats.

3.3.10 ZAP-70(AS) Cells Form Immune Synapses on 1st Generation SLBs

Cells were also tested for the formation of immune synapses and accumulation of pMHC and ICAM-1 on SLBs (Figure 23). Samples were left to settle on 1st generation agonist-presenting SLBs with labelled pMHC and ICAM-1 for 10 minutes at room temperature and fixed prior to imaging (same preparation as in section 3.3.6). Similarly to 1G4^{hi} cells, J-AS^{hi} cells readily accumulate pMHC and ICAM-1 under activating conditions, whereas J-AS^{lo} cells do not generally show significant pMHC accumulation. However, they show clear spreading and accumulation of ICAM-1, indicating productive signalling through the TCR. DKO-AS cells show negligible pMHC accumulation on bilayers, and some visible ICAM-1 accumulation, which is not unexpected since the cells are imaged in a buffer containing magnesium ions, which are known to stabilise a conformation of LFA-1 that is more permissive to ICAM-1 binding (see section 1.4.2).

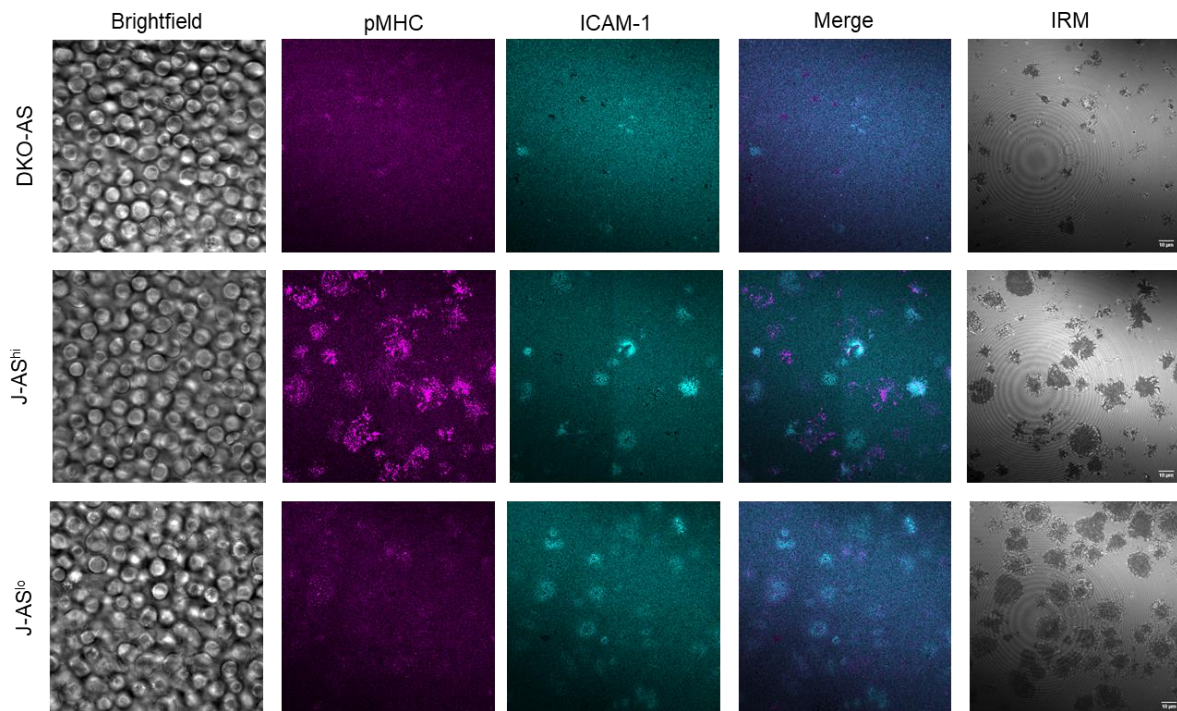


Figure 23 **ZAP-70(AS)-expressing cell lines accumulate pMHC and ICAM-1 and form immune synapses on 1st generation agonist pMHC-presenting SLBs** Approximately 5×10^5 cells were harvested, washed in PBS-MgSO₄ and left to settle on 1st generation agonist-presenting SLBs with labelled pMHC and ICAM-1 for 10 minutes before imaging to demonstrate immune synapse formation. IRM footprints of cells illustrate spreading caused by TCR signalling which is absent in DKO-AS cells. SLBs comprised proteins at the following concentrations: agonist pMHC 0.3 ng/ μ l, null pMHC 9.7 ng/ μ l, ICAM-1 1.2 ng/ μ l. Scale bar 10 μ m.

3.3.11 Effect of ZAP-70(AS) Inhibition by 3-MB-PP1

After confirming that the functionality of ZAP-70(AS)-Halo is comparable to wildtype ZAP-70 by various methods, and that the HaloTag provides a suitable labelling method, the next step was to confirm the ability of the small molecule inhibitor 3-MB-PP1 to ablate its kinase activity.

Firstly, calcium flux assays were carried out on 1st generation agonist-presenting SLBs, where after Fluo-4 AM labelling, aliquots of J-AS^{hi} cells were either washed and resuspended in various concentrations of 3-MB-PP1 in PBS-MgSO₄ or the maximum equivalent volume of DMSO as a control (Figure 24). Previous studies use concentrations between 2.5 μ M and 10 μ M 3-MB-PP1^{223,382-385} so this range was selected for testing. A dose-dependent effect on the fraction of cells signalling could be observed (Figure 24B), with virtually no signalling

(average 2.7%) at a concentration of 10 μM of 3-MB-PP1. In contrast, ZAP-70 wildtype-expressing cells were not affected by 10 μM 3-MB-PP1 (average of 64% control vs 60% treated), indicating the effect is specific to ZAP-70(AS).

Inhibition of ZAP-70(AS) with 3-MB-PP1 was confirmed with J-AS^{lo} and DKO-AS cell lines (Figure 24C). Like J-AS^{hi}, J-AS^{lo} cells had an almost complete ablation of signalling (average 2.5%) on 1st generation bilayers, although this did not reach statistical significance, likely due to the large spread of data (SD 11.3%) for J-AS^{lo} cells under control conditions.

Treatment with 3-MB-PP1 also has effects on the qualitative nature of calcium flux. As the concentration of the drug was increased, the number of calcium spikes per cell decreased (Figure 24D). This effect became significant at 5 and 10 μM where 19.2% cells had more than one calcium spike at 5 μM , decreasing to 7.2% at 10 μM . Whilst not statistically significant due to high variability (and lower power from a smaller sample size of cells signalling with increasing 3-MB-PP1), there was also a trend towards smaller amplitudes of calcium spikes, decreasing from 8.1 x baseline intensity for control cells to 4.3 x baseline intensity with 10 μM 3-MB-PP1 (Figure 24E), and longer median signalling times (DMSO treated: 77 seconds, 10 μM 3-MB-PP1 treated: 202 seconds) with increasing concentrations of 3-MB-PP1 (Figure 24F).

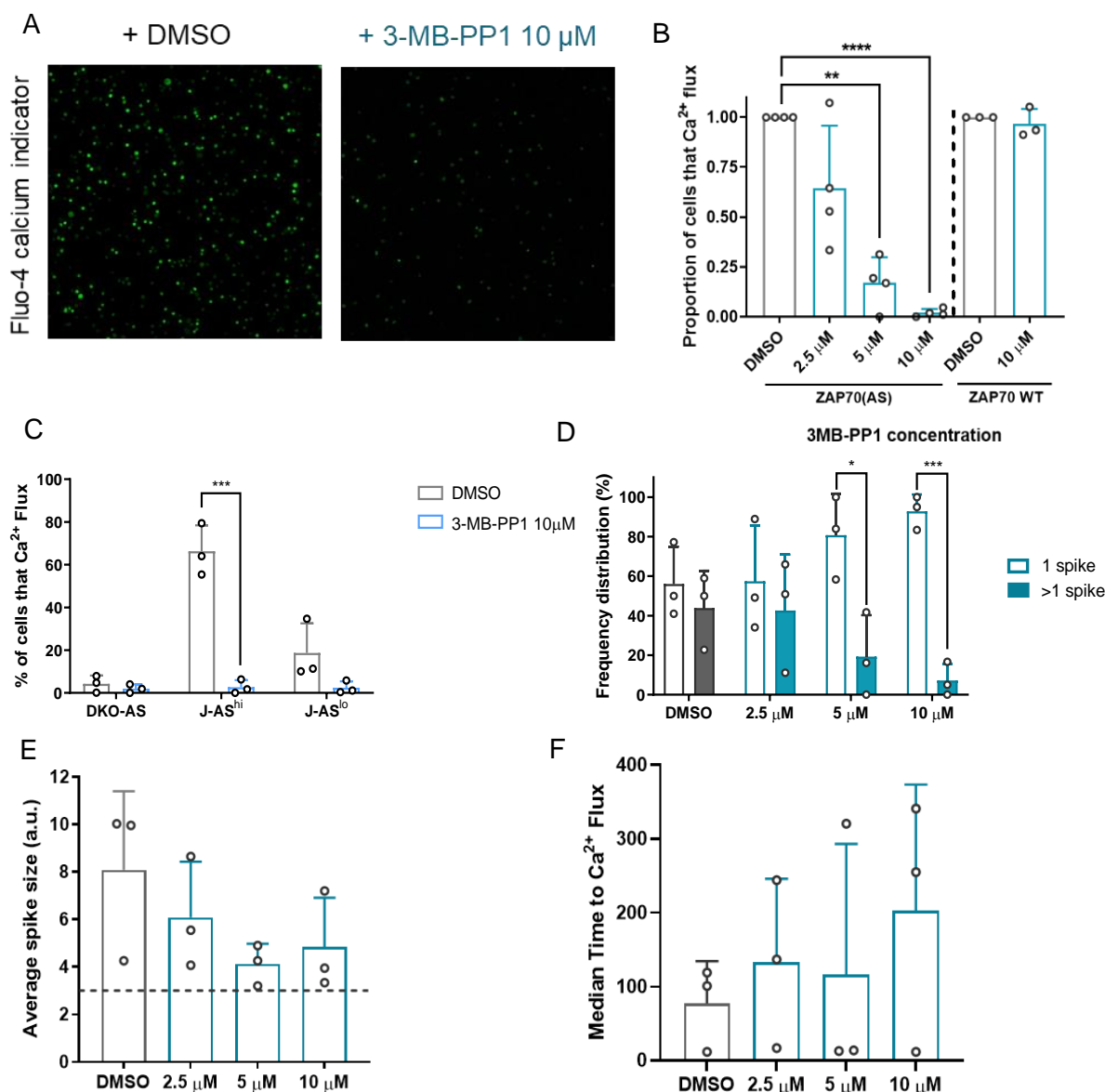


Figure 24 3-MB-PP1 abolishes TCR signalling in ZAP-70(AS)-expressing cells (A) Representative image of a field of view of cells labelled with Fluo-4 AM on 1st generation agonist-presenting SLBs under control conditions (left) or after washing in PBS-MgSO₄ containing 10 μM 3-MB-PP1 (right). (B) Normalised fraction of cells triggering on 1st generation agonist-presenting SLBs with increasing concentrations of 3-MB-PP1. Analysed with an RM one-way ANOVA with DMSO as the control condition. No significant difference in triggering occurred in ZAP-70 wildtype cells, determined by Student's t-test. (C) ZAP-70(AS) cells with different TCR expression were treated with DMSO or 10 μM 3-MB-PP1 and placed onto 1st generation agonist-presenting SLBs. A significant decrease in signalling was observed with J-AS^{hi} cells, but not J-AS^{lo} or DKO-AS under these conditions. Each condition was tested per cell line using a Student's t-test. (D) The same experiment as (B), with the spike frequency plotted for each condition. (E) Average calcium spike size for cells used in (B) Dashed line indicates the threshold for cells to be considered triggered. (F) Median time to triggering for cells used in (B). Statistical analysis in (E) and (F) conducted using ordinary one-way ANOVA with DMSO as the control group. Mean ± SD plotted in all graphs. ~200-1000 cells analysed per repeat. *** = p < 0.001, ** = p < 0.01 * = p < 0.05. Non-significant comparisons not shown.

3.3.12 ZAP-70(AS) Cells Activate on Protein-Coated Surfaces and APCs

Finally, to further confirm that the downstream signalling pathways were intact, and compare functional responses to naturally-presented antigen, the ZAP-70(AS) and ZAP-70 wildtype cells were subjected to activation assays on activating surfaces and APCs (Figure 25). Activation protocols are described in detail in section 3.2.7 and 3.2.8, but in brief, 96-well plates were coated with either OKT3 antibody, or U-2 OS APCs which were pulsed with 9V peptide. Cells were allowed to interact with these surfaces/cells in the presence of 10 μ M 3-MB-PP1, 10 μ M PP2, or matched volume of DMSO, for 18 hours before collection and staining with antibodies against CD3 ϵ , CD8 α , CD25 and CD69 in separate 96-well plates. Cells were gated on live singlets expressing CD8 and expression levels for each protein were normalised to an unstimulated control condition.

Overall, results between ZAP-70(AS) and ZAP-70 wildtype cell lines were similar. All cell lines expressing TCR showed marked downregulation of the TCR as the concentration of OKT3 increased – an average reduction of 92% for J-AS^{hi} and 63% for J-AS^{lo}, while 1G4^{hi} and 1G4^{lo} were reduced by 88% and 37% respectively. TCR downregulation was unaffected by the presence of signal-inhibiting drugs 3-MB-PP1 and PP2, corroborating another study which suggests this process may be regulated by pathways separate to those inducing T-cell activation³⁹¹ (Figure 25A, left panels). This effect however was generally less pronounced on U-2 OS APCs (Figure 25B, left panels), with J-AS^{hi} and J-AS^{lo} decreasing expression by 59% and 42% respectively, 1G4^{hi} by 78%, and 1G4^{lo} by 33%. When signalling was inhibited, TCR expression only decreased by 14% for J-AS^{hi}, 19% for J-AS^{lo}, 43% for 1G4^{hi} and 14% for 1G4^{lo}. TCR negative cells (i.e., TCR KO or DKO-AS) maintained a negligible level of TCR expression across all conditions.

Cell lines with low TCR expression had little to no increase in activation markers on OKT3-coated surfaces – the highest average fraction of CD25⁺ J-AS^{lo} cells was 1.2% and 1.7% for 1G4^{lo}, and for CD69 this was 3.1% and 2.9% (Figure 25A, middle and right panels). However,

they did demonstrate some ability to activate when incubated with peptide-pulsed U-2 OS cells (Figure 25B, middle and right panels). J-AS^{lo} cells had a CD25 positive fraction of up to 7.4% and CD69 positive up to 28% while 1G4^{lo} cells were up to 8.3% CD25 positive and 22.1% CD69 positive. Inhibiting TCR signalling reduced both activation markers to negligible values, although the inhibiting effect was smaller at higher levels of stimulus.

Cells with physiological TCR expression unsurprisingly showed more pronounced activation. On OKT3, the CD25 positive fraction of J-AS^{hi} reached up to 12% and 21% for 1G4^{hi} cells, and the CD69 positive fractions were 35% and 44% respectively (Figure 25A, middle and right panels). Once again on APCs, these fractions were increased (Figure 25B, middle and right panels). The maximum fraction of CD25 positive cells was 23% for J-AS^{hi} and 45% for 1G4^{hi} while the CD69 positive fraction was 59% for J-AS^{hi} and 58% for 1G4^{hi}. Cells incubated with 3-MB-PP1 had negligible activation on either surface, but PP2 only had a large effect on activation of ZAP-70 wildtype cells on OKT3. On U-2 OS cells, CD25 and CD69-positive fractions of 1G4^{hi} and 1G4^{lo} cells were reduced but not to a comparable level to TCR KO cells. Since PP2 is known to inhibit TCR signalling, it is most likely that its effect did not last over time under such strong signalling conditions.

TCR negative cells did not show any significant increase in the activation markers CD25 and CD69 (<2%) under any activating conditions, as expected (Figure 25A and B, middle and right panels).

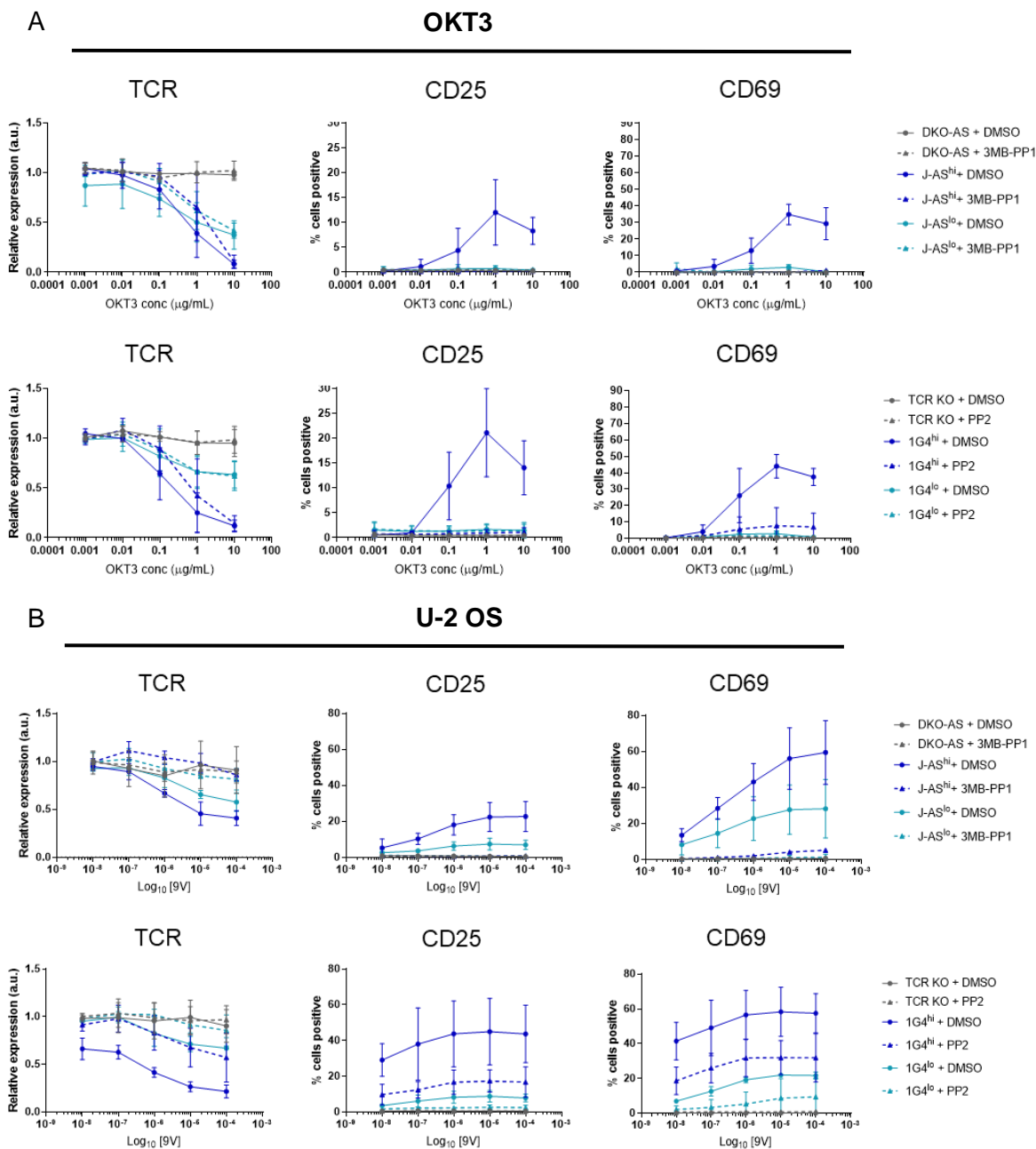


Figure 25 Comparison of activation markers between ZAP-70(AS) and ZAP-70 wildtype cells
 (A) Cells were prepared in complete medium with either 10 μ M 3-MB-PP1, 10 μ M PP2, or matched volume of DMSO and incubated with increasing concentrations of OKT3 for 18 hours before staining, washing, fixing and analysis of TCR, CD25 and CD69 expression by flow cytometry. The top panels indicate ZAP-70(AS) cell lines, and the bottom panels are ZAP-70 wild-type cells. Conditions are the same in (B) but with U-2 OS APCs pulsed with increasing concentrations of 9V peptide. All values are normalised to an unstimulated control condition and dashed lines indicate signalling-inhibited cells. Mean \pm SD plotted in all graphs. $\geq 3 \times 10^4$ cells analysed per condition. Each concentration of OKT3/9V was prepared in triplicate. 3 repeats of the entire experiment were carried out.

3.4 Discussion

In this chapter, several cell lines were created with different TCR affinities and expression levels to assess the requirements for TCR density, affinity and signalling capacity on early T-cell contact formation, activation and microcluster formation. Using the well-established Jurkat T cell line as a starting point, gp100 or 1G4 TCR-expressing CD4- CD8+ T cells with either a physiological (i.e., 'high') or low TCR expression level were created using CRISPR/Cas9 gene editing and lentiviral transduction.

Additional cell lines were created with endogenous ZAP-70 replaced by ZAP-70(AS)-Halo, which can be used to uncouple TCR binding from signalling and labelled in live cells for imaging. ZAP-70 was chosen as a target molecule because it exists proximally to the TCR in the signalling cascade, is responsible for phosphorylating key molecules including LAT, and has previously been implicated in actin architecture and integrin signalling^{384,392}, two key aspects which could affect contact formation and morphology of T cells.

These cell lines all produced a robust early response to TCR stimulation and comparable expression of key surface and intracellular proteins to Jurkats, suggesting no gross signalling abnormalities were introduced by genetic manipulation.

3.4.1 1G4 and gp100 TCR-Expressing Cell Lines as Model T-Cells

Whilst the Jurkat T cell, and model cell lines in general, are largely accepted as faithful models of primary T cells, their limitations must be acknowledged. Jurkats have an unusual karyotype, and several proteins involved in T-cell signalling, such as PTEN, SHIP, CTLA-4 and SYK, are not expressed in Jurkats³⁹³. Furthermore, LFA-1 in Jurkats is known to be relatively low³⁸⁶, and although this protein is not known to affect the signalling mechanism of the TCR, it can modulate T-cell sensitivity by anchoring the T cell to the SLB or APC^{90,331,350,386}. Boosting CD11a and CD18 on the cell lines, therefore, made their interaction

with ICAM-1 on SLBs more representative of primary cells (see section 8.3), a phenomenon which has been noted by other groups³⁸⁶. Additionally, since Jurkat cells are of the CD4+ lineage, but pMHCs used in this thesis were MHC class I-restricted, the cell lines were modified to express CD8 and not CD4. Functional data from this chapter suggests that the cell lines derived from Jurkats are still fit-for-purpose and that the proteins most likely to affect T-cell signalling are present at suitable expression levels. Additionally, cells were regularly tested for these markers to prevent phenotypic drift between experiments. However, the functionality of CD8 was not directly tested here.

CRISPR/Cas9 was used during the construction of all cell lines to create efficient and permanent knockout of proteins such as TCR α , TCR β , CD4 and ZAP-70. Based on the analysis by flow cytometry and Western blot, protein knockdowns were stable and effective. Often, studies using CRISPR/Cas9 for knocking out protein expression use single-cell methods to generate clones which are then sequenced and grown for further use. Instead, here a bulk approach was used. This is much more efficient than generating clones and is advantageous because any off-target mutations are less likely to become dominant within the bulk cell population. Testing of the cell lines' signalling competence suggests no significant changes in behaviour, but without full genetic sequencing it is impossible to know whether undesirable mutations were introduced to the cell lines.

3.4.2 ZAP-70(AS) As a Tool to Regulate TCR Signalling

ZAP-70(AS)-expressing cells have been used in several studies to control T-cell signalling. Cell lines created here were tested to ensure similarity to ZAP-70 wildtype cells in both early and later stages of signalling and were generally comparable, as expected, since the ZAP-70(AS) construct is known to function as effectively as wildtype ZAP-70 in cells when 3-MB-PP1 is not present^{223,382-385}. Furthermore, the addition of a conjugated HaloTag means that most ZAP-70 in the cell can be labelled, facilitating quantitative studies.

By using an inducible model such as ZAP-70(AS), rather than creating a knockout cell line, the cells can serve as their own controls in experiments, thus avoiding any discrepancies in cell growth or signalling that may occur by generating and culturing two genetically different cell lines. However, the replacement of endogenous ZAP-70 with a modified version requires more extensive genetic editing than a simple knockout cell line or a ZAP-70-deficient line such as the Jurkat derivative P116¹⁶¹. As with any genetic modification, this runs the risk of disturbing the genome in an unpredictable manner, and although reasonable checks were undertaken to ensure no relevant changes occurred in these cells, the possibility of aberrant genetic modifications remains. Additionally, the expression of ZAP-70(AS)-Halo in the cell lines is noticeably higher than endogenous ZAP-70 expression in Jurkats (Figure 19). Since sorting these cells for ZAP-70 in comparison to Jurkats is not possible, they were instead sorted for similar expression between cell lines, since this is how comparisons will be made in experiments.

The use of 3-MB-PP1, as with any small molecule inhibitor, has some drawbacks. It is possible that some ZAP-70(AS) molecules evade the drug within a cell, given that a very small fraction of cells sometimes signal after treatment with 3-MB-PP1. However, these cells can easily be excluded from most analyses or considered separately. Overall, 3-MB-PP1 appears to work rapidly with negligible off-target effects and suppress ZAP-70 kinase activity for up to 18 hours, as demonstrated here and in another study³⁸⁵.

3.4.3 SLBs as a Model of Antigen Presenting Cells

SLBs decorated with proteins have been established as a mainstay of investigating T-cell biology. They present a highly customisable system, with finely tuneable protein densities and free lateral diffusion^{332,394}, and have been shown to be sufficient for T-cell signalling and activation^{96,332}.

However, there are two main criticisms of this system. The first is that it is currently impossible to fully recapitulate the protein complexity of a real APC in this model, meaning that subtle differences, for example in T-cell adhesion and scanning, might be lost. The majority of experiments carried out in this thesis are focused on the differences in T-cell behaviour with and without TCR signalling or with different TCR densities, and since pMHC alone is sufficient to cause early T-cell signalling (Figure 16), and pMHC with ICAM-1 (i.e. 1st generation SLBs) is sufficient for immune synapse formation (Figure 17)⁹⁶, it is likely that the results found here are representative of what might occur *in vivo*.

Secondly, by having glass as the underlying substrate of SLBs, T cells interact with a surface far harder than anything they would encounter in the body. The estimated stiffness of glass is 10^7 - 10^8 times that of APCs³³⁷ and T cells are known to change their behaviour depending on substrate stiffness³³⁸ which presents a potential problem for glass-SLBs. However, a recent study using polydimethylsiloxane-SLBs with variable stiffnesses determined that T-cell signalling (measured by calcium flux), along with accumulation and exclusion of CD2 and CD45, respectively, appear to be largely unaffected by the underlying substrate³⁴⁰ suggesting that the SLBs used in this thesis are suitable models to study early signalling events.

4 The Relationship between Early T-Cell Contacts and TCR Signalling

4.1 Introduction

T cells must scan and respond to antigen rapidly to mount an effective immune response. In line with this, studies have indicated that T cells spend only a few minutes scanning APCs *in vivo*^{395,396} illustrating the significance of early T-cell contacts with an APC. A seminal study by Chang et al.¹³⁵ demonstrated the importance of T-cell 'close contacts' – which are areas of T cell/target cell membrane apposition of less than about 15 nm – in initiating TCR signalling, suggesting an important role for topography in early contacts and TCR signal initiation.

Recently, studies have turned to the potential role of microvilli specifically and have shown that T cells are covered in hundreds of these dynamic membrane protrusions which cumulatively scan almost the entire cell surface in just 1 minute²²³. A recent modelling-based study suggested that the size of close contacts must be carefully regulated to maintain TCR discrimination, and the optimal radius for these contacts – about 200 nm – is comparable with the size of microvilli¹⁹⁵. Furthermore, there is evidence that microvilli are enriched in proteins important for TCR signalling such as CD4, Lck, and the TCR itself^{103,194}, adding weight to the argument for their role in signal initiation.

T-cell microvilli have been measured between 70-500 nm in diameter and 100 to several hundred nm in length^{103,194}, making them challenging to image in a dynamic cell-cell context, but readily observable on two-dimensional surfaces, such as SLB-bound quantum dots, using diffraction-limited microscopy²²³. 1st generation SLBs are generally not suitable for imaging microvilli and cell topography as they lack proteins which can either be excluded or bound at close contacts, and IRM does not usually provide adequate resolution to image

single contacts. Because of this, the role and regulation of cell topography in initial contact formation is still largely unexplored.

One question that arises from the new-found importance of T-cell topography in contact formation is whether TCR-based signalling may be involved, and studies so far are divided. Cai and colleagues²²³ showed that blocking T-cell signalling using the ZAP-70(AS) system (see section 3.3.7) in transgenic murine cells did not seem to affect the scanning nature of microvilli in mouse T cells, however in another study³⁸⁴, which also used murine ZAP-70(AS)-expressing cells, the authors noted that while T cells adhered to target cells regardless of ZAP-70 activity, T cell/target cell conjugates did not progress to the formation of characteristic CTL secretory clefts, and instead showed long-lived close contacts dominated by T-cell membrane protrusions into the target cell.

Further to this, there is room to explore the role of TCR triggering, especially involving ZAP-70, during the time of significant morphological change induced after antigen is found on an APC. During this process, the T cell rapidly changes shape, polarising towards the area of membrane where the TCR is engaged and spreads over the surface of the APC to enhance further scanning³⁹⁷. This is controlled by a complex network of signalling mechanisms which modulate the cytoskeleton and is the subject of much study. Previous studies have provided evidence for ZAP-70 having a role in cytoskeletal modulation as well as signal propagation^{383,384}, therefore making use of the ZAP-70(AS) and SLB systems here could provide insights as to the role of TCR signalling in the regulation of this process.

Given the potential importance of microvilli in T-cell activation, and the lack of consistent results thus far, further study is needed to identify factors that control the functions of T-cell microvilli and the transition of the T cell from antigen scanning to spreading on the APC surface. Given the technical difficulty of imaging small and dynamic contacts in a cell-cell setting, SLBs present a good model system for directly observing early contacts. For this purpose, complex SLBs containing the glycocalyx proteins CD43 and CD45 (which are

excluded by T-cell close contacts) and the small adhesion protein CD58 (which binds CD2 at close contacts), in addition to pMHC and ICAM-1 were created (see also section 2.5.2). These SLBs are hereafter referred to as 2nd generation SLBs.

Using 2nd generation SLBs, small structures such as T-cell close contacts, presumably made by microvilli, can be readily observed using TIRFM. The three ZAP-70(AS) cell lines provide a way to test the potential role of TCR triggering on the formation of these early contacts in two ways: firstly, by presenting different densities of TCRs available for antigen binding; and secondly by controlling the ability of the TCR to signal productively. Therefore, this chapter will focus on the characterisation of T-cell microvilli, the transition between scanning and spreading on both 1st and 2nd generation SLB surfaces, and how this is modulated by TCR signalling and expression.

4.2 Materials and Methods

4.2.1 Confocal Z-Stack Imaging

Sterile μ -Slide 8 well glass chambers (Ibidi) were prepared with a PLL coating as previously described (section 2.5.3). 1×10^6 cells were centrifuged at 2000 rpm for 90 seconds in a MiniSpin (Eppendorf) and resuspended in PBS containing the appropriate dilution of relevant Fab or antibody (CD3 ϵ – Fab-Halo made in-house clone UCHT1, CD62L – BioLegend antibody clone DREG-56, CD2 – Biolegend antibody clone RPA-2.10, CD11a – BioLegend antibody clone HI111). Samples were left covered on ice for one hour before centrifuging as before and washing twice in 500 μ l PBS containing either 10 μ M 3-MB-PP1 or equivalent volume of DMSO. Labelled cells were fixed in 200 μ l of 4% PFA with 0.25% glutaraldehyde (Sigma Aldrich) in PBS (plus DMSO or 3-MB-PP1), covered, at room temperature for 30 minutes. 22 μ l of a 10X solution of Cell Mask (final concentration 0.5 μ g/ml, Thermo Fisher) was added for the final 15 minutes. Cells were finally centrifuged and resuspended in 100 μ l PBS before adding to PLL-coated slides. Samples were imaged immediately.

Images were acquired on a Zeiss 880 LSM inverted confocal microscope. Cells were selected for acquisition using the Cell Mask channel to find non-apoptotic cells. The first and last Z stack positions were selected to cover the entirety of the cell body. Laser powers were adjusted to avoid bleaching the sample over the acquisition time. Each Z-slice was taken with the smallest spacing possible and high averaging (8x).

To determine relative localisation of cell surface proteins, composite Z-projections of Cell Mask membrane dye and relevant label (i.e., antibody or Fab against protein of interest) were created in Fiji from 2-4 slices of the cell midplane, in order to include as much signal as possible from each microvillus, given that they could be captured in multiple focal planes. Freehand line profiles were created for several microvilli between 100-500 nm in length per cell, using only the Cell Mask channel to blind results. The intensity profiles for each

channel, as well as distance, were min-max normalised to ensure reproducibility across different microvilli. The average intensity values for each channel were calculated for each 1/5th of the microvillus, and the 'label' intensity was divided by the Cell Mask intensity. This gave an average value of correlation between the label and cell membrane for each 1/5th of the microvillus. Values across different microvilli and cells were pooled and analysed.

4.2.2 2nd Generation SLB-Bound Protein Production

Other His-tagged proteins such as ICAM-1, CD45RABC, CD58, and CD43 were purified as previously described, with FPLC and Coomassie staining analysis to determine monomeric protein fractions for future use (section 2.3.6 and 2.3.7). Proteins were diluted and stored in PBS at -80°C after snap freezing in a dry ice and isopropanol mixture.

4.2.3 Initial Adhesion to SLBs

Cells were labelled and processed as previously described (section 2.5.5.1) for calcium flux experiments with DMSO or 3-MB-PP1 treatment and placed onto prepared, equilibrated and washed agonist 1st or 2nd generation SLBs. Timelapse images were acquired as with calcium flux experiments and analysed using the same custom MATLAB code.

Tables were constructed using the data provided for time to adherence per cell, with cells still not adhered after the length of the video given a value of 700 seconds (total length of the video was 600 seconds). Using these values, the fraction of adherence during the video could be calculated, as well as the median time to adhere and frequency distribution charts for each cell line and condition. Cells landing on the SLBs later in the video (≤ 300 seconds before the end of acquisition) were automatically excluded to avoid being counted as non-adherent.

4.2.4 Protein accumulation on SLBs – Imaging and Analysis

1st or 2nd generation agonist-presenting SLBs were created with labelled pMHC and ICAM-1. Approximately 5×10^5 cells were centrifuged at 2000 rpm for 90 seconds in a MiniSpin (Eppendorf) and washed twice in 500 μ l pre-warmed 0.22 μ m-filtered PBS-MgSO₄ and 10 μ M 3-MB-PP1 or matched volume of DMSO. Cells were finally resuspended in 50 μ l of the same solution, placed onto washed SLBs and left to interact with the bilayer for 10 minutes at room temperature. Excess liquid was then removed from the wells and 15 μ l of 4% PFA with 0.25% glutaraldehyde was added. Samples were fixed for 30 minutes at room temperature before washing with PBS and immediate imaging of the SLB proteins and IRM footprints. Images were acquired on a Zeiss 880 LSM inverted confocal microscope.

Images were analysed using Fiji. Areas under the cells were defined by manual thresholding based on the IRM channel intensity and masks were created for numerous individual cells, which were used to determine the maximum and average intensity in the area using the analyse particles tool. The average background intensity of each SLB protein was determined by selecting 5 areas spread across the field of view where no cells were present, to mitigate for small variations in illumination. These areas were as large as possible to ensure best possible averaging of results. The average intensity across these areas was determined and this was used as a baseline for calculating the relative enrichment of SLB proteins under each cell by dividing the average intensity under the cell to the average background intensity.

4.2.5 Confocal IRM-based Cell Area Imaging and Analysis

Interference reflection microscopy was carried out to assess the size of cell 'footprints' (i.e., the area of close contact between the cell and surface). Approximately 5×10^5 cells were centrifuged at 2000 rpm for 90 seconds in a MiniSpin (Eppendorf) and labelled with UCHT1 Fab-488 (final concentration 20 μ g/ml) at 37°C for 10 minutes in complete RPMI media

(total volume 200 μ l). Cells were then centrifuged as before and washed twice in 500 μ l pre-warmed 0.22 μ m-filtered PBS-MgSO₄ and 10 μ M 3-MB-PP1 or matched volume of DMSO. Cells were finally resuspended in 50 μ l of the same solution and placed onto 1st generation agonist-presenting SLBs after 3 minutes equilibration in the microscope incubator. Images were acquired on a Zeiss 880 LSM inverted confocal microscope. Images were taken every 10 seconds for 65 frames (~11 minutes), with definite autofocus applied every frame.

The IRM channel was opened in Fiji and thresholded manually. Cells with uneven illumination (e.g., the sides of the field of view), focus fluctuations affecting IRM, or those positioned on the edge of the field of view were discarded, as well as those reaching their maximum area at the final frame (to only include cells which were certain to have reached their maximum size). The 'analyse particles' tool was used to measure the size of each cell 'footprint' for each frame, which was then used to determine the maximum size reached and speed of spreading over time.

4.2.6 Microvillar Contact Imaging

Approximately 5×10^5 cells were centrifuged at 2000 rpm for 90 seconds in a MiniSpin (Eppendorf) and labelled with 1 μ l Fluo-4 AM (Thermo Fisher; stock prepared at 500 μ g/ml in DMSO) and Cell Mask-647 (Thermo Fisher, final concentration 0.5 μ g/ml) at 37°C for 10 minutes in complete RPMI media (total volume 200 μ l). Cells were then centrifuged as before and washed twice in 500 μ l pre-warmed 0.22 μ m-filtered PBS-MgSO₄ and 10 μ M 3-MB-PP1 or matched volume of DMSO. Cells were finally resuspended in 50 μ l of the same solution and placed onto 2nd generation agonist-presenting SLBs with CD43 and CD45 labelled with Alexa Fluor-555 after 3 minutes equilibration in the microscope incubator. Images were acquired using a custom-built TIRF microscope (Klenerman group). Images were taken with 100 ms exposure every 2 seconds for 15 minutes, with perfect autofocus applied. Laser powers used were optimised for good signal to noise and to avoid bleaching.

4.2.7 Close Contact Analysis

Quantitative image analysis was performed with custom software (written by Markus Körbel, Klenerman group) run on Python³⁹⁸ with Numpy³⁹⁹, Matplotlib⁴⁰⁰, Pandas⁴⁰¹, Scikit-image⁴⁰², Scipy⁴⁰³).

Three-colour timelapse images were acquired by TIRFM for T cell/SLB contact analysis. The channel corresponding to the cell membrane dye was used to segment each cell using the Watershed algorithm and the 488 channel was used to identify the calcium flux within each cell. Pre-analysis image processing included Difference of Gaussian filtering, binary mark generation by global threshold, small object removal and hole filling. T cells interacting with the bilayer show minimal (x, y) position variation over time therefore leading to overlapping masks in time. A larger Difference of Gaussian filter was used in the final frame to define cell positions defined by local maxima and separated by at least the cell radius. These were then used as seeds for Watershed segmentation. Disconnected regions were assigned to the most proximally labelled region not further than twice the cell radius. To analyse close contacts, TIRFM images were divided by the flat-field, which was obtained by summing and normalising a separate image stack of the SLB before cells were added. A rolling ball filter was applied in the time dimension followed by a Gaussian filter in x & y on this image stack. The Laplacian of the filtered image was calculated using the Sobel operator for partial derivatives. The images were then binarized using hysteresis thresholding. The two thresholds were defined as $mean(I_{notCZ}) + h \cdot std(I_{notCZ})$, with $h = 2, 4$ and I_{notCZ} all pixel intensities of the calculated Laplacian outside of contact zones. Close contacts bigger than a minimum size were labelled. Cells reaching their maximum size or maximum number of Close contacts at the last frame of the timelapse were excluded from some analyses (max CC size, max CZ size and max number of CCs) to avoid including cells which had appeared late in the timelapse and were likely still in the process of spreading.

Additionally, the calcium response was measured for each cell. This was calculated by taking the mean fluorescence intensity at a circle centred at the centroid of a close contact. If a contact zone was missing at a timepoint, it was linearly interpolated from the next neighbouring centroids for that cell. Calcium traces for each cell were used to determine time to calcium signalling and cell adhesion. Features for contact zones and close contacts are determined by pixel intensity values. Cells that did not flux calcium were excluded from the control DMSO condition and vice versa under 3-MB-PP1 treatment.

4.3 Results

Cell morphology, protein localisation and contact formation with SLBs were analysed to determine if, and how, TCR signalling and expression may affect these interactions.

4.3.1 Cell Morphology is not Affected by TCR or ZAP-70 at Rest

Since ZAP-70 is known to regulate T-cell morphology^{383,384}, cells were initially observed in a resting state to see whether the morphology of ZA70(AS) cells is as expected and if TCR or ZAP-70 signalling affects cell shape before it encounters an SLB.

3D projections of J-AS^{hi}, J-AS^{lo} and DKO-AS cells were made by washing cells in PBS-MgSO₄ and either 10 µM 3-MB-PP1 or equivalent volume of DMSO, then fixing for 30 minutes in a solution containing Cell Mask membrane dye before placing onto washed poly-L-lysine coated slides to prevent movement during imaging. After setting the first and last z-stack locations (i.e., the top and bottom of the cell) on a randomly-chosen cell, 20-40 image slices were acquired with minimal gaps between slices and high averaging across the entire size of the cell. These were then processed in Fiji to obtain reconstructed Z-projections of an entire cell.

Microvilli were readily observed on the surface of all T-cell lines, as well as other features in the membrane such as membrane ruffles which are typical of resting T cells^{194,223}. Three representative cells for each condition are shown in Figure 26. A semi-quantitative analysis confirmed that there was no substantial difference in the size or morphology of cells treated with 3-MB-PP1 or DMSO.

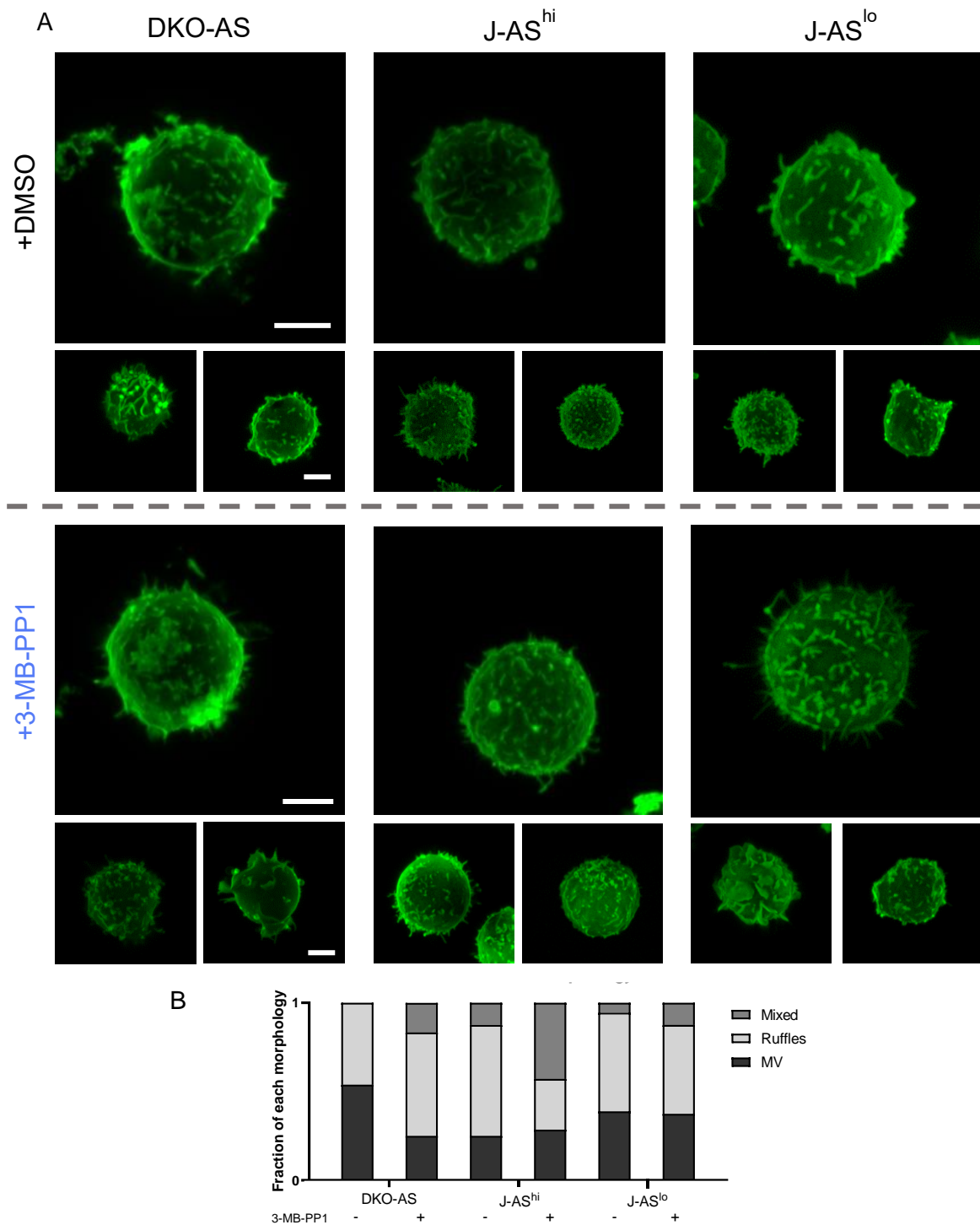


Figure 26 T-cell morphology at rest is not affected by TCR or ZAP-70 (A) Approximately 1×10^6 cells labelled with UCHT1 Fab at $20 \mu\text{g/ml}$ on ice for one hour in the dark before centrifuging washing in PBS with ether $10 \mu\text{M}$ 3-MB-PP1 or DMSO. Labelled cells were fixed in 4% PFA with 0.25% glutaraldehyde and DMSO/3-MB-PP1, covered, at room temperature for 30 minutes, with Cell Mask-647 added for the final 15 minutes. Cells were centrifuged and resuspended before being placed onto PLL-coated slides. Samples were imaged immediately on a Zeiss 880 confocal using the Z-stack function. Images show cells with different morphologies as occurred across all cell lines and conditions tested. Scale bar $5 \mu\text{m}$. (B) Cells were categorised manually as having a morphology dominated by microvilli (MV), ruffles, or a mixture of both. No substantial differences were observed between any cell lines or conditions. 7-19 cells per condition were acquired across 3 repeats and pooled. Statistical testing was not performed.

4.3.2 The TCR is Slightly Enriched on Microvilli Tips

Previous studies have suggested that microvilli are enriched in signalling proteins, adhesion proteins, and the TCR itself^{103,194}. To test this, cells were prepared as above but with an additional initial step of labelling TCR complexes using UCHT1 Fab-488. Cells were labelled for an hour in the dark on ice before washing in PBS-MgSO₄ with DMSO or 3-MB-PP1, fixing, and labelling the membrane with Cell Mask-647.

Cells were selected using only the Cell Mask channel to minimise bias. Z-stacks of individual cells were taken in both Cell Mask and UCHT1 Fab channels in the same manner as before. Some cells were acquired in totality for illustrative purposes, but for analysis, a 3-5 slice Z-stack was acquired from many cells at the approximate midplane to capture complete profiles of several microvilli for analysis.

Relative protein enrichment graphs were constructed by Z-projecting the stacks taken of the cell midplanes in each channel, then merging them to form a composite image. Intensity values and distance across the cell body and into the microvillus were normalised and the intensity of UCHT1 Fab was divided by the Cell Mask intensity, giving a relative enrichment score where a value of 1 indicates no enrichment or depletion, while values higher or lower than this suggest enrichment or depletion of labelled protein respectively. Relative distance was separated into 1/5th sections, to incorporate the cell body in the first 1/5th of the distance and several sections of the entire microvillus in the rest.

Firstly, a positive control stain of CD62L (L-selectin) was acquired and analysed in this way for method validation, since this protein is known to be enriched on microvillar tips⁴⁰⁴ (Figure 27A). Indeed, analysis of CD62L-stained cells showed strong and significant enrichment on microvillar tips (enrichment score 3.0), and depletion on the cell body (score of 0.57).

J-AS^{hi} and J-AS^{lo} cells were analysed separately to see whether there was a difference in TCR localisation when TCR density is different. Despite high variability, both cell lines cells showed a small but significant enrichment of TCRs towards the tips of microvilli (Figure 27B and C), corroborating previous work^{103,194}. Average enrichment scores for the cell body were 0.96 and 1.33 for J-AS^{hi} and J-AS^{lo} respectively, while the most distal portion had an average enrichment of 1.81 for J-AS^{hi} and 1.84 for J-AS^{lo}. While there was a trend towards TCR depletion on the middle portion of the microvilli, this was not significant in either case.

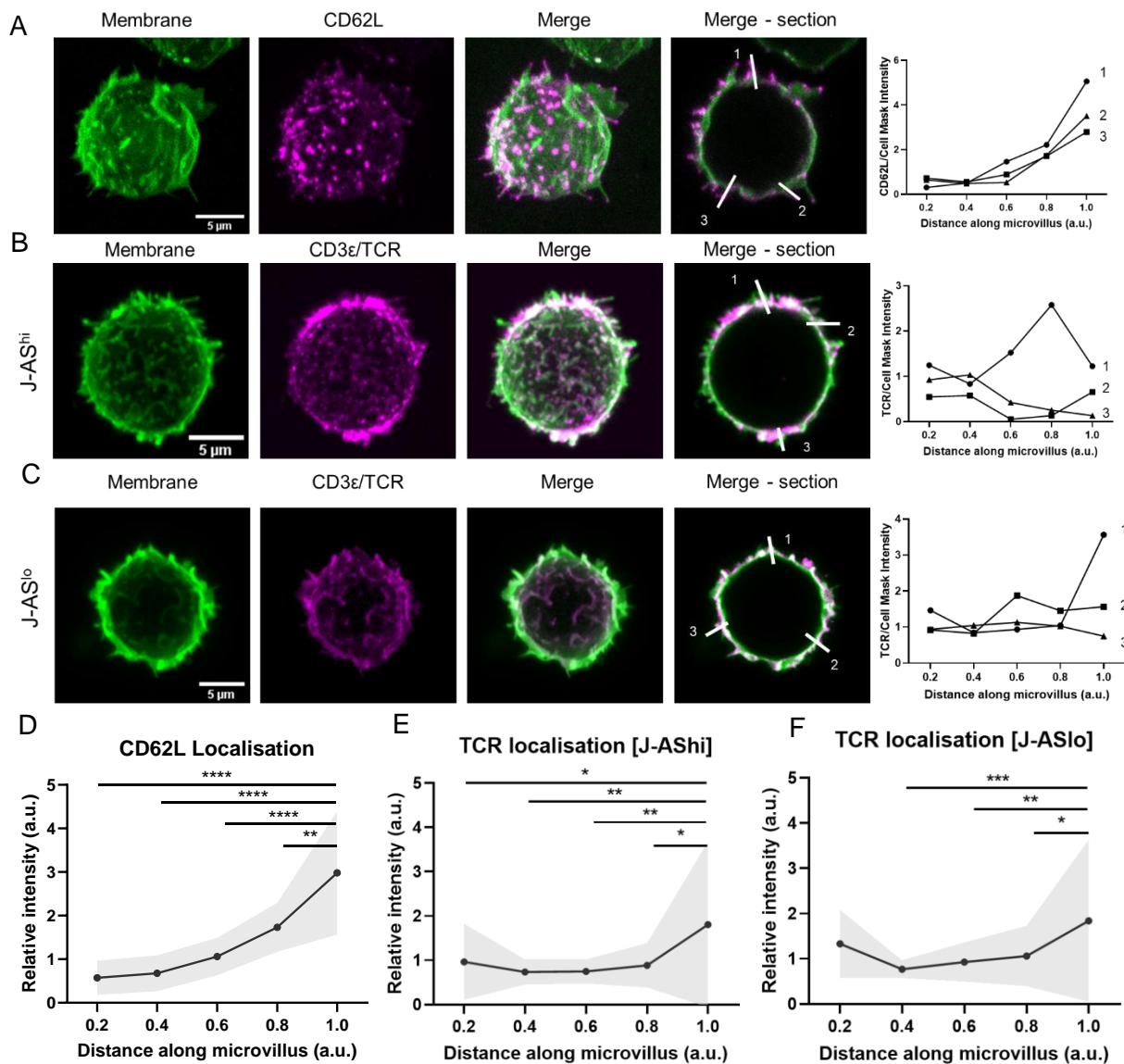


Figure 27 The TCR displays a slight preference for microvillar tips Cells were labelled with antibody or Fab against the relevant surface protein and Cell Mask membrane dye on ice, then washed, and fixed in suspension. (A) Representative image of a J-AS^{hi} cell stained with anti-CD62L antibodies. Relative intensity plots for each microvillus are shown on the right. (B) and (C) Representative images of J-AS^{hi} and J-AS^{lo} cells stained with UCHT1 Fab-Halo, and individual microvilli plots on the right. (D) Pooled relative intensity CD62L of 9 microvilli from 3 cells (mean ± SD plotted) against the relative distance away from the cell body. (E) Same plot for intensity of TCR on J-AS^{hi} cells pooled from 23 microvilli across 8 cells (F) Same plot for intensity of TCR on J-AS^{lo} cells pooled from 26 microvilli across 9 cells. 3 biological repeats were acquired for each condition and the mean intensity score at each distance was analysed by ordinary one-way ANOVA with Tukey's multiple comparisons. **** = p < 0.0001 *** = p < 0.001, ** = p < 0.01 * = p < 0.05. Non-significant comparisons not shown.

4.3.3 The Adhesion Proteins CD2 and LFA-1 have Broadly Homogeneous Distribution Across Microvilli

This analysis was also carried out for CD2, a small adhesion molecule on T cells which is involved in early contact formation^{100,185} and CD11a, the subunit of LFA-1 which is unique to this integrin heterodimer⁹⁴. Both proteins are involved in signalling pathways which interlink with the TCR^{90,97,350}, therefore may influence antigen-stimulated changes in T-cell behaviour.

Pooled data from CD11a-stained cells did not show any significant enrichment of the protein to a specific portion of the microvilli (Figure 28A). Enrichment values were 1.05 for the cell body and 1.41 at the tip, so there is a small trend towards a preference for more distal portions. Localisation for CD2 was very similar (Figure 28B), showing a trend towards tip enrichment, which would be expected based on previous work¹⁰³. At the cell body the enrichment score was 1.02, increasing to 1.26 at the microvillus tip. A significant change in localisation was present between the middle and tip of the microvillus, but this did not hold true for other segments.

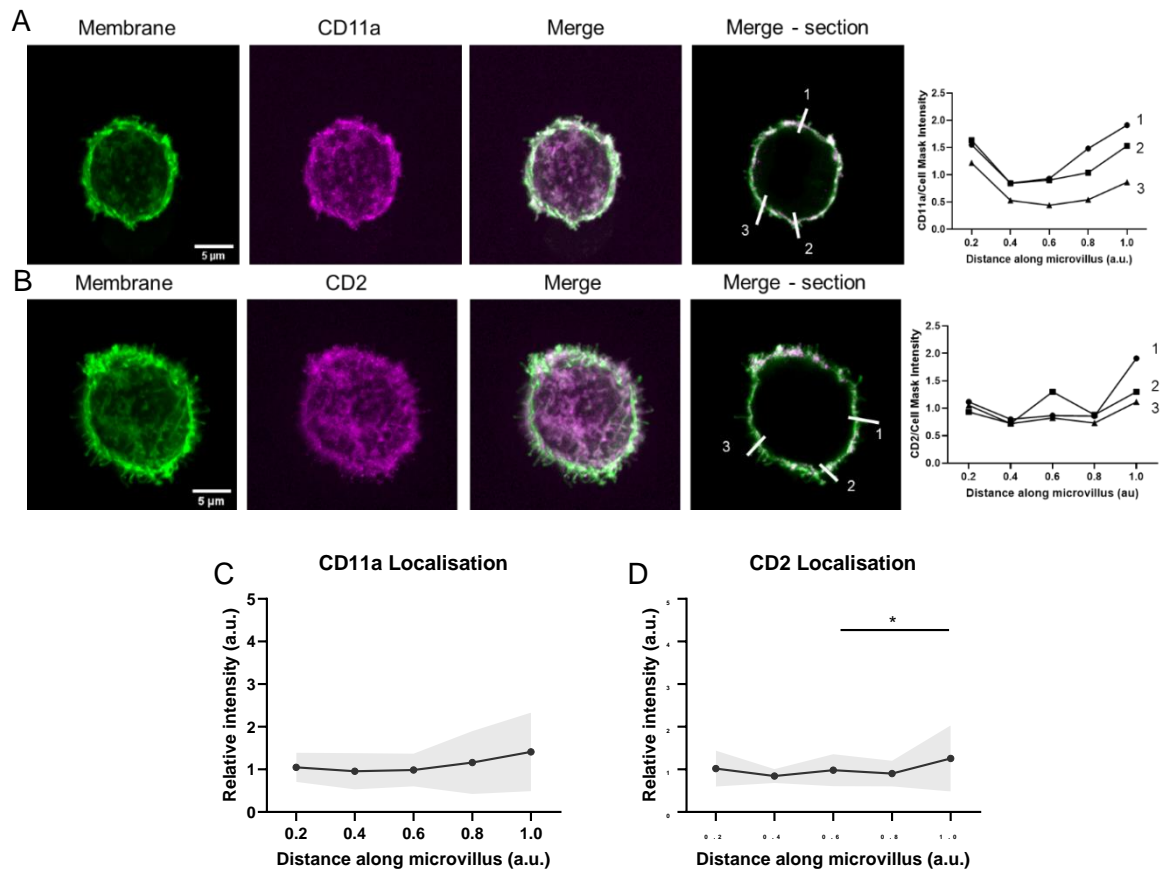


Figure 28 CD11a and CD2 have broadly homogeneous distribution on the cell membrane J-AS^{hi} cells were labelled with antibody or Fab against the relevant surface protein and Cell Mask membrane dye on ice, washed, and fixed in suspension. (A) Representative image of a cell stained with anti-CD11a antibodies. Relative intensity plots for each microvillus are shown on the right. (B) Representative images of cells stained with anti-CD2 antibody, and individual microvilli plots on the right. (C) Pooled relative intensity CD11a of 24 microvilli from 7 cells (mean \pm SD plotted) against the relative distance away from the cell body. (D) Same plot for relative intensity of CD2 pooled from 24 microvilli across 6 cells. 3 biological repeats were acquired for each condition and the mean intensity score at each distance was analysed by ordinary one-way ANOVA with Tukey's multiple comparisons. *** = $p < 0.001$, ** = $p < 0.01$ * = $p < 0.05$. Non-significant comparisons not shown.

4.3.4 T-Cell Interactions with 1st Generation SLBs: Dependence on TCR expression and Signalling

4.3.4.1 Adhesion to 1st Generation SLBs is Independent of TCR and ZAP-70

T cells must adhere to an APC or target cell before close contacts are made. Therefore, adhesion to agonist-presenting SLBs was tested under signalling and non-signalling (i.e., ZAP-70-inhibited) conditions.

Cells were prepared as per the standard protocol for calcium flux videos (section 2.5.5.1) with washing in either DMSO or 3-MB-PP1-containing PBS-MgSO₄, and placed onto

prepared, washed and equilibrated agonist-presenting SLBs for timelapse imaging. Using pooled data from thousands of cells per condition, the total fraction of cells adhering to the SLB, and the frequency distributions of adhesion times were analysed (Figure 29).

When looking at the total fraction of cells adhering to the SLBs (Figure 29A, left panel), all cells and conditions had an average total adhesion of $\geq 81\%$. On 1st generation SLBs, the average fraction of cells adhering under control conditions was 92%, 98% and 96% for DKO-AS, J-AS^{lo} and J-AS^{hi} respectively. When ZAP-70 was inhibited by 3-MB-PP1 treatment, the matching fractions were 86%, 87% and 97%. While there was greater variability during 3-MB-PP1 treatment, this did not significantly affect total adhesion.

Looking more closely, the median time to adhere on 1st generation SLBs was 56 s under control conditions versus 64 s with ZAP-70 inhibition for DKO-AS cells, 30 s versus 29 s for J-AS^{hi} and 28 s versus 47 s for J-AS^{lo} (Figure 29A, right panel). There was no significant difference between either cell lines or treatments, although there was a trend towards longer adhesion times for DKO-AS cells in both conditions.

Finally, cumulative frequency distribution graphs were constructed to visualise the rate at which cells adhere to the SLBs under each condition (Figure 29B). Rates of adhesion between control and ZAP-70-inhibited conditions overlapped substantially in all cell lines, suggesting that initial adhesion is not dependent on either TCR expression or signalling capacity. This corroborates well with previous studies examining cell-cell contacts^{383,384}.

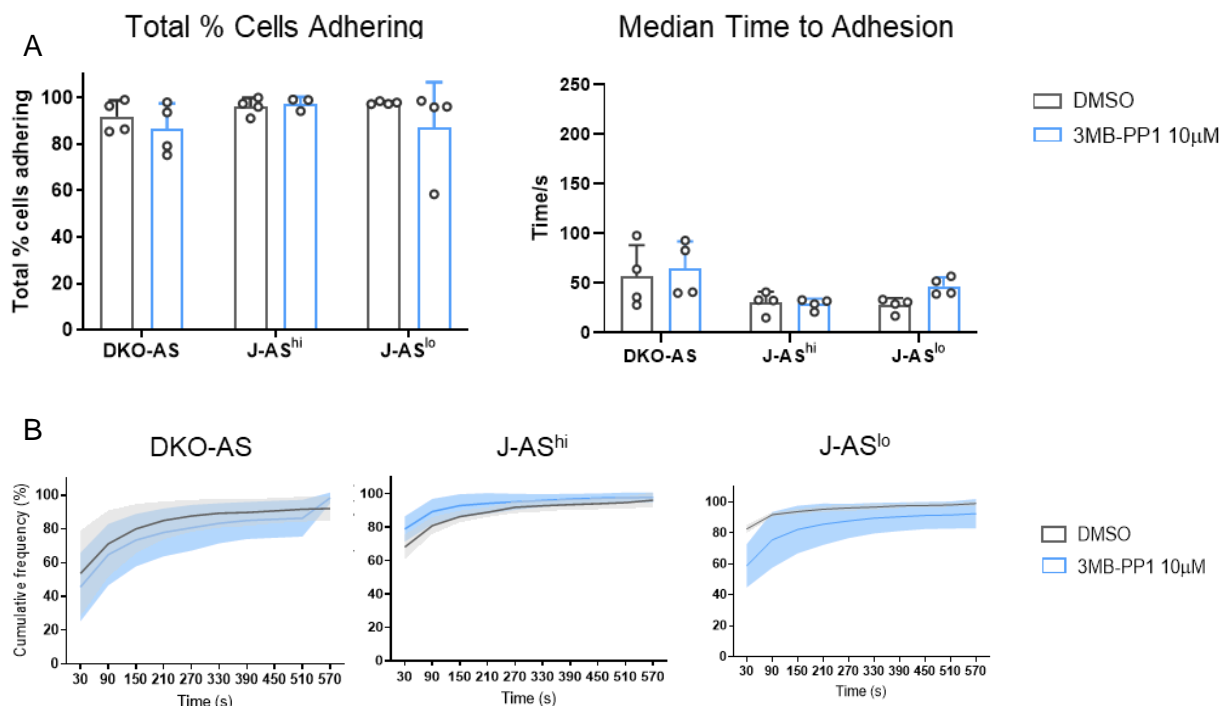


Figure 29 Initial adhesion to 1st generation SLBs is independent of TCR expression and ZAP-70 activity Cells were labelled with Fluo-4 AM, washed in PBS-MgSO₄ with DMSO or 3-MB-PP1 and placed onto agonist-presenting 1st generation SLBs. Custom MATLAB code was used to analyse various biophysical metrics of hundreds of cells per repeat over 3-5 repeats. (A) Percentage of cells adhering to the SLBs over the course of a 10 minute timelapse (left) and median time to adhesion per cell (right) for 1st generation SLBs. (B) Pooled data from all repeats per condition showing the rate of adhesion to 1st generation SLBs in a cumulative frequency distribution plot. Mean \pm SD plotted in all graphs. No statistically significant difference was found between any of the cell lines or treatments for any of the metrics analysed using a two-way ANOVA test with Šídák's multiple comparisons (only tested in panel A).

4.3.4.2 pMHC and ICAM-1 Accumulation are Regulated by TCR Density and ZAP-70 Signalling on 1st Generation SLBs

Interaction of both adhesion proteins and TCR/pMHC on the T cell and APC facilitate and induce T-cell activation^{96,99,102}. Therefore next, the effect of TCR expression and signalling was assessed on the cells' ability to accumulate pMHC and ICAM-1 on SLBs.

1st and 2nd generation agonist-presenting SLBs were created with labelled pMHC and ICAM-1. A high concentration (0.3 ng/ μ l) of agonist pMHC was used so that relative accumulation could be observed under cells, since the concentrations usually used to induce signalling (typically 0.05 ng/ μ l or ≤ 10 molecules/ μ m² on 2nd generation SLBs, 0.2 ng/ μ l on 1st

generation SLBs) are not readily visible. Approximately 5×10^5 cells from each cell line (DKO-AS, J-AS^{hi} and J-AS^{lo}) were placed onto agonist-presenting SLBs and left for 10 minutes at room temperature after being washed in PBS-MgSO₄ and 10 μ M 3-MB-PP1 or matched volume of DMSO. After fixing and washing, images were taken of several fields of view after focussing on the SLB surface, and dozens of cell footprints were analysed to determine relative protein enrichment by comparing mean intensity under each cell to the background intensity where no cells were present. Cells with a comparable intensity of SLB proteins relative to the background would produce a relative intensity value around 1, while accumulation and exclusion under a cell would result in values higher or lower than 1 respectively. Since ICAM-1 is usually simultaneously excluded and accumulated under an activating cell (probably due to topography fluctuations and variations in LFA-1 binding affinity due to signalling), the spread of relative intensity values for ICAM-1 is generally greater than for pMHC and often reaches values lower than 1. To avoid bias, all cells in a field of view were analysed unless there was a valid reason to exclude them (e.g., if dead or blocked by debris).

Figure 30 shows the degree of protein accumulation by cells on 1st generation SLBs. DKO-AS cells, as expected, showed negligible pMHC accumulation (average fold increase <1.6), which was similar for ICAM-1 (average <1.6). There was no significant change in ICAM-1 accumulation when ZAP-70 was inhibited, which again is expected since there is no TCR signalling in these cells. J-AS^{hi} cells on the other hand showed visible accumulation of pMHC with an average fold increase of 2.3, which significantly increased upon 3-MB-PP1 treatment to 3.9, suggesting some effect leading to more TCRs being available for binding. ICAM-1 accumulation was also significantly affected in J-AS^{hi} cells by 3-MB-PP1 treatment, decreasing from 2.0-fold enrichment under control conditions to 1.3-fold enrichment. The level of pMHC accumulation in J-AS^{lo} cells was not significantly different from DKO-AS (≤ 1.5 under any condition), which is not surprising given the low density of TCRs available for binding. Interestingly, the degree of ICAM-1 accumulation was not significantly different

between J-AS^{hi} and J-AS^{lo} cells on 1st generation SLBs with J-AS^{lo} cells having an enrichment of 1.9-fold. This decreased to 1.3-fold with ZAP-70 inhibition, which was significant.

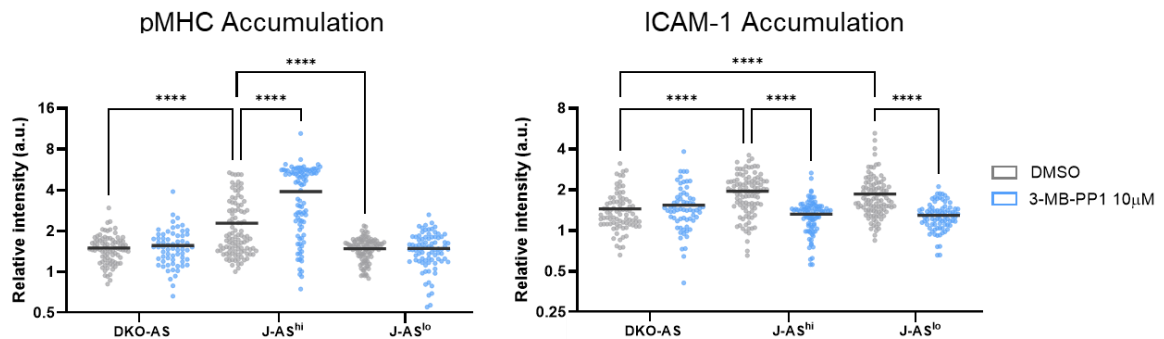


Figure 30 TCR expression and signalling capacity modulate pMHC and ICAM-1 binding on 1st generation SLBs Cells were washed in PBS-MgSO₄ with DMSO or 3-MB-PP1 before placing on SLBs with labelled pMHC and ICAM-1. After 10 minutes incubation, excess cells were gently washed away and remaining cells were fixed to analyse protein accumulation. (A) Relative accumulation of pMHC (left) and ICAM-1 (right) under cells on 1st generation SLBs. Between 65-104 cells for each condition were pooled from 3 repeats. Statistical significance was tested by ordinary one-way ANOVA with Tukey's multiple comparisons. **** = $p < 0.0001$ *** = $p < 0.001$, ** = $p < 0.01$ * = $p < 0.05$. Non-significant comparisons not shown.

4.3.4.3 ZAP-70 Activity, but not TCR Density, Regulates Cell Spreading on 1st Generation SLBs

The change in protein accumulation, in particular pMHC, on SLBs provided some evidence that ZAP-70 signalling may be changing the morphology of the cell as it interacts with an agonist-presenting SLB. Therefore, experiments were conducted where live cells were imaged interacting with these surfaces under different signalling conditions.

Approximately 5×10^5 cells of each cell line were washed PBS-MgSO₄ and 10 μ M 3-MB-PP1 or matched volume of DMSO. Cells were resuspended and placed onto prepared, washed and temperature-equilibrated 1st generation agonist-presenting SLBs after 3 minutes equilibration at 37°C. Timelapse images were taken every 10 seconds for 15 minutes, and cell footprints as determined by IRM signal were analysed over time (Figure 31A). All cells were analysed to avoid bias except where IRM signal was disrupted or where cells were cut off by the field of view.

Firstly, analysis was directed at the maximum surface area achieved by cells in each condition (Figure 31B). DKO-AS cells did not spread very much (average surface area of $30 \mu\text{m}^2$) and significantly less than all TCR-expressing cells. Interestingly, this decreased to $6 \mu\text{m}^2$ with 3-MB-PP1, which was significant. As expected, J-AS^{hi} and J-AS^{lo} cells both showed substantial cell spreading after contacting the SLB, with similar maximum sizes of $123 \mu\text{m}^2$ for J-AS^{hi} and $116 \mu\text{m}^2$ for J-AS^{lo}, indicating that reduced TCR density does not affect spreading in this manner. The TCR-expressing cell lines also both showed a significant and substantial decrease in the maximum size reached when ZAP-70 was inhibited by 3-MB-PP1, down to $13 \mu\text{m}^2$ for J-AS^{hi} and $20 \mu\text{m}^2$ for J-AS^{lo}, suggesting a strong role for ZAP-70 in regulating cell spreading.

The mean cell area across the timelapse, which indicates how long the cell spends in a spread morphology, was then analysed (Figure 31C). Once again under control conditions, the surface area for DKO-AS cells was relatively small ($19 \mu\text{m}^2$) and much lower than J-AS^{hi} and J-AS^{lo} cells, which had an average area of $44 \mu\text{m}^2$ and $63 \mu\text{m}^2$ respectively. Upon treatment, mean areas decreased to $4 \mu\text{m}^2$ for DKO-AS cells, $5 \mu\text{m}^2$ for J-AS^{hi} and $10 \mu\text{m}^2$ for J-AS^{lo} cells. This was significant for all cell lines.

Finally, similar patterns were observed when the speed of cell spreading up to its maximum size was measured (Figure 31D). There was no difference between J-AS^{hi} and J-AS^{lo} cells (both $0.7 \mu\text{m}^2/\text{s}$), which both spread much faster than DKO-AS at $0.1 \mu\text{m}^2/\text{s}$. Both cell lines showed reduction to a similar speed of spreading when 3-MB-PP1 was applied, down to $0.09 \mu\text{m}^2/\text{s}$ for J-AS^{hi} and $0.15 \mu\text{m}^2/\text{s}$ for J-AS^{lo}, and this was significant for both cell lines. DKO-AS cells were reduced to a speed of just $0.03 \mu\text{m}^2/\text{s}$. This again suggests a vital, but not necessarily TCR-dependent, role for ZAP-70 in regulating cell morphology and size.

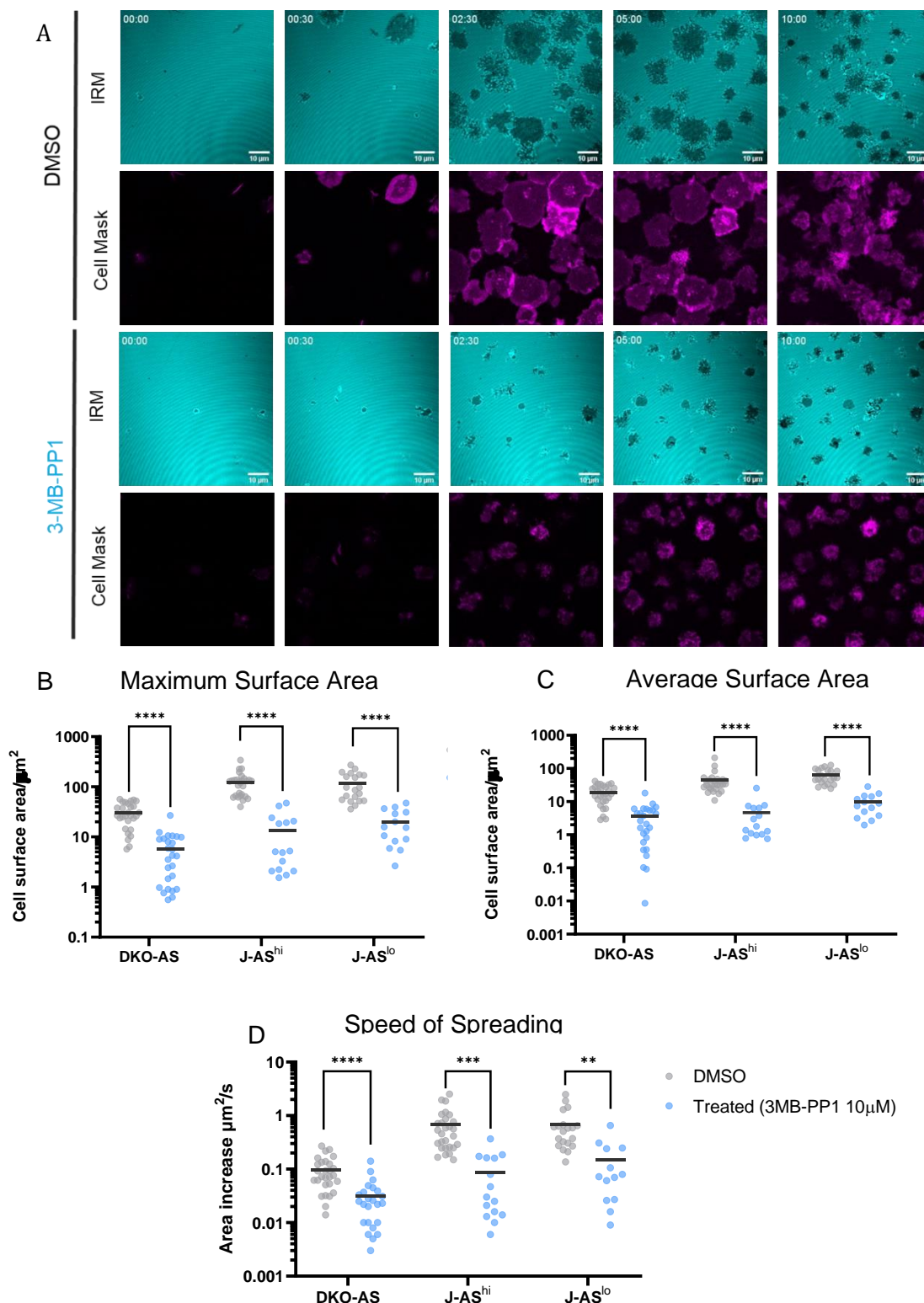


Figure 31 ZAP-70 controls cell spreading on 1st generation SLBs Cells were washed in PBS-MgSO₄ with DMSO or 3-MB-PP1 before placing on 1st generation agonist-presenting SLBs. IRM was used to measure the footprint of the cells over a 15-minute timelapse. (A) Representative timelapse of J-AS^{hi} cells spreading on 1st generation agonist-presenting SLBs under control and ZAP-70-inhibited conditions. Dark areas on the IRM channel represent areas of contact between the cell and SLBs (B) Maximum surface area reached by cells (C) Average surface area of cells over the course of the timelapse (D) Rate of area increase of cells from landing to their maximum size. Dark bars indicate the mean value for each condition. Between 14-28 pooled cells were analysed per condition, over 3 repeats.. Conditions within cell lines were compared in a pairwise manner using a Student’s t-test. **** = p < 0.0001 *** = p < 0.001, ** = p < 0.01.

4.3.5 T-Cell Interactions with 2nd Generation SLBs: Dependence on TCR expression and Signalling

Adhesion, protein accumulation and cell spreading were then tested on 2nd generation SLBs to assess whether there may be differences when cells interact with a more physiological SLB containing adhesion and glycocalyx proteins. Cells and SLBs were prepared in the same manner as in section 4.3.4.

4.3.5.1 Adhesion to SLBs is Independent of TCR and ZAP-70 on 2nd Generation SLBs

There was no substantial difference between adhesion on 1st and 2nd generation SLB systems, while the pattern of greater variability upon 3-MB-PP1 treatment was recapitulated (Figure 32A, left panel). The total fraction of DKO-AS, J-AS^{lo} and J-AS^{hi} cells adhering on 2nd generation SLBs were 94%, 91% and 82%. Upon ZAP-70 inhibition, the respective values were 95%, 84% and 81%.

For 2nd generation SLBs, adhesion times were generally longer (Figure 32A, right panel), which is expected since these surfaces are known to be less adhesive due to the inclusion of the glycocalyx proteins CD43 and CD45 (thesis of Edward Jenkins, Davis group). The median times for control and 3-MB-PP1-treated cells on 2nd generation SLBs were 54 s versus 114 s for DKO-AS, 86 s versus 110 s for J-AS^{hi} and 46 s versus 92 s for J-AS^{lo}. Once again, neither cell line nor treatment had a significant effect on these times, although greater variability was observed with 3-MB-PP1 treatment.

Like with 1st generation SLBs, the rate of cell adhesion between DMSO and 3-MB-PP1-treated cells overlapped substantially with all cell lines, which all generally adhered at a slower rate on 2nd generation SLBs compared to 1st generation (Figure 32B).

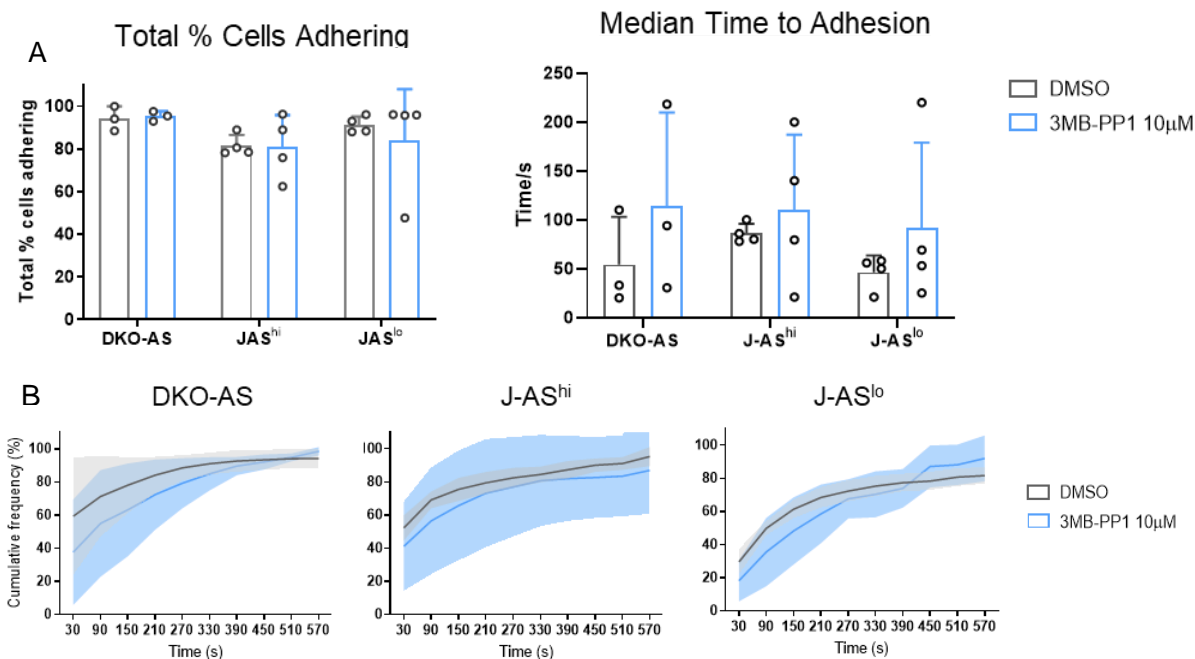


Figure 32 Initial adhesion to 2nd generation SLBs is independent of TCR expression and ZAP-70 activity Cells were labelled with Fluo-4 AM, washed in PBS-MgSO₄ with DMSO or 3-MB-PP1 and placed onto agonist-presenting 2nd generation SLBs. Custom MATLAB code was used to analyse various biophysical metrics of hundreds of cells per repeat over 3-5 repeats. (A) Percentage of cells adhering to the SLBs over the course of a 10 minute timelapse (left) and median time to adhesion per cell (right) (B) Pooled data from all repeats per condition showing the rate of adhesion in a cumulative frequency distribution plot. Mean \pm SD plotted in all graphs. No statistically significant difference was found between any of the cell lines or treatments for any of the metrics analysed using a two-way ANOVA test with Šídák's multiple comparisons (only tested in panel A).

4.3.5.2 pMHC and ICAM1 Accumulation are Regulated by TCR and ZAP-70 Signalling on 2nd Generation SLBs

Results for pMHC and ICAM-1 accumulation are summarised in Figure 33. DKO-AS cells once again did not accumulate pMHC or ICAM-1 under any conditions. J-AS^{hi} cells visibly accumulated pMHC on 2nd generation SLBs (1.9-fold increase), which significantly increased to 2.5-fold with ZAP-70 inhibition similarly to 1st generation SLBs. ICAM-1 accumulation under J-AS^{hi} cells decreased slightly, but significantly, from 1.4 to 1.1-fold with ZAP-70 inhibition. J-AS^{lo} cells once again did not show substantial pMHC accumulation (1.2-fold under control conditions), and this did not change with 3-MB-PP1 treatment (1.2-fold). A decrease in ICAM-1 accumulation was observed, but this was not significant (1.2 to 1.3-fold enrichment with control vs ZAP-70-inhibited conditions). Interestingly, the degree of ICAM-

1 accumulation was significantly different between J-AS^{hi} and J-AS^{lo} cells on 2nd generation SLBs, possibly suggesting that signal integration from more TCRs affects LFA-1 binding, at least in some conditions. Average accumulation on these SLBs was 1.9 down to 1.3 with ZAP-70 inhibition and 1.7 to 1.1 on 2nd generation SLBs.

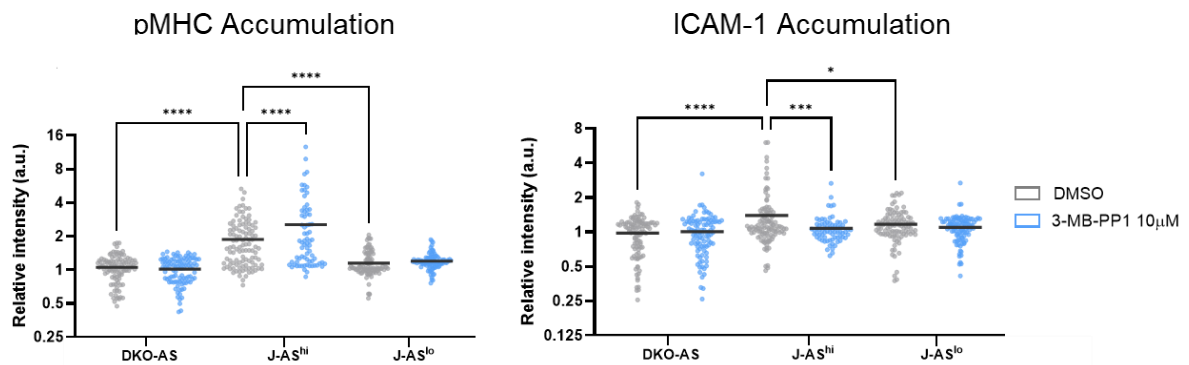


Figure 33 TCR expression and signalling capacity modulate pMHC and ICAM-1 binding on 2nd generation SLBs Cells were washed in PBS-MgSO₄ with DMSO or 3-MB-PP1 before placing on SLBs with labelled pMHC and ICAM-1. After 10 minutes incubation, excess cells were gently washed away and remaining cells were fixed to analyse protein accumulation. (A) Relative accumulation of pMHC (left) and ICAM-1 (right) under cells on 2nd generation SLBs. Between 72-107 cells for each condition were pooled from 3 repeats. Statistical significance was tested by ordinary one-way ANOVA with Tukey's multiple comparisons. **** = $p < 0.0001$ *** = $p < 0.001$, * = $p < 0.05$. Non-significant comparisons not shown.

4.3.5.3 ZAP-70 Activity, but not TCR Density, Regulates Cell Spreading on 2nd Generation SLBs

The size and speed of cell surface area increase was also measured on 2nd generation agonist-presenting SLBs (Figure 34). Cell size was measured using the custom Python close contact code (section 4.2.7) which automatically segments and tracks areas of Cell Mask-labelled membrane over time for multiple cells in a field of view.

Cells were harvested and labelled with Cell Mask and Fluo-4 AM, then washed and resuspended in PBS-MgSO₄ and 10 μ M 3-MB-PP1 or matched volume of DMSO. Cells were placed onto labelled 2nd generation agonist-presenting SLBs after 3 minutes equilibration in the microscope incubator and an image was taken every 2 seconds for 15 minutes with autofocus applied to avoid focal drift. Representative timelapse images for J-AS^{hi} cells under each experimental condition is shown in Figure 34A.

The maximum surface area reached by each cell line under control conditions was $59 \mu\text{m}^2$ for DKO-AS, $130 \mu\text{m}^2$ for J-AS^{hi} and $130 \mu\text{m}^2$ for J-AS^{lo}. When ZAP-70 was inhibited this decreased significantly to $39 \mu\text{m}^2$ for J-AS^{hi} cells and $29 \mu\text{m}^2$ for J-AS^{lo} cells, but stayed similar at $57 \mu\text{m}^2$ for DKO-AS (Figure 34B), suggesting a strong effect of ZAP-70 activity, but only when TCR is present. Furthermore, the average surface area across the timelapse (Figure 34C) was $31 \mu\text{m}^2$ regardless of treatment for DKO-AS cells, while J-AS^{hi} cells decreased significantly from $63 \mu\text{m}^2$ (control) to $19 \mu\text{m}^2$ (3-MB-PP1), and for J-AS^{lo} the decrease was $59 \mu\text{m}^2$ (control) to $15 \mu\text{m}^2$ (3-MB-PP1) and this was also significant. Finally, the speed of spreading was analysed (Figure 34D). DKO-AS cells again did not demonstrate any substantial changes – their average area increase was $0.1 \mu\text{m}^2/\text{s}$ regardless of treatment, whereas J-AS^{hi} cells decreased from $0.44 \mu\text{m}^2/\text{s}$ (control) to $0.07 \mu\text{m}^2/\text{s}$ (3-MB-PP1) and J-AS^{lo} also decreased from $0.52 \mu\text{m}^2/\text{s}$ (control) down to $0.08 \mu\text{m}^2/\text{s}$ (3-MB-PP1) with ZAP-70 inhibition, and both of these changes were significant.

In summary, inhibition of ZAP-70 in these cell lines on 2nd generation SLBs had no significant effect on DKO-AS cells and reduced both the total cell surface area and speed of cell spreading of TCR-expressing cell lines to match DKO-AS cells. This data is in overall in good agreement with the experiments conducted on 1st generation SLBs (section 4.3.4.3), except for DKO-AS cells which appear to be affected by 3-MB-PP1 treatment only on 1st generation SLBs.

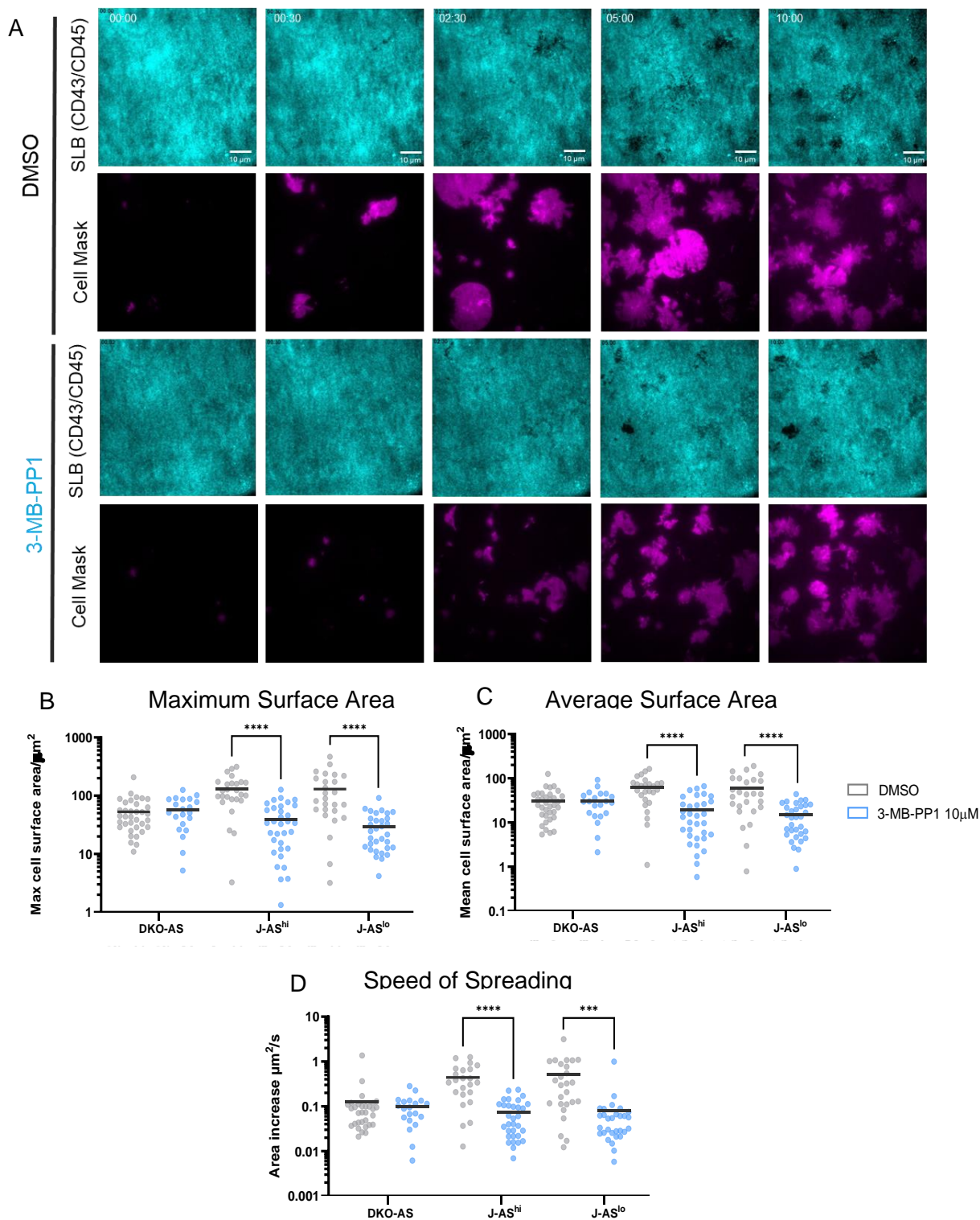


Figure 34 **ZAP-70 controls cell spreading on 2nd generation SLBs** Cells were washed in PBS-MgSO₄ with DMSO or 3-MB-PP1 before placing on 2nd generation agonist-presenting SLBs. Cell size was measured over a 15-minute timelapse by tracking cell membrane area dyed with Cell Mask. (A) Representative timelapse of J-AS^{hi} cells spreading on 1st generation agonist-presenting SLBs under control and ZAP-70-inhibited conditions. Dark areas in the SLB represent areas of close contact between the cell and SLBs (B) Maximum surface area reached by cells (C) Average surface area of cells over the course of the timelapse (D) Rate of area increase of cells from landing to their maximum size. Dark bars indicate the mean value for each condition. Between 21-35 pooled cells were analysed per condition, over 3 repeats. Conditions within cell lines were compared in a pairwise manner using a Student's t-test. **** = p < 0.0001 *** = p < 0.001.

4.3.5.4 ZAP-70 Activity, but not TCR Density, Affects Close Contacts on 2nd Generation SLBs

The data acquired so far suggests that, while inhibiting ZAP-70 signalling in T cells does not affect initial adhesion to SLBs, it appears to influence their subsequent morphology in a manner that is at least partially independent of TCR density, or even presence. Using 2nd generation SLBs, the smallest initial contacts, likely made by microvilli, can be directly observed as they initiate cell/SLB contact and progress through cell spreading. Using the ZAP-70(AS) system combined with 2nd generation SLBs and a custom MATLAB analysis code the size and rate of growth of these contacts can be quantified under different experimental conditions (Figure 35).

2nd generation SLBs were set up with labelled glyocalyx proteins CD43 and CD45. These proteins are very dense on the SLB when introduced at physiological levels (see section 2.5.2) and so create a homogenous plane which can be disrupted as cells bind to small adhesion proteins and pMHC, excluding these large molecules^{135,185}. Areas of close contact (CC) between the cell and SLB appear as dark spots in the labelled SLB surface (see Figure 35B-D). Cells were prepared as in section 4.3.5.3.

There was no significant difference between control or treated DKO-AS cells in any of the metrics tested, suggesting a TCR-dependent effect of ZAP-70 in the regulation of close contacts (Figure 35E-I). The growth of all close contacts per cell over time in these cells overlapped closely between conditions (Figure 35E, left panel) and likely demonstrate a passive spreading event on the SLBs, rather than true active spreading seen with signalling cells. Interestingly, this suggests different spreading behaviour from DKO-AS cells on 1st generation SLBs as determined in the previous experiments looking at overall cell surface area with IRM.

Notably, there was no significant increase in the speed of first close contact formation between any of the cell lines when ZAP-70 was inhibited, with the mean of all conditions lying between 260-447 s (see section 8.4, Figure 52B), although there was a trend towards longer times to close contact formation when ZAP-70 was inhibited. The total area occupied by close contacts per cell was significantly smaller when ZAP-70 was inhibited, reducing from $7.5 \mu\text{m}^2$ (control) to $3.0 \mu\text{m}^2$ (3-MB-PP1) for J-AS^{hi} cells and from $7.2 \mu\text{m}^2$ (control) and $3.5 \mu\text{m}^2$ (3-MB-PP1) for J-AS^{lo} cells (Figure 35H). J-AS^{hi} and J-AS^{lo} cells both showed a peak in the growth of their close contacts between 300-400 seconds, taking an average of 396 s and 312 s respectively to reach the maximum close contact size per cell (Figure 35I). This was longer during ZAP-70 inhibition at 454 s and 509 s, although the change was only significant for J-AS^{lo} cells.

Both J-AS^{hi} and J-AS^{lo} cells had significant reductions in the number of close contacts formed per cell, from an average of 22 and 26 respectively under control conditions to 9 and 8 when treated with 3-MB-PP1 (Figure 35F), however when these were normalised for the cell surface area there was no significant difference between any cell conditions with close contact densities all falling between 0.21-0.34 CCs/ μm^2 (see section 8.4, Figure 52A). However, the average size per close contact (determined by dividing the total CC area per cell by the maximum number of CCs per cell, Figure 35G) was significantly larger for J-AS^{lo} cells when treated with 3-MB-PP1, increasing from $0.27 \mu\text{m}^2$ to $0.42 \mu\text{m}^2$. J-AS^{hi} cells did not show a significant change but did increase in size ($0.36 \mu\text{m}^2$ control to $0.39 \mu\text{m}^2$ with 3-MB-PP1), whereas DKO-AS cells had a non-significant decrease in CC size ($0.41 \mu\text{m}^2$ control to $0.33 \mu\text{m}^2$ with 3-MB-PP1).

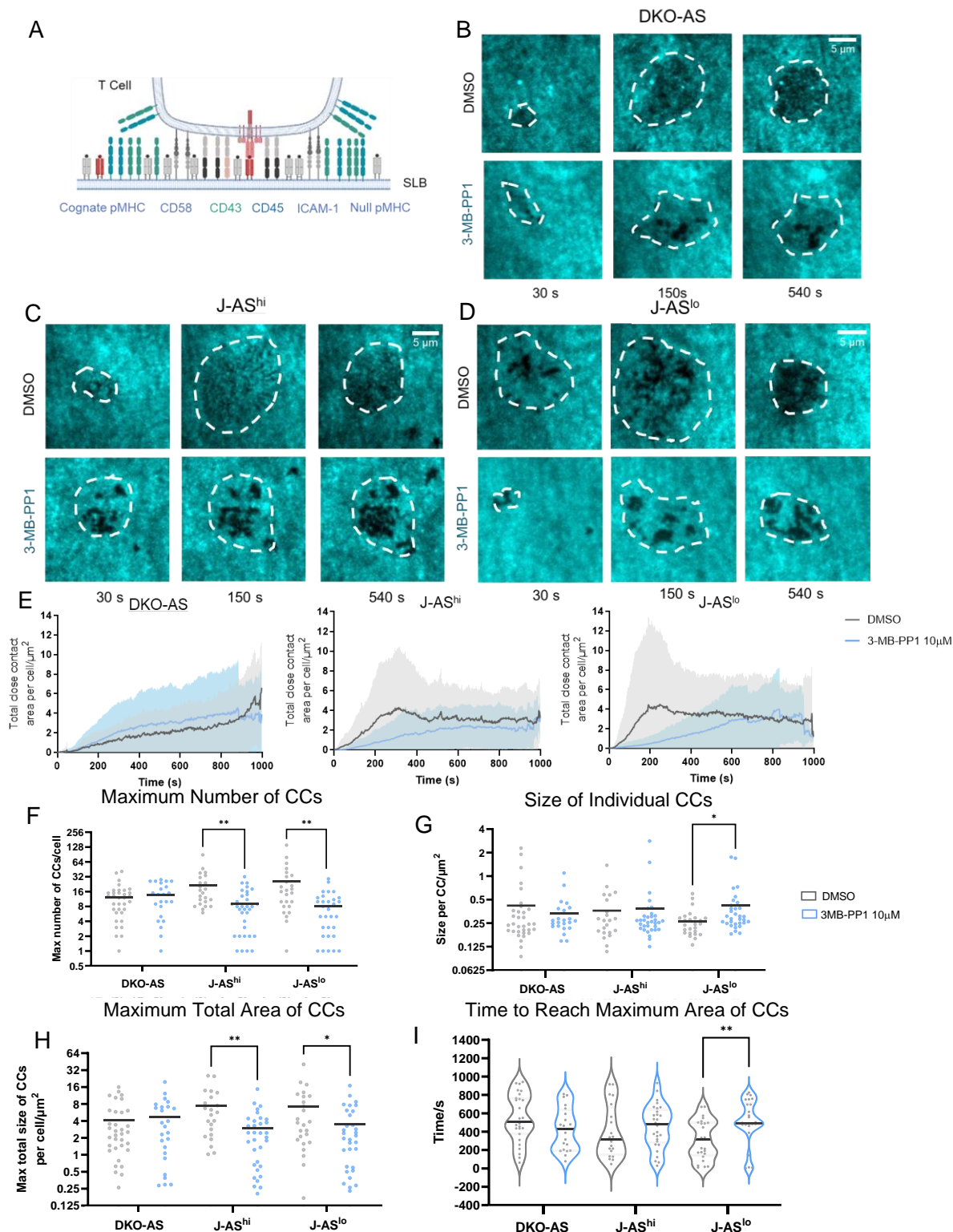


Figure 35 TCR expression and ZAP-70 activity affect some metrics of T cell close contacts Cells were labeled with Fluo-4 AM and Cell Mask, washed in PBS-MgSO₄ with DMSO or 3-MB-PP1, and placed onto 2nd generation SLBs with CD43 and CD45 labelled. A custom Python code was used to analyse areas of CC between the cell and SLB, schematically depicted in (A). (B-D) Timelapse images of representative cells for each cell line with and without ZAP-70 inhibition. (E) Total size of CCs over time for each condition and cell line (mean \pm SD plotted). (F) Maximum number of CCs per cell. (G) Average area per CC in μm^2 . (H) Maximum total area of CCs reached per cell. (I) Time taken to reach the maximum CC size per cell. Dark bar represents the median value for each condition in violin plots, and mean in scatter plots. Between 22-69 cells were analysed per condition over 3 repeats. Statistical testing was carried out pairwise within cell lines using a Student's t-test. ** = $p < 0.01$ * = $p < 0.05$.

4.4 Discussion

The experiments in this chapter were designed to investigate whether TCR signalling capacity or expression influences the formation and dynamics of contacts between T cells and SLBs.

The resting morphology of the three ZAP-70(AS) T-cell lines were found to be similar regardless of ZAP-70 activity and TCR expression, and a slight enrichment for the TCR, but not CD2 or LFA-1, was observed on microvilli. Cells adhered to 1st and 2nd generation SLBs in a similar manner regardless of TCR expression or 3-MB-PP1 treatment. Interestingly, while ICAM-1 accumulation was generally reduced on SLBs in the absence of TCR signalling, pMHC accumulation increased substantially, but only in J-AS^{hi} cells where accumulation was observable. Cell spreading on 1st generation SLBs was found to be markedly reduced by ZAP-70 inhibition in all cell lines, however the effect on 2nd generation SLBs was only apparent for J-AS^{hi} and J-AS^{lo} cells. Similarly, the size and number of close contacts was smaller when ZAP-70 was inhibited, although the density of close contacts remained consistent, suggesting no gross changes in morphology. Finally, the time taken to reach the maximum close contact size in TCR-expressing cell lines was longer with 3-MB-PP1 treatment, but this only reached significance for J-AS^{lo} cells.

Overall, the results here suggest that T-cell microvilli may be structured to facilitate TCR signalling, although initial adhesion to SLBs and some protein binding on SLBs can occur without signalling. ZAP-70 activity affects cell spreading substantially but close contacts are more subtly changed, and usually these effects are only noticeable in TCR-expressing cells.

4.4.1 Differential Protein Localisation on the T-Cell Surface

Z-stack projections of resting T cells suggested that TCR expression and signalling likely do not have a role in regulating morphology at rest. However, more cells would need to be imaged and quantitatively analysed before a firm conclusion can be made.

Intensity-based analysis of key proteins on T-cell microvilli showed homogeneous distribution of CD2 and LFA-1, but a slight enrichment of TCR towards the microvilli tips. The methodology used to determine relative enrichment was first verified for CD62L, which is known to be preferentially located on microvilli⁴⁰⁴, and by analysing cells fixed in suspension rather than when interacting with a surface, contact formation between the cell and surface that could cause redistribution of proteins (for example exclusion of large molecules) are avoided. Furthermore, fixing in solution prevents non-specific TCR triggering as observed on a variety of surfaces, even those traditionally considered to be inert^{135,304,334}. By using a Fab to label the TCR rather than an antibody, and labelling all samples at 4°C, activation of the cells and subsequent protein clustering is unlikely. By additionally measuring CD44, which is said to localise around the base of microvilli¹⁹⁴, the method could be further tested.

However, this method is still relatively crude (diffraction-limited images and manual analysis) therefore conclusions drawn should be taken in context of results from other work using different methods, such as super-resolution and 3D imaging. Additionally, the result for CD2 does not agree as well with a previous publication which found a strong preference for CD2 on microvilli tips¹⁰³.

4.4.2 The Role of TCR and ZAP-70 in T-Cell Interaction with SLBs

TCR expression, nor signalling capacity, appear to influence initial adhesion to model APCs, as all cell lines regardless of treatment adhered to SLBs comparably.

While adhesion has not been studied by others in this manner, studies in cell-cell settings confirm that ZAP-70 inhibition does not change the number of conjugates formed between T cells and APCs or target cells^{383,384}, suggesting the results here are likely accurate despite being unable to recapitulate every surface protein interaction.

Accumulation of pMHC and ICAM-1 on SLBs could however be different from a cell-cell context. While many examples of protein reorganisation on T cells interacting with SLBs, such as TCR and LFA-1 accumulation, hold true for cell-cell settings^{215,405} it is uncertain whether the results observed here would have a meaningful translation to an *in vivo* setting. It is too impractical to fully recapitulate the complex protein surface of an APC and the enrichment values obtained here are likely higher than reality. However, these conclusions were made in the context of relative change between conditions where the SLBs were identical (as far as is possible), and protein densities were designed to match physiological levels measured on APCs.

4.4.3 Regulation of T-Cell Contacts on 1st and 2nd Generation SLBs by TCR and ZAP-70

ZAP-70 activity, but not TCR density (or even expression in some cases) was found to modulate T-cell contacts with 1st and 2nd generation SLBs.

Changes in the cell surface area and speed of spreading for the DKO-AS line did not match between 1st and 2nd generation SLBs – there was a significant decrease in both metrics on 1st generation SLBs with ZAP-70 inhibition which was not observed on 2nd generation SLBs. The reduction in speed and size of J-AS^{hi} and J-AS^{lo} cells was also more subtle, although still highly significant, on 2nd generation SLBs. Overall, this suggests either a reduced effect of ZAP-70 inhibition on 2nd generation SLBs, or a technical difference in measurements and analysis. Discrepancies could occur in cell surface area measurements between IRM and direct cell membrane area, since the area of the cell in close contact with the SLB and within

the TIRF evanescent field may not fully overlap, or due to the different experimental set ups (i.e., different objectives, magnifications, and analysis methods)

Second generation SLBs provide a novel system to study close contact formation in a manner that is arguably more physiologically relevant than other methods such as quantum dot exclusion used in other studies²²³. SLBs however are still imperfect, as close contacts smaller than the resolution of the microscope (approximately 100 nm), or those not excluding enough glyocalyx proteins to be identified by the code, could be missed.

One key aspect of SLBs that may affect T-cell morphology is the stiffness of the underlying substrate. As previously discussed, (section 3.4.3), early events in T-cell signalling, as well as protein reorganisation, seem to be largely unaffected by substrate stiffness³⁴⁰, but there is evidence that stiffness can affect T-cell migration, activation, and spreading^{337,406}. Therefore, these interactions may not be well recapitulated in SLBs given that they provide the T cell with a very stiff substrate containing unanchored, rapidly diffusing proteins which would not provide the same mechanical resistance as a real APC. Nevertheless, the comparative nature of the experimental set up can provide insight into the differences in T-cell behaviour when ZAP-70 activity and TCR expression are changed under certain conditions.

5 Microclusters and their Relationship with Microvilli

5.1 Introduction

TCR microclusters (MCs), small units typically made up of 40-200 TCRs^{172,213,216}, have been studied extensively in the context of T-cell signalling and synapse formation. TCR MCs are proposed to be the initiators of T-cell signalling for several reasons. Firstly, they appear very shortly after T cells contact model APCs^{172,213}, exclude CD45²¹¹, colocalise with signalling and scaffold molecules such as ZAP-70, Lck and LAT^{172,213,214,216}, and appear concomitantly with²¹⁵, or prior to¹⁷², calcium flux. Additionally, it is well known that clustering TCRs with antibodies or multimeric agonist pMHC can induce signalling in solution, whereas monomeric ligands cannot¹⁷⁴. Furthermore, a recent study using optogenetic techniques has shown that clustering CD3 ζ alone can cause T-cell signalling⁴⁰⁷.

It is becoming increasingly clear that T cells do not form homogenous, flat contacts with model APC surfaces, and that these fluctuations in topography may represent an important mechanism for T cells to regulate their signalling^{135,195,223,408}. MCs of TCRs (and indeed ZAP-70) in microscopy studies are observed as local increases in protein intensity at the cell membrane. Therefore, these could be the result of: (1) artefacts caused by variations in protein intensity due to cell topography, where protein intensity changes relative to the cell membrane position within the evanescent TIRF field (2) clusters of protein created by passively binding ligand on an activating surface or (3) physical complexes of TCR molecules in the T-cell membrane. Given the recent highlighting of the role of topography in T-cell signalling, microscopy studies have started to consider the possible link between the appearance of MCs and T-cell topography.

A study by Cai et al.²²³ used a technique called 'synaptic contact mapping' to measure close contacts made by live T cells on agonist pMHC-presenting 1st generation SLBs. The experimental set up included quantum dots of ~16 nm diameter on SLBs which were

excluded at close contacts. Using this method, they demonstrated distinct small points of close contact under spread T cells (similar to images of glycocalyx exclusion on 2nd generation SLBs from section 4.3.5.4), suggesting that fluctuations in the T-cell membrane are present during antigen scanning and spreading on the SLB surface. Furthermore, they observed a strong correlation between close contacts and TCR or ZAP-70 MCs, which suggests that observed MCs may be due to fluctuations in membrane topography. Additionally, it was demonstrated that early TCR MCs colocalised with actin, suggesting that microvilli (dynamic actin-rich protrusions on the T cell surface) may be the cause of these clusters. However, this association was weaker in later stages of contact. In line with this, another study found that pre-treatment of cells with an actin-inhibiting drug, which abolishes microvilli, prevented microcluster formation¹⁷². Finally, TCR microclusters have been shown to passively exclude CD45²¹¹ and their size^{103,211,216} is similar to that of microvilli tips^{103,194,223}. These results therefore suggest that either apparent MCs may represent fluctuations in topography, or that actin is required to facilitate MC formation.

In addition to this, Cai et al.²²³ noted that close contact areas which contained detectable TCR were much longer lived than those without, suggesting a passive mechanism of MC formation based on TCR occupancy by agonist pMHC. This idea is supported by another study which demonstrated a link between agonist pMHC density on the SLB and the size of TCR clusters²¹³. Furthermore, it has been suggested that pMHC attached to the SLB with GPI anchors (used in studies such as Varma et al.²¹¹) induces clustering of cell surface proteins⁴⁰⁹. Additionally, blocking access to agonist pMHC on an SLB with antibodies was shown to prevent formation of new TCR MCs²¹¹. Finally, one study²²² using a DNA-CAR (chimeric antigen receptor) as a model TCR demonstrated that the ligand binding rate of receptors was increased by ≥ 350 -fold in areas near ligand-bound receptors. This suggests a mechanism for the appearance of TCR MCs which relies on ligand-binding events regulated by an as yet unknown mechanism.

Several studies^{192,211} which imaged T-cell membrane simultaneously to TCR did not find a strong correlation between their intensity. Another study determined that microcluster size is independent of pMHC affinity¹⁹², suggesting that binding pMHC may not be the only reason for the appearance of MCs, and MCs of similar sizes have also been observed in SLBs using a range of different agonist pMHC densities²¹¹. Stimulation of T cells with a low density of antigen also leads to less TCR MC translocation and little/no cSMAC formation⁴¹⁰. A super-resolution imaging study demonstrated that ZAP-70 was recruited to TCR MCs regardless of their size²²⁰, and another showed that TCRs signal when MCs are as small as 11 TCRs in size²¹¹. Finally, ZAP-70 MCs appeared as distinct structures on glass slides homogeneously coated with OKT3, a TCR-binding antibody, in another super-resolution study⁴¹¹, suggesting that MCs are not simply an artefact of ligand binding by the TCR. Given the differing findings presented by these studies, a consensus on the appearance of MCs, especially with regard to T-cell membrane topography, has yet to be reached.

Finally, while substantial efforts have been made in characterising TCR MCs, the role of ZAP-70 kinase activity in regulating TCR MCs has not been examined by imaging studies. Interestingly, imaging studies of TCR and ZAP-70 have demonstrated the potential for ZAP-70 MCs to form around a few, or possibly even a single, TCR^{172,213}, suggesting relatively large TCR clusters may not be necessary for ZAP-70 recruitment. Additionally, a study by Katz et al.⁴¹² demonstrated that ZAP-70 kinase activity was required for release of ZAP-70 from the TCR ζ chains, which suggests a mechanism for early signal amplification.

By comparing J-AS^{hi} and J-AS^{lo} cells (described in 3.3.7), which have dramatically different TCR expression levels, the mechanics behind the appearance of TCR microclusters can be investigated. For example, it would be more difficult to form MCs when TCR density is very low (at least at a similar time scale to cells with physiological TCR expression), especially if they are a result of passive pMHC binding. ZAP-70 recruitment in cells with different densities of TCR will be quantified using the ZAP-70(AS)-HaloTag chimeric protein, which

can also be used to investigate the effect of ZAP-70 signalling during early contact formation without affecting ligand binding. This will help to dissect the factors controlling the appearance of TCR and ZAP-70 MCs. 2nd generation SLBs presenting labelled CD43 and CD45 (i.e., a glycocalyx) will be used to visualise T cell close contacts using TIRFM. By correlating glycocalyx intensity with labelled TCR and ZAP-70, the relationship between T-cell topography and apparent MCs will be quantified. Finally, the role of actin will be investigated by using pharmacological inhibitors to disrupt the cytoskeleton in different ways, while observing the effects on close contact formation and T-cell signalling.

This chapter will be divided into two parts: firstly, investigating the effect of different TCR expression, as well as ZAP-70 inhibition, on the formation of TCR MCs. Secondly, examining the relationship of cell topography and actin to the appearance of MCs, and its effect on TCR triggering.

5.2 Materials and Methods

5.2.1 TCR and ZAP-70 Microcluster Assays

Approximately 5×10^5 cells were labelled with Janelia Fluor-646 HaloTag ligand as previously described (final concentration 200 nM; section 2.5.6). Cells were then centrifuged at $395 \times g$ and incubated with UCHT1 Fab-Halo (488) at 20 $\mu\text{g}/\text{ml}$ in 50 μl total volume of complete RPMI for 10 minutes at 37°C . Cells were centrifuged as before and washed twice in 500 μl pre-warmed 0.22 μm -filtered PBS-MgSO₄ and 10 μM 3-MB-PP1 or matched volume of DMSO. The sample was finally resuspended in 50 μl of the same solution and placed onto 1st generation SLBs which had been prepared and washed in 0.22 μm -filtered PBS-MgSO₄ at room temperature. Cells were allowed to settle on the SLBs for 5 minutes before removal of excess liquid in the SLB wells and addition of 15 μl of a 4% PFA solution with 0.25% glutaraldehyde. Samples were fixed at room temperature for 30 minutes before washing with 0.22 μm -filtered PBS and immediate imaging.

Images were taken on an Olympus IX83 inverted TIRF microscope. Laser powers and exposure times were adjusted to achieve maximum dynamic range for each channel and kept constant over the course of each experiment. Every cell in a field of view was analysed to avoid bias, except those that were dead or on the edge of the frame. Images were analysed in Fiji. Cells were segmented using the IRM channel and MCs of TCR or ZAP-70 were defined as pixels within the top 20% of intensity within a cell (this was chosen empirically based on cells in control conditions). The 'analyse particles' feature was used to determine the number, intensity and size of 'MCs' (i.e., high-intensity spots) within the cell. Intensity values were normalised to the average intensity of the cell background. Detected TCR spots with an area greater than 1 μm^2 were excluded, and ZAP-70 spots greater than 2 μm^2 were excluded to avoid counting the cSMAC or clusters forming very close together as a single

cluster. These values were based on doubling microcluster area measurements for each protein^{211,413} to include changes in microcluster size.

5.2.2 Cell Topography in Relation to Microclusters

Approximately 5×10^5 cells were labelled as above (section 5.2.1). The sample was finally resuspended in 50 μl of PBS-MgSO₄ with 10 μM 3-MB-PP1 or matched volume of DMSO and placed onto 2nd generation SLBs containing Alexa Fluor 555-labelled CD43 and CD45 which had been prepared and washed in 0.22 μm -filtered PBS-MgSO₄ at room temperature. Cells were allowed to settle on the SLBs for 5 minutes before fixing and imaging as above.

Images were analysed using the Coloc2 tool in Fiji with default PSF and Costes randomisation settings. A mask was created for each cell using its IRM footprint, which was used to define an area to analyse the colocalisation of TCR vs glyocalyx, ZAP-70 vs glyocalyx or TCR vs ZAP-70 as a positive control using Pearson's correlation.

5.2.3 Early Signalling and Contact Area with Actin Inhibition

Different versions of 2nd generation SLBs were prepared: either excluding glyocalyx proteins (i.e., just pMHC, CD58 and null pMHC block) or with the glyocalyx included (i.e., a normal 2nd gen bilayer).

Approximately 1×10^6 cells were centrifuged at 2000 rpm for 90 seconds in a MiniSpin (Eppendorf), washed in 500 μl PBS and incubated in 1 μM latrunculin B, 10 μM cytochalasin D or 100nM jasplakinolide or equivalent volume DMSO in 100 μl RPMI (with no supplements) for 1 hour in a tissue culture incubator at 37°C and 5% CO₂. Cells were centrifuged, washed twice in 500 μl warmed PBS-MgSO₄ and the appropriate concentration of drug or matched volume of DMSO. Cells were finally resuspended in 50 μl of the same solution and left to incubate for 3 minutes in the microscope incubator while SLBs were washed in the relevant PBS-MgSO₄ with drug or DMSO. Approximately 5 μl of the cell

suspension was added to the SLB and an image was taken every second for 600 frames/10 minutes (for calcium flux assays) or every 10 seconds for 60 frames/10 minutes for contact analysis. Images were acquired on a Zeiss 780 (calcium) and 880 (contact formation) inverted confocal microscope. Calcium flux data was analysed using a bespoke MATLAB code (section 2.6). Contact zone analysis was carried out using a custom Python code (section 4.2.7).

5.3 Results

Many studies of TCR MCs have been conducted on SLBs presenting agonist pMHC and ICAM-1 (i.e., 1st generation SLBs) or antibody-coated glass. Glass surfaces however do not allow for MC translocation across the cell surface as would happen at a T cell/target cell contact^{211,213,215}. Therefore, J-AS^{hi} and J-AS^{lo} cells were compared on agonist- and null-presenting SLBs both with and without ZAP-70 inhibition to assess the role of TCR expression levels and ZAP-70 signalling on TCR and ZAP-70 MC formation. 2nd generation SLBs were also used to investigate the relationship between MCs, actin, and T-cell topography.

5.3.1 Early TCR Signalling Microclusters are not Affected by TCR Expression

J-AS^{hi} and J-AS^{lo} cells were labelled with UCHT1 Fab-Halo and a Janelia Fluor HaloTag ligand before washing and resuspension in warm PBS-MgSO₄ with either 10 μ M 3-MB-PP1 or DMSO. A small amount of the cell suspension was placed onto 1st generation agonist or null pMHC-presenting SLBs and cells were allowed to settle for 5 minutes before washing with PBS and fixing with 4% PFA with 0.25% glutaraldehyde. A relatively low density (1-10 pMHC/ μ m²) of agonist pMHC was used to mimic the physiological stimulus leading to signalling.

Images were taken immediately by TIRFM, as this allows the best signal-to-noise ratio for surface protein measurements. The strategy for analysing MCs is shown in Figure 36. The footprint of each cell was determined using IRM and the average background intensity for each cell was measured. Each cell was subjected to thresholding in each channel (TCR or ZAP-70) and the top 20% of pixel intensities were empirically defined as 'MCs' for analysis, to account for variations in TCR or ZAP-70 expression between cells in the same condition. The 'analyse particles' feature of Fiji was used to measure the number, size, and intensity of MCs for each channel.

Cells interacting with null pMHC-presenting SLBs, where little to no TCR signalling occurs (see section 8.4, Figure 51), also demonstrated areas of increased TCR intensity which were of comparable size and density to cells settled on agonist-presenting SLBs (Figure 36), however these were less bright both in absolute terms and relative to the cell background, suggesting that these 'MCs' likely represent areas of different membrane proximity to the SLB and/or stochastic variations in receptor density on the cell surface.

J-AS^{hi} cells formed an average of 22 MCs per cell and J-AS^{lo} cells formed 21 (Figure 37A). The average microcluster size was also very similar between both cell lines – 0.31 μm^2 for J-AS^{hi} cells and 0.29 μm^2 for J-AS^{lo} cells (Figure 37C). When comparing the intensity - and therefore number of TCRs present - in each microcluster, the absolute intensity of each microcluster was 2.6-fold higher for J-AS^{hi} cells compared to J-AS^{lo} cells, a difference that was significant (Figure 37D). When these values were normalised to the background intensity for each cell (i.e. representing the fold-change in intensity for a microcluster compared to the average intensity across the cell), a small but significant difference in values remained at 1.62 for J-AS^{hi} and 1.58 for J-AS^{lo} (Figure 37E). Therefore, TCR expression does not affect TCR MC density or size, however there is a small but significant decrease in the density of TCRs at individual MCs.

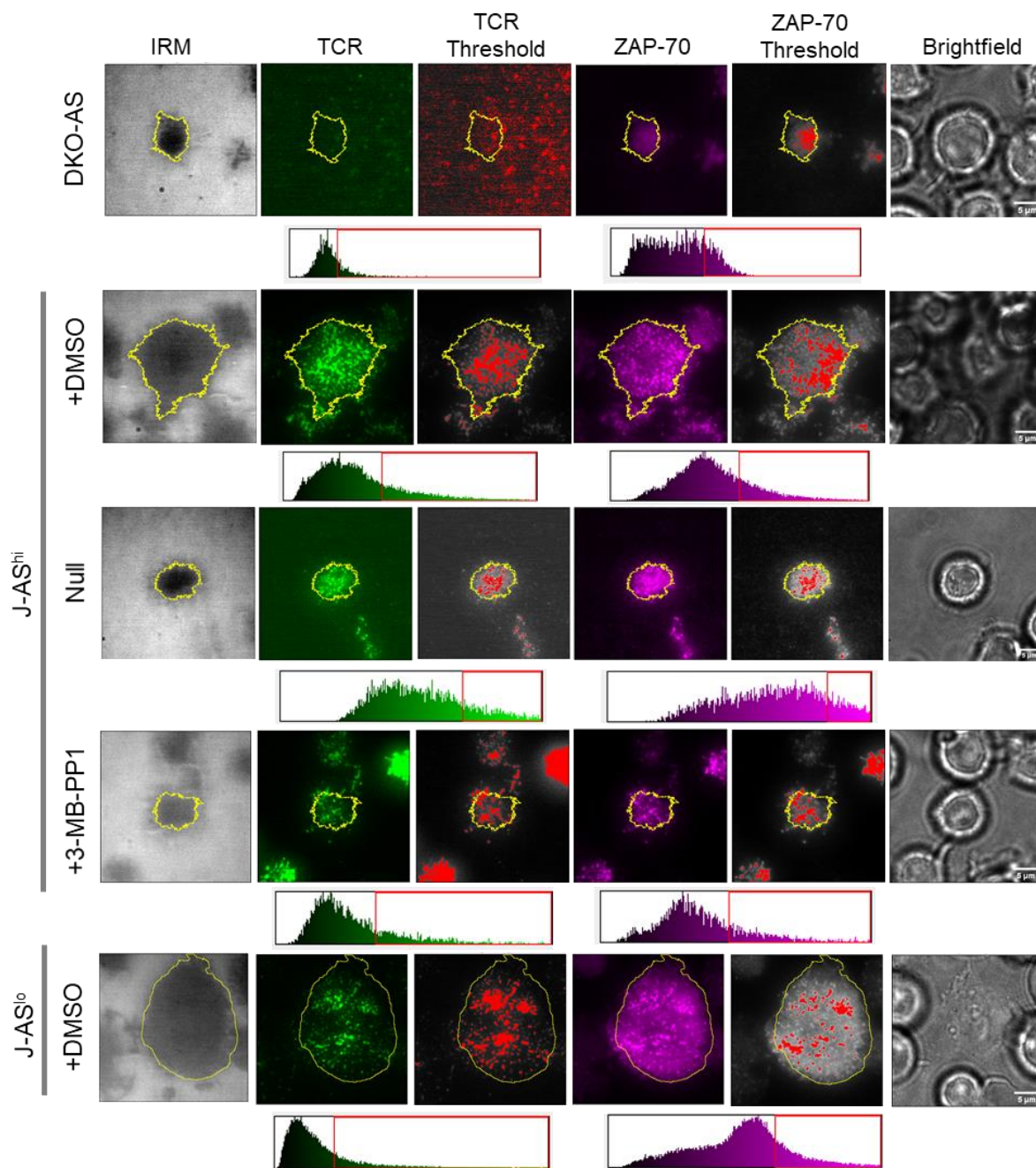


Figure 36 **Strategy for analysing TCR and ZAP-70 microclusters** Approximately 5×10^5 cells were labelled with HaloTag ligand and UCHT1 Fab-Halo. Cells were washed in PBS-MgSO₄ and 10 μ M 3-MB-PP1 or DMSO then placed onto agonist- or null pMHC-presenting 1st generation SLBs. Cells were allowed to settle on the SLBs for 5 minutes before fixation and immediate imaging on a TIRF microscope. Images show cells representative of each condition. After selecting a cell contact area based on IRM, channels representing TCR or ZAP-70 were individually subjected to thresholding to select pixels in the top 20% of intensities within the cell for analysis (this value was determined empirically). Red areas highlight the areas selected by this thresholding method. Intensity histograms below cells in each condition illustrate the distribution of intensities for cells in each condition, with the red box indicating the pixel intensities selected for analysis.

5.3.2 Early TCR Signalling Microclusters are not Substantially Affected by ZAP-70 Inhibition

When ZAP-70 was inhibited, the number of TCR MCs on J-AS^{hi} cells was reduced from 25 to 8 per cell for J-AS^{hi} and 9 for J-AS^{lo} cells. As described in Chapter 4, inhibition of ZAP-70 reduces the surface area of T cells on agonist-presenting SLBs, so TCR microcluster frequencies were normalised for cell surface area (Figure 37B). This gave similar densities across both cell lines of 0.13 MCs/ μm^2 for J-AS^{hi} and 0.16 MCs/ μm^2 for J-AS^{lo} cells, or one microcluster per 6.3-7.2 μm^2 of cell surface area. This did not change significantly with ZAP-70 inhibition.

The size of TCR MCs increased slightly for each cell line with ZAP-70 inhibition, from 0.31 μm^2 to 0.34 μm^2 for J-AS^{hi} and 0.29 μm^2 to 0.31 μm^2 for J-AS^{lo} cells (Figure 37C). Neither change was significant, however. Furthermore, the absolute intensity of TCR MCs was not significantly different between control or ZAP-70-inhibited cells (Figure 37C). The relative intensity was significantly higher for J-AS^{lo} cells treated with 3-MB-PP1 (Figure 37D) rather than DMSO, although the magnitude of the change was very small (1.58-fold higher than background vs 1.63). Overall, TCR MCs are not substantially affected by ZAP-70 activity, with the exception of an increase in MC intensity in J-AS^{lo} cells where ZAP-70 was inhibited.

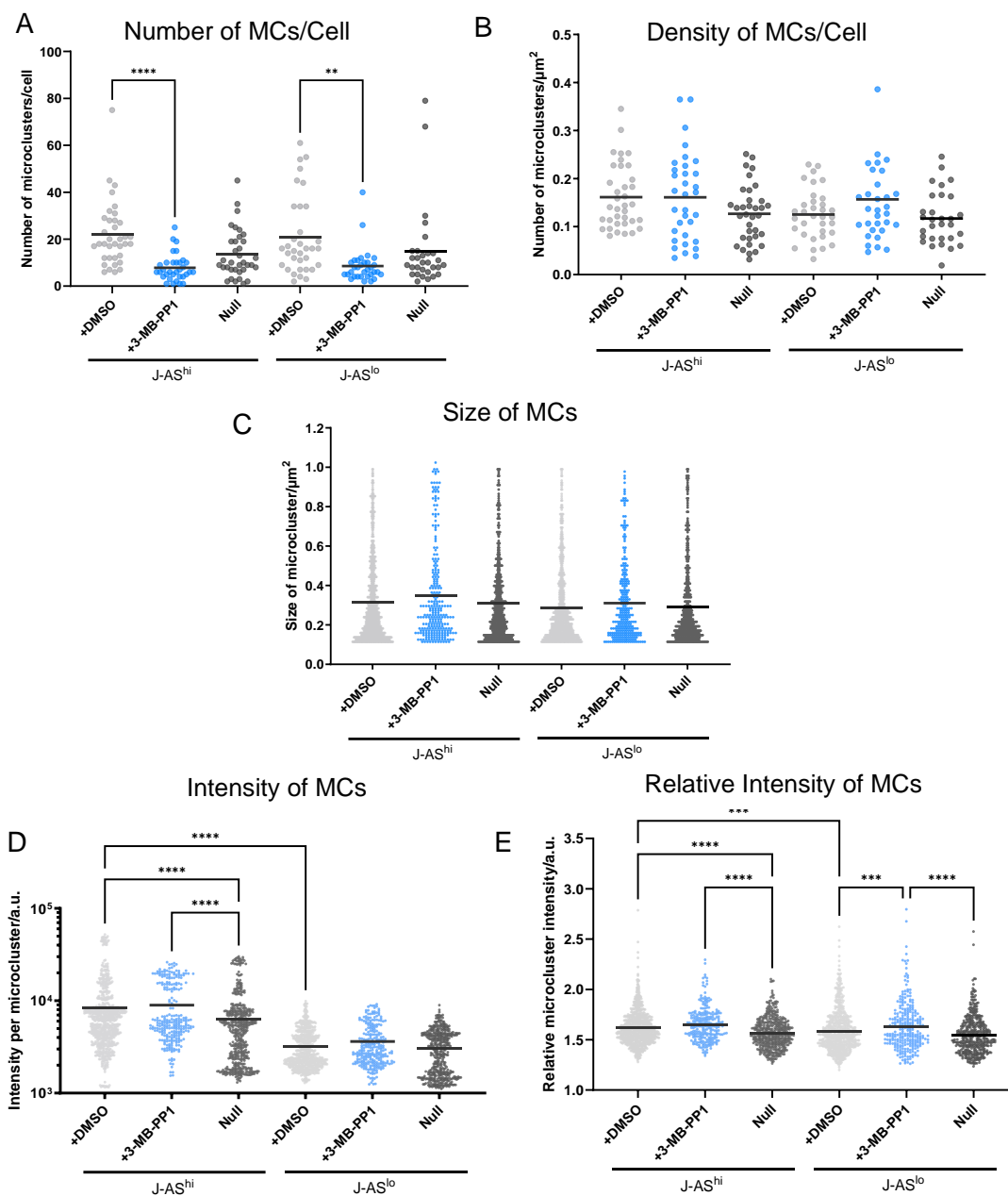


Figure 37 Characteristics of early TCR microclusters in cells with different TCR expression and signalling capacity Approximately 5×10^5 cells were labelled with HaloTag ligand and UCHT1 Fab-Halo. Cells were washed in PBS-MgSO₄ and 10 μ M 3-MB-PP1 or DMSO then placed onto agonist- or null pMHC-presenting 1st generation SLBs. Cells were allowed to settle on the SLBs for 5 minutes before fixation and immediate imaging on a TIRF microscope. Microclusters were defined as pixels within the top 20% of intensity values for each cell. (A) Absolute number of microclusters per cell. (B) Density of microclusters per cell (i.e., number of microclusters divided by the surface area of the cell). (C) Size of each microcluster in μm^2 . (D) Raw intensity value per microcluster. (E) Relative intensity of each microcluster (i.e., the intensity of each microcluster divided by the average intensity value across the entire cell). Dark grey bars represent the mean value in all graphs. Between 18-36 cells analysed per condition spread over three independent repeats. A total of 256-786 microclusters were analysed per condition over the 3 repeats. Values for each cell/microcluster were pooled and analysed by ordinary one-way ANOVA. **** = $p < 0.0001$ *** = $p < 0.001$, ** = $p < 0.01$. Non-significant comparisons not shown.

5.3.3 Appearance of ZAP-70 Signalling Microclusters is Independent of TCR Expression

Appearance of ZAP-70 MCs is easily distinguished via TIRFM as discrete puncta of molecules recruited to the TCR standing out against the homogeneous cytoplasmic background (see Figure 4, Figure 20, Figure 36). By measuring the mean intensity per cell an overall value for ZAP-70 recruitment can be obtained with TIRFM, as only the molecules closest to the cell membrane will be illuminated (Figure 38A). Several cells were measured for each condition and normalised to DKO-AS cells which cannot recruit ZAP-70 to the membrane as they have no TCR. Indeed, on agonist-presenting 1st generation SLBs J-AS^{hi} cells recruited approximately 2-fold more ZAP-70 to the cell membrane than DKO-AS cells, while J-AS^{lo} cells did not have a value significantly different from DKO-AS cells, suggesting the amount of ZAP-70 recruited to the surface of the J-AS^{lo} cells is very low. Both J-AS^{lo} and J-AS^{hi} cells placed on null pMHC-presenting SLBs exhibited significantly fewer ZAP-70 'MCs' than for those on agonist pMHC-presenting SLBs (average of 10 per cell for J-AS^{hi} and 8 for J-AS^{lo}), although there were more detected under these conditions than in DKO-AS cells (significantly for both cell lines, data not shown), possibly suggesting some amount of signalling on null SLBs or transient association of ZAP-70 with the TCR (Figure 38B and C).

The average number of ZAP-70 MCs per cell on agonist-presenting SLBs for J-AS^{hi} cells was 24 vs 17 for J-AS^{lo} cells (this was not significantly different; Figure 38B), however when this was normalised for the cell surface area (determined by IRM; data not shown) the values were 0.16 MCs/ μm^2 for J-AS^{hi} and 0.09/ μm^2 for J-AS^{lo}, which were significantly different (Figure 38C). Interestingly, the average microcluster size for J-AS^{hi} cells was 0.42 μm^2 and for J-AS^{lo} cells was 0.40 μm^2 , which were not statistically different (Figure 38D). However, the absolute intensity of MCs was almost 2-fold higher in J-AS^{hi} cells than J-AS^{lo} cells (Figure 38E). This was significantly different, and so was the relative intensity of ZAP-70 MCs (1.55 for J-AS^{hi} vs 1.52 for J-AS^{lo}) even though the fold change was small (Figure 38F).

In summary, J-AS^{lo} cells recruited less ZAP-70 to their surface overall and had a reduced density of MCs. ZAP-70 MCs were also less intense for J-AS^{lo} cells compared with J-AS^{hi}.

5.3.4 ZAP-70 Microcluster Intensity, but not Size or Number is Affected by ZAP-70 Inhibition

While the kinase activity of ZAP-70 is not required for its recruitment to phosphorylated TCR ζ chains, ZAP-70 is known to phosphorylate other ZAP-70 molecules in *trans*¹⁶⁰, and this has previously been shown to facilitate ZAP-70 binding and dissociation from the TCR⁴¹². Therefore, ablating its kinase activity could affect ZAP-70 recruitment to the TCR as well as preventing downstream signalling. Overall recruitment of ZAP-70 was not significantly different in either cell line when treated with 3-MB-PP1 (Figure 38A), with both control and treated J-AS^{hi} cells demonstrating relative ZAP-70 recruitment values of ~2-fold higher than DKO-AS cells, and J-AS^{lo} cells appearing comparable to DKO-AS cells in both cases (likely due to their low TCR density).

As with the TCR MCs, the number of ZAP-70 MCs decreased significantly for each cell line, dropping from 25 to 8 from J-AS^{hi} cells and 20 to 8 for J-AS^{lo} cells when ZAP-70 was inhibited (Figure 38B). The density of MCs however was not significantly different in either cell line when ZAP-70 was inhibited (Figure 38C). The size of ZAP-70 MCs was also not significantly different with 3-MB-PP1 treatment, increasing slightly from 0.42 μm^2 (DMSO) to 0.47 μm^2 (3-MB-PP1 treated) for J-AS^{hi} and from 0.40 μm^2 (DMSO) to 0.46 μm^2 (3-MB-PP1 treated) for J-AS^{lo} cells (Figure 38D). Interestingly, the absolute intensity values per microcluster were similar between DMSO and ZAP-70-inhibited J-AS^{hi} cells (Figure 38E), whereas for J-AS^{lo} cells there was a significant 1.7-fold increase in intensity between control and ZAP-70-inhibited cells (Figure 38F). When microcluster intensity was normalised to the cell background, J-AS^{hi} cells has a small but significant decrease in intensity (1.55 DMSO to 1.50

3-MB-PP1) while the opposite effect occurred for J-AS^{lo} cells (1.53 DMSO to 1.63 3-MB-PP1), which was significant (Figure 38F).

Overall ZAP-70 inhibition did not significantly change the number or size of ZAP-70 MCs formed in either cell line. It did however increase MC intensity in absolute and relative terms for J-AS^{lo} cells, whereas J-AS^{hi} cells had a small but significant decrease in relative intensity.

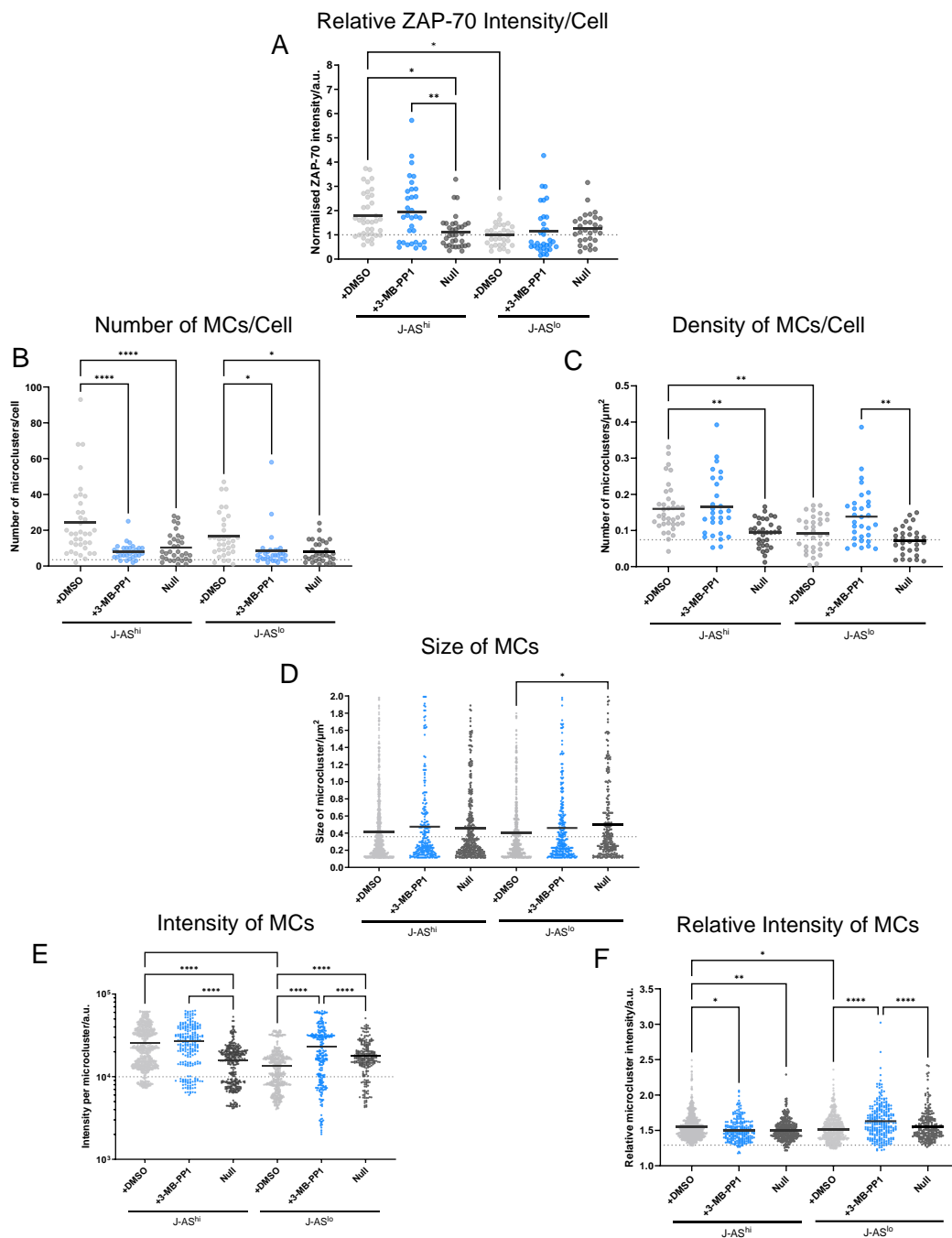


Figure 38 Characteristics of early ZAP-70 microclusters in cells with different TCR expression and signalling capacity Approximately 5×10^5 cells were labelled with HaloTag ligand and UCHT1 Fab-Halo. Cells were washed in PBS-MgSO₄ and 10 μ M 3-MB-PP1 or DMSO then placed onto agonist- or null pMHC-presenting 1st generation SLBs. Cells were allowed to settle on the SLBs for 5 minutes before fixation and immediate imaging on a TIRF microscope. Microclusters were defined as pixels within the top 20% of intensity values for each cell. (A) Average ZAP-70 intensity per cell normalised to DKO-AS cells. (B) Absolute number of microclusters per cell. (C) Density of microclusters per cell (i.e., number of microclusters divided by the surface area of the cell). (D) Size of each microcluster in μm^2 . (E) Raw intensity value per microcluster. (F) Relative intensity of each microcluster (i.e., the intensity of each microcluster divided by the average intensity value across the entire cell). Dark grey bars represent the mean value in all graphs and light grey dotted line represents the average value obtained for the control cell line DKO-AS. Between 29-37 cells analysed per condition spread over three independent repeats. A total of 102-840 microclusters were analysed per condition over the 3 repeats. Values for each cell/microcluster were pooled and analysed by ordinary one-way ANOVA. **** = $p < 0.0001$, *** = $p < 0.001$, ** = $p < 0.01$, * = $p < 0.05$. Non-significant comparisons not shown.

5.3.5 TCR and ZAP-70 Microclusters do not Appear Exclusively at Close Contacts

As previously demonstrated (section 4.3.5.4, Figure 35), small variations in T-cell topography, where the cell makes a close contact with pMHC and/or CD58, can be visualised using 2nd generation SLBs with labelled glyocalyx proteins (CD43 and/or CD45). If TCR and/or ZAP-70 MCs appear only at these areas of close contact, it would suggest there is a relationship between T cell topography and microcluster location on the cell. J-AS^{hi} cells were therefore imaged on these SLBs to determine whether there is a relationship between TCR or ZAP-70 MCs and close contacts. By comparing TCR, ZAP-70, and glyocalyx colocalisation on SLBs presenting agonist pMHC, null pMHC or with ZAP-70 inhibited by 3-MB-PP1, their spatial relationship can be examined.

Cells were labelled with Janelia Fluor-646 HaloTag ligand followed by UCHT1 Fab-Halo (488) to visualise TCR and ZAP-70. Cells were then washed in warmed PBS-MgSO₄ and 10 μ M 3-MB-PP1 or a matched volume of DMSO. The sample was resuspended in the same solution and placed onto 2nd generation agonist-presenting or null-presenting SLBs presenting Alexa Fluor 555-labelled CD43 and CD45 which had been prepared and washed with PBS-MgSO₄ at room temperature. A relatively low density of agonist pMHC (1-10 pMHC/ μ m²) was used to provide a physiological level of antigen presentation and prevent artefactual clustering of TCRs caused by passively binding dense pMHC. Cells were allowed to interact with the SLBs for 5 minutes before fixation at room temperature for 30 minutes before washing with PBS and immediate imaging. Images were analysed using the Coloc2 tool in Fiji where a mask was created for each cell using its IRM footprint and each channel was analysed against every other using Pearson's correlation.

Colocalisation was first tested between TCR and ZAP-70 as a positive control, which would be expected to colocalise upon TCR stimulation (Figure 39B, left panel). On agonist-presenting SLBs, the average coefficient of TCR vs ZAP-70 was 0.45 which indeed indicates a relatively strong colocalisation between these two proteins. ZAP-70 and TCR had a

correlation coefficient of 0.29 on null -presenting SLBs and 0.47 on agonist-presenting SLBs when treated with 3-MB-PP1. Correlation on null-presenting SLBs was significantly different from the other two conditions, suggesting ZAP-70 recruitment to the TCR on agonist-presenting SLBs, even when ZAP-70 is unable to further propagate signalling.

The TCR analysed against the glycocalyx on agonist-presenting SLBs showed no correlation with a coefficient value of 0.05 (Figure 39B, middle panel). Interestingly, this decreased to -0.20 on null-presenting SLBs which was similar to cells treated with 3-MB-PP1 at -0.27. Both values were significantly different to the coefficient on agonist-presenting SLBs, suggesting that upon T-cell signalling, the TCR does not strongly localise to close contacts. This is similar to the results of a study which used SLBs containing agonist pMHC and quantum dots to mark T-cell close contacts²²³.

Similarly, ZAP-70 analysed against the glycocalyx on agonist-presenting SLBs gave an average correlation coefficient of 0 (Figure 39B, right panel). There was a stronger anticorrelation of -0.31 on null-presenting SLBs and -0.40 on agonist-presenting SLBs where cells were treated with 3-MB-PP1, which was statistically significant for both and again suggests a shift in ZAP-70 localisation away from close contacts upon T-cell signalling.

These observations suggest that during T-cell spreading and synapse formation MCs are real objects, distinct from close contacts made by the T cell and SLB, and not imaging artefacts. Cells on null pMHC-presenting SLBs, or those treated with 3-MB-PP1 by contrast showed strong anti-correlation between TCR or ZAP-70 and SLB exclusion, suggesting that under these conditions TCR and ZAP-70 are linked to close contacts.

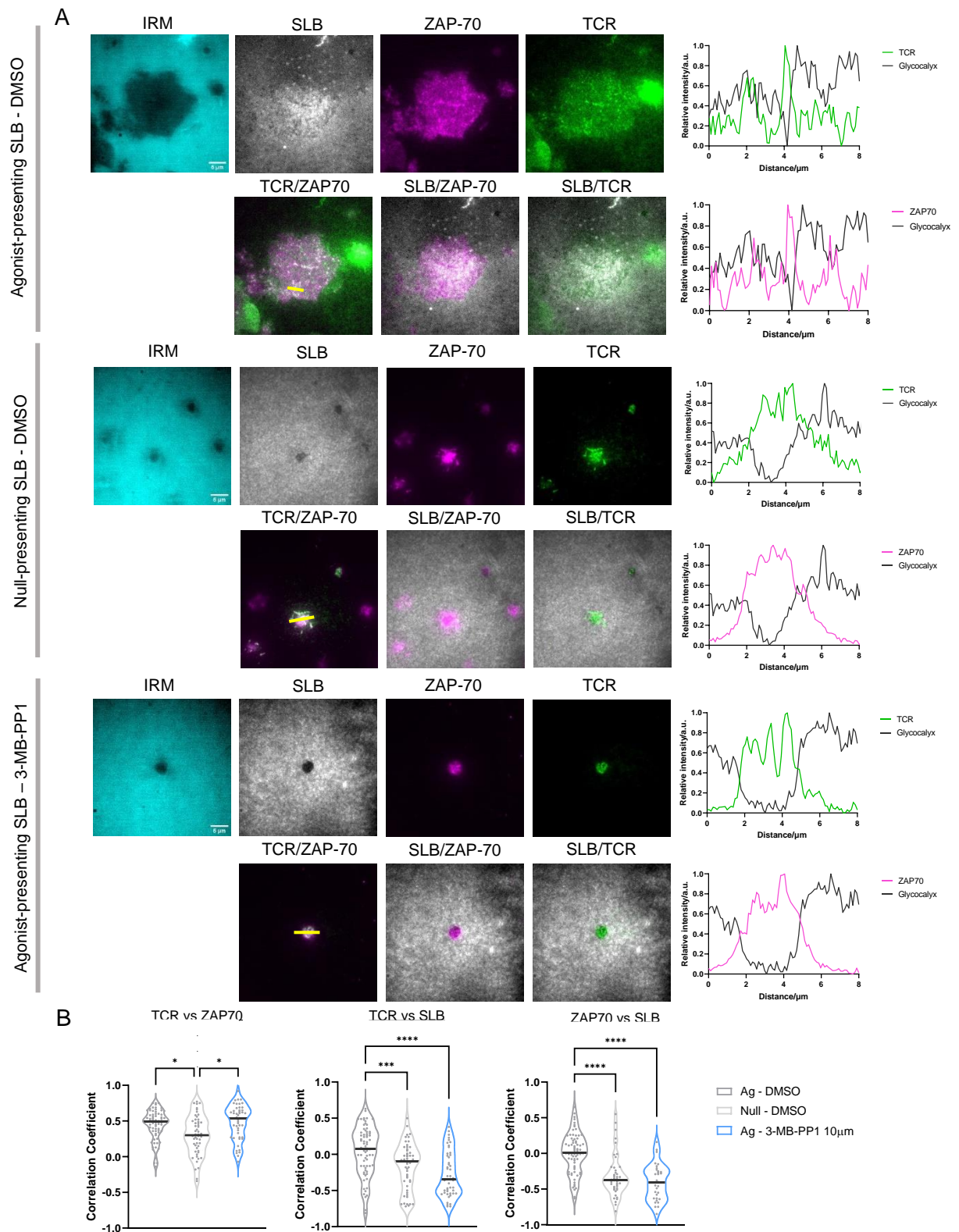


Figure 39 TCR and ZAP-70 microclusters do not appear exclusively at close contacts

Approximately 5×10^5 J-AS^{hi} cells were harvested, labelled with UCHT1 Fab-Halo and Janelia Fluor HaloTag ligand, then washed in PBS-MgSO₄ with either DMSO or matched volume of 3-MB-PP1. Cells were then allowed to interact with 2nd generation agonist- or null- presenting SLBs for 5 minutes before fixation and imaging on a TIRF microscope. Colocalisation between TCR, ZAP-70 and SLB (i.e. CD43 and CD45) was determined using Pearson's correlation in Fiji (Coloc2 tool) (A) Representative images of labelled J-AS^{hi} cells on 2nd generation SLBs (left) with different patterns of colocalisation between channels (right). (B) Violin plot indicating the correlation coefficient generated for comparisons between each channel. Dark lines represent median values. 47-72 cells analysed per condition for 3-4 biological repeats. Analysed by one-way ANOVA with Šidák's multiple comparisons. **** = $p < 0.0001$ *** = $p < 0.001$, * = $p < 0.05$. Non-significant comparisons not shown.

5.3.6 Actin Inhibition Disrupts Close Contact Formation¹

To test the role of actin within early contact formation and signalling, cells were washed and incubated in different actin-modulating drugs or control DMSO for an hour at 37°C before placing onto 2nd generation SLBs with labelled glycoalyx proteins (i.e., CD43 and CD45) and acquiring timelapse images for 10 minutes to image close contact formation and dynamics (Figure 40B and C). A high concentration of agonist pMHC was used (50-100 molecules/ μm^2) so that finding ligand was not a limiting factor. A custom Python code, described previously (section 4.2.7), was used to analyse close contacts including their size, number, and formation relative to the cell first appearing in the TIRF field.

Several different drugs were selected to disrupt actin in these cells. Jasplakinolide (Jasplak) prevents actin remodelling by stabilising pre-formed filaments⁴¹⁴. Cells treated with jasplakinolide therefore appear 'frozen' and retain the actin-mediated morphological features present before treatment. This means that any changes in cell behaviour observed after jasplakinolide treatment are likely due to the loss of the dynamic properties of microvilli specifically, rather than their removal. In contrast, cytochalasin D (CytoD) and latrunculin B (LatB) mainly inhibit actin polymerisation^{415,416} and cause loss of actin-mediated structures such as microvilli (Figure 40A).

Treatment with any of these drugs compared to DMSO significantly reduced the fraction of cells able to form close contacts on 2nd generation SLBs, from 70% of cells under control conditions to 20%, 43% and 38% with Jasplak, CytoD and LatB treatment respectively (Figure 40B). This indicates that a dynamic actin network is important in forming the close contacts required for TCR signal initiation. Additionally, the median time taken to form the first close contact (Figure 40C) was lengthened when cells were treated with CytoD and

¹ These experiments were carried out jointly with Edward Jenkins (Davis group) who also analysed the close contact formation using a CD4⁺ CD8⁺ LFA-1^{hi} cell line expressing the 1G4 TCR at physiological levels and with no conjugated tags, called J8. Cells also expressed a genetically encoded calcium indicator GjCamp7S³²⁵ to measure calcium flux without the need for Fluo-4 AM labelling.

LatB, from 80 s (DMSO) to 160 s and 170 s respectively, showing that cells incapable of forming microvilli struggle to penetrate the glycocalyx and form close contacts. Jasplak treatment did slightly increase the time taken for close contact formation to 130 s, but this was not significant, suggesting that immobile microvilli can penetrate the glycocalyx rapidly, but that active processes are required to form normal close contacts. On the other hand, since the sample number was lower for the Jasplak condition, this may be the reason for not reaching significance.

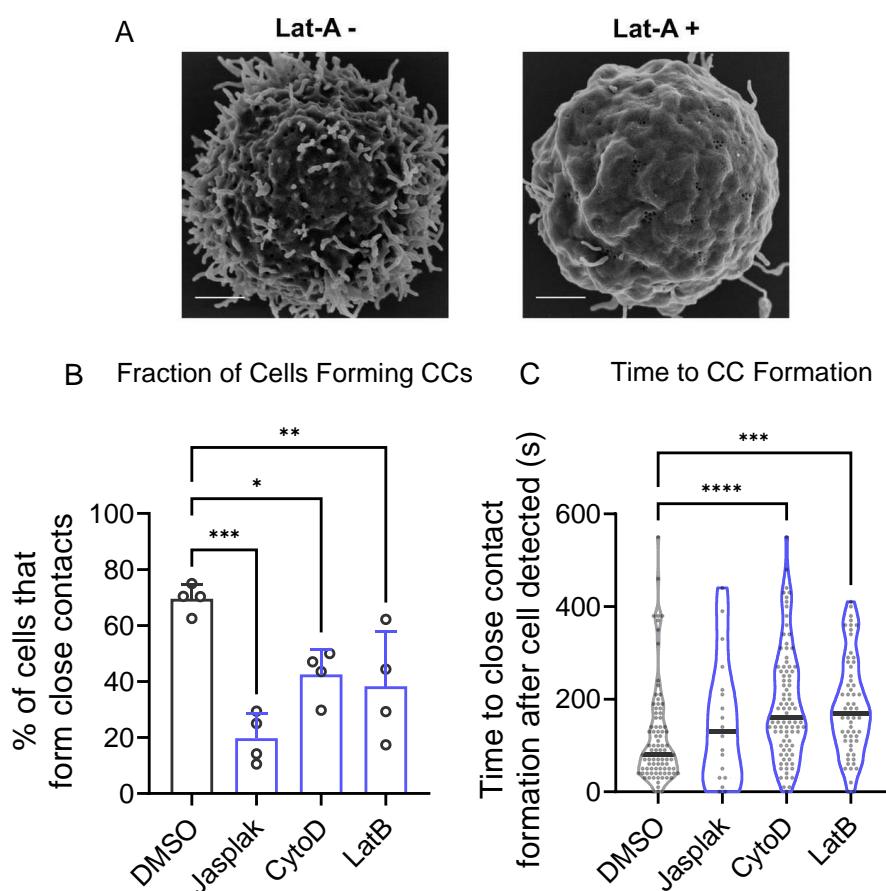


Figure 40 Dynamic microvilli are required to form normal close contacts on 2nd generation SLBs Cells were incubated with actin-modulating drugs or matched volume of DMSO before washing in PBS-MgSO₄ and being placed on 2nd generation SLBs with a high concentration of agonist pMHC. (A) Example of the effect of actin-inhibiting drugs on T cells, adapted from ref¹⁹⁴ (B) Fraction of cells forming close contacts under each condition. Mean ± SD plotted. Data from 13-113 cells over 4 biological repeats. (C) Time between a cell first being detected (using Cell Mask) and its first close contact formation. Bars represent the median value. Data from 18-93 cells over 4 biological repeats. Analysis was carried out by one-way ANOVA with Tukey's multiple comparisons assigning DMSO as the control group. **** = $p < 0.0001$ *** = $p < 0.001$, ** = $p < 0.01$ * = $p < 0.05$. Non-significant comparisons not shown.

5.3.7 Actin Inhibition Does Not Prevent TCR Triggering²

Finally, to test whether actin-based structures are essential to T-cell signalling, cells were prepared with either DMSO or actin-inhibiting drugs as before, washed in PBS-MgSO₄ with DMSO or the drug, and placed on either 2nd generation agonist-presenting SLBs or SLBs with only pMHC and CD58, to create a surface with no steric hindrance for T-cell scanning. Agonist pMHC densities used here were between 50-100 molecules/ μm^2 to ensure pMHC availability was not limiting. Under control conditions, there was no difference in signalling observed between the two SLB types tested (2nd generation or pMHC + CD58 only, Figure 41). When treated with any of the actin-inhibiting drugs however, there were substantial and significant decreases in the fraction of cells signalling on 2nd generation SLBs compared to the pMHC + CD58 SLBs only (Figure 41). Jasplak treatment reduced the fraction of cells signalling from 53% (2nd generation SLB) to 26% (pMHC + CD58 only), while for CytoD this was reduced from 57% to 22%, and 67% down to 31% with LatB. This strongly suggests that the actin cytoskeleton is not required for TCR triggering *per se* but does facilitate signalling in an environment where agonist pMHC is presented with a glycocalyx. However, the fraction of cells signalling on pMHC + CD58 only SLBs is slightly lower with actin-inhibiting drug treatment compared to the control, and this is significant for Jasplak and CytoD (Figure 41), suggesting another effect on the cells which is reducing their ability to signal.

² Experiments and analysis were carried out jointly with Edward Jenkins (Davis group) as in the previous section.

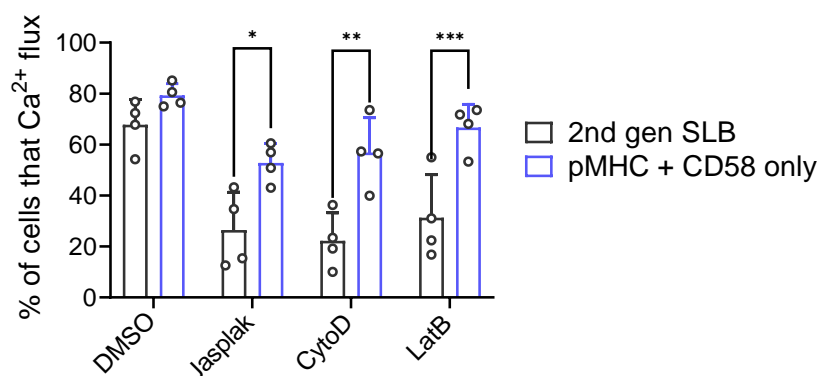


Figure 41 **Actin inhibition reduces TCR signalling when a glycocalyx is present** Cells were incubated with actin-modulating drugs or matched volume of DMSO before washing in PBS-MgSO₄ and being placed either on 2nd generation SLBs or SLBs comprised of pMHC and CD58 only. Mean ± SD plotted. Data from 138-785 cells per repeat over 4 biological repeats. Analysed using two-way ANOVA with Šidák's correction. *** = p < 0.001, ** = p < 0.01 * = p < 0.05. NB. Significant decreases between control and Jasplak (**), as well as CytoD-treated cells (*) was found on pMHC + CD58 SLBs as determined using ordinary one-way ANOVA with Dunnett's multiple comparisons. All conditions were found to be significantly different (**) from DMSO on 2nd generation SLBs as determined using ordinary one-way ANOVA with Dunnett's multiple comparisons.

5.4 Discussion

The aim of this chapter was to address whether TCR expression levels and signalling capacity (through ZAP-70) contribute to MC formation and whether MCs are an artefact of microvilli binding laterally mobile agonist pMHC on SLBs.

TCR MC size, intensity and density was found to be independent of TCR expression, and TCR and ZAP-70 MCs formed in the same manner irrespective of TCR expression level. The intensity of ZAP-70 MCs was increased, surprisingly, upon 3-MB-PP1 treatment but no other characteristics (i.e., size and number of MCs) were significantly affected. Cells interacting with agonist-presenting 2nd generation SLBs did not show a statistically significant correlation between TCR or ZAP-70 and glyocalyx (CD43 and CD45) exclusion, however a significant anticorrelation between TCR/ZAP-70 and the glyocalyx was found under non-signalling conditions (i.e., null-presenting SLBs or agonist-presenting SLBs where cells were treated with 3-MB-PP1). Finally, chemical modulation of the actin cytoskeleton was shown to reduce the ability of cells to form close contacts with SLBs but did not significantly inhibit the fraction of cells signalled, as long as access to agonist pMHC was not hindered by a glyocalyx on the SLB.

5.4.1 The Effect of TCR Expression and ZAP-70 Activity on Early Signalling Microclusters

TCR expression did not affect the normalised number, size or intensity of TCR or ZAP-70 MCs. ZAP-70 inhibition on the other hand increased ZAP-70 microcluster intensity but did not affect TCR clusters significantly.

Defining and characterising MCs for quantitative analysis, especially with standard-resolution microscopy techniques, is difficult. Studies of MCs often define them as a certain threshold intensity based on the density of TCRs on the cell¹⁷² or relative to a single isolated fluorophore²¹³. Furthermore, many of these studies were conducted on primary cells which

have different TCR density and overall size to Jurkat cells. Since the experiments here compared cell lines with different TCR expression, absolute intensity values could not be used to define a MC, so a value of relative intensity per cell (within the top 20%) was empirically determined to be a suitable value. While this meant that control cells placed on a surface that does not induce strong signalling (i.e., SLBs with null pMHC) were counted as having TCR and ZAP-70 MCs, the characteristics of these were generally different to *bona fide* signalling MCs (for example being present at lower densities and/or lower intensities) as expected on agonist pMHC-presenting SLBs (see Figure 37 and Figure 38), suggesting the method of analysis is valid.

However, ZAP-70 cluster size and intensity was higher for J-AS^{lo} cells on a null-presenting SLB than agonist-presenting SLB, suggesting that either error in the analysis method used here may not be low enough to determine small changes in ZAP-70 intensity in J-AS^{lo} cells, or that the 'null' surfaces were causing more signalling than expected for the cells analysed. The latter possibility is unlikely as cells were previously determined to signal negligibly on such SLBs (i.e., only a small fraction of total cells flux calcium, Figure 51). Using a surface such as fibronectin-coated glass, which does not induce TCR signalling (data not shown), could help capture the TCR and ZAP-70 in a more representative 'resting' state.

Since ZAP-70 expression was similar between the cell lines, and higher than wildtype Jurkats (see Figure 19), any differences in ZAP-70 recruitment must be attributable to changes in TCR expression or ZAP-70 signalling rather than differences in protein expression. However, since the expression of ZAP-70 is not comparable to wildtype cells, it is possible that ZAP-70 behaviour in these cells may not be reflective of wholly physiological conditions.

It has been shown that, when T-cells are placed on activating surfaces, new MCs are continuously generated at the periphery and translocated into the centre of the cell where they form a cSMAC^{211,213}. Here, MCs were analysed from the entire surface of the cell, which

would capture them at slightly different timepoints in their 'lifecycle'. While most cells did not form a cSMAC in the 5-minute time period before fixation, since all cells in a given field of view were analysed, those that did were included in analysis and could skew the MC distribution towards larger, brighter clusters. Excluding clusters bigger than $1 \mu\text{m}^2$ for TCR or $2 \mu\text{m}^2$ for ZAP-70 was used to negate this effect but these size restraints were based on only single studies measuring MC size^{211,413}. Furthermore, given that ZAP-70-inhibited cells do not progress to full spreading, they are likely stuck in the 'antigen scanning' stage. Future experiments could involve restricting analysis to different areas within a spread cell, or to the periphery only to select newly formed signalling TCR MCs. Treating cells with 3-MB-PP1 after spreading and analysing these newly formed MCs could provide a way to study the effect of ZAP-70 inhibition on MCs at a more comparable stage to control cells. Additionally, using more sophisticated thresholding methods could help to identify MCs across regions of uneven illumination rather than simply selecting the brightest clusters across the entire cell.

As previously discussed, (section 1.9, section 4.1 and demonstrated in section 4.3.5.4 and 5.3.5), T cells interacting with SLBs do not form completely flat contacts which creates slightly uneven illumination on the cell surface. Furthermore, since the experiments conducted here were carried out with standard diffraction-limited microscopy, MCs smaller than one pixel ($\sim 100 \text{ nm}$ for the microscope used) cannot be distinguished and therefore all MCs as defined here will have a size of at least one pixel, which may not be reflective of the size of the smallest signalling MCs. This presents an issue for standard microscopy techniques in quantifying MCs. However, some super-resolution techniques can measure cell membrane distance from a surface as well as localisation of fluorophores¹⁹⁴. Using this method could overcome any fluctuations in cell topography that may be causing apparent differences in protein localisation, as well as increasing the sensitivity of imaging to the smallest MCs, which some groups have suggested could be as small as 11 TCRs each²¹¹.

However, analysis of protein clustering by super-resolution techniques can be prone to molecule overcounting errors^{300,301}.

5.4.2 The Relationship between Microclusters and T-Cell Topography

Colocalisation analysis showed a strong correlation between TCR and ZAP-70 on agonist-presenting SLBs, regardless of ZAP-70 kinase activity, but only significant anticorrelation between TCR or ZAP-70 and the glycocalyx when cells did not signal (null-presenting SLBs or agonist-presenting SLBs with 3-MB-PP1 treatment). This suggests that TCR and ZAP-70 MCs are indeed real structures and not artefacts of TIRFM in cells interacting with an activating surface, while in conditions of little/no signalling (i.e., null pMHC-presenting SLBs or 3-MB-PP1-treated cells), TCR and ZAP-70 localisation is strongly linked to close contacts. SLBs may not be able to fully capture the complex topography of a T cell since only relatively large proteins are labelled in the present experimental setup. A real APC, with a more complex surface proteome and different stiffness to glass-SLBs, may induce more subtle fluctuations in the T-cell membrane that would not be apparent in this context. A low density of agonist pMHC was used here to provide a more physiological surface, however numerous T-cell studies use high densities (≥ 100 molecules/ μm^2) of agonist pMHC which may influence TCR MC size through passive binding. Future experiments could therefore be carried out at higher agonist pMHC densities.

Pearson's correlation coefficient is useful for determining the strength of colocalisation between two channels in an image as it analyses both the overlap between channels and their intensity. It is not affected by the absolute intensity of either channel meaning that differences in labelling of the proteins of interest is unlikely to affect results, unless there is a large inefficiency of labelling or large variability in labelling efficiency across samples. However, Pearson's correlation coefficient is only accurate for linear relationships and does not necessarily imply a causative effect between the two variables measured, neither does it account for differences caused by a potential third variable.

J-AS^{hi} cells on null-presenting SLBs or agonist-presenting SLBs with 3-MB-PP1 treatment do not spread out as much as control-treated cells on agonist-presenting SLBs (see section 4.3.4.3 and 4.3.5.3), meaning that the area used for analysis is much smaller. The Pearson's correlation coefficient analysed channel intensities for each pixel so that even small clusters will not be overlooked, however the images analysed were diffraction-limited and therefore using super-resolution imaging may provide more accurate information about relative localisation of proteins within and around the cell.

Treating cells with the actin-inhibiting drugs Jasplakinolide, Cytochalasin D, and Latrunculin B disturbed T cell-SLB contact formation by reducing the number of cells forming close contacts and increasing the time taken to form close contacts. However, there was still a small decrease in the fraction of cells signalling on pMHC + CD58-presenting SLBs when cells were treated with actin inhibitors compared to DMSO-treated cells, which was significant in the case of Jasplak and CytoD, suggesting that the drugs used reduce signalling capacity to some extent. It is possible that the cells' signalling capacity decreased due to a general disruption of key processes regulated by the cytoskeleton, but this was not investigated further here and therefore is an opportunity for future study.

6 Lymphocyte Receptors as Individual Functional Entities

6.1 Introduction

It is widely accepted that TCRs can be triggered and activated by a very small number of ligands; even as low as a single pMHC per APC^{184,208}. This extreme sensitivity is not surprising given the rarity of agonist pMHC present in the body for any given TCR. What has not yet been conclusively determined is the mechanism by which a single ligand can induce signalling and activation of a T cell with both high specificity and sensitivity.

Since there is substantial evidence for a monomeric distribution of resting TCRs^{179,190,191,303}, and that ligand recognition must occur before TCR triggering, it seems likely that monomeric TCRs can produce the initial signal in T cells. Indeed, a recent paper used several fluorescence microscopy techniques to show that monomeric TCRs are responsible for ligand recognition¹⁷⁹, and imaging studies in live T cells have demonstrated ZAP-70 recruitment to a single TCR-engaged pMHC on an SLB⁴¹⁷ as well as calcium flux in response to single pMHC molecules on APCs⁴¹⁸. Evidence from this thesis, where cells expressing very low densities of TCR (i.e. 1G4^{lo} and J-AS^{lo}), or without a functional actin cytoskeleton signal robustly (section 3.3.4, 3.3.5 and 5.2.3), and another study where low TCR-expressing cells signal readily in response to superantigen²¹⁰, suggest higher oligomeric states of the TCR may not be strictly necessary for triggering.

Both the conformational change and the KS model of TCR triggering, as well as the serial triggering hypothesis which aims to explain T cell sensitivity, do not require TCR clustering for induction of signalling. Therefore, assuming a monomeric TCR at rest, testing key predictions of each model can be used to determine the correct mechanism. One prediction made by the KS model, but not others, is that slowing the diffusion of the TCR within a close contact increases the probability of triggering^{185,195}. This can be readily examined using versions of pMHC with and without a histidine tag. Histidine-tagged pMHC will directly bind

to TCR and nickel-containing SLBs simultaneously, thus restricting the free diffusion of the TCR. pMHC adducts without these tags will be dragged across the SLB surface in close contacts between the T cell and SLB, and therefore will slow the diffusion of TCR without directly anchoring it to the SLB. Additionally, measuring cell signalling on gp100 pMHC-presenting SLBs with a very low density of agonist pMHC could be used to test whether a single TCR/pMHC interaction can induce triggering without the need for serial binding, as the extremely high affinity of this TCR/pMHC pair³⁷⁶ favours very long binding times. As coreceptors have been implicated in increasing TCR sensitivity to pMHC¹⁶, the role of CD8 can also be tested using MHC mutants with different affinities for the coreceptor on SLBs.

The triggering mechanism of the BCR is also highly debated. As with the TCR, receptor crosslinking has been shown to induce signalling, but considering many antigens are presented to B cells on the surface of other cells^{267,268,305}, and indeed monomeric antigen can induce signalling at a surface²⁹⁵, another mechanism must also occur. While numerous models have been proposed (see section 1.11), recent unpublished work in the Davis group (thesis of Martin Wilcock) has suggested a role for KS in BCR signalling. It was demonstrated that while monomeric ligands cannot trigger the BCR in solution, they induce robust signalling when presented on a surface. Furthermore, B cells interacting with antigen at a surface exhibit exclusion of the phosphatases CD45 and CD148 and this is dependent on the size of the protein extracellular domains. By testing other key predictions of the KS model in B cells the correct mechanism for BCR triggering may become apparent. For example, a monomeric BCR distribution (predicted by KS) directly excludes the possibility of the dissociation-activation model of BCR triggering (see section 1.11.1) which has persisted for over a decade. Therefore, elucidating the resting stoichiometry of the BCR is essential to determine the BCR triggering mechanism.

While numerous studies have investigated the effect of reducing ligand density on TCR signalling^{192,211,213}, few have changed the density of the TCR itself^{82,419}, and none of these

have looked at the effect of TCR density on early TCR signalling events. The cell lines created in this thesis with very low TCR expression, therefore, provide a unique opportunity to test the functional limits of single TCRs, since MCs would likely not form at all, or as readily, as under physiological TCR expression levels. If ligand density is decreased to a suitable level, single pMHC/TCR interactions can reasonably be assumed. Furthermore, by using a model B cell line with known antigen specificity, key experiments can be carried out in a different lymphocyte model to determine whether principles regulating TCR triggering apply to other immune cells.

Evidence from both this thesis and the literature suggests that the TCR may be capable of triggering without forming MCs. Therefore, the aim of this final chapter is to investigate the role of the TCR as a monomeric functional molecule and determine whether signalling MCs are necessary for TCR triggering. Furthermore, experiments will also be conducted in a model B cell line to determine the generalisability of TCR triggering mechanisms to other immune receptors, to the extent that stoichiometry can be used to distinguish between theories.

6.2 Materials and Methods

6.2.1 TCR Triggering in Solution

Non-triggering and non-adhesive SLB surfaces were created on glass coverslips using a 100% POPC SUV solution at the same concentration as the mixed 98% POPC 2% Ni-NTA-DGS solution. Lipids were dried, resuspended, mixed and sonicated as before and SLBs were created using the previously defined method (section 2.5.1). SLBs were temperature-equilibrated in the microscope chamber for 5 minutes before use.

Cells were tested for their signalling capacity on OKT3-coated surfaces before each experiment. For solution signalling experiments, approximately 5×10^5 gp100^{hi} cells were incubated in 20 μ L of complete RPMI containing 1 μ L of Fluo-4 AM (final concentration 25 μ g/ml) for 15 minutes, before being washed in 1 ml pre-warmed PBS and resuspended in the same. 1 μ L of the cell suspension was added to POPC SLBs and cells were allowed to settle for 3 minutes, while being monitored to ensure negligible signalling at this stage. 2 μ L of either 1 μ M unlabelled UCHT1 antibody, gp100 pMHC (no tags), gp100 pMHC (2xHis tags), or PBS was added to the settled cells and timelapse acquisition was started.

For TCR diffusion signalling experiments, approximately 5×10^5 gp100^{hi} cells were incubated in 20 μ L of complete RPMI containing 1 μ L of Fluo-4 AM (final concentration 25 μ g/ml) and either 1 μ M unlabelled UCHT1 Fab, gp100 pMHC (no tags), gp100 pMHC (2x6His tags), or RPMI alone. Proteins were centrifuged at 17,000 x g for 5 minutes at 4 °C prior to use to remove aggregates, and both pMHC types were additionally subjected to size-exclusion chromatography (AKTA Pure system) to ensure only monomeric fractions were used. Cells were incubated for 15 min at 37 °C, washed with 1 ml pre-warmed PBS, and resuspended in the same buffer. 1 μ L of the cell suspension was placed onto SLBs presenting a high density of CD58 only (approximately 3600 molecules/ μ m²). This density was non-

saturating to ensure some free nickel chelating sites would be available for binding to gp100 pMHC with 2x6His tags.

Timelapse images were acquired every second for 600 frames/10 minutes. Custom MATLAB code (section 2.6) was used to analyse cell signalling.

6.2.2 H2Kb mutant pMHC production

A refolded pMHC with an enhanced CD8 binding mutation was made. This pMHC comprised of the $\alpha 1/\alpha 2$ peptide binding platform of HLA-A2 and the $\alpha 3$ domain of H2-Kb, derived from murine HLA-A2⁴²⁰. This was refolded with human $\beta 2$ microglobulin and the gp100 peptide used previously in this thesis (see section 2.3.8 for full details). As with other pMHCs produced for use on SLBs, a dual histidine tag (2 x 6His-linker-2 x6 His) was added onto the C terminus of HLA-A2 to facilitate SLB binding through nickel-chelating lipids.

6.2.3 Serial Triggering Experiments

Approximately 5×10^5 gp100^{lo} cells were harvested, centrifuged at 2000 rpm for 90 seconds in a MiniSpin and labelled with 1 μ l Fluo-4 AM (final concentration 2.5 μ g/ml) and Cell Mask-647 (final concentration 0.5 μ g/ml) at 37°C for 10 minutes in complete RPMI media (total volume 200 μ l). Cells were then centrifuged as before and washed twice in 500 μ l pre-warmed 0.22 μ m-filtered PBS-MgSO₄ before being resuspended in 50 μ l of the same solution. After 3 minutes equilibration in the microscope incubator a small volume of the cell suspension was placed onto 2nd generation agonist-presenting SLBs. The concentration of agonist pMHC used was 0.005 ng/ μ l, equivalent to <1 pMHC per μ m².

Images were taken every 10 seconds for 60 frames/10 minutes and cell signalling was analysed with a custom MATLAB code (section 2.6).

6.2.4 Single Molecule TIRFM for BCR Tracking (DySCo)

Approximately 1×10^6 cells with low BCR expression (HyHEL10 receptor expressed in the pHRI vector) were harvested and centrifuged at 2000 rpm for 90 seconds in a Minispin. Cells were then resuspended in complete RPMI with 20 $\mu\text{g}/\text{ml}$ each of monomeric HEL labelled with either SMNAP Cell-505-Star or SNAP- 647 SiR and incubated for 15 minutes at 37°C. Cells were washed twice in 500 μl 0.22 μm -filtered PBS before placing on a PBS-washed fibronectin-coated glass coverslip (which does not induce signalling; data not shown).

Imaging was undertaken on a custom-built TIRF microscope with collaborators in Cambridge (James McColl, Klenerman group). Once cells had settled on the surface, high-intensity laser power was used to bleach already visible fluorophores on the cell surface. Then, image acquisition was started to capture labelled BCRs diffusing onto the cell surface in the evanescent field. Timelapse images were analysed using the established method Dynamic Single-Molecule Colocalisation (DySCo)³⁰², which tracks each fluorophore over time and determines the rate and length of colour coincidence.

6.2.5 dSTORM Imaging

MD4 cells were purified as previously described (section 2.1.6), resuspended in PBS and kept at 4°C. Approximately 1×10^6 cells were harvested and centrifuged at 2000 rpm in a Minispin. For surface labelling, cells were then resuspended in various concentrations of Alexa Fluor 647-labelled monomeric HEL (between 0.004-20 $\mu\text{g}/\text{ml}$) in PBS and left to incubate for one hour in the dark at 4°C. Cells were then washed twice in 1 ml PBS and fixed with freshly diluted 4% PFA and 0.25% glutaraldehyde for 30 minutes at room temperature, before a final wash (500 μl PBS) and resuspension in PBS for imaging.

For clathrin-labelled samples, cells were first fixed in freshly diluted 4% PFA for 30 minutes at room temperature, then incubated with blocking buffer (0.2% TritonX-100, 30 $\mu\text{g}/\text{ml}$ BSA in PBS) for one hour at room temperature. Cells were then centrifuged as before and

resuspended in permeabilisation buffer (0.5% TritonX-100, 30 $\mu\text{g}/\text{ml}$ BSA in PBS) for 2 minutes at room temperature before being centrifuged and resuspended in 200 μl blocking buffer containing between 1-20 $\mu\text{g}/\text{ml}$ of Alexa Fluor 647-labelled anti-clathrin antibody (Abcam ab 21679, labelled with an antibody labelling kit from Thermo Fisher) for one hour in the dark at 4°C. Cells were washed in 500 μl of permeabilisation buffer twice and resuspended in 4% PFA solution for 30 minutes before centrifugation and a final resuspension in PBS. All samples were stored in the dark at 4°C until imaging.

Images were acquired on a custom-built TIRF microscope (described in section 2.5.4) with collaborators in Cambridge (James McColl and Gregory Chant, Klenerman and Lee groups). PLL-coated glass coverslips were prepared, washed, and coated with gold nanobeads for microscope drift correction. Gold nanobeads (100 nm diameter, suspension in 0.1 mM PBS, Sigma Aldrich) were pelleted by centrifugation at 17,000 x g for 30 minutes and washed and resuspended in Milli-Q water. The bead suspension was then passed through a 200 nm pore to remove clusters and diluted 200-fold for use on slides. A small number of labelled cells were centrifuged at 2000 rpm in a MiniSpin then resuspended in a solution containing TN buffer (50mM Tris pH 8.0, 10 nM NaCl), an oxygen scavenging system (0.5 mg/mL glucose oxidase (Sigma Aldrich), 40 $\mu\text{g}/\text{mL}$ catalase (Sigma Aldrich), and 10% (w/v) glucose) and 10 mM 2-aminoethanethiol/cysteamine (Sigma Aldrich) and placed on the slides⁴²¹. A thin pad made of 1% molecular grade agarose solution (Thermo Fisher) in PBS was then placed on top of the cells to increase adhesion to the surface and reduce cell movement. Images were acquired using the 640 nm (1-1.2 kW/cm²) and 405 nm (100mW laser with filters restricting transmission to 12.5%) lasers at 1 frame per 33 ms for $\geq 10,000$ frames.

6.2.6 dSTORM Analysis

dSTORM image reconstruction involves creating precise localisations from each bright spot by fitting a two-dimensional Gaussian profile to the individual point-spread function

created by a fluorophore and compiling all frames together to collect all localisations within a sample³⁶⁴.

Analysis of dSTORM data was carried out by James McColl (Klenerman group) and Gregory Chant (Lee group). Images were reconstructed using the GDSC SMLM plugin in Fiji. Frames over time were corrected for drift by aligning each frame to the localisation of gold nanobeads present within the same field of view as the cell. This resulted in a higher precision of localisations over the frames. To avoid artefacts created by the edges of the cells (i.e., acquiring localisations within the TIRF field which are slightly higher up on the cell membrane) a square area from the middle of each cell was sampled for analysis. This area was kept as large as possible without including the edges of the cell.

Relative distribution of localisations was analysed by an established code³⁰⁰ which was run on MATLAB.

Firstly, binary masks of clusters were generated for the reconstructed super-resolution images. The number of localisations per μm^2 in clusters (ρ) was plotted against the number of total localisations per μm^2 . The y-intercept value of this graph (ρ_0) was used to normalise ρ values. Normalised localisation densities (ρ/ρ_0) were finally plotted against η , which is the relative area coverage by the binary cluster masks. This is carried out for multiple labelling densities creating a spread of data which can be fitted with a curve. Clustered localisations result in a steeper curve whereas the fit for random localisations remains essentially flat.

6.3 Results

Calcium flux-based signalling experiments were conducted to determine whether the TCR could induce signalling without the need for clustering and then to examine the similarities and differences in BCR and TCR signalling.

6.3.1 Early Signalling Response is Similar Between 1G4^{lo} and 1G4^{hi} Cells

If the TCR can trigger without clustering, it would be expected that cells expressing a low density of TCRs respond in the same way as those expressing a high density, provided the concentration of agonist pMHC is not a limiting factor.

Approximating the surface area of the cells to a sphere (see section 8.6), 1G4^{hi} cells have an average surface area of 452 μm^2 and 1G4^{lo} cells have a surface area of 483 μm^2 . Based on the quantification of TCR expression in Figure 12, 1G4^{hi} cells have ~ 38 TCRs/ μm^2 and 1G4^{lo} cells have 0.5 TCRs/ μm^2 , resulting in <1 TCR per microvillar contact (using microvillar measurements from Cai et al.²²³). These are likely to be an underestimate of density given the number of microvillar protrusions on the cell which increase its surface area. This significant difference in TCR density means that the 1G4^{hi} and 1G4^{lo} cell lines provide a useful tool for investigating the potential of single TCR triggering. Therefore, the calcium flux response of 1G4^{hi} and 1G4^{lo} cells was compared (Figure 42).

Approximately 1×10^6 TCR KO, 1G4^{hi} or 1G4^{lo} cells were labelled with Fluo4-AM, washed and equilibrated in the microscope incubator. Agonist-presenting SLBs were created with either a low (0.2 ng/ μl) or high (2 ng/ μl) concentration of agonist pMHC (i.e., HLA-A2-9V) and a null pMHC block (HLA-A2-gp100), washed and equilibrated as previously described. Cells were then placed onto each SLB and a timelapse video was acquired for signalling analysis with a custom MATLAB code (section 2.6).

TCR KO cells did not signal substantially ($<10\%$) with any tested concentration of pMHC on SLBs (Figure 42A). On SLBs presenting a high concentration (2 ng/ μl) of agonist pMHC, the

average fraction of 1G4^{hi} and 1G4^{lo} cells that signalled was 70% and 44% respectively, and not statistically different. However, when the concentration was reduced to 0.2 ng/ μ l, 1G4^{hi} cells signalled again on average 70% while for 1G4^{lo} cells this was reduced to 26%, which was statistically significant (Figure 42A). This demonstrates that 1G4^{lo} cells are more sensitive to changes in pMHC density. This data however implies that robust triggering of TCRs at very low density with a physiological affinity TCR/pMHC interaction is possible when agonist pMHC concentration is not a limiting factor. Since each concentration of agonist pMHC used here resulted in either a comparable or statistically different fraction of cells signalling for each cell line, these conditions were used for testing for any differences in the qualitative nature of calcium response (as a proxy for TCR triggering) between the 1G4^{hi} and 1G4^{lo} cells.

Closer examination of the signalling characteristics on SLBs presenting a high concentration of agonist pMHC revealed that the frequency distribution of calcium spikes between cell lines was similar with 55% of cells fluxing calcium only once for 1G4^{hi} cells and 64% for 1G4^{lo} (Figure 42B). The amplitude of calcium spikes for each cell line was almost identical at 10.5 x baseline for 1G4^{hi} and 10.6 x baseline for 1G4^{lo} cells (Figure 42C), although there was much higher variability of results for 1G4^{lo} cells (SD 2.4 vs. 0.3 for 1G4^{hi}). Finally, the median time to the first calcium spike was 66 s for 1G4^{hi} cells and 118 s for 1G4^{lo} cells (Figure 42D), but this was not statistically significant due to high variability within both cell lines (SD of 32 s for 1G4^{hi} and 25 s for 1G4^{lo}).

Since the similarity of calcium spike characteristics could be explained by the high concentration of pMHC leading to a saturating response, these parameters were also tested on low concentration agonist-presenting pMHC SLBs (Figure 42). Here, both 1G4^{hi} and 1G4^{lo} cells exhibited comparable frequency distributions of calcium spikes with 67% and 53% of cells signalling only once during the 10-minute timelapse respectively (Figure 42B). Further, the median spike amplitude for 1G4^{hi} cells was 7.2 x baseline intensity whilst for

1G4^{lo} cells it was 5.7 x baseline (Figure 42C). The median signalling time for 1G4^{hi} and 1G4^{lo} cells was 143 s and 197 s respectively (Figure 42D). None of these parameters were statistically different between the 1G4^{hi} and 1G4^{lo} cell lines. These data together show that the qualitative aspects of calcium flux response are similar regardless of TCR density.

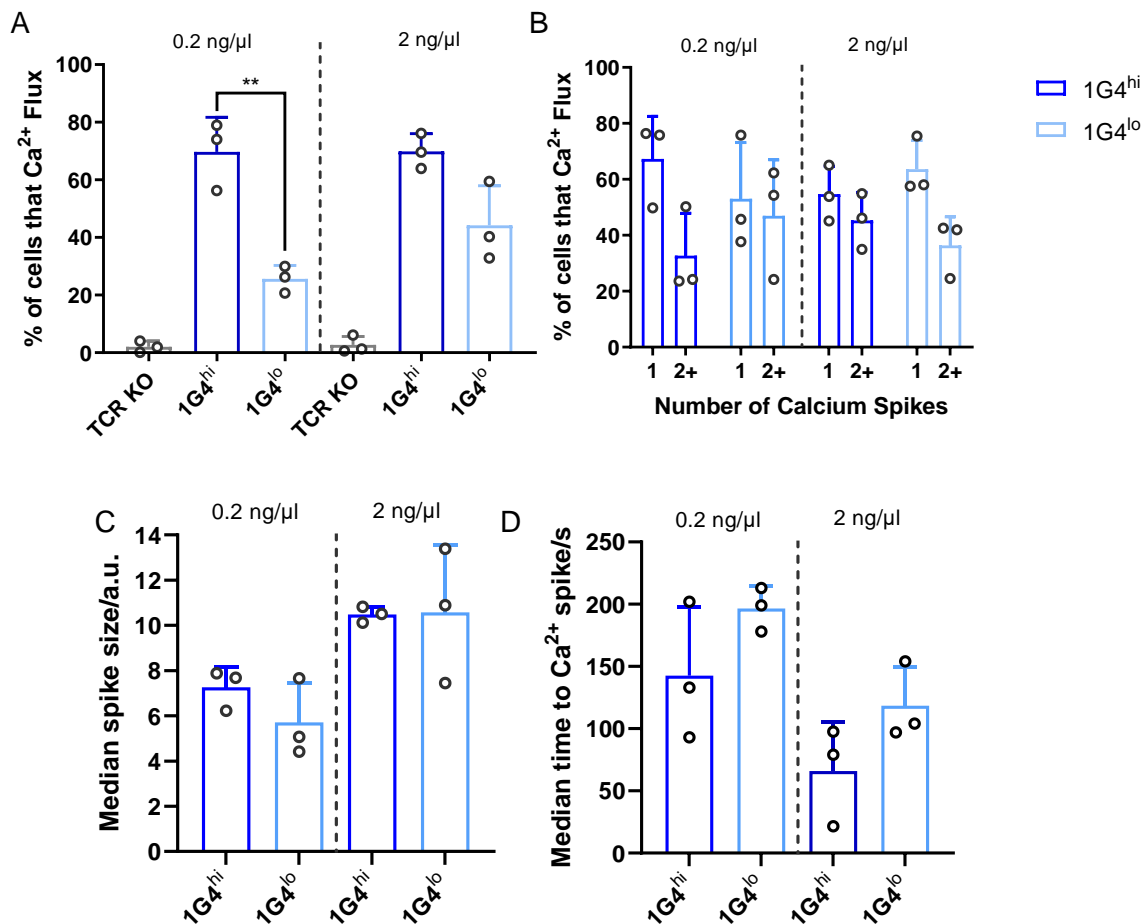


Figure 42 1G4^{hi} and 1G4^{lo} cells do not have significantly different calcium flux characteristics
 Approximately 1 x 10⁶ cells of 1G4^{hi} and 1G4^{lo} lines were harvested and labelled with Fluo4-AM for calcium flux experiments on SLBs made with a high (2 ng/μl) or low (0.2 ng/μl) concentration of agonist pMHC. (A) Fraction of cells triggering on each SLB type. Mean ± SD plotted. (B) Frequency distribution of the number of calcium spikes per cell between each cell line on each concentration of agonist pMHC. Mean ± SD plotted. (C) Median spike size, relative to the baseline intensity values per cell for each cell line on each concentration of agonist pMHC. Median ± SD plotted. (D) Median time to the first calcium spike for each cell on each concentration of agonist pMHC. Median ± SD plotted. Between 200-1000 cells were analysed and averaged per repeat for 3 biological repeats. Analysis was carried out between 1G4^{hi} and 1G4^{lo} cells using an unpaired student's t-test. ** = p < 0.01. Non-significant comparisons are not shown. Nb. Differences between TCR KO cells and 1G4^{hi} and 1G4^{lo} cells were not tested statistically.

6.3.2 Slowing TCR Diffusion Increases the Probability of Receptor Triggering³

It has previously been shown that monomeric ligand cannot induce TCR triggering in solution^{112,174}, but since the TCR can respond to single ligands in a cell-cell setting, crosslinking cannot be the only mechanism by which triggering is induced. The KS model postulates that single receptors can be triggered in such a context, if they are trapped in a phosphatase-excluding close contact for long enough to achieve net phosphorylation and induce downstream signalling¹⁸⁵. These predictions can be tested by comparing T-cell responses to monomeric ligands in solution and at a surface, and by slowing the diffusion of single TCRs within T-cell close contacts.

T cells were first presented with monomeric and crosslinking ligands in solution and on surfaces to investigate their effect on early signalling (i.e., calcium flux). Due to the relatively low affinity of the 1G4 TCR/9V-pMHC interaction, gp100^{hi} T cells and gp100-pMHC were used in these experiments. This ensures sustained binding of TCR and pMHC, and the possibility for conformational changes to occur, if this is part of the mechanism.

Functionally inert SLB surfaces were created using the vesicle fusion method with 100% POPC SUVs (described in section 6.2.1). Cells placed on these SLBs do not adhere or trigger, demonstrating the lack of interaction of the cells with this surface (data not shown). Gp100^{hi} cells were labelled with Fluo-4 AM as previously described (section 2.5.5.1), washed in PBS-MgSO₄, then placed onto 100% POPC SLBs and allowed to settle for 3 minutes. The microscope chamber was maintained at 37°C. Monomeric gp100 pMHC, PBS, or UCHT1 antibody was then gently added to the cells and a timelapse video was started with a frame being taken every second for 600 frames/10 minutes. Two versions of gp100 pMHC, with and without a dual 6x histidine tag, were created to investigate the role of slowing TCR

³ Triggering experiments carried out with, and analysed by, Edward Jenkins (Davis group). TCR diffusion experiments carried out, and analysed, by Kevin Chen and Markus Körbel (Klenerman group). The experiments described here formed part of a publication (see ref¹⁹⁶)

diffusion in close contacts in subsequent experiments. Therefore, both versions of pMHC were tested here. The addition of UCHT1 antibody led to strong calcium signalling (average 69%) whereas for all other reagents this was negligible ($\leq 5\%$) (Figure 43B, left). This confirms that the monomeric ligands used here, which cannot crosslink the TCR, do not induce triggering in solution despite a very high affinity.

To test signalling responses of the cells with modulated TCR diffusion, a calcium flux assay was carried out (Figure 43B, right panel). SLBs presenting labelled CD58 (approximately 3600 molecules/ μm^2) were created to allow cells to adhere and create close contacts without involving TCR/ligand binding. Not all nickel chelating sites were saturated with CD58 to ensure some free sites would be available to bind the dual 6x histidine tag used on one version of the soluble pMHC, thus linking the TCR directly to the SLB (Figure 43A). The pMHC adduct with no tags was predicted to slow TCR diffusion by dragging across the SLB surface. Cells were first labelled with Fluo-4 AM and gp100 pMHC with or without a dual 6x histidine tag, or equivalent volume of PBS. Cells were washed, resuspended in pre-warmed filtered PBS and placed onto CD58-presenting SLBs after temperature equilibration to 37°C. OKT3-coated glass with mock (i.e., PBS) labelled cells was used as a positive control for surface signalling experiments and induced an average of 73% of cells to signal (Figure 43B, right panel). PBS-incubated cells signalled <11% on CD58-presenting SLBs, likely representing the fraction of cells displaying the baseline level of ligand-independent triggering induced by random TCR diffusion in close contacts which have been depleted of CD45 phosphatase activity¹⁸⁵. Incubating cells with gp100 pMHC (no tags) significantly increased the fraction of cells signalling to 36%, while incubation with gp100 pMHC (dual 6x histidine tags) increased this further to 64% - statistically indistinguishable from the OKT3 condition, and significantly higher than gp100 pMHC with no tags. These results suggest firstly, that the TCR can be triggered in the absence of any ligand, and secondly that slowing the diffusion of the TCR in a close contact can induce signalling.

The effect of these adducts on TCR diffusion in the same cells were quantified in a recent study¹⁹⁶. Particle-tracking analysis of the TCRs in close contacts (defined as regions of CD58 accumulation) formed by these cells showed that TCR diffusion was reduced from 0.064 $\mu\text{m}^2/\text{s}$ (TCR with no adduct) to 0.013 $\mu\text{m}^2/\text{s}$ with pMHC (no tags) and 0.0043 $\mu\text{m}^2/\text{s}$ with pMHC (2 x histidine tags). As a negative control, in fixed cells, the TCR was found to have a diffusion rate of 0.00068 $\mu\text{m}^2/\text{s}$ (much slower than any other condition). Accordingly, here, the fraction of cells signalling was higher for cells incubated with pMHC (dual 6x histidine tags), which caused the largest decrease in TCR diffusion speed. Therefore, slowing TCR diffusion increases the probability of TCR triggering proportionally to the degree of receptor slowing.

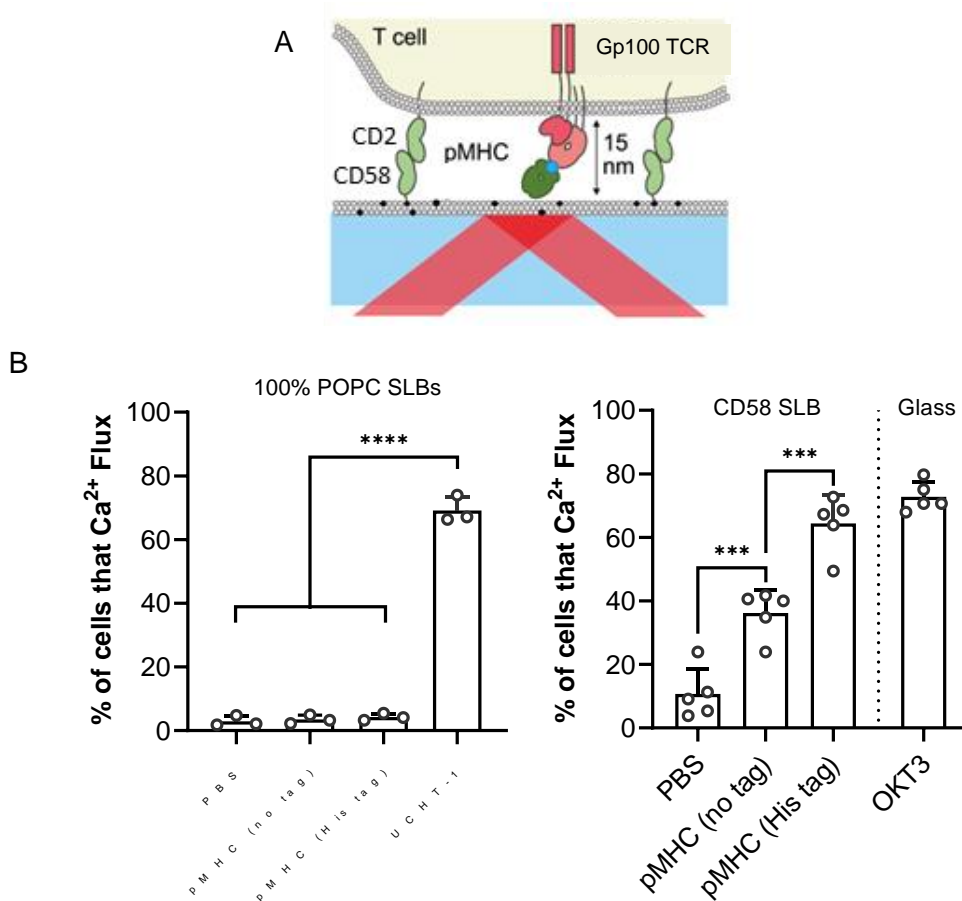


Figure 43 **Slowing TCR diffusion increases the probability of triggering** (A) Schematic illustrating the experimental set-up for slowing TCR diffusion with pMHC (no tags) on CD58-presenting SLBs. Figure adapted from ref¹⁹⁶ (B, left) Fluo-4 AM-labelled cells were allowed to settle on POPC SLBs for 3 minutes before adding PBS, gp100 pMHC without tags or gp100 pMHC with a dual histidine (2 x His) tag. UCHT1 antibody was used as a positive control. The graph shows the fraction of cells triggering during the subsequent 10 minutes. (B, right) Cells were incubated with PBS, gp100 pMHC (no tags) or gp100 pMHC (2 x His tag) for 15 minutes at 37°C before washing and placing on CD58-presenting SLBs. The graph shows the fraction of cells triggering during the subsequent 10 minutes. Significance was tested with a one-way ANOVA with Tukey's multiple comparisons. Mean \pm SD plotted in all graphs. **** = $p < 0.0001$ *** = $p < 0.001$. Non-significant comparisons not shown.

6.3.3 High Affinity pMHC does not Induce Significant TCR Triggering at Very Low Densities on 2nd Generation SLBs

T cells with low TCR expression have previously been shown to signal robustly on 1st generation and agonist pMHC-presenting SLBs (section 3.3.5 and this chapter). When TCR and pMHC interact at low densities, it is unclear whether a single occurrence of agonist pMHC binding a TCR could be enough to induce triggering, or whether this could be

explained by serial binding and unbinding of TCR(s) and pMHC. The serial triggering hypothesis, which stipulates that one agonist pMHC binding several TCRs on a T cell leads to a biological response^{173,209}, could explain the ability of low pMHC density to lead to robust signalling. Therefore, the gp100 TCR, with an extremely high affinity (11 pM^{376}) for its cognate pMHC, was used to test whether serial binding is necessary to induce TCR triggering in a situation where TCR/pMHC interactions are infrequent. Gp100^{lo} cells were used to reduce the likelihood of TCR clustering and pMHC serially binding multiple TCRs in close proximity, since the density of TCR on this cell line is likely to be $\leq 1 \text{ TCR}/\mu\text{m}^2$ based on surface area measurements made in other cell lines.

2nd generation SLBs were used to provide a more physiological surface on which T cells have been shown to be more sensitive to changes in pMHC density (unpublished work of Edward Jenkins, Davis group). The concentration of agonist pMHC used was $0.005 \text{ ng}/\mu\text{l}$ which is equivalent to $< 1 \text{ pMHC per } \mu\text{m}^2$ and therefore should equate to $< 1 \text{ pMHC per microvillar contact}$ based on the known size of microvilli^{194,223}. Therefore, if signalling occurs it is likely due to a single agonist pMHC interacting with a single TCR. Null SLBs were created in parallel with only HLA-A2-9V, which does not induce signalling through the gp100 TCR (see appendix Figure 51).

Cells were harvested and labelled with Fluo-4 AM and Cell Mask-647 before being washed and resuspended in PBS-MgSO₄. After equilibration to 37°C cells were placed onto 2nd generation agonist- or null-presenting SLBs and imaged every 10 seconds for 60 frames or ~10 minutes.

The average fraction of cells signalling on a null-presenting SLB was 29%, whereas 30% of cells signalled on agonist-presenting SLBs (Figure 44). This suggests that under the conditions tested, single TCR/pMHC interactions are not able to induce signalling beyond background levels, which are likely a result of ligand-independent triggering¹⁸⁵, and/or some triggering of the high-affinity gp100 TCR in response to 9V-pMHC (see also Figure 51).

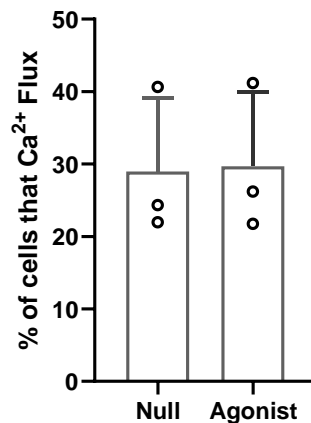


Figure 44 **Agonist pMHC at a very low concentration does not induce significant triggering on 2nd generation SLBs** Approximately 5×10^5 cells were harvested and labelled with Fluo-4 AM and Cell Mask-647 at 37°C for 10 minutes in complete RPMI media. Cells were washed twice in warm PBS-MgSO₄ before being resuspended in the same solution and placed onto agonist- or null-presenting 2nd generation SLBs. Mean \pm SD plotted. 45-56 cells were analysed per repeat for 3 independent repeats. Experiments were matched between null and agonist-presenting SLBs.

6.3.4 MHC Affinity for CD8 does not Substantially Affect TCR Triggering Induced by High-Affinity Ligands

Despite extensive research, the role and importance of coreceptors in TCR triggering remains somewhat unclear. While T cells are capable of signalling and activating without coreceptor presence¹³¹, it has been suggested that they may have a role in enhancing ligand discrimination by the TCR^{130,131}, which could be especially important when ligands (or receptors) are present at low densities. Therefore T-cell responses to pMHC molecules with different affinities for CD8 were tested to see whether coreceptor interactions of different affinities might affect early signalling when ligand density is varied.

To be comparable with the solution vs surface signalling experiments, the gp100 TCR-expressing cell lines were used here. Both gp100^{hi} and gp100^{lo} cells were compared to determine whether coreceptor affinity may have a more pronounced effect where TCR/pMHC binding is limited. To test this, a mutant pMHC (hereafter H2Kb mutant), which has a relatively high affinity for CD8 ($K_D \sim 10 \mu\text{M}$, compared with wildtype $K_D \sim 150 \mu\text{M}$)⁴²⁰ was cloned with a dual histidine tag and refolded with the gp100 peptide. The protein was

then analysed on an FPLC column and Coomassie gels to ensure only high-quality monomeric protein was used (for full details see sections 2.3.8 and 6.2.2).

1st generation SLBs were created with very high (5 ng/ μ l) or low (0.05 ng/ μ l) concentrations of agonist pMHC (either wildtype/WT or H2Kb), null pMHC block (HLA-A2-9V at 5-9.95 ng/ μ l depending on agonist pMHC concentration) and ICAM-1 (1.2 ng/ μ l), then washed in PBS-MgSO₄ and allowed to equilibrate in the microscope chamber at 37°C for 5 minutes. gp100^{hi} or gp100^{lo} cells were labelled with Fluo4-AM, washed in PBS-MgSO₄ and equilibrated in the microscope chamber at 37°C before being placed onto the SLBs.

On SLBs presenting a high density of agonist pMHC (Figure 45A, left panel), on average 75% of gp100^{hi} cells signalled on wildtype pMHC and 90% on the H2Kb mutant. For gp100^{lo} cells the matching fractions were 26% (wildtype) and 30% (H2Kb). There was no statistically significant difference between either pMHC type for each cell line. Considering the median signalling time (Figure 45, right panel), there was no statistically significant difference between either cell line or pMHC type. The average median time for gp100^{hi} cells was 18 s with wildtype MHC and 27s with the H2Kb mutant, while for gp100^{lo} cells this was 22 s vs. 24 s respectively.

The fraction of cells signalling on the very low concentration of pMHC (0.05 ng/ μ l; a 100-fold decrease) was only slightly lower (Figure 45B, left panel). For gp100^{hi} cells the fraction signalling was 69% with wildtype MHC vs. 74% with H2Kb and for gp100^{lo} cells this was 11% and 14% respectively. Median signalling time (Figure 45B, right panel) was much longer on low density pMHC-presenting SLBs with the average median signalling times of gp100^{hi} cells at 85 s for wildtype MHC and 25 s with the H2Kb mutant, which is the only comparison reaching statistical significance. Median signalling times were 91 s and 65 s for gp100^{lo} cells on wildtype and H2Kb mutant respectively.

Taken together, these data suggest that the role of CD8 affinity for MHC is negligible in inducing signalling by high-affinity pMHC/TCR interactions, except for decreasing the time taken to induce signalling in situations where ligand, but not TCR, is sparse.

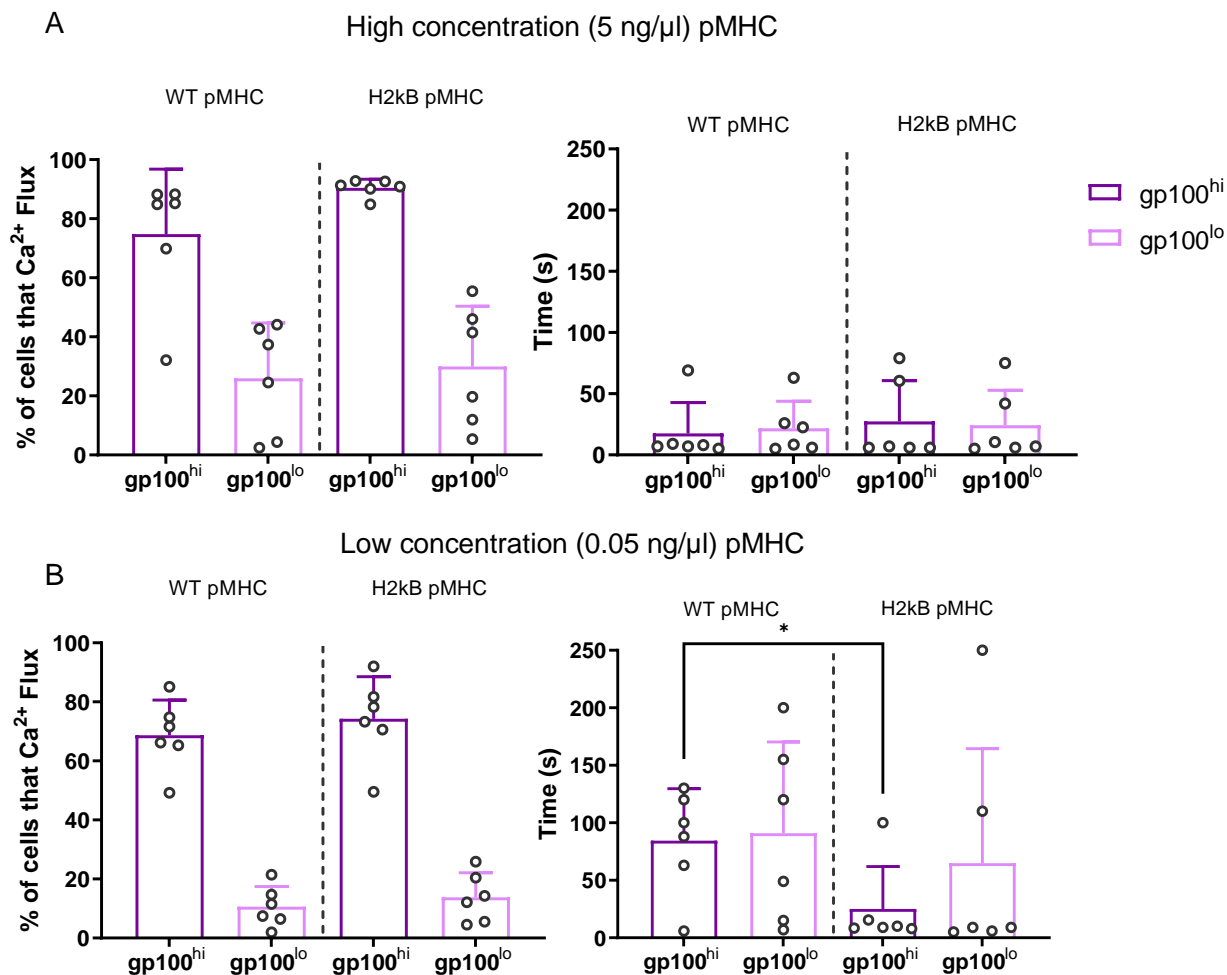


Figure 45 MHC affinity for CD8 does not affect TCR triggering induced by high-affinity ligands
 Approximately 1×10^6 gp100^{hi} or gp100^{lo} cells were labelled with Fluo4-AM and placed onto 1st generation SLBs presenting either wildtype or H2Kb mutant agonist pMHC. (A) Fraction of cells triggering (left) and median triggering time (right) for each cell line and pMHC type on SLBs with a high concentration of pMHC (5 ng/μl). (B) Same data for SLBs presenting pMHC at a low (0.05 ng/μl) density. Mean \pm SD is plotted in all graphs. Data pooled from ~200-1000 cells per repeat for 6 biological repeats. Cell lines were compared between WT and H2kB conditions pairwise by student's t-test * = $p < 0.05$. Non-significant comparisons are not shown.

6.3.5 The BCR Behaves as a Monomer on Live B Cells⁴

The fact that monomeric ligands can trigger the BCR on a surface²⁹⁵ suggests a triggering mechanism other than receptor crosslinking must be occurring, which may be initiated by single receptors. By determining the resting stoichiometry of the BCR, the number of appropriate models to explain triggering can be refined. Therefore, the stoichiometry on resting live B cells was analysed.

The model selected for these experiments is the HyHEL10 BCR transduced in A20 murine cells with their endogenous BCR removed by CRISPR/Cas9 (described in section 2.1.5). Given that the HyHEL10 BCR can be readily labelled in numerous colours via its ligand HEL (which binds with high affinity and is fused to a SNAP-Tag and a HaloTag), this presented an ideal opportunity to investigate receptor stoichiometry on live B cells. HyHEL10 BCR cells with low BCR expression (produced by transducing the BCR in a pHRI vector) were used, as a low density of labelled receptors was required for accurate measurements in diffraction-limited single-molecule microscopy experiments.

Dynamic Single-Molecule Colocalisation (DySCo)³⁰², which involves tracking multiple fluorophores over time to assess their coincidence rate, was performed on live B cells incubated with labelled HEL. Since the BCR has two ligand-binding sites, saturated BCRs on cells will each be labelled with two HEL proteins. Therefore, if labelling is maintained at saturation, ~50% of BCRs will be labelled with HEL of both colours, and the remaining ~50% will be split between single-coloured species if the BCR is monomeric. The presence of higher-order oligomers will increase the fraction of diffraction-limited spots labelled with both colours above 50%, while a majority monomeric BCR will result in ≤50% spots containing both colours. The ratio of these different colour combinations can therefore be used to determine the stoichiometry of the BCR in live cells.

⁴ Two-colour BCR tracking experiments were carried out jointly with Martin Wilcock (Davis group) and James McColl, who also performed data analysis (Klenerman group).

HyHEL10-expressing B cells with low BCR expression were harvested and incubated with equimolar concentrations of HEL labelled via SNAP-Tag with two non-spectrally overlapping fluorophores. Another aliquot of cells was labelled with the same fluorophores intracellularly via a HaloTag on the cytoplasmic domain of the Ig α chain and extracellularly with labelled HEL to act as a positive colocalisation control. After washing, cells were placed onto glass coverslips coated with fibronectin (which does not induce cell adhesion or signalling; data not shown) for imaging on a custom TIRF microscope. Labels on the cell surfaces were bleached with a high laser power which was immediately lowered for subsequent image acquisition as labelled BCRs diffused back into the TIRF evanescent field (Figure 46B). Timelapse images were acquired every 33 ms for 100 frames and then analysed with the DySCo method, using a custom MATLAB code utilising a Bayesian algorithm³⁰². Colour coincidence (i.e., putative dimers, or dual-labelled BCR monomers) is reported where two fluorophores track together over several frames, which is unlikely to happen given a random distribution of monomeric labelled proteins.

In addition to this, HyHEL10 antibody (i.e., a soluble BCR, made in-house) was labelled in the same manner as the cell-bound HyHEL10 and allowed to settle on a PLL-coated glass coverslip before imaging. Since the cell-bound BCR comprises two ligand binding sites, if it is monomeric, it should appear comparable to the soluble BCR/antibody control.

DySCo analysis gave an average coincidence value of 29.4% for the BCR on live cells, while for the HyHEL10 antibody/soluble BCR this was 37.2%, and 82.5% for the dual-labelled BCR positive control (Figure 46C). There was no statistically significant difference between the cell-bound BCR and soluble antibody, while both of these were significantly different from the positive control. While these values were lower than the predicted 50% coincidence for a dimer (i.e., dual-labelled BCR), this is likely due to labelling of the proteins not reaching saturation. Nevertheless, this implies a monomeric BCR on the surface of live B cells.

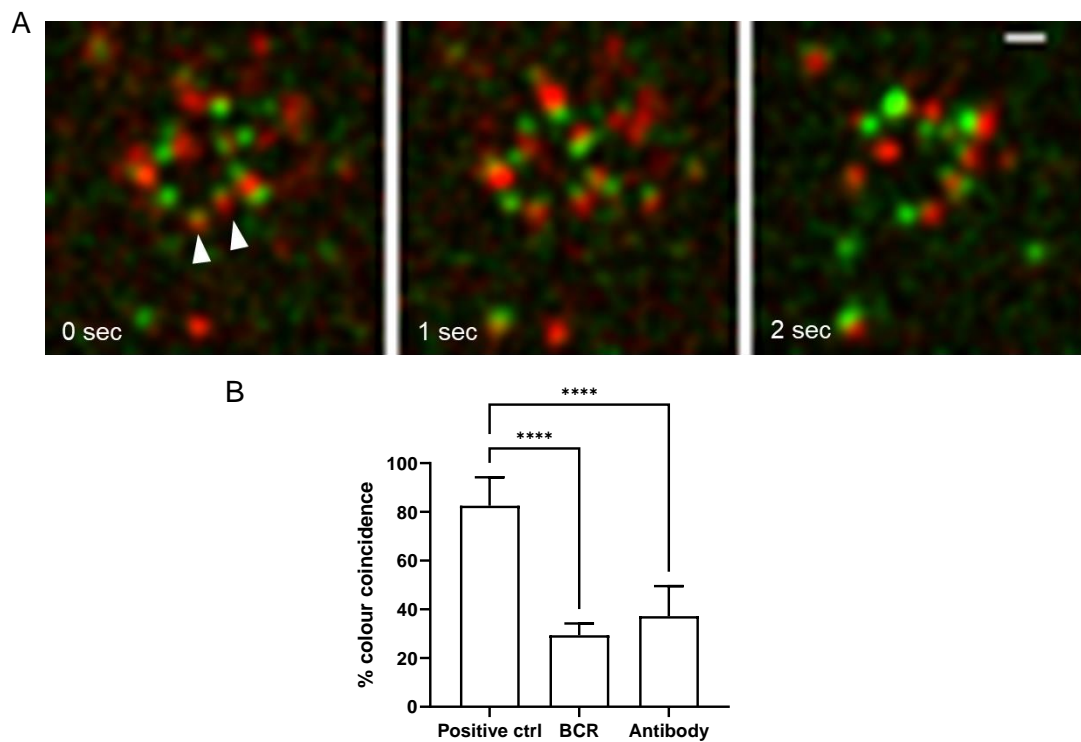


Figure 46 Two-colour coincidence analysis suggests a monomeric BCR on live B cells
 Approximately 1×10^6 cells expressing the HyHEL10 BCR at low expression levels were incubated with equimolar concentrations of HEL labelled with two different colours and placed on a fibronectin-coated glass coverslip. Other HyHEL10-expressing B cells were labelled intracellularly with a HaloTag ligand and externally in a different colour via HEL as a positive coincidence control. After bleaching of visible fluorophores, timelapse images were taken every 33 ms for 100 frames. HyHEL10 antibody was finally labelled in the same manner as the HyHEL10 BCR on the B cells and adsorbed onto a PLL-coated surface to prevent movement. Timelapse images of all three conditions were analysed by the DySCo method, using a custom MATLAB code. (A) Representative example of single molecules moving on a B-cell surface over time. Arrows indicate overlapping channels and therefore a dual-labelled BCR. Scale bar 2 μ m. (B) Percentage colour coincidence of the HEL + Halo-labelled BCR (positive control), HEL-labelled BCR, and HEL-labelled HyHEL10 antibody on glass. 8-10 whole cells per condition, and 86 individual antibodies were analysed in total. Mean \pm SD plotted. Statistical analysis was carried out by ordinary one-way ANOVA. **** = $p < 0.0001$

6.3.6 The BCR is Unclustered on Naïve Primary B Cells⁵

While experiments on live cells provide useful information about receptor mobility, the densities of BCR present on this cell line was much lower than physiological levels to facilitate single molecule tracking and counting at diffraction-limited resolution. To assess BCR stoichiometry in a more physiological setting, primary cells were used. One of the reasons the HyHEL10 receptor was chosen as a model BCR was because of the availability of transgenic mice with B cells expressing the same receptor. This enables experiments to be conducted using the same BCR model and reagents as for the B cell lines, but in a more physiological setting.

Primary murine MD4 B cells were purified via magnetic separation (described in section 2.1.6; Figure 47A). A negative selection method was chosen to avoid any interaction of naïve B cells with antibodies or beads which may cause BCR triggering, and purification was carried out in a tissue culture hood to avoid B cell activation by microbial contaminants. This ensures that the receptor stoichiometry is representative of cells in a resting, naïve state as triggering may change BCR distribution^{293, 296, 297, 310, 311}. Primary MD4 cells express approximately 4×10^5 BCRs per cell²⁷⁰ which is a density impossible to resolve by diffraction-limited microscopy. Therefore, super-resolution techniques were employed.

Direct stochastic optical resolution microscopy (dSTORM)³⁶⁴ is a technique which relies on observing fluorophore localisations over time, rather than simultaneously, to achieve sub-diffraction-limited (resolution of up to ~ 20 nm) images. The method was developed as a modification to traditional STORM which used the photophysical properties of a fluorophore pair to create cycles of fluorescence and darkness. Certain fluorophores, such as Alexa Fluor-647, exhibit cyclic photoswitchable properties when exposed to two

⁵ Experiments carried out with João Ferreira Fernandes (Davis group), James McColl (Klenerman group) and Gregory Chant (Lee group). Image analysis was performed by Gregory Chant and James McColl.

different laser wavelengths simultaneously. This 'blinking' is random and can be adjusted with laser power such that only a small fraction of total fluorophores is observed at a single time point. Therefore, by collecting localisations over a large period (several thousand frames) eventually every labelled protein will be acquired.

MD4 B cells were obtained from a fresh mouse spleen as per the method described in section 2.1.6 and their purity (typically ~80%) was confirmed by flow cytometry (Figure 47A). Cells were harvested and incubated with several concentrations of Alexa Fluor-647 labelled HEL in PBS for 1 hour in the dark at 4°C. Clathrin was used as a cluster control, since it is a well-known multimeric protein³⁰⁰. To label clathrin, cells were first fixed and permeabilised before labelling with different concentrations of anti-clathrin Alexa Fluor-647 labelled antibodies. Cells were then washed and fixed before finally being resuspended in PBS.

Images were acquired on a custom TIRF microscope with collaborators in Cambridge (Klenerman lab) by placing cells on PLL-coated glass coverslips seeded with gold nanobeads as fiducial markers, adding a buffer containing glucose oxidase and an oxygen scavenging system and gently placing a thin pad made from 1% agarose on top of the cells to prevent movement. Once a cell had been located, the 640 and 405 nm lasers were used simultaneously to induce fluorophore blinking and 10,000-15,000 frames (enough to capture most to all localisations) were acquired (see section 6.2.5 for details).

Timelapse images were then reconstructed in Fiji to produce a super-resolved image of each cell acquired by using the GDSC SMLM plugin to identify the centre of each bright point caused by a fluorophore (Figure 47B). Frames over time were aligned based on the localisations from the gold nanobeads to correct for microscope drift which would otherwise reduce the localisation accuracy. Analysis of the distribution of labels on each cell over a variety of labelling densities was carried out using an established method³⁰⁰ which relies on code run in MATALB.

Briefly, the clustering analysis normalises the average density of localisations within apparent clusters (ρ) to the intersection of the density curves with the y-axis (ρ_0). This is then plotted against the relative area coverage by the cluster masks (η) within the sample. This is calculated for multiple cells across a range of labelling densities to obtain a spread of data which can be fitted. A perfectly random distribution of localisations produces a flat line whereas more clustered localisation distributions form a steeply sloped line (see also section 6.2.6).

As seen in Figure 47C, BCRs labelled with HEL follow a pattern similar to a simulated perfect monomer when analysed by this method. Although a monomeric BCR would appear as a dimer due to its two ligand binding sites, current methods are not sensitive enough to distinguish between a monomer and dimer in such a case. In contrast, labelled clathrin produced a much steeper slope, similar to data from another study³⁰⁰. Therefore, this data is suggestive of an unclustered BCR on resting primary B cells.

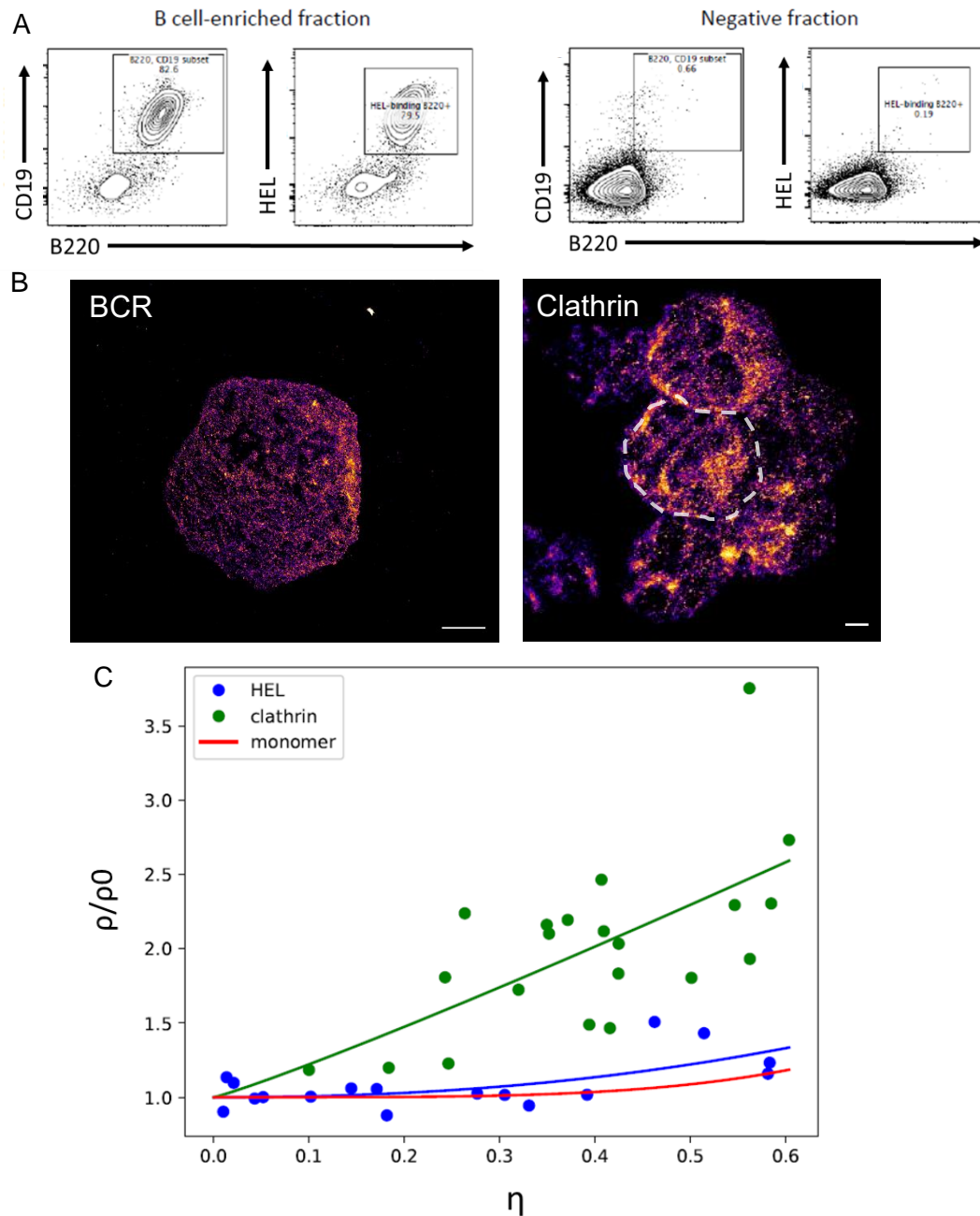


Figure 47 The BCR appears unclustered in primary murine B cells using dSTORM (A) Primary murine MD4 B cells, expressing the HyHEL10 BCR, were purified via magnetic separation using negative selection. B cell-enriched and B cell-depleted fractions were then analysed by flow cytometry to determine purity of separation which was typically ~80%. B220 (i.e. CD45) and CD19 are common markers of B cells. HEL binding, indicating the specificity of the BCR, was also analysed. (B) Representative reconstructed images of primary B cells labelled with either HEL or anti-clathrin antibodies placed onto PLL-coated slides. A gold nanobead, used for correcting microscope drift, can be observed in the top right corner of the BCR sample. One cell is outlined in white in the clathrin-labelled sample. Scale bars 2 μm . (C) Analysis of localisations for HEL and anti-clathrin labelled primary B cells over a range of labelling densities. Normalised localisation densities (ρ/ρ_0) are plotted against η (relative area coverage by the binary cluster masks). Each point represents one cell with a different density of labelling.

6.4 Discussion

In this chapter, the ability of the TCR to induce triggering without crosslinking or MC formation was explored. Using 1G4 TCR-expressing T cells with different receptor densities, it was shown that while 1G4^{lo} cells are more sensitive to changes in pMHC density on SLBs, the qualitative nature of their calcium response was indistinguishable from 1G4^{hi} cells. Furthermore, at high ligand density, the fraction of 1G4^{hi} and 1G4^{lo} cells signalling was comparable. Monomeric ligands could not induce signalling of gp100^{hi} cells in solution, but could when slowing TCR diffusion via interacting with the SLB, suggesting that an additional triggering mechanism operated beyond receptor crosslinking. Investigation of the resting stoichiometry of the BCR on both cell lines and primary B cells suggested a monomeric distribution of receptors using two experimental methods (two-colour tracking, and direct super-resolution imaging of the BCR). This evidence directly contradicts the dissociation-activation model of triggering allowing the possibility that monomeric receptors can induce BCR triggering.

6.4.1 Robust Signalling by 1G4^{lo} Cells

Characteristics of 1G4^{lo} calcium spikes, such as amplitude, frequency, and time to signalling were comparable to 1G4^{hi} cells on SLBs presenting different densities of agonist pMHC. 1G4^{lo} cells also signal at a comparable level to 1G4^{hi} cells when agonist pMHC density is high. The main disadvantage of these experiments is that all cell lines will express a range of TCR densities within their population. While TCR expression can be monitored and sorting implemented, it is impossible to maintain a population of cells with TCR expression spanning less than about 10-fold (see Figure 10 and Figure 11). This means that it is impossible to quantify signalling behaviour beyond the “average” cell. Therefore, the cells signalling may be those on the upper end of the TCR distribution of the 1G4^{lo} cells which could overlap with the TCR density of the lower end of the 1G4^{hi} cell line. One way to circumvent this would be to label the TCR on cells in a manner that would not affect ligand

binding (such as via intracellular SNAP-Tag) and create a way to screen cells based on the TCR signal intensity before analysing calcium flux.

6.4.2 Slowing TCR Diffusion Using His-Tagged pMHC on Ni-NTA-containing SLBs

Soluble, monomeric agonist pMHC molecules with and without histidine tags were used to confirm that monomeric ligands cannot trigger the TCR in solution, and further demonstrate that slowing TCR diffusion within a close contact is sufficient to induce triggering.

It is possible that models where the TCR is considered a mechanosensor, and/or changes conformation under force, could explain why anchored (i.e., pMHC with dual 6x histidine tag) and diffusion-restricted (i.e., pMHC with no tags), but not soluble monomeric ligands, induced signalling. However, TCRs were unlikely to be exposed to substantial forces as all components on the SLB are laterally mobile, and anchoring cells to the SLB with the small adhesion protein pair CD58/CD2 would likely insulate the TCR from bearing significant force. Furthermore, similar signalling results were observed¹⁹⁶ in a different TCR (1G4) and using a generic Fab ligand (UCHT1) which binds to a different part of the TCR complex than pMHC, which would not be expected if (force-induced) conformational changes were required to initiate TCR signalling. Finally, modelling of this system¹⁹⁶ demonstrated that the effect of diffusion alone was sufficient to explain the increase in signalling observed. However, it is impossible to rule force out completely in this experiment as it was not measured.

Using the gp100 pMHC/TCR pair is not a physiologically accurate model, since their binding affinity (11 pM³⁷⁶) is much higher than anything a TCR would encounter *in vivo*³⁷⁸. However, using a more representative receptor/ligand pair in this experiment would not permit the long binding times required to affect TCR diffusion and rule out rapid rebinding of TCRs by pMHC. Additionally, since similar results were observed with a non-pMHC generic TCR

ligand (UCHT1 Fab) bound to a different TCR (1G4),¹⁹⁶ it seems that the effects observed were not solely attributable to the high affinity of this interaction.

6.4.3 Gp100 TCR Triggering on Low Density Agonist-Presenting 2nd Generation SLBs

Gp100^{lo} cells were allowed to interact with 2nd generation agonist-presenting or null SLBs and the fraction of cells signalling was analysed. The concentration of agonist pMHC on the SLB was calculated to be < 1 pMHC per μm^2 which equates to < 1 pMHC per microvillar contact. This, combined with the high-affinity gp100 TCR receptor/ligand pair means that serial unbinding and rebinding of TCR and pMHC is highly unlikely, as is aggregation of more than one TCR on the cell surface. There was essentially no (~1%) difference in the fraction of cells signalling in either condition.

While this experiment demonstrates that agonist pMHC at this density does not robustly induce TCR triggering, it does not necessarily mean that single TCR/pMHC pairs cannot induce triggering. Assuming a similar surface area of gp100^{lo} cells to other cell lines used in this thesis, the density of TCRs should be approximately 1 TCR/ μm^2 . Given that the pMHC density used was < 1 pMHC/ μm^2 , this may reduce the likelihood of pMHC/TCR contact too much, extending it beyond the range of time acquired during the imaging period (~10 minutes). Additional experiments could therefore be carried out with a range of pMHC densities which, alongside modelling of TCR/pMHC encounters, could provide information about the minimum density of TCR and pMHC required to induce triggering. Comparing the behaviour of gp100 TCR-expressing cells with 1G4 TCR-expressing cells under the same conditions would provide more information about whether serial binding of pMHC/TCR is required to induce signalling. Furthermore, following individual pMHC molecules and TCRs on live cells would provide a more direct approach to determine whether single pMHC/TCR interactions can lead to triggering, and gp100 TCR-expressing cells would be an excellent system to use for this given the extremely high pMHC affinity.

6.4.4 The Effect of MHC Affinity for CD8

Gp100^{hi} and gp100^{lo} cells were tested for signalling on SLBs presenting agonist pMHC of either a wildtype or CD8 affinity-enhanced HLA-A2 pMHC. Across a hundred-fold dilution in agonist pMHC concentration, both cell lines signalled comparably on either type of MHC in terms of the fraction of cells undergoing calcium flux and the median time to trigger.

Gp100 TCR-expressing cells were chosen since this would be more comparable to results from the previous solution signalling experiments, which required the use of a high-affinity ligand. However, the high affinity nature of this TCR/pMHC interaction may mask subtle effects of MHC affinity for the CD8 coreceptor. Indeed, a previous study has shown that high-affinity TCR/pMHC interactions induce signalling regardless of CD8 activity¹³¹. Future experiments using 1G4 expressing cell lines and 9V-loaded pMHC would provide a more physiological context.

6.4.5 The BCR is Monomeric on Resting or Naïve B Cells

Using a combination of techniques and cell models, the final aim of this chapter was to address the stoichiometry of the resting BCR. Two-colour tracking of single receptors on live cells with low BCR density suggested a monomeric, freely diffusing BCR. Data from additional experiments using super-resolution dSTORM imaging on primary B cells also indicates a monomeric BCR. The results found in this chapter were corroborated by another group using a different super-resolution technique³²⁴, however other studies contradict this^{270,298}.

One caveat of the DySCo experiments is that they were conducted in a B cell line with a low BCR expression. This was necessary to resolve single molecules without super-resolution methods (which are especially complex for live cells), while still labelling as many BCRs as possible (to achieve the most robust colour coincidence measurements). However, it is possible that diffusion and clustering of BCRs could be affected by BCR density on the cell

surface, which is why other experimental methods were used to validate the results found here. Additionally, while monomeric antigen in solution is known not to induce BCR signalling²⁹⁵, the possibility of HEL binding disturbing the true resting state of the BCR cannot be ruled out, given that it is the cognate ligand for this BCR. Furthermore, in line with results described for the TCR in section 6.3.2, it is also possible that HEL would act as an adduct for the BCR, dragging it on the fibronectin surface and increasing the likelihood of BCR triggering. Future experiments on live B cells could therefore involve suspending cells in a gel to prevent any effects of imaging at a surface, as was demonstrated in a recent study⁴²².

The primary MD4, HyHEL10 BCR-expressing murine cells obtained were typically at a high, although not perfect, purity level. It was not possible to sort the B cells further before use as this would involve labelling the BCR in some manner, which could induce signalling and disturb their naïve state. This may introduce some noise in the data collection, however cells with a very low number of localisations of HEL-labelled BCR were not selected for acquisition which should remove the possibility of acquiring non-B cells. With clathrin-labelled samples, non-B cells would be harder to distinguish from B cells, so a larger number of cells were analysed to negate the effect of the imperfect purity.

Super-resolution techniques such as dSTORM, while powerful, have limitations. One drawback of dSTORM concerns overcounting of fluorophores, which can arise from using labelling reagents with more than one fluorophore per probe, or which bind the target more than once (e.g., a polyclonal Fab), and because fluorophores can blink more than once over the time period of data collection^{300,301,423}. It is very difficult to separate a single fluorophore which fluoresces on and off over time from a local cluster of fluorophores in a very close proximity and this is especially challenging if there is any drift present in the sample platform as data is acquired. Since drift correction was implemented here using gold

nanobeads as fiducial markers, each fluorophore should not appear in more than one location in the sample over time.

The analysis method used in the present study aims to overcome artefacts of overcounting as it relies on comparing the trend in the density of localisations per cluster as labelling increases, rather than analysing localisations present at a single (saturating) label density. Randomly distributed proteins will lead to a constant density of localisations per cluster as the relative area covered by apparent clusters will increase steadily with increasing concentration of label. Clustered proteins, in contrast, would result in a change in the density of localisations per cluster, proportional to the concentration of label, since the relative area covered by clusters will saturate.

Although saturating concentrations of HEL and anti-clathrin antibodies were used to stain cells (data not shown) it is impossible to label every target protein. The rate of label fall off was minimised by labelling at low temperatures, but nevertheless some localisations will inevitably be missed. Given the very high number of localisations acquired for all samples, this should not make an appreciable difference to the analysis, however. Additionally, naïve MD4 B cells express both IgM and IgD isotypes²⁷⁰, but HEL labels all BCRs regardless of isotype. Some papers have suggested differential clustering of BCRs depending on isotype²⁹⁹ which would not be accounted for in the present study.

A further possible issue is the differences in labelling between HEL and anti-clathrin antibodies. HEL proteins were all labelled in a 1:1 stoichiometry with Alexa Fluor-647 whereas the anti-clathrin antibodies were labelled with a lysine labelling kit. Although the antibodies were confirmed to have an average labelling efficiency of one fluorophore per antibody with a NanoDrop II, the bulk sample was not purified further meaning there will be a spread in the number of fluorophores for each antibody molecule. Since clathrin is relatively abundant, and should bind multiple antibodies per cluster, this should not have a large effect on the data acquired. Furthermore, although each BCR should be labelled with

two HEL molecules, the effects this would have on overcounting can be overcome by the analysis method used here and also by future comparison to suitable controls (e.g., soluble HyHEL10 antibody labelled in the same manner). However, ideally all proteins of interest should be labelled in a 1:1 dye/protein stoichiometry for more direct comparison, which could be achieved by creating HaloTag-conjugated fabs against the target protein. Finally, production of a reagent to label a presumed monomeric protein such as CD45³⁰³ could be used in future experiments to provide another control for labelling and analysis.

7 General Discussion

The main aims of this thesis were to better understand the regulation of TCR signalling in early T-cell contacts, by examining the influence of TCR expression and ZAP-70 activity on TCR triggering, T cell spreading, close contact formation, signalling microclusters, and T-cell activation. Furthermore, key principles of the kinetic segregation (KS) model were tested in T- and B-cell lines to examine whether principles governing TCR triggering are also applicable to the BCR.

In Chapter 3, cell lines with different TCR specificities and expression levels, and controllable early signalling through ZAP-70(AS) were created and characterised. Next, in Chapter 4, the formation and regulation of early T-cell contacts was studied. In Chapter 5, the effect of TCR expression and signalling capacity on TCR and ZAP-70 microclusters (MCs), and T-cell topography, was investigated. Lastly, in Chapter 6, experiments were carried out to examine whether predictions of the KS model were applicable in both T and B cells.

The key findings from this thesis can be summarised as follows:

- i. Cells with a very low TCR density produce robust early activation responses (i.e., calcium flux) but do not activate fully (i.e., CD25 and CD69 expression), suggesting that the engagement of a threshold number of TCRs is required to produce full T-cell activation.
- ii. T-cell spreading on activating SLBs is unaffected by TCR density but is reduced when signalling is inhibited by ablating ZAP-70 kinase activity. Therefore, ZAP-70 activity is required for T-cell spreading on activating surfaces.
- iii. T-cell close contacts made with SLBs increase in size when ZAP-70 activity is blocked but are comparable in size and intensity across cell lines with different TCR densities. Therefore, ZAP-70 activity, but not TCR expression level, controls the structure of T-cell close contacts on activating surfaces.

- iv. ZAP-70 MCs in T cells interacting with activating SLBs increase in intensity when cells are treated with a ZAP-70 kinase inhibitor, suggesting that ZAP-70's kinase activity controls its association with the TCR.
- v. T cells treated with actin inhibitors activate on agonist-presenting SLBs, but only if the SLBs do not additionally present a glycocalyx (CD43 and CD45). This suggests that, while T cells do not require actin for TCR signalling, they are dependent on a dynamic cytoskeleton to facilitate early TCR signalling when a glycocalyx is present.
- vi. Slowing TCR diffusion in T-cell close contacts using receptor adducts increases the probability of TCR triggering and adducts which slow the TCR to a greater extent cause more TCR triggering. This confirms a key prediction of the KS model, which states that TCRs confined in a phosphatase-depleted zone (i.e., a close contact) are more likely to be signalled as the time spent in these areas increases.
- vii. The BCR is unclustered in resting B cells, as shown by both live-cell single-molecule tracking experiments and super-resolution imaging of primary B cells. This directly excludes the dissociation-activation model as an explanation of BCR triggering.

7.1 The Transition from TCR Triggering to T-Cell Activation

7.1.1 Early Signalling is Unimpeded in T Cells with Low TCR Densities

T cells can be activated by sparse ligands^{184,208}, and monomeric TCRs have been shown to drive ligand recognition¹⁷⁹, which raises the question of whether single TCRs can induce T-cell signalling. In Chapter 6, it was shown that when agonist pMHC was not a limiting factor, many aspects of signalling were comparable between cells with a ~76-fold difference in TCR density. Calcium flux was not significantly different in terms of the fraction of cells signalling and in the qualitative nature of the calcium flux (such as amplitude, frequency, and time of occurrence). Cells with low TCR density were more sensitive to changes in agonist pMHC concentration, implying that a threshold density of TCRs is required to induce triggering when agonist pMHC is limited. A study by Viola et al²¹⁰, which used T-cell clones expressing different numbers of TCRs interacting with APCs, found that cells with as few as 3000 TCRs produced calcium flux in response to antigen. However, they noted that calcium flux was less sustained in cells with the lowest levels of TCR expression. In contrast, experiments in the present study (where TCR density was lower than in Viola et al.) showed that calcium spike size was similar between cells with different TCR densities.

Serial binding of pMHC/TCR has been proposed as a mechanism to explain T-cell sensitivity to sparse ligand¹⁷³. Therefore, this was tested by measuring triggering at very low TCR and agonist pMHC densities in T cells expressing a TCR which binds its ligand with very high affinity. No agonist pMHC-induced signalling was observed (Figure 44). This suggests that either single, long-lived pMHC/TCR interactions do not induce triggering at the timescales tested, or that the pMHC and/or TCR density was too low to facilitate pMHC/TCR encounters. While there is evidence that a single ligand can induce T-cell activation^{184,208}, direct observation of single TCRs interacting with single pMHC molecules has not yet been achieved. One study⁴¹⁷ observed ZAP-70 molecules being recruited to single TCR-bound pMHC molecules on an SLB but did not simultaneously image TCR, therefore, it cannot be

certain that this was a 1:1 pMHC/TCR interaction. Lin and colleagues²⁰⁵ showed that T cells displayed NFAT translocation (a relatively early activation marker) in response to a single long-lived pMHC/TCR binding event (where dwell time was an order of magnitude larger than the mean binding duration), suggesting that single pMHC/TCR interactions lead to triggering if the binding is sustained for a sufficient time. Indeed, the cells used in the present experiments, where unbinding of pMHC and TCR is highly unlikely, were shown to signal robustly on SLBs (Figure 16) when agonist pMHC was present at a higher density, which suggests that sustained interactions are more likely to be the cause of signalling than serial binding, at least in this cell line. These results imply that serial pMHC/TCR engagement may not be necessary for T-cell triggering. However, additional experiments using the same cell line (i.e., with a low density of TCR and a high-affinity pMHC ligand) where agonist pMHC density is titrated, especially with simultaneous imaging of pMHC, TCR, and activation markers such as calcium flux or NFAT translocation, are required to confirm this.

7.1.2 Cells with Low TCR Density do not Fully Activate

After finding that cells with low TCR expression responded robustly (regarding calcium flux) to their cognate pMHC (figures 16, 22, 42), a logical next step was to examine how TCR density might affect later activation markers. T cells with a low TCR density tested in the present study did not show substantial activation when compared to cells with high TCR density (Figure 25). The apparent discrepancy between TCR triggering and full activation could be explained by signal integration in the T cell. Serial binding of multiple TCRs by a single ligand (i.e., serial triggering model) was proposed as a mechanism to explain the discrepancy between the number of agonist pMHCs present on APCs and the extent of TCR downregulation observed on T cells, given that only triggered TCRs are internalised¹⁷³. In line with this, a single-molecule tracking study demonstrated that NFAT translocation occurs in response to several relatively short-lived pMHC/TCR binding events if they occur

in close spatial and temporal proximity (but not simultaneously)²⁰⁵. Thus, the sparse TCRs may not be able to facilitate sequential ligand/receptor interaction. Furthermore, Schodin and colleagues⁴¹⁹ found that high-affinity ligands at high density can activate CTLs with only 1000 TCRs available (a comparable level to cells with a low TCR expression used here), whereas at low ligand density (regardless of affinity), almost all of a cell's TCRs were required for an effector response. In summary, cells tested here with a low TCR density may not be able to achieve the level of signal integration required from a threshold number of TCR/pMHC interactions, either due to TCR expression levels or ligand density being limiting factors. An explanation for these results is not explored here and poses an interesting question for future work.

7.2 Regulation of Early T-Cell Contact Formation by TCR Density and ZAP-70 Activity

7.2.1 Differential Protein Organisation on the Resting T-Cell Surface

Many studies have demonstrated that the T-cell surface is not homogenous in terms of topography and surface proteins^{103,194,223}. In Chapter 4, no gross differences in morphology were observed between resting control and ZAP-70-inhibited cells by confocal microscopy (figure 26). This is supported by another study using light sheet microscopy²²³. The TCR, but not CD2 or LFA-1, was observed to be significantly enriched on microvilli (Figures 27 & 28), adding to the evidence that these structures are likely important in facilitating T-cell signalling initiation. The degree of enrichment observed in this thesis (~1.8-fold at microvillar tips), however, was more subtle than measured elsewhere. One study for example observed $\geq 90\%$ of the cell's TCRs to be localised on microvilli¹⁰³, and another observed a 4-6-fold increase in TCR density on microvilli compared to the cell body¹⁹⁴.

In contrast to the results here, other studies have showed enrichment of LFA-1 on the T-cell body^{245,424}. The ICAM-1/LFA-1 interaction is important for T-cell activation and

trafficking^{90,92,95} but its role in early contact formation seems less critical. Accordingly, Hashimoto-Tane et al. showed that LFA-1 tends to segregate away from the TCR in small zones termed 'micro-adhesion rings'²¹², which is supported by other studies demonstrating anti-correlation of ICAM-1 and TCR in early T-cell contacts²²³. Conversely, the small adhesion molecule CD2 is unlikely to be passively excluded from close contacts (CD2/CD58 height is estimated to be ~15 nm, comparable to TCR/pMHC¹⁰¹) and indeed does colocalise with the TCR in imaging studies¹⁰². Therefore, it seems likely that LFA-1 does not play a role in close contact formation, and this may instead be carried out by CD2.

7.2.2 T-Cell Spreading on Activating SLBs is Regulated by ZAP-70 Activity, but not TCR Density

T-cell spreading occurs in response to an activating ligand¹⁷² and is proportional to the potency of the stimulus⁴²⁵. During spreading, large scale protein reorganisation occurs, eventually leading to the formation of the immune synapse^{96,426}. In this study, removing TCR signalling, either through TCR knockout or ZAP-70 inhibition, reduced the size and speed of cell spreading (Figure 31 and Figure 34) and caused cells to spread in a more passive fashion, likely driven by ICAM-1/LFA-1 and/or CD58/CD2 interactions as previously discussed. T cells with different TCR densities spread at the same speed and to the same size, suggesting that very few TCRs are required to initiate cell spreading. This fits well with the general principle of a small number of agonist pMHCs being required to induce TCR signalling. Indeed, cells treated with PP2¹⁷², or placed on surfaces which do not induce activation (such as null pMHC-presenting SLBs, Figure 51) do not spread as vigorously as signalling-competent cells^{172,427} (see Figure 39 and Figure 54).

Cells without TCR exhibited a 5-fold decrease in spreading with ZAP-70 inhibition on 1st generation SLBs, which is unexpected since they presumably cannot recruit ZAP-70 to their surface where it is known to function⁴¹². This suggests a potential role for ZAP-70 in T-cell spreading that is not kinase- or TCR-dependent. Indeed, a 2010 study by Au-Yeung et al.³⁸⁵

showed that kinase-inhibited ZAP-70 can still induce conformational changes in integrins. However, this was only tested in TCR-expressing cells. Alternatively, this behaviour may reflect differences in adhesive characteristics of the two SLB types, mainly due to the inclusion of CD58 in 2nd generation SLBs which stabilises T-cell close contacts through CD2. In line with this, all cell lines spread slightly more on 2nd generation SLBs, and cells without TCR expression did not show a difference in spreading with ZAP-70 inhibition on this surface.

Overall, this data is in general agreement with there being an important role for ZAP-70 downstream of the TCR in cytoskeletal regulation of cell spreading, which has been shown previously in cell-cell contacts³⁸⁴, but not with model APC systems.

7.2.3 T-Cell Close Contacts with Activating SLBs are Regulated by ZAP-70 Activity but not TCR Density

T cells must make close physical contacts with target cells to become activated, and how this process is regulated is an area of active research. In this work and elsewhere^{194,223}, microvilli were shown to be prominent structures in resting cells (Figure 26) and likely during all stages of T-cell interaction with SLBs, as small areas of close contact between the T cell and SLB were observed from contact initiation to cell spreading (Figure 35). Furthermore, these close contacts were observed in all cell lines, regardless of TCR expression, signalling capacity, or even presence (of TCR) (Figure 35). This is likely due to the binding of CD2 on the T cell to the small adhesion molecule CD58 on the SLB as discussed previously (7.2.2). This shows that TCR/pMHC binding is not required for close contact formation. In contrast to these observations, a study by Cai and colleagues²²³, which studied close contacts in primary mouse cells expressing the ZAP-70(AS) mutant, observed that contacts containing TCRs had a persistence time almost 3-fold higher than those without TCR (or those formed on null- and weak agonist-presenting SLBs). They concluded that close contacts were stabilised by binding of pMHC, which is supported by a previous study

where T-cell contacts on an OKT3-coated surface persisted for longer than those on an anti-IgG1-coated surface⁴²⁸. However, TCR binding of static surfaces is known to induce different T-cell behaviour to mobile surfaces (i.e., SLBs), for example in TCR translocation, so a direct comparison cannot be made. In the study by Cai et al.²²³, the use of a 1st generation SLB could force the TCR to act as both a signalling and adhesion molecule (since ICAM-1 was shown to be excluded from close contacts), thus causing the strong dependence on the TCR for contact stabilisation. Since the density of agonist pMHC used is not stated, it may also be the case that TCR-mediated contact stabilisation occurs when the density of pMHC is very high, although this cannot be confirmed.

Interestingly, an increase in the size of individual close contacts (Figure 35) was observed for TCR-expressing cells when ZAP-70 was inhibited (although this was not significant for both cell lines), which could explain the more significant accumulation of agonist pMHC in drug-treated cells (Figure 30 and Figure 33). This contrasts with the study by Cai et al. which showed that close contacts in ZAP-70-inhibited cells were no different in size from control cells, and that microvillar structure did not change during interaction with an agonist-presenting APC²²³ (at a timescale when activation presumably occurs, although this was not tested). The size of microvilli is likely to be of crucial importance to T-cell antigen discrimination, which is presumably why different T cell types have similar microvilli sizes^{194,240}. Modelling of T-cell close contacts¹⁹⁵ suggests that the optimal contact diameter to carry out efficient, specific, and sensitive antigen recognition is ~440 nm, comparable to microvilli size measurements in the literature^{194,223}, and implied by close contact area measured in the present study (Figure 35). Therefore, this result suggests an important role for ZAP-70 in maintaining the structure of T-cell microvillar contacts, and therefore in upholding antigen discrimination. This interesting observation warrants further investigation.

7.3 Regulation of Signalling Microclusters by TCR Density and ZAP-70 Activity

7.3.1 Signalling Microclusters Appear in Cells with Low TCR Density

MCs of TCR and ZAP-70 have been observed consistently on T cells interacting with activating surfaces and are assumed to be the drivers of TCR signalling^{211,213}. TCR MCs were found to be broadly similar in cell lines with different TCR expression, except for a higher intensity of these MCs in cells with higher TCR expression (Figure 37). Cells with low TCR expression recruited approximately half as much ZAP-70 to their membrane and had less intense ZAP-70 MCs. These results suggest, as expected, that cells with fewer TCRs form less dense TCR MCs which therefore recruit less ZAP-70. However, cells with low TCR density were shown to signal robustly (Figure 22 and other data not shown) and produced a comparable number of ZAP-70 MCs when compared to cells with physiological TCR expression, suggesting that the level of recruitment of ZAP-70 is sufficient to drive early signalling. In line with this, it has been shown that TCR MCs as small as 11 TCRs can drive signalling²¹¹, and that crosslinking just two or three TCRs can induce signalling¹⁷⁴. Furthermore, a super-resolution study showed that ZAP-70 is recruited to TCR MCs independently of TCR cluster size⁴²⁹.

While no studies investigating MCs have involved changing TCR expression, studies changing the ligand concentration have shown that TCR MCs appear to change structurally in response to varying agonist pMHC concentration. For example, a study by Yokosuka et al.²¹³ showed that increasing antigen concentration did not increase the number of TCR MCs but did increase their intensity, which mirrors results here where the intensity, but not the number, of TCR MCs was decreased in cells with lower TCR expression. Another study by Varma and colleagues²¹¹ showed that calcium signalling does not change substantially over a large range of agonist pMHC densities, which aligns with the similarities in calcium flux characteristics between cells with different TCR densities shown in Figure 16, 22 and 42.

However, similarities in calcium flux in the study by Varma et al. could be a result of signal amplification by a few pMHCs engaging many TCRs, which is less likely to occur in the cells with a low density of TCR used in this thesis. Furthermore, ZAP-70 MC size was reduced with lower antigen dose in a study by Hashimoto-Tane et al.⁴¹⁰, suggesting a discrete T-cell response at this early stage of signalling. In the present study, in cells with low TCR expression, ZAP-70 MCs were comparable in size to those in high TCR expression cells but were not as intense (Figure 38), which fits with this idea.

7.3.2 ZAP-70 Activity Regulates the Density of Signalling Microclusters

TCR MCs were observed in ZAP-70-inhibited cells (Figure 37), which fits well with findings from several studies that have shown that TCR MCs appear in the presence of pharmacological inhibitors such as PP2 (which broadly inhibits Src-family kinases)²¹³. Interestingly, the intensity of ZAP-70 MCs increased in cells with low TCR expression when ZAP-70 was inhibited. Accordingly, a recent paper by Katz et al.⁴¹² found that ZAP-70 kinase activity was required for its release from the TCR ITAMs, as this process is mediated by *trans*-autophosphorylation. Katz et al. showed that ZAP-70 was continuously recruited to, activated at, and released from, the TCR under activating conditions, where it was retained at the T-cell surface for a short period of time. Thus, inhibiting ZAP-70 kinase activity in T cells may impede ZAP-70 release from the TCR. Cells with a physiological TCR density in comparison only had a small increase in absolute ZAP-70 MC intensity with ZAP-70 inhibition, which translated to a small relative decrease in MC intensity. This could be explained by a dependence of this mechanism on TCR density, or by an increase in overall ZAP-70 intensity at the membrane of these cells (which was shown in Figure 38). These findings suggest that ZAP-70 kinase activity is responsible for its release from TCR ζ chains, possibly contributing to signal amplification, especially where TCR density is low. Further study, especially in live T cells, is required to follow up this interesting result.

7.4 The Relationship between T-Cell Topography and Early Signalling

7.4.1 The Actin Cytoskeleton is Required to Facilitate T-Cell Signalling in the Presence of a Glycocalyx

Studies showing that treatment of T cells with actin-inhibiting drugs quenches TCR signalling²⁴³ and prevents MC formation¹⁷² have led to speculation about the role of actin in the initiation of TCR signalling. In Chapter 5, treatment of cells with actin-inhibiting drugs slightly decreased T-cell triggering compared to control cells on SLBs presenting agonist pMHC with CD58 (Figure 41). However, all conditions still induced robust early T-cell activation, suggesting that actin disruption *per se* does not prevent TCR triggering. This result is consistent with another study which demonstrated that calcium flux occurs before substantial cytoskeletal reorganisation⁴³⁰. However, many studies have observed disruption in MC formation^{172,211} and translocation⁴³¹ when cells are treated with an actin inhibitor, although pre-existing MCs are not affected by actin inhibition²¹¹. These data together suggest that a functional cytoskeleton is not required for early TCR signalling.

Treatment with actin-inhibiting drugs significantly reduced the incidence and speed of close contact formation on 2nd generation SLBs (which present a glycocalyx), and substantially reduced the fraction of cells signalling. One study observing T-cell contacts with 1st generation agonist-presenting SLBs found that actin density was higher at newly formed TCR MCs than established ones²²³, and other studies have demonstrated actin foci at TCR MCs, which are synthesised as a result of TCR signalling^{242,432,433}. This is consistent with a role for a dynamic actin cytoskeleton in microvilli structure⁴³⁴, thereby regulating close contact formation, and suggests that microvillar activity is essential in facilitating TCR signal initiation where the glycocalyx provides physical hindrance to agonist pMHC.

7.4.2 TCR and ZAP-70 Microclusters do not Correlate with Areas of Close Contact

Given that T-cell close contacts are caused by variations in membrane topography, and that TCR signalling is initiated at close contacts¹³⁵, it is possible that apparent MCs may be a result of membrane fluctuations in the TIRF evanescent field causing intensity variations in labelled proteins or through TCR passively binding agonist pMHC in close contacts. In fixed samples analysed in the present study, no correlation was found between TCR or ZAP-70 fluorescence intensity and areas of close contact with an activating SLB (Figure 39). Similarly, other TIRFM studies^{192,211}, including one using super-resolution microscopy⁴³⁵, which labelled cell membrane and TCR simultaneously, have shown a lack of correlation between these parameters in cells interacting with activating SLBs. Additionally, another TIRFM study²¹¹ showed that a 100-fold change in agonist pMHC density only resulted in a ~2-fold change in TCR MC size, suggesting that agonist pMHC density is not directly linked to MC size. In the present study, cells placed on null-presenting SLBs, or on agonist-presenting SLBs but with ZAP-70 inhibition, showed a strong correlation between close contacts and TCR or ZAP-70 fluorescence (Figure 39). These cells do not progress to the spreading stage seen in cells interacting with agonist-presenting SLBs (e.g., Figure 39, top panel). Therefore, MCs appearing at this stage cannot be separated as distinct structures, at least as determined by the methods used here. In contrast, a study by Cai et al. observed a strong correlation between TCR and ZAP-70 intensity and areas of close contact on 1st generation SLBs regardless of TCR signalling capacity, but dependent on TCR presence²²³ (discussed in section 7.2.3). This may be due to a difference in SLB composition used by Cai et al. versus the present study.

Overall, these data support the idea of MCs being real structures which are not artefacts of pMHC binding or intensity fluctuations of labelled proteins in TIRFM. Additional experiments tracking MCs in cells interacting with different agonist pMHC densities, and

over time, would be useful to determine the likely mechanism underlying the initial appearance of MCs.

7.5 Kinetic Segregation-Based Signalling of Lymphocyte Receptors

7.5.1 Slowing TCR Diffusion Increases TCR Triggering

One theory of signalling which can explain triggering by individual TCRs is the KS model. Therefore, a key prediction of this model was tested in a T cell line expressing physiological levels of TCR with a high affinity for its cognate pMHC. Slowing TCR diffusion speed with different adducts was shown to increase the fraction of T cells fluxing calcium to a comparable level as a crosslinking antibody (Figure 43). While monomeric pMHC in solution did not produce a response from the T cells, 36% of cells incubated with pMHC (with no tags) signalled when allowed to settle on CD58-presenting SLBs, and those incubated with pMHC containing a histidine tag activated comparably to cells incubated with a TCR-crosslinking antibody. These TCR adducts were shown to slow the diffusion of the TCR by 5- and 15- fold (pMHC no tags and pMHC with histidine tag, respectively) in close contacts. This result has additionally been shown with a different TCR and the anti-CD3 ϵ Fab UCHT1¹⁹⁶. These results provide experimental evidence to support a key prediction made by the KS model - that increasing the time a TCR spends in a phosphatase-depleted area increases the probability of TCR triggering, regardless of TCR occupancy. While the role of (force-induced) conformational change cannot be directly excluded from this experiment, the similarities between the effect seen with a pMHC and UCHT1 Fab ligand, which bind the TCR at different places, suggest the induction of signalling is caused by their effect on diffusion rather than force applied or conformational change induced on the TCR. Furthermore, no consistent structural change in TCRs interacting with ligands have been demonstrated by structural studies^{83,84}. Overall, these data provide strong evidence for a KS-based model of signalling for the TCR.

7.5.2 The BCR is Unclustered in Resting, Naïve B Cells

To test the compatibility of the KS model with signalling by other lymphocyte receptors, two methods were employed to investigate the resting stoichiometry of the BCR. Dual-colour single-molecule tracking experiments on resting B cells showed that the percentage colour coincidence value obtained for membrane-bound BCR molecules was comparable to an antibody in solution labelled in the same manner (Figure 46). In support of this finding, coincidence values for the membrane bound BCR and antibody were similar to a known dimer, the costimulatory receptor CD28, measured and analysed using the same technique on T cells³⁰². In further support of this finding, another study by Tolar et al.²⁹³ used FRET to demonstrate that BCRs are largely present as monomers in live resting B cells.

To support the live cell data, dSTORM imaging on fixed primary B cells indicated that the BCR distribution matched well with a simulation of a perfect randomly distributed monomer, and was different to the distribution of clathrin, a known multimeric protein³⁰⁰ (Figure 47). Consistent with this, a recent paper by Gomes de Castro et al.³²⁴ using stimulated emission depletion (STED) microscopy and STORM on a human B cell line found the resting BCR to be distributed largely as monomers and dimers, which agrees with a previous study using dSTORM on human B cells²⁹⁹. In contrast, a study by Mattila et al.²⁷⁰ using STORM concluded that MD4 BCRs form nanoclusters under resting conditions. However, they allowed cells to settle on an antibody-coated glass slide (and no apparent blocking agent) before fixing, whereas cells were fixed in solution in the present study and by Gomes de Castro et al. Given that B cells signal non-specifically on glass (data not shown), it is possible that a significant fraction of these cells were not captured under truly resting conditions.

These results argue against the possibility of dissociation-activation as a model for BCR signalling by showing BCRs are unclustered in resting cells.

7.6 Concluding Remarks

The overarching aims of this thesis were to investigate the effect of TCR density and ZAP-70 signalling capacity on TCR triggering, MCs and early T-cell contacts. Overall, cells expressing a low density of TCR were found to behave almost indistinguishably from those with a physiological TCR expression level with regards to calcium flux, contact formation with SLBs, and the appearance of MCs. However, cells with a low TCR density were severely impaired with respect to activation compared to those with high (i.e., physiological) TCR density. These results imply different cellular requirements for TCR triggering vs T-cell activation, where triggering can be induced by a very low number of TCRs, but full activation requires integration across a threshold number of TCRs. ZAP-70 was shown to have a role in regulating T-cell contact formation with SLBs, both at the whole-cell level (i.e., spreading) and the close contact level, where changes in the speed of close contact formation and size of individual close contacts were observed. This could have important implications for antigen discrimination which likely relies on highly restrained close contact sizes. Finally, experiments were undertaken on the BCR to determine its stoichiometry, which was found to be randomly distributed and unclustered. This is compatible with a triggering mechanism based on receptor crosslinking or phosphatase exclusion and argues directly against the dissociation-activation model of BCR triggering. Overall, the work in this thesis provides insight into the molecular details of TCR and BCR triggering mechanisms which contribute to the understanding of how these receptors function *in vivo*.

8 Appendix

8.1 Creation of a UCHT1 Fab-Halo for Imaging TCRs on T-cells Interacting with SLBs

As the cell lines in this thesis were largely to be used for imaging experiments, UCHT1 binding was also tested for microscopy. For this, a novel UCHT1 Fab-Halo was designed and purified (see 2.3.9). This Fab could be labelled with a very high - up to 99% - efficiency through the HaloTag, while also ensuring a 1:1 dye/Fab stoichiometry which would be useful for quantitative single-molecule imaging in future experiments. The UCHT1 Fab-Halo was made with Strep-tag II³⁷² rather than a histidine tag to avoid binding labelled TCR to nickel-chelating lipids in SLBs and altering their diffusion (see section 6.3.2 and ref 308). The UCHT1 Fab-Halo labelled the TCR comparably to a commercial UCHT1 antibody and could be used with various dyes to visualise the TCR (Figure 48).

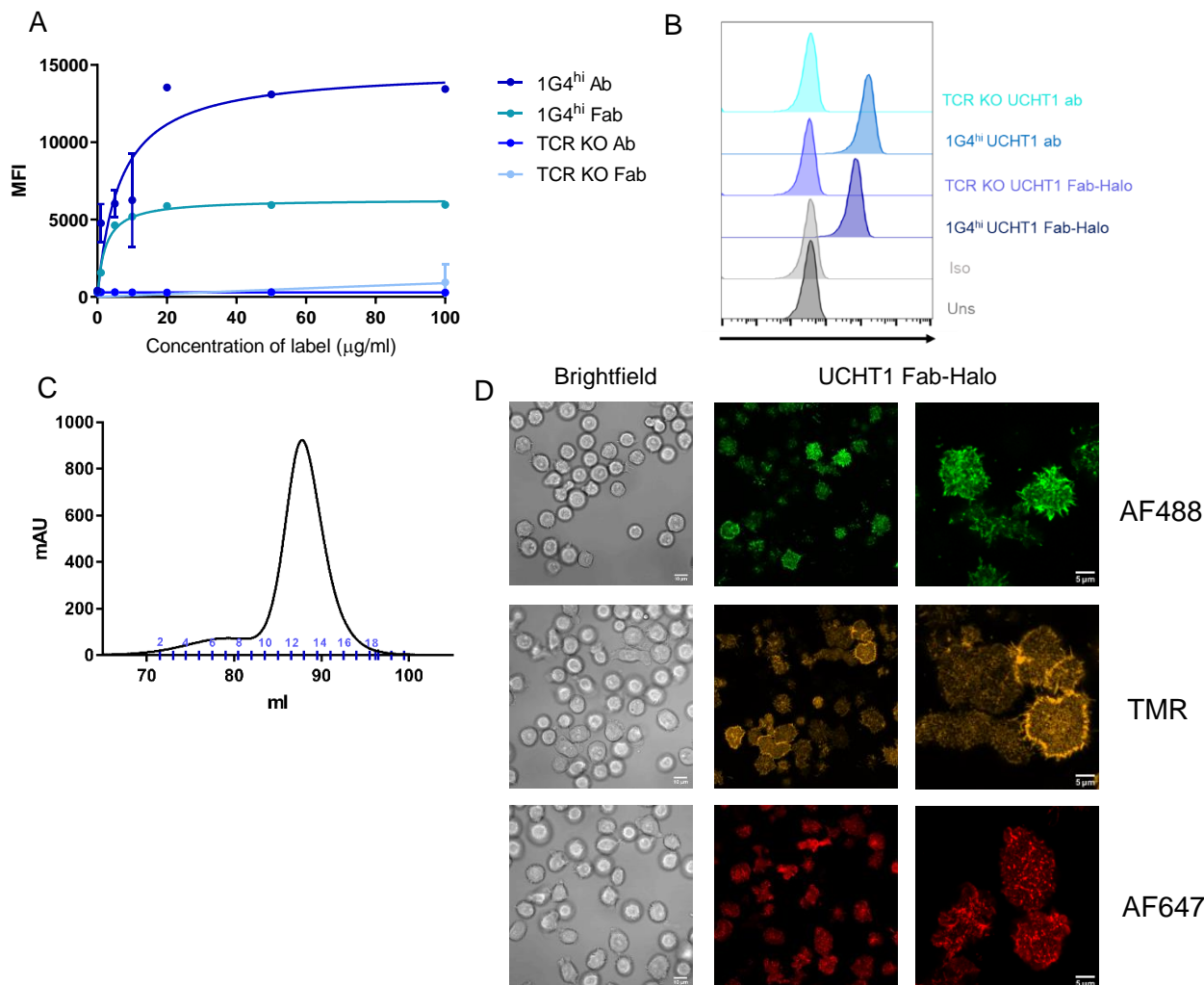


Figure 48 **Creation of a UCHT1 Fab-Halo for T-cell labelling and imaging** (A) 1G4^{hi} cells were stained with either UCHT1 Fab or commercial labelled UCHT1 antibody at varying concentrations, washed and fixed. Lower intensity values for the Fab are expected due to the 1:1 labelling stoichiometry, while a commercially labelled antibody is likely to contain multiple fluorophores per antibody. Negligible staining is observed on TCR KO cells, indicating good specificity of the UCHT1 Fab-Halo. (B) 1G4^{hi} cells were stained with either UCHT1 Fab-Halo or commercial labelled UCHT1 antibody, washed, fixed, and analysed by flow cytometry. (C) FPLC trace of UCHT1 Fab-Halo illustrating its elution as a monomer. Fractions from the centre of the peak were selected for use. (D) Cells were labelled with UCHT1 Fab-Halo with different fluorophores and allowed to settle on an OKT3 surface for 5 minutes before fixation. Left and middle panels are at the same scale. Right panels are examples of cells from middle panels at higher magnification.

8.2 Overcoming the Effect of 'Free' Nickel-Chelating Sites on SLBs

SLBs containing a small percentage of nickel-chelating lipids (such as DGS-Ni-NTA used in this thesis), which can then bind strongly to histidine-tagged proteins, are used frequently in T-cell signalling studies^{135,196,332,354}. They are readily and quickly formed on glass surfaces and remain stable for long periods of time, as long as they remain hydrated. Proteins anchored to nickel-chelating lipids diffuse freely and can remain bound for hours³⁹⁴ making the SLB system a robust and reproducible reductionist model system to investigate T-cell signalling. Several studies however have shown that T cells can bind, and signal in response to, SLBs containing nickel-chelating lipids, an effect that is dependent on the TCR^{334,422}. Indeed, both gp100 and 1G4 TCR-expressing T cells bound and signalled substantially (up to 30% of cells over 10 minutes) on SLBs with 2% Ni-NTA and no protein, whereas TCR or ZAP-70 KO cells do not signal much (<10%), indicating that the response observed is dependent on the TCR (Figure 49).

Therefore, in using SLBs for this thesis it was important to ensure there were as few 'free' (i.e., unbound by protein) nickel cation sites as possible. Based on previous work carried out by Edward Jenkins (Davis group), unbound nickel-chelating lipids were sequestered using an inert protein – null pMHC (i.e., a pMHC that is known not to induce signalling, or strongly bind, the specific TCR). This was chosen for several reasons: first, it makes the SLB systems more representative of a real APC, as there will be a high density of non-agonist pMHCs presented to each T cell as they interact with its surface; secondly, a 2xHis-tagged pMHC binds as strongly to the bilayer as other 2xHis-tagged proteins used; and finally, it is small in size so unlikely to be excluded from a cell-SLB contact¹⁸⁵, thus not disturbing the relative density of other SLB-bound proteins. As expected, adding increasing concentrations of a null pMHC to an otherwise protein-free SLB decreased the fraction of 1G4^{hi} cells signalling to an insignificant level ($\leq 5\%$). Therefore, the null pMHC 'block' was used in all SLBs in the present study, except where explicitly stated.

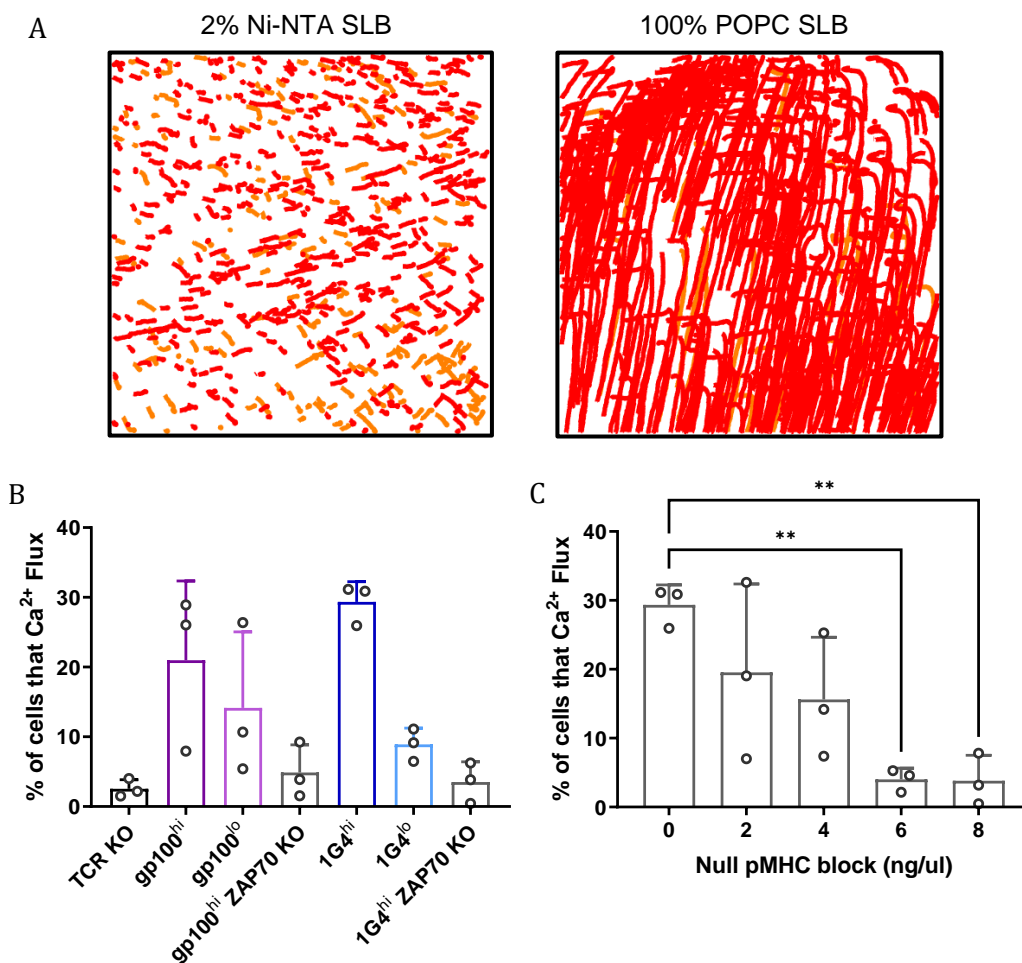


Figure 49 Exposed nickel-chelating lipids on SLBs cause T cell adhesion and triggering through the TCR Cells were labelled with Fluo-4 AM and dropped onto SLBs containing either 2% Ni-NTA lipids or 100% POPC lipids with no protein. (A) Representative images showing tracks of cells over 10 minute timelapses after being placed either on unblocked 2% Ni-NTA SLBs (left) or POPC-only SLBs (right). Longer tracks indicate a longer time for adhesion. Red tracks indicate non-triggering cells and orange tracks indicate triggering cells. (B) Fraction of cells triggering on unblocked 2% Ni-NTA SLBs (B) Fraction of 1G4^{hi} cells triggering on 2% Ni-NTA lipids with increasing concentrations of a null pMHC (i.e., gp100) added to the SLB. Tested with a one-way ANOVA with Dunnett’s multiple comparisons, with 0 ng/ul as the control condition. ** = p < 0.01. Mean ± SD plotted in all graphs.

8.3 LFA-1 Boosting is Required to Facilitate Immune Synapse Formation in Jurkat-Derived T Cells

Jurkat T cells have a comparatively low expression of CD11a and CD18 (i.e., LFA-1) compared to primary cells³⁸⁶. This means that accumulation of ICAM-1 on SLBs, interaction with ICAM-1 on APCs, and signalling through LFA-1 on the cell lines used in this thesis would be weakened compared to primary cells, and the formation of mature immune synapses would be compromised (see Figure 50A). This has also been observed in a recent study, where boosting the expression of LFA-1 on Jurkat cells was sufficient to rescue a robust immune synapse formation and enhance TCR-based calcium signalling³⁸⁶. Noting the low expression levels in cell lines created in section 3.3.1, LFA-1 was boosted in the cells using the standard lentiviral transduction method for CD11a and CD18 cloned into pHR vectors (section 2.2.2.8). The increased expression of LFA-1 on the T cells did not affect their growth rate but did cause them to grow in larger clumps which required dissociating by agitation before use in experiments (Figure 50B & C). Importantly, in combination with the PBS-MgSO₄ buffer, it rescued their ability to bind ICAM-1 on SLBs and form immune synapses (Figure 50A and Figure 17).

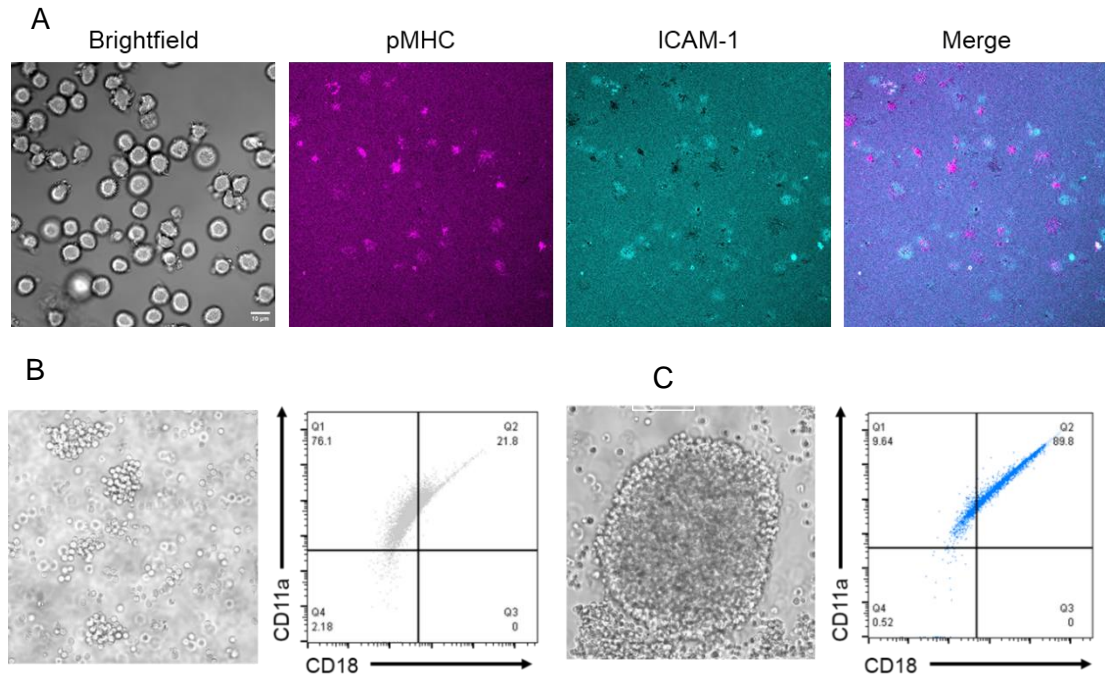


Figure 50 LFA-1 boosting in cells is required to facilitate immune synapse formation (A) Approximately 5×10^5 $1G4^{hi}$ $LFA-1^{lo}$ cells were harvested and washed twice in PBS-MgSO₄ before being placed on 1st generation agonist-presenting SLBs with labelled pMHC and ICAM-1. pMHC accumulation is apparent but ICAM-1 accumulation is weak, with many ICAM-1 exclusion areas. Typical immune synapse structures cannot be observed in most cells. (B) Typical behaviour of cells in culture before LFA-1 boosting (left) and dot plot of the same cells labelled for CD11a and CD18, the two subunits of LFA-1. Quadrants were based on the isotype staining levels. (C) Typical behaviour of cells in culture after LFA-1 boost (left) and dot plot of CD11a and CD18 staining (right). $1G4^{hi}$ cells are used as a representative example.

8.4 Cell Lines do not Signal Significantly on Non-Cognate pMHC

To confirm that cell lines created in Chapter 3 do not respond to null pMHC used on SLBs as a blocking agent (see also section 8.2), 1st generation null pMHC-presenting SLBs were created for each TCR specificity used. Cells were labelled with Fluo4-AM, washed in warmed filtered PBS-MgSO₄, and placed on SLBs. Imaging was immediately started, and a frame was taken every second for 600 frames/10 minutes. Image analysis was carried out with a custom MATLAB code (see section 2.6). The average fraction of cells triggering was ≤11% for all cell lines on their respective null-presenting SLB, and gp100 TCR-expressing cells were more reactive to their null pMHC (HLA-A2-9V) than 1G4-expressing cells were to HLA-A2-gp100 (Figure 51). Triggering values were not significantly different from TCR DKO cells tested on the same SLB type. This confirms that TCR reactivity to null-presenting SLBs is generally negligible, however it should be noted that a greater percentage of gp100 TCR-expressing cells signal on their respective null pMHC compared to 1G4 TCR-expressing cells, suggesting some cross-reactivity of the gp100 TCR.

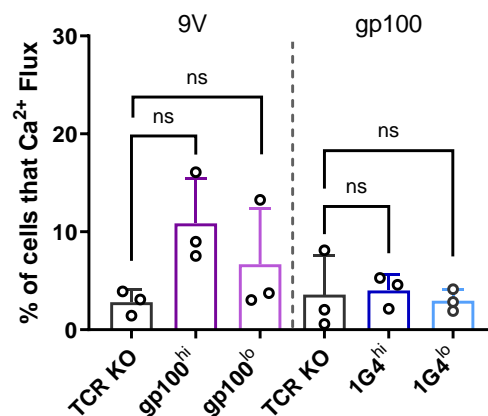


Figure 51 Cell lines do not signal significantly on non-cognate pMHC Approximately 5×10^5 cells from each cell line were harvested and labelled with Fluo-4 AM before being washed in PBS-MgSO₄, equilibrated to 37°C and placed on null pMHC-presenting SLBs. Timelapse images were acquired every second for 600 frames/10 minutes. Graph shows the average fraction of cells triggering on null pMHC-presenting SLBs. The null pMHC in each case is indicated above the bars and was added to a final concentration of 10 ng/μl. ICAM-1 was used at a concentration of 1.2 ng/μl. Mean ± SD plotted. Data acquired from ~200-1000 cells per repeat, with 3 biological repeats per condition. Comparisons were made between TCR KO and other cell lines within the same condition by a one-way ANOVA, with TCR KO as the control condition.

8.5 Further Analysis of T-Cell Close Contact Formation

Other metrics analysed by or derived from the custom Python code included the close contact density and time for formation of the first close contact per cell. Dividing the maximum number of close contacts per cell by the average maximum surface area for each condition (Figure 34B) gives an approximate density of close contacts per μm^2 which gives similar values between all conditions: 0.34 CCs/ μm^2 , 0.34 CCs/ μm^2 and 0.21 CCs/ μm^2 for DKO-AS, J-AS^{hi} and J-AS^{lo} under control conditions and 0.27 CCs/ μm^2 , 0.31 CCs/ μm^2 and 0.27 CCs/ μm^2 respectively when treated with 3-MB-PP1 (Figure 52A). The time to the formation of the first close contact per cell was found to be highly variable and not significantly different between any of the cell lines or conditions, however there is a trend towards longer times with 3-MB-PP1 treatment (Figure 52B). DKO-AS cells had a mean time to close contact formation of 260 s under control conditions and 323 s with ZAP-70 inhibition. For J-AS^{hi} cells, this was 291 s under control conditions and 358 s with ZAP-70 inhibition, and for J-AS^{lo} cells these values were 335 s (control) and 447 s (3-MB-PP1).

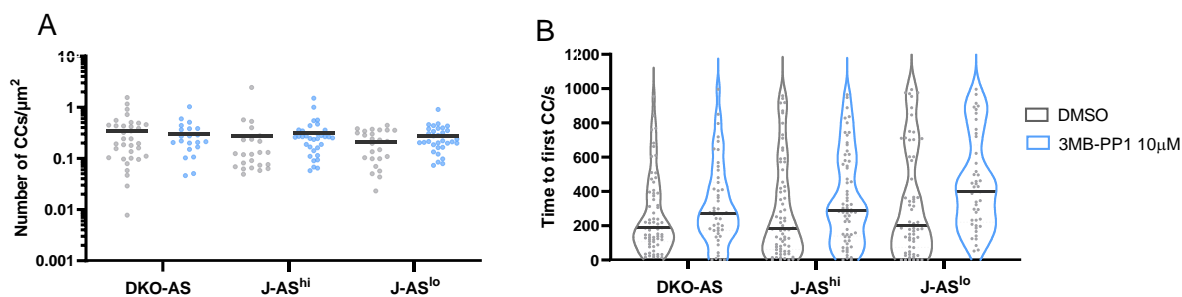
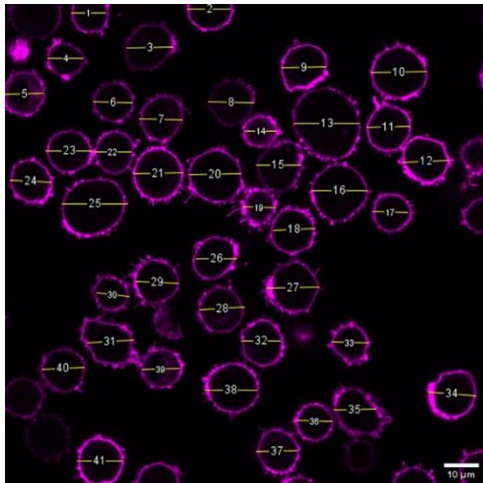


Figure 52 Close contact density and time to the formation of the first close contact does not change with TCR expression or ZAP-70 inhibition Cells were labelled with Cell Mask-647 and Fluo-4 AM before being washed in PBS-MgSO₄ with DMSO or 3-MB-PP1 and placed on 2nd generation SLBs for analysis with a custom Python code. (A) Density of CCs within each condition. Dark grey lines indicate mean values. Conditions within each cell line were compared by Student's t-test and no significance was found. (B) Time to the formation of the first CC. Dark grey lines indicate the median value. Conditions within each cell line were compared by Student's t-test and no significance was found. Between 22-69 cells were analysed per condition over 3 repeats.

8.6 Calculating the Surface Area of Cell Lines

To estimate the density of TCRs on each cell line, the diameter of several dozen cells was measured using Fiji. Cells were labelled with Cell Mask-647 (Thermo Fisher, final concentration 0.5 $\mu\text{g}/\text{ml}$) at 37°C for 10 minutes in complete RPMI media (total volume 200 μl), then fixed with 4% PFA and placed on PLL-coated glass slides (prepared as in section 2.5.3). The approximate midplane of the cells was found (giving the most accurate diameter) and measured using a line profile (Figure 53). The average diameter for each cell line was then used to calculate the surface area, if the cell is approximated to a sphere, using the equation $S = 4\pi r^2$.



Cell line	Diameter/ μm	Surface area/ μm^2	TCR density/ μm^2
1G4 ^{hi}	12.01 \pm 1.63	452	38
1G4 ^{lo}	12.45 \pm 1.67	483	0.5
J-AS ^{hi}	12.17 \pm 1.95	465	39
J-AS ^{lo}	12.42 \pm 1.20	483	3

Figure 53 **Approximating the surface area of cell lines** Approximately 1×10^6 cells were harvested and labelled with Cell Mask-647 for 15 minutes at 37°C before being washed in PBS-MgSO₄ and fixed in 4% PFA for 30 minutes at room temperature. Cells were then added to prepared and washed PLL-coated slides and imaged immediately. Line profiles were drawn through the centre of each cell. The average diameter of each cell per cell line was then used to calculate the surface area of each cell, approximated to a sphere. 47-73 cells measured per cell line over 2-3 biological repeats.

8.7 Characterisation of Early TCR and ZAP-70 Microclusters

As described in section 5.3, the number, size, and intensity of TCR and ZAP-70 microclusters formed after 5 minutes of interaction with agonist- or null pMHC-presenting SLBs were analysed. Representative images of cells in each condition analysed are shown in Figure 54.

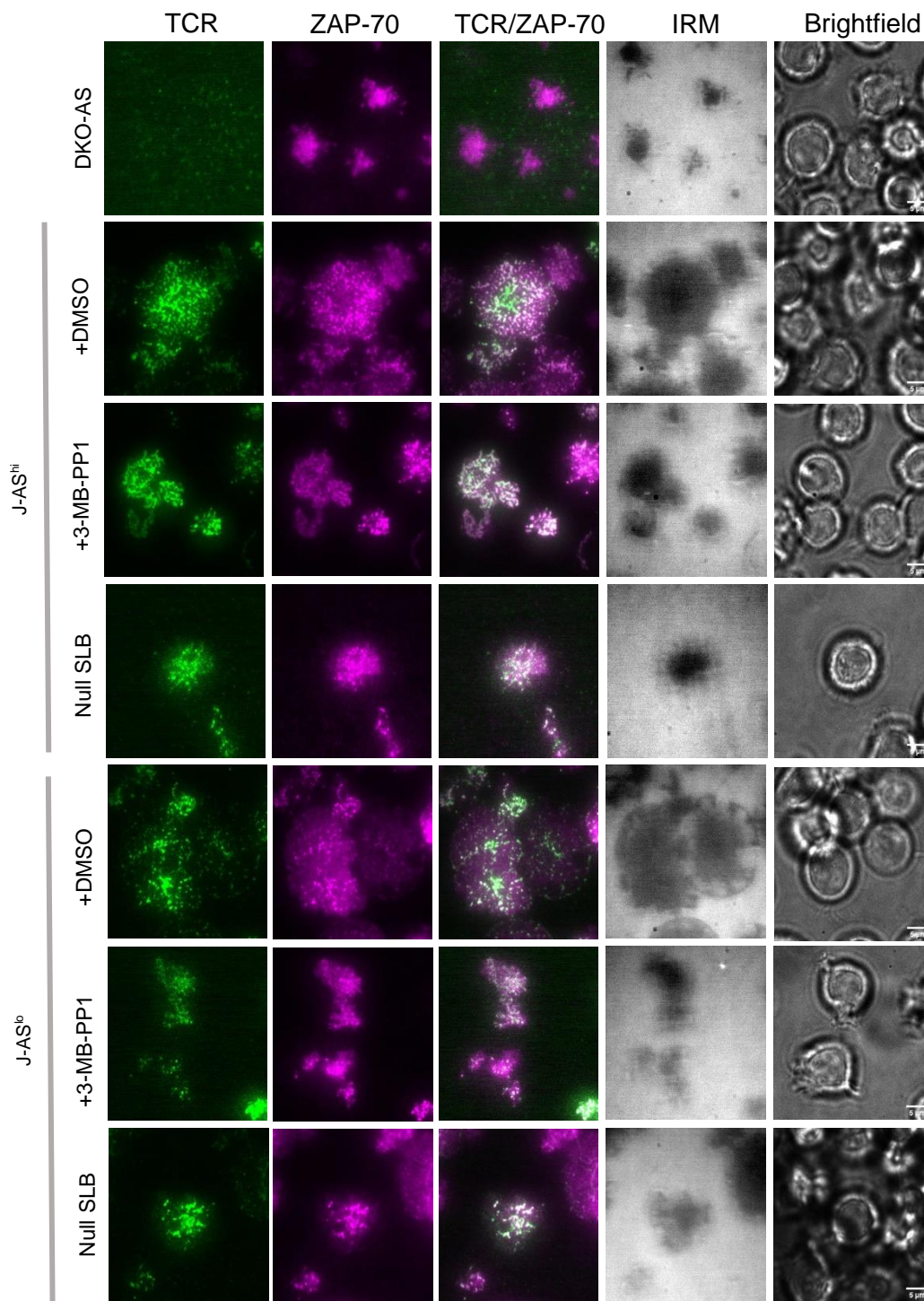


Figure 54 **Characterisation of early TCR and ZAP-70 microclusters under different signalling conditions** Approximately 5×10^5 cells were labelled with HaloTag ligand and UHCT1 fab-Halo before being washed twice in PBS-MgSO₄ with 10 μM 3-MB-PP1 or DMSO. Cells were placed onto 1st generation agonist- or null-presenting SLBs and allowed to settle for 5 minutes before fixation and immediate imaging on a TIRF microscope. SLBs are agonist-presenting unless specified. Representative cells for each condition. Intensities were adjusted for each condition to illustrate microclusters but were not modified for analysis.

9 References

1. Schindelin, J. *et al.* Fiji: an open-source platform for biological-image analysis. *Nature Methods* 2012 9:7 9, 676–682 (2012).
2. Cooper, M. D. & Alder, M. N. The Evolution of Adaptive Immune Systems. *Cell* **124**, 815–822 (2006).
3. Buettner, M. & Lochner, M. Development and Function of Secondary and Tertiary Lymphoid Organs in the Small Intestine and the Colon. *Front Immunol* **7**, 342 (2016).
4. Hampton, H. R. & Chtanova, T. Lymphatic migration of immune cells. *Front Immunol* **10**, 1168 (2019).
5. Pitzalis, C., Jones, G. W., Bombardieri, M. & Jones, S. A. Ectopic lymphoid-like structures in infection, cancer and autoimmunity. *Nat Rev Immunol* **14**, 447–462 (2014).
6. Beutler, B. Innate immunity: an overview. *Mol Immunol* **40**, 845–859 (2004).
7. Janeway, C. A. & Medzhitov, R. Innate Immune Recognition. <https://doi.org/10.1146/annurev.immunol.20.083001.084359> **20**, 197–216 (2003).
8. Akira, S., Uematsu, S. & Takeuchi, O. Pathogen Recognition and Innate Immunity. *Cell* **124**, 783–801 (2006).
9. Chien, Y. hsiu & Jores, R. $\gamma\delta$ T Cells: T cells with B-cell-like recognition properties. *Current Biology* **5**, 1116–1118 (1995).
10. Woo, S. R., Corrales, L. & Gajewski, T. F. Innate Immune Recognition of Cancer. <http://dx.doi.org/10.1146/annurev-immunol-032414-112043> **33**, 445–474 (2015).
11. da Silva, E. Z. M., Jamur, M. C. & Oliver, C. Mast Cell Function: A New Vision of an Old Cell. *Journal of Histochemistry and Cytochemistry* **62**, 698–738 (2014).
12. Paul, S. & Lal, G. The molecular mechanism of natural killer cells function and its importance in cancer immunotherapy. *Front Immunol* **8**, 1124 (2017).
13. Banchereau, J. & Steinman, R. M. Dendritic cells and the control of immunity. *Nature* 1998 392:6673 **392**, 245–252 (1998).
14. Kalyan, S. & Kabelitz, D. Defining the nature of human $\gamma\delta$ T cells: a biographical sketch of the highly empathetic. *Cellular & Molecular Immunology* 2013 10:1 **10**, 21–29 (2012).
15. Bach, F. H., Bach, M. L. & Sondel, P. M. Differential function of major histocompatibility complex antigens in T-lymphocyte activation. *Nature* **259**, 273–281 (1976).
16. Mørch, A. M., Bálint, Š., Santos, A. M., Davis, S. J. & Dustin, M. L. Coreceptors and TCR Signaling – the Strong and the Weak of It. *Front Cell Dev Biol* **8**, 1147 (2020).
17. Drayton, D. L., Liao, S., Mounzer, R. H. & Ruddle, N. H. Lymphoid organ development: from ontogeny to neogenesis. *Nature Immunology* 2006 7:4 **7**, 344–353 (2006).
18. Halle, S., Halle, O. & Förster, R. Mechanisms and Dynamics of T Cell-Mediated Cytotoxicity In Vivo. *Trends Immunol* **38**, 432–443 (2017).
19. Luckheeram, R. V., Zhou, R., Verma, A. D. & Xia, B. CD4+T Cells: Differentiation and Functions. *Clin Dev Immunol* **2012**, 12 (2012).

20. Workman, C. J., Szymczak-Workman, A. L., Collison, L. W., Pillai, M. R. & Vignali, D. A. A. The Development and Function of Regulatory T Cells. *Cell Mol Life Sci* **66**, 2603 (2009).
21. Chen, X. & Jensen, P. E. The role of B lymphocytes as antigen-presenting cells. *Arch. Immunol. Ther. Exp* **56**, 77–83 (2008).
22. Allman, D. & Pillai, S. Peripheral B cell subsets. *Curr Opin Immunol* **20**, 149 (2008).
23. LeBien, T. W. & Tedder, T. F. B lymphocytes: how they develop and function. *Blood* **112**, 1570 (2008).
24. de Silva, N. S. & Klein, U. Dynamics of B cells in germinal centres. *Nat Rev Immunol* **15**, 137–148 (2015).
25. Rothstein, T. L., Griffin, D. O., Holodick, N. E., Quach, T. D. & Kaku, H. Human B-1 cells take the stage. *Ann N Y Acad Sci* **1285**, 97 (2013).
26. Eberl, G., Colonna, M., Santo, J. P. D. & McKenzie, A. N. J. Innate lymphoid cells: A new paradigm in immunology. *Science (1979)* **348**, (2015).
27. Walsh, K. P. & Mills, K. H. G. Dendritic cells and other innate determinants of T helper cell polarisation. *Trends Immunol* **34**, 521–530 (2013).
28. van Gisbergen, K. P. J. M., Sanchez-Hernandez, M., Geijtenbeek, T. B. H. & van Kooyk, Y. Neutrophils mediate immune modulation of dendritic cells through glycosylation-dependent interactions between Mac-1 and DC-SIGN. *Journal of Experimental Medicine* **201**, 1281–1292 (2005).
29. Jonuleit, H., Schmitt, E., Schuler, G., Knop, J. & Enk, A. H. Induction of Interleukin 10–Producing, Nonproliferating Cd4+ T Cells with Regulatory Properties by Repetitive Stimulation with Allogeneic Immature Human Dendritic Cells. *Journal of Experimental Medicine* **192**, 1213–1222 (2000).
30. Spits, H. Development of $\alpha\beta$ T cells in the human thymus. *Nature Reviews Immunology* *2002 2:10* **2**, 760–772 (2002).
31. Joachims, M. L., Chain, J. L., Hooker, S. W., Knott-Craig, C. J. & Thompson, L. F. Human $\alpha\beta$ and $\gamma\delta$ Thymocyte Development: TCR Gene Rearrangements, Intracellular TCR β Expression and $\gamma\delta$ Developmental Potential – Differences between Men and Mice. *J Immunol* **176**, 1543 (2006).
32. Blom, B. *et al.* TCR Gene Rearrangements and Expression of the Pre-T Cell Receptor Complex During Human T-Cell Differentiation. *Blood* **93**, 3033–3043 (1999).
33. Glusman, G. *et al.* Comparative Genomics of the Human and Mouse T Cell Receptor Loci. *Immunity* **15**, 337–349 (2001).
34. Schatz, D. G. & Ji, Y. Recombination centres and the orchestration of V(D)J recombination. *Nature Reviews Immunology* *2011 11:4* **11**, 251–263 (2011).
35. Janeway, C., Travers, P. & Walport, M. *Immunobiology: The Immune System in Health and Disease*. (New York: Garland Science, 2001).
36. Xing, Y. & Hogquist, K. A. T-Cell Tolerance: Central and Peripheral. *Cold Spring Harb Perspect Biol* **4**, 1–15 (2012).
37. Singer, A., Adoro, S. & Park, J. H. Lineage fate and intense debate: myths, models and mechanisms of CD4/CD8 lineage choice. *Nat Rev Immunol* **8**, 788 (2008).

38. Carding, S. R. & Egan, P. J. $\gamma\delta$ T cells: functional plasticity and heterogeneity. *Nature Reviews Immunology* 2002 2:5 **2**, 336–345 (2002).
39. Stinchcombe, J. C., Bossi, G., Booth, S. & Griffiths, G. M. The immunological synapse of CTL contains a secretory domain and membrane bridges. *Immunity* **15**, 751–761 (2001).
40. Zhang, N. & Bevan, M. J. CD8+ T Cells: Foot Soldiers of the Immune System. *Immunity* **35**, 161 (2011).
41. Masopust, D. & Schenkel, J. M. The integration of T cell migration, differentiation and function. *Nature Reviews Immunology* 2013 13:5 **13**, 309–320 (2013).
42. Ley, K., Laudanna, C., Cybulsky, M. I. & Nourshargh, S. Getting to the site of inflammation: the leukocyte adhesion cascade updated. *Nature Reviews Immunology* 2007 7:9 **7**, 678–689 (2007).
43. Adams, D. H. & Shaw, S. Leucocyte-endothelial interactions and regulation of leucocyte migration. *The Lancet* **343**, 831–836 (1994).
44. Potter, T. A., Grebe, K., Freiberg, B. & Kupfer, A. Formation of supramolecular activation clusters on fresh ex vivo CD8+ T cells after engagement of the T cell antigen receptor and CD8 by antigen-presenting cells. *Proceedings of the National Academy of Sciences* **98**, 12624–12629 (2001).
45. Lowin, B., Hahne, M., Mattmann, C. & Tschopp, J. Cytolytic T-cell cytotoxicity is mediated through perforin and Fas lytic pathways. *Nature* **370**, 650–652 (1994).
46. Peters, P. J. *et al.* Cytotoxic T lymphocyte granules are secretory lysosomes, containing both perforin and granzymes. *Journal of Experimental Medicine* **173**, 1099–1109 (1991).
47. Stinchcombe, J. C., Majorovits, E., Bossi, G., Fuller, S. & Griffiths, G. M. Centrosome polarization delivers secretory granules to the immunological synapse. *Nature* **443**, 462–465 (2006).
48. Young, J. D. E., Podack, E. R. & Cohn, Z. A. Properties of a purified pore-forming protein (perforin 1) isolated from H-2-restricted cytotoxic T cell granules. *J Exp Med* **164**, 144–155 (1986).
49. Poenie, M., Tsien, R. Y. & Schmitt-Verhulst, A. M. Sequential activation and lethal hit measured by $[Ca^{2+}]_i$ in individual cytolytic T cells and targets. *EMBO J* **6**, 2223–2232 (1987).
50. Munger, W. E., Berrebi, G. A. & Henkart, P. A. Possible involvement of CTL granule proteases in target cell DNA breakdown. *Immunol Rev* **103**, 99–109 (1988).
51. Suda, T. & Nagata, S. Purification and characterization of the Fas-ligand that induces apoptosis. *J Exp Med* **179**, 873 (1994).
52. Krammer, P. H. CD95's deadly mission in the immune system. *Nature* 2000 407:6805 **407**, 789–795 (2000).
53. Slifka, M. K. & Whitton, J. L. Antigen-Specific Regulation of T Cell-Mediated Cytokine Production. *Immunity* **12**, 451–457 (2000).
54. Weant, A. E. *et al.* Apoptosis Regulators Bim and Fas Function Concurrently to Control Autoimmunity and CD8+ T Cell Contraction. *Immunity* **28**, 218–230 (2008).

55. Ahmed, R. & Gray, D. Immunological Memory and Protective Immunity: Understanding Their Relation. *Science* (1979) **272**, 54–60 (1996).
56. Obar, J. J. & Lefrançois, L. Memory CD8+ T cell differentiation. *Ann N Y Acad Sci* **1183**, 251 (2010).
57. de Jong, E. C., Smits, H. H. & Kapsenberg, M. L. Dendritic cell-mediated T cell polarization. *Springer Semin Immunopathol* **26**, 289–307 (2005).
58. Boehm, U., Klamp, T., Groot, M. & Howard, J. C. Cellular responses to interferon-gamma. *Annu Rev Immunol* **15**, 749–795 (1997).
59. Murray, H. W., Rubin, B. Y., Carriero, S. M., Harris, A. M. & Jaffee, E. A. Human mononuclear phagocyte antiprotozoal mechanisms: oxygen-dependent vs oxygen-independent activity against intracellular *Toxoplasma gondii*. *The Journal of Immunology* **134**, (1985).
60. Zhu, J. & Paul, W. E. CD4 T cells: fates, functions, and faults. *Blood* **112**, 1557–1569 (2008).
61. Couper, K. N., Blount, D. G. & Riley, E. M. IL-10: The Master Regulator of Immunity to Infection. *The Journal of Immunology* **180**, 5771–5777 (2008).
62. Korn, T. *et al.* IL-21 initiates an alternative pathway to induce proinflammatory TH17 cells. *Nature* **448**, 484 (2007).
63. Nurieva, R. I. *et al.* Generation of follicular helper T cells is mediated by IL-21 but independent of TH1, TH2 or TH17 lineages. *Immunity* **29**, 138 (2008).
64. Fazilleau, N., Mark, L., McHeyzer-Williams, L. J. & McHeyzer-Williams, M. G. FOLLICULAR HELPER T CELLS: LINEAGE AND LOCATION. *Immunity* **30**, 324 (2009).
65. Vinuesa, C. G., Tangye, S. G., Moser, B. & Mackay, C. R. Follicular B helper T cells in antibody responses and autoimmunity. *Nature Reviews Immunology 2005 5:11* **5**, 853–865 (2005).
66. Vignali, D. A. A., Collison, L. W. & Workman, C. J. How regulatory T cells work. *Nat Rev Immunol* **8**, 523 (2008).
67. The major histocompatibility complex and its functions - Immunobiology - NCBI Bookshelf. <https://www.ncbi.nlm.nih.gov/books/NBK27156/>.
68. Halenius, A., Gerke, C. & Hengel, H. Classical and non-classical MHC I molecule manipulation by human cytomegalovirus: so many targets—but how many arrows in the quiver? *Cellular & Molecular Immunology 2015 12:2* **12**, 139–153 (2014).
69. Wiczorek, M. *et al.* Major histocompatibility complex (MHC) class I and MHC class II proteins: Conformational plasticity in antigen presentation. *Front Immunol* **8**, 292 (2017).
70. Zacharias, M. & Springer, S. Conformational Flexibility of the MHC Class I α 1- α 2 Domain in Peptide Bound and Free States: A Molecular Dynamics Simulation Study. *Biophys J* **87**, 2203–2214 (2004).
71. Matsumura, M., Fremont, D. H., Peterson, P. A. & Wilson, I. A. Emerging Principles for the Recognition of Peptide Antigens by MHC Class I Molecules. *Science* (1979) **257**, 927–934 (1992).
72. Hunt, D. F. *et al.* Characterization of Peptides Bound to the Class I MHC Molecule HLA-A2.1 by Mass Spectrometry. *Science* (1979) **255**, 1261–1263 (1992).

73. Jardetzky, T. S., Lane, W. S., Robinson, R. A., Madden, D. R. & Wiley, D. C. Identification of self peptides bound to purified HLA-B27. *Nature* 1991 353:6342 **353**, 326–329 (1991).
74. Rötzschke, O. *et al.* Isolation and analysis of naturally processed viral peptides as recognized by cytotoxic T cells. *Nature* 1990 348:6298 **348**, 252–254 (1990).
75. van Bleek, G. M. & Nathenson, S. G. *Isolation of an endogenously processed immunodominant viral peptide from the class I H-2Kb molecule The major Kb-restricted N peptide.*
76. Chicz, R. M. *et al.* Predominant naturally processed peptides bound to HLA-DR1 are derived from MHC-related molecules and are heterogeneous in size. *Nature* 1992 358:6389 **358**, 764–768 (1992).
77. Rock, K. L., Reits, E. & Neefjes, J. Present Yourself! By MHC Class I and MHC Class II Molecules. *Trends Immunol* **37**, 724–737 (2016).
78. Raghavan, M., del Cid, N., Rizvi, S. M. & Peters, L. R. MHC class I assembly: out and about. *Trends Immunol* **29**, 436 (2008).
79. ten Broeke, T., Wubbolts, R. & Stoorvogel, W. MHC Class II Antigen Presentation by Dendritic Cells Regulated through Endosomal Sorting. *Cold Spring Harb Perspect Biol* **5**, (2013).
80. Kobayashi, K. S. & van den Elsen, P. J. NLRC5: a key regulator of MHC class I-dependent immune responses. *Nature Reviews Immunology* 2012 12:12 **12**, 813–820 (2012).
81. Embgenbroich, M. & Burgdorf, S. Current concepts of antigen cross-presentation. *Front Immunol* **9**, 1643 (2018).
82. Labrecque, N. *et al.* How much TCR does a T cell need? *Immunity* **15**, 71–82 (2001).
83. Rudolph, M. G., Stanfield, R. L. & Wilson, I. A. HOW TCRS BIND MHCS, PEPTIDES, AND CORECEPTORS. <http://dx.doi.org/10.1146/annurev.immunol.23.021704.115658> **24**, 419–466 (2006).
84. Dong, D. *et al.* Structural basis of assembly of the human T cell receptor–CD3 complex. *Nature* 2019 573:7775 **573**, 546–552 (2019).
85. Kuhns, M. S. & Davis, M. M. Disruption of Extracellular Interactions Impairs T Cell Receptor-CD3 Complex Stability and Signaling. *Immunity* **26**, 357–369 (2007).
86. Garcia, K. C. *et al.* An $\alpha\beta$ T Cell Receptor Structure at 2.5 Å and Its Orientation in the TCR-MHC Complex. *Science* (1979) **185**, 209–219 (1996).
87. Wang, J. H. *et al.* Atomic structure of an alphabeta T cell receptor (TCR) heterodimer in complex with an anti-TCR fab fragment derived from a mitogenic antibody. *EMBO J* **17**, 10–26 (1998).
88. Hennecke, J. & Wiley, D. C. T Cell Receptor–MHC Interactions up Close. *Cell* **104**, 1–4 (2001).
89. Xu, X., Li, H. & Xu, C. Structural understanding of T cell receptor triggering. *Cellular & Molecular Immunology* 2020 17:3 **17**, 193–202 (2020).
90. Verma, N. K. & Kelleher, D. Not Just an Adhesion Molecule: LFA-1 Contact Tunes the T Lymphocyte Program. *The Journal of Immunology* **199**, 1213–1221 (2017).

91. Purification and structural characterization of LFA-1, a lymphocyte function-associated antigen, and Mac-1, a related macrophage differentiation antigen associated with the type three complement receptor - PubMed. <https://pubmed.ncbi.nlm.nih.gov/6749860/>.
92. Smith, A. *et al.* The role of the integrin LFA-1 in T-lymphocyte migration. *Immunol Rev* **218**, 135–146 (2007).
93. Shimaoka, M., Takagi, J. & Springer, T. A. Conformational Regulation of Integrin Structure and Function. <http://dx.doi.org/10.1146/annurev.biophys.31.101101.140922> **31**, 485–516 (2003).
94. Tan, S. M. The leucocyte $\beta 2$ (CD18) integrins: the structure, functional regulation and signalling properties. *Biosci Rep* **32**, 241–269 (2012).
95. Walling, B. L. & Kim, M. LFA-1 in T cell migration and differentiation. *Front Immunol* **9**, 952 (2018).
96. Grakoui, A. *et al.* The immunological synapse: a molecular machine controlling T cell activation. *Science* **285**, 221–7 (1999).
97. Binder, C. *et al.* CD2 Immunobiology. *Front Immunol* **11**, 1090 (2020).
98. van der Merwe, P. A. *et al.* Human cell-adhesion molecule CD2 binds CD58 (LFA-3) with a very low affinity and an extremely fast dissociation rate but does not bind CD48 or CD59. *Biochemistry* **33**, 10149–10160 (1994).
99. Springer, T. A., Dustin, M. L., Kishimoto, T. K. & Marlin, S. D. The Lymphocyte Function Associated LFA-1, CD2, and LFA-3 Molecules: Cell Adhesion Receptors of the Immune System. <http://dx.doi.org/10.1146/annurev.iy.05.040187.001255> **5**, 223–252 (2003).
100. Davis, S. J. & van der Merwe, P. A. The structure and ligand interactions of CD2: implications for T-cell function. *Immunol Today* **17**, 177–187 (1996).
101. Anton van der Merwe, P., McNamee, P. N., Davies, E. A., Barclay, A. N. & Davis, S. J. Topology of the CD2–CD48 cell-adhesion molecule complex: implications for antigen recognition by T cells. *Current Biology* **5**, 74–84 (1995).
102. Kaizuka, Y., Douglass, A. D., Vardhana, S., Dustin, M. L. & Vale, R. D. The coreceptor CD2 uses plasma membrane microdomains to transduce signals in T cells. *J Cell Biol* **185**, 521–534 (2009).
103. Ghosh, S. *et al.* ERM-Dependent Assembly of T Cell Receptor Signaling and Costimulatory Molecules on Microvilli prior to Activation. *Cell Rep* **30**, 3434–3447.e6 (2020).
104. Möckl, L. The Emerging Role of the Mammalian Glycocalyx in Functional Membrane Organization and Immune System Regulation. *Front Cell Dev Biol* **8**, 253 (2020).
105. Bell, G. I., Dembo, M. & Bongrand, P. Cell adhesion. Competition between nonspecific repulsion and specific bonding. *Biophys J* **45**, 1051–1064 (1984).
106. Ardman, B., Sikorski, M. A. & Staunton, D. E. CD43 interferes with T-lymphocyte adhesion. *Proceedings of the National Academy of Sciences* **89**, 5001–5005 (1992).
107. Rosenstein, Y., Santana, A. & Pedraza-Alva, G. CD43, a molecule with multiple functions. *Immunol Res* **20**, 89–99 (1999).
108. Walker, J. & Green, J. M. Structural Requirements for CD43 Function. (1999).

109. Mueller, D. L., Jenkins, M. K. & Schwartz, R. H. Clonal Expansion Versus Functional Clonal Inactivation: A Costimulatory Signalling Pathway Determines the Outcome of T Cell Antigen Receptor Occupancy. <http://dx.doi.org/10.1146/annurev.iy.07.040189.002305> **7**, 445–480 (2003).
110. Hubo, M. *et al.* Costimulatory molecules on immunogenic versus tolerogenic human dendritic cells. *Front Immunol* **4**, 82 (2013).
111. Chen, L. & Flies, D. B. Molecular mechanisms of T cell co-stimulation and co-inhibition. *Nature Reviews Immunology* **2013 13:4** **13**, 227–242 (2013).
112. van der Merwe, P. A. & Dushek, O. Mechanisms for T cell receptor triggering. *Nature Reviews Immunology* **2011 11:1** **11**, 47–55 (2010).
113. Weiss, A. & Littman, D. R. Signal transduction by lymphocyte antigen receptors. *Cell* **76**, 263–274 (1994).
114. Huse, M. *et al.* Spatial and Temporal Dynamics of T Cell Receptor Signaling with a Photoactivatable Agonist. *Immunity* **27**, 76–88 (2007).
115. Geahlen, R. L. Syk and pTyr'd: Signaling through the B cell antigen receptor. *Biochimica et Biophysica Acta (BBA) - Molecular Cell Research* **1793**, 1115–1127 (2009).
116. Reth, M. & Alarcon B Wileman, C. H. Antigen receptor tail clue. *Nature* **1989 338:6214** **338**, 383–384 (1989).
117. Underhill, D. M. & Goodridge, H. S. The many faces of ITAMs. *Trends Immunol* **28**, 66–73 (2007).
118. Wang, Y. *et al.* A Conserved CXXC Motif in CD3 ϵ Is Critical for T Cell Development and TCR Signaling. *PLoS Biol* **7**, (2009).
119. Call, M. E., Pyrdol, J. & Wucherpfennig, K. W. Stoichiometry of the T-cell receptor–CD3 complex and key intermediates assembled in the endoplasmic reticulum. *EMBO J* **23**, 2348–2357 (2004).
120. Call, M. E. *et al.* The Structure of the $\zeta\zeta$ Transmembrane Dimer Reveals Features Essential for Its Assembly with the T Cell Receptor. *Cell* **127**, 355–368 (2006).
121. Love, P. E. & Hayes, S. M. ITAM-mediated Signaling by the T-Cell Antigen Receptor. *Cold Spring Harb Perspect Biol* **2**, a002485 (2010).
122. Wittlich, M., Koenig, B. W., Hoffmann, S. & Willbold, D. Structural characterization of the transmembrane and cytoplasmic domains of human CD4. *Biochimica et Biophysica Acta (BBA) - Biomembranes* **1768**, 2949–2960 (2007).
123. The T8 antigen is a multimeric complex of two distinct subunits on human thymocytes but consists of homomultimeric forms on peripheral blood T lymphocytes - PubMed. <https://pubmed.ncbi.nlm.nih.gov/6605969/>.
124. Snow, P. M., Coligan, J. E. & Terhorst, C. Analysis of the structure of the human T cell surface antigen T8 by limited proteolysis and chemical cleavage. *Journal of Biological Chemistry* **260**, 2700–2708 (1985).
125. Kim, P. W., Sun, Z. Y. J., Blacklow, S. C., Wagner, G. & Eck, M. J. A zinc clasp structure tethers Lck to T cell coreceptors CD4 and CD8. *Science* **301**, 1725–1728 (2003).
126. Leahy, D. J. A structural view of CD4 and CD8. *The FASEB Journal* **9**, 17–25 (1995).

127. Li, Y., Yin, Y. & Mariuzza, R. A. Structural and biophysical insights into the role of CD4 and CD8 in T cell activation. *Front Immunol* **4**, 206 (2013).
128. Jönsson, P. *et al.* Remarkably low affinity of CD4/peptide-major histocompatibility complex class II protein interactions. **113**, (2016).
129. Artyomov, M. N., Lis, M., Devadas, S., Davis, M. M. & Chakraborty, A. K. CD4 and CD8 binding to MHC molecules primarily acts to enhance Lck delivery. *Proc Natl Acad Sci U S A* **107**, 16916–16921 (2010).
130. Hampl, J., Chien, Y. H. & Davis, M. M. CD4 Augments the Response of a T Cell to Agonist but Not to Antagonist Ligands. *Immunity* **7**, 379–385 (1997).
131. Holler, P. D. & Kranz, D. M. Quantitative Analysis of the Contribution of TCR/pepMHC Affinity and CD8 to T Cell Activation. *Immunity* **18**, 255–264 (2003).
132. Byth, K. F. *et al.* CD45-null transgenic mice reveal a positive regulatory role for CD45 in early thymocyte development, in the selection of CD4+CD8+ thymocytes, and B cell maturation. *Journal of Experimental Medicine* **183**, 1707–1718 (1996).
133. Tchilian, E. Z. *et al.* A Deletion in the Gene Encoding the CD45 Antigen in a Patient with SCID. *The Journal of Immunology* **166**, 1308–1313 (2001).
134. Okumura, M. *et al.* Comparison of CD45 extracellular domain sequences from divergent vertebrate species suggests the conservation of three fibronectin type III domains. *The Journal of Immunology* **157**, (1996).
135. Chang, V. T. *et al.* Initiation of T cell signaling by CD45 segregation at 'close contacts'. *Nat Immunol* **17**, 574–582 (2016).
136. Hermiston, M. L., Xu, Z. & Weiss, A. CD45: A Critical Regulator of Signaling Thresholds in Immune Cells. <http://dx.doi.org/10.1146/annurev.immunol.21.120601.140946> **21**, 107–137 (2003).
137. Altin, J. G. & Sloan, E. K. The role of CD45 and CD45-associated molecules in T cell activation. *Immunol Cell Biol* **75**, 430–445 (1997).
138. Davis, S. J. & van der Merwe, P. A. Lck and the nature of the T cell receptor trigger. *Trends Immunol* **32**, 1–5 (2011).
139. Palacios, E. H. & Weiss, A. Function of the Src-family kinases, Lck and Fyn, in T-cell development and activation. *Oncogene 2004 23:48* **23**, 7990–8000 (2004).
140. Rossy, J., Williamson, D. J. & Gaus, K. How does the kinase Lck phosphorylate the T cell receptor? Spatial organization as a regulatory mechanism. *Front Immunol* **3**, (2012).
141. Straus, D. B. & Weiss, A. Genetic evidence for the involvement of the lck tyrosine kinase in signal transduction through the T cell antigen receptor. *Cell* **70**, 585–593 (1992).
142. Boggon, T. J. & Eck, M. J. Structure and regulation of Src family kinases. *Oncogene 2004 23:48* **23**, 7918–7927 (2004).
143. Xu, H. & Littman, D. R. A kinase-independent function of Lck in potentiating antigen-specific T cell activation. *Cell* **74**, 633–643 (1993).
144. van Laethem, F. *et al.* Deletion of CD4 and CD8 Coreceptors Permits Generation of $\alpha\beta$ T Cells that Recognize Antigens Independently of the MHC. *Immunity* **27**, 735–750 (2007).

145. Yamaguchi, H. & Hendrickson, W. A. Structural basis for activation of human lymphocyte kinase Lck upon tyrosine phosphorylation. *Nature* **384**, 484 (1996).
146. Kapiloff, M. S. *et al.* Structure of the regulatory domains of the Src-family tyrosine kinase Lck. *Nature* *1994* **368**:6473 **368**, 764–769 (1994).
147. Xu, W., Doshi, A., Lei, M., Eck, M. J. & Harrison, S. C. Crystal Structures of c-Src Reveal Features of Its Autoinhibitory Mechanism. *Mol Cell* **3**, 629–638 (1999).
148. Nada, S., Okada, M., MacAuley, A., Cooper, J. A. & Nakagawa, H. Cloning of a complementary DNA for a protein-tyrosine kinase that specifically phosphorylates a negative regulatory site of p60c-src. *Nature* *1991* **351**:6321 **351**, 69–72 (1991).
149. Nika, K. *et al.* Constitutively Active Lck Kinase in T Cells Drives Antigen Receptor Signal Transduction. *Immunity* **32**, 766 (2010).
150. McNeill, L. *et al.* The differential regulation of Lck kinase phosphorylation sites by CD45 is critical for T cell receptor signaling responses. *Immunity* **27**, 425–437 (2007).
151. Wong, N. K. Y., Lai, J. C. Y., Birkenhead, D., Shaw, A. S. & Johnson, P. CD45 down-regulates Lck-mediated CD44 signaling and modulates actin rearrangement in T cells. *J Immunol* **181**, 7033–7043 (2008).
152. Timson Gauen, L. K., Kong, A. N., Samelson, L. E. & Shaw, A. S. p59fyn tyrosine kinase associates with multiple T-cell receptor subunits through its unique amino-terminal domain. *Mol Cell Biol* **12**, 5438–5446 (1992).
153. Appleby, M. W. *et al.* Defective T cell receptor signaling in mice lacking the thymic isoform of p59fyn. *Cell* **70**, 751–763 (1992).
154. Iwashima, M., Irving, B. A., van Oers, N. S. C., Chan, A. C. & Weiss, A. Sequential Interactions of the TCR with Two Distinct Cytoplasmic Tyrosine Kinases. *Science* *(1979)* **193**, 4279–4282 (1994).
155. Chan, A. C., Iwashima, M., Turck, C. W. & Weiss, A. ZAP-70: a 70 kd protein-tyrosine kinase that associates with the TCR zeta chain. *Cell* **71**, 649–662 (1992).
156. Deindl, S. *et al.* Structural Basis for the Inhibition of Tyrosine Kinase Activity of ZAP-70. *Cell* **129**, 735–746 (2007).
157. Neumeister, E. N. *et al.* Binding of ZAP-70 to phosphorylated T-cell receptor zeta and eta enhances its autophosphorylation and generates specific binding sites for SH2 domain-containing proteins. *Mol Cell Biol* **15**, 3171 (1995).
158. Watts, J. D. *et al.* Identification by electrospray ionization mass spectrometry of the sites of tyrosine phosphorylation induced in activated Jurkat T cells on the protein tyrosine kinase ZAP-70. *Journal of Biological Chemistry* **269**, 29520–29529 (1994).
159. Kong, G. *et al.* Distinct tyrosine phosphorylation sites in ZAP-70 mediate activation and negative regulation of antigen receptor function. *Mol Cell Biol* **16**, 5026 (1996).
160. Wang, H. *et al.* ZAP-70: An Essential Kinase in T-cell Signaling. *Cold Spring Harb Perspect Biol* **2**, (2010).
161. Williams, B. L. *et al.* Genetic evidence for differential coupling of Syk family kinases to the T-cell receptor: reconstitution studies in a ZAP-70-deficient Jurkat T-cell line. *Mol Cell Biol* **18**, 1388–1399 (1998).

162. Kuhns, M. S. *et al.* Evidence for a functional sidedness to the $\alpha\beta$ TCR. *Proc Natl Acad Sci U S A* **107**, 5094 (2010).
163. Garcia, K. C., Teyton, L. & Wilson, I. A. STRUCTURAL BASIS OF T CELL RECOGNITION. <http://dx.doi.org/10.1146/annurev.immunol.17.1.369> **17**, 369–397 (2003).
164. Xu, C. *et al.* Regulation of T cell Receptor Activation by Dynamic Membrane Binding of the CD3 ϵ Cytoplasmic Tyrosine-Based Motif. *Cell* **135**, 702 (2008).
165. Fernandes, R. A. *et al.* T cell receptors are structures capable of initiating signaling in the absence of large conformational rearrangements. *Journal of Biological Chemistry* **287**, 13324–13335 (2012).
166. Imbert, V. *et al.* Induction of tyrosine phosphorylation and T-cell activation by vanadate peroxide, an inhibitor of protein tyrosine phosphatases. *Biochemical Journal* **297**, 163–173 (1994).
167. Mingueneau, M. *et al.* The proline-rich sequence of CD3 ϵ controls T cell antigen receptor expression on and signaling potency in preselection CD4+CD8+ thymocytes. *Nature Immunology* 2008 9:5 **9**, 522–532 (2008).
168. Li, Y.-C. *et al.* Cutting Edge: Mechanical Forces Acting on T Cells Immobilized via the TCR Complex Can Trigger TCR Signaling. *The Journal of Immunology* **184**, 5959–5963 (2010).
169. Ma, Z., Sharp, K. A., Janmey, P. A. & Finkel, T. H. Surface-Anchored Monomeric Agonist pMHCs Alone Trigger TCR with High Sensitivity. *PLoS Biol* **6**, e43 (2008).
170. Kuhns, M. S., Davis, M. M. & Garcia, K. C. Deconstructing the Form and Function of the TCR/CD3 Complex. *Immunity* **24**, 133–139 (2006).
171. Sun, Z. Y. J., Kim, K. S., Wagner, G. & Reinherz, E. L. Mechanisms Contributing to T Cell Receptor Signaling and Assembly Revealed by the Solution Structure of an Ectodomain Fragment of the CD3 $\epsilon\gamma$ Heterodimer. *Cell* **105**, 913–923 (2001).
172. Campi, G., Varma, R. & Dustin, M. L. Actin and agonist MHC–peptide complex–dependent T cell receptor microclusters as scaffolds for signaling. *Journal of Experimental Medicine* **202**, 1031–1036 (2005).
173. Valitutti, S., Miller, S., Cella, M., Padovan, E. & Lanzavecchia, A. Serial triggering of many T-cell receptors by a few peptide-MHC complexes. *Nature* **375**, 148–151 (1995).
174. Boniface, J. J. *et al.* Initiation of signal transduction through the T cell receptor requires the multivalent engagement of peptide/MHC ligands [corrected]. *Immunity* **9**, 459–466 (1998).
175. Hu, K. H. & Butte, M. J. T cell activation requires force generation. *Journal of Cell Biology* **213**, 535–542 (2016).
176. Ma, R. *et al.* DNA probes that store mechanical information reveal transient piconewton forces applied by T cells. *Proc Natl Acad Sci U S A* **116**, 16949–16954 (2019).
177. Göhring, J. *et al.* Temporal Analysis of T-Cell Receptor-Imposed Forces via Quantitative Single Molecule FRET Measurements. *bioRxiv* 2020.04.03.024299 (2020) doi:10.1101/2020.04.03.024299.

178. Liu, Y. *et al.* DNA-based nanoparticle tension sensors reveal that T-cell receptors transmit defined pN forces to their antigens for enhanced fidelity. *Proc Natl Acad Sci U S A* **113**, 5610–5615 (2016).
179. Brameshuber, M. *et al.* Monomeric TCRs drive T cell antigen recognition article. *Nat Immunol* **19**, 487–496 (2018).
180. Casas, J. *et al.* Ligand-engaged TCR is triggered by Lck not associated with CD8 coreceptor. *Nat Commun* **5**, 1–11 (2014).
181. Juang, J. *et al.* Peptide-MHC heterodimers show that thymic positive selection requires a more restricted set of self-peptides than negative selection. *Journal of Experimental Medicine* **207**, 1223–1234 (2010).
182. Krogsgaard, M., Juang, J. & Davis, M. M. A role for “self” in T-cell activation. *Semin Immunol* **19**, 236–244 (2007).
183. Schilham, M. W. *et al.* Alloreactive cytotoxic T cells can develop and function in mice lacking both CD4 and CD8. *Eur J Immunol* **23**, 1299–1304 (1993).
184. Sykulev, Y., Joo, M., Vturina, I., Tsomides, T. J. & Eisen, H. N. Evidence that a Single Peptide–MHC Complex on a Target Cell Can Elicit a Cytolytic T Cell Response. *Immunity* **4**, 565–571 (1996).
185. Davis, S. J. & van der Merwe, P. A. The kinetic-segregation model: TCR triggering and beyond. *Nature Immunology* *2006 7:8* **7**, 803–809 (2006).
186. Irlles, C. *et al.* CD45 ectodomain controls interaction with GEMs and Lck activity for optimal TCR signaling. *Nature Immunology* *2002 4:2* **4**, 189–197 (2002).
187. Lin, J. & Weiss, A. The tyrosine phosphatase CD148 is excluded from the immunologic synapse and down-regulates prolonged T cell signaling. *Journal of Cell Biology* **162**, 673–682 (2003).
188. Wild, M. K. *et al.* Dependence of T Cell Antigen Recognition on the Dimensions of an Accessory Receptor–Ligand Complex. *J Exp Med* **190**, 31 (1999).
189. Choudhuri, K., Wiseman, D., Brown, M. H., Gould, K. & van der Merwe, P. A. T-cell receptor triggering is critically dependent on the dimensions of its peptide-MHC ligand. *Nature* **436**, 578–582 (2005).
190. Rossoth, B. *et al.* TCRs are randomly distributed on the plasma membrane of resting antigen-experienced T cells. *Nature Immunology* *2018 19:8* **19**, 821–827 (2018).
191. Fernández-Miguel, G. *et al.* Multivalent structure of an $\alpha\beta$ T cell receptor. *Proceedings of the National Academy of Sciences* **96**, 1547–1552 (1999).
192. Crites, T. J. *et al.* TCR Microclusters Pre-Exist and Contain Molecules Necessary for TCR Signal Transduction. *The Journal of Immunology* **193**, 56–67 (2014).
193. Schamel, W. W. A. *et al.* Coexistence of multivalent and monovalent TCRs explains high sensitivity and wide range of response. *J Exp Med* **202**, 493–503 (2005).
194. Jung, Y. *et al.* Three-dimensional localization of T-cell receptors in relation to microvilli using a combination of superresolution microscopies. *Proc Natl Acad Sci U S A* **113**, E5916–E5924 (2016).
195. Fernandes, R. A. *et al.* A cell topography-based mechanism for ligand discrimination by the T cell receptor. *Proc Natl Acad Sci U S A* **116**, 14002–14010 (2019).

196. Chen, K. Y. *et al.* Trapping or slowing the diffusion of T cell receptors at close contacts initiates T cell signaling. *Proc Natl Acad Sci U S A* **118**, 2024250118 (2021).
197. Hořejší, V. Lipid rafts and their roles in T-cell activation. *Microbes Infect* **7**, 310–316 (2005).
198. van der Merwe, P. A. & Dushek, O. Mechanisms for T cell receptor triggering. *Nature Reviews Immunology* vol. 11 47–55 Preprint at <https://doi.org/10.1038/nri2887> (2011).
199. Urbančič, I. *et al.* Aggregation and mobility of membrane proteins interplay with local lipid order in the plasma membrane of T cells. *FEBS Lett* **595**, 2127–2146 (2021).
200. Harder, T. & Sangani, D. Plasma membrane rafts engaged in T cell signalling: New developments in an old concept. *Cell Communication and Signaling* **7**, 1–7 (2009).
201. Dinic, J., Riehl, A., Adler, J. & Parmryd, I. The T cell receptor resides in ordered plasma membrane nanodomains that aggregate upon patching of the receptor. *Scientific Reports 2015 5:1* **5**, 1–9 (2015).
202. Hashimoto-Tane, A. *et al.* T-Cell Receptor Microclusters Critical for T-Cell Activation Are Formed Independently of Lipid Raft Clustering. *Mol Cell Biol* **30**, 3421–3429 (2010).
203. Mckeithan, T. W. *Kinetic proofreading in T-cell receptor signal transduction (protein-tyrosine kinase/major histocompatibility complex/mathematical model)*. *Immunology* vol. 92 (1995).
204. Matsui, K., Boniface, J. J., Steffner, P., Reay, P. A. & Davis, M. M. Kinetics of T-cell receptor binding to peptide/I-Ek complexes: correlation of the dissociation rate with T-cell responsiveness. *Proc Natl Acad Sci U S A* **91**, 12862–12866 (1994).
205. Lin, J. J. Y. *et al.* Mapping the stochastic sequence of individual ligand-receptor binding events to cellular activation: T cells act on the rare events. *Sci Signal* **12**, (2019).
206. Govern, C. C., Paczosa, M. K., Chakraborty, A. K. & Huseby, E. S. Fast on-rates allow short dwell time ligands to activate T cells. *Proc Natl Acad Sci U S A* **107**, 8724–8729 (2010).
207. Stone, J. D., Chervin, A. S. & Kranz, D. M. T-cell receptor binding affinities and kinetics: impact on T-cell activity and specificity. *Immunology* **126**, 165 (2009).
208. Huang, J. *et al.* A single peptide-major histocompatibility complex ligand triggers digital cytokine secretion in CD4+ T cells. *Immunity* **39**, 846–857 (2013).
209. Valitutti, S. The serial engagement model 17 years after: From tcr triggering to immunotherapy. *Front Immunol* **3**, 272 (2012).
210. Viola, A. & Lanzavecchia, A. T Cell Activation Determined by T Cell Receptor Number and Tunable Thresholds. *Science (1979)* **273**, 104–106 (1996).
211. Varma, R., Campi, G., Yokosuka, T., Saito, T. & Dustin, M. L. T Cell Receptor-Proximal Signals Are Sustained in Peripheral Microclusters and Terminated in the Central Supramolecular Activation Cluster. *Immunity* **25**, 117–127 (2006).
212. Hashimoto-Tane, A. *et al.* Micro-adhesion rings surrounding TCR microclusters are essential for T cell activation. *J Exp Med* **213**, (2016).

213. Yokosuka, T. *et al.* Newly generated T cell receptor microclusters initiate and sustain T cell activation by recruitment of Zap70 and SLP-76. *Nat Immunol* **6**, 1253–1262 (2005).
214. Yi, J., Balagopalan, L., Nguyen, T., McIntire, K. M. & Samelson, L. E. TCR microclusters form spatially segregated domains and sequentially assemble in calcium-dependent kinetic steps. *Nature Communications* 2019 10:1 **10**, 1–13 (2019).
215. Krummel, M. F., Sjaastad, M. D., Wulfig, C. W. & Davis, M. M. Differential clustering of CD4 and CD3 ζ during T cell recognition. *Science (1979)* **289**, 1349–1352 (2000).
216. Lillemeier, B. F. *et al.* TCR and Lat are expressed on separate protein islands on T cell membranes and concatenate during activation. *Nature Immunology* 2009 11:1 **11**, 90–96 (2009).
217. Pigeon, S. v. *et al.* Functional role of T-cell receptor nanoclusters in signal initiation and antigen discrimination. *Proc Natl Acad Sci U S A* **113**, E5454–E5463 (2016).
218. Bunnell, S. C. *et al.* T cell receptor ligation induces the formation of dynamically regulated signaling assemblies. *Journal of Cell Biology* **158**, 1263–1275 (2002).
219. Hsu, C. J. & Baumgart, T. Spatial association of signaling proteins and F-actin effects on cluster assembly analyzed via photoactivation localization microscopy in T cells. *PLoS One* **6**, (2011).
220. Sherman, E. *et al.* Functional nanoscale organization of signaling molecules downstream of the T cell antigen receptor. *Immunity* **35**, 705–20 (2011).
221. Freiberg, B. A. *et al.* Staging and resetting T cell activation in SMACs. *Nature Immunology* 2002 3:10 **3**, 911–917 (2002).
222. Taylor, M. J., Husain, K., Gartner, Z. J., Mayor, S. & Vale, R. D. A DNA-Based T Cell Receptor Reveals a Role for Receptor Clustering in Ligand Discrimination. *Cell* **169**, 108-119.e20 (2017).
223. Cai, E. *et al.* Visualizing dynamic microvillar search and stabilization during ligand detection by T cells. *Science (1979)* **356**, (2017).
224. Zhang, W., Sloan-Lancaster, J., Kitchen, J., Tribble, R. P. & Samelson, L. E. LAT: the ZAP-70 tyrosine kinase substrate that links T cell receptor to cellular activation. *Cell* **92**, 83–92 (1998).
225. Wardenburg, J. B. *et al.* Phosphorylation of SLP-76 by the ZAP-70 protein-tyrosine kinase is required for T-cell receptor function. *J Biol Chem* **271**, 19641–19644 (1996).
226. Smith-Garvin, J. E., Koretzky, G. A. & Jordan, M. S. T Cell Activation. *Annu Rev Immunol* **27**, 591 (2009).
227. Joseph, N., Reicher, B. & Barda-Saad, M. The calcium feedback loop and T cell activation: How cytoskeleton networks control intracellular calcium flux. *Biochimica et Biophysica Acta (BBA) - Biomembranes* **1838**, 557–568 (2014).
228. d'Ambrosio, D., Cantrell, D. A., Frati, L., Santoni, A. & Testi, R. Involvement of p21ras activation in T cell CD69 expression. *Eur J Immunol* **24**, 616–620 (1994).
229. Genot, E. & Cantrell, D. A. Ras regulation and function in lymphocytes. *Curr Opin Immunol* **12**, 289–294 (2000).
230. Schulze-Luehrmann, J. & Ghosh, S. Antigen-Receptor Signaling to Nuclear Factor κ B. *Immunity* **25**, 701–715 (2006).

231. Lafferty, K. J. & Cunningham, A. J. A new analysis of allogeneic interactions. *Aust J Exp Biol Med Sci* **53**, 27–42 (1975).
232. Croft, M. *et al.* TNF superfamily in inflammatory disease: translating basic insights. *Trends Immunol* **33**, 144 (2012).
233. Harding, F. A., McArthur, J. G., Gross, J. A., Raulet, D. H. & Allison, J. P. CD28-mediated signalling co-stimulates murine T cells and prevents induction of anergy in T-cell clones. *Nature* 1992 356:6370 **356**, 607–609 (1992).
234. Chemnitz, J. M., Parry, R. v., Nichols, K. E., June, C. H. & Riley, J. L. SHP-1 and SHP-2 Associate with Immunoreceptor Tyrosine-Based Switch Motif of Programmed Death 1 upon Primary Human T Cell Stimulation, but Only Receptor Ligation Prevents T Cell Activation. *The Journal of Immunology* **173**, 945–954 (2004).
235. Linsley, P. S. & Ledbetter, J. A. The Role of the CD28 Receptor During T Cell Responses to Antigen. <http://dx.doi.org/10.1146/annurev.iy.11.040193.001203> **11**, 191–212 (2003).
236. Curtsinger, J. M. & Mescher, M. F. Inflammatory Cytokines as a Third Signal for T Cell Activation. *Curr Opin Immunol* **22**, 333 (2010).
237. Monks, C. R. F., Freiberg, B. A., Kupfer, H., Sciaky, N. & Kupfer, A. Three-dimensional segregation of supramolecular activation clusters in T cells. *Nature* **395**, 82–86 (1998).
238. Davis, D. M. & Dustin, M. L. What is the importance of the immunological synapse? doi:10.1016/j.it.2004.03.007.
239. Ueda, H., Morphew, M. K., McIntosh, J. R. & Davis, M. M. CD4 + T-cell synapses involve multiple distinct stages. *Proc Natl Acad Sci U S A* **108**, 17099–17104 (2011).
240. Majstoravich, S. *et al.* Lymphocyte microvilli are dynamic, actin-dependent structures that do not require Wiskott-Aldrich syndrome protein (WASp) for their morphology. *Blood* **104**, 1396–1403 (2004).
241. Rozdzial, M. M., Malissen, B. & Finkel, T. H. Tyrosine-phosphorylated T cell receptor zeta chain associates with the actin cytoskeleton upon activation of mature T lymphocytes. *Immunity* **3**, 623–633 (1995).
242. Kumari, S., Curado, S., Mayya, V. & Dustin, M. L. T cell antigen receptor activation and actin cytoskeleton remodeling. *Biochim Biophys Acta* **1838**, 546–556 (2014).
243. Valitutti, S., Dessing, M., Aktories, K., Gallati, H. & Lanzavecchia, A. Sustained signaling leading to T cell activation results from prolonged T cell receptor occupancy. Role of T cell actin cytoskeleton. *J Exp Med* **181**, 577 (1995).
244. Sage, P. T. *et al.* Antigen recognition is facilitated by invadosome-like protrusions formed by memory/effector T cells. *J Immunol* **188**, 3686–3699 (2012).
245. Berlin, C. *et al.* $\alpha 4$ integrins mediate lymphocyte attachment and rolling under physiologic flow. *Cell* **80**, 413–422 (1995).
246. Jung, Y., Wen, L., Altman, A. & Ley, K. CD45 pre-exclusion from the tips of T cell microvilli prior to antigen recognition. *Nature Communications* 2021 12:1 **12**, 1–16 (2021).
247. Cooper, M. D., Peterson, R. D. A. & Good, R. A. DELINEATION OF THE THYMIC AND BURSAL LYMPHOID SYSTEMS IN THE CHICKEN. *Nature* **205**, 143–146 (1965).

248. Oettinger, M. A., Schatz, D. G., Gorka, C. & Baltimore, D. RAG-1 and RAG-2, adjacent genes that synergistically activate V(D)J recombination. *Science* **248**, 1517–1523 (1990).
249. Chang, Y., Bosma, M. J. & Bosma, G. C. Extended Duration of DH–JH Rearrangement in Immunoglobulin Heavy Chain Transgenic Mice: Implications for Regulation of Allelic Exclusion. *Journal of Experimental Medicine* **189**, 1295–1305 (1999).
250. van der Burg, M. *et al.* Ordered recombination of immunoglobulin light chain genes occurs at the IGK locus but seems less strict at the IGL locus. *Blood* **97**, 1001–1008 (2001).
251. King, L. B., Norvell, A. & Monroe, J. G. Antigen Receptor-Induced Signal Transduction Imbalances Associated with the Negative Selection of Immature B Cells Transduction . (1999).
252. Zouali, M. & Richard, Y. Marginal Zone B-Cells, a Gatekeeper of Innate Immunity. *Front Immunol* **2**, (2011).
253. Shlomchik, M. J. & Weisel, F. Germinal center selection and the development of memory B and plasma cells. *Immunol Rev* **247**, 52–63 (2012).
254. Li, Z., Woo, C. J., Iglesias-Ussel, M. D., Ronai, D. & Scharff, M. D. The generation of antibody diversity through somatic hypermutation and class switch recombination. *Genes Dev* **18**, 1–11 (2004).
255. Stavnezer, J., Guikema, J. E. J. & Schrader, C. E. Mechanism and Regulation of Class Switch Recombination. *Annu Rev Immunol* **26**, 261 (2008).
256. Victora, G. D. & Nussenzweig, M. C. Germinal Centers. <https://doi.org/10.1146/annurev-immunol-020711-075032> **30**, 429–457 (2012).
257. Eisen, H. N. Affinity Enhancement of Antibodies: How Low-Affinity Antibodies Produced Early in Immune Responses Are Followed by High-Affinity Antibodies Later and in Memory B-Cell Responses. *Cancer Immunol Res* **2**, (2014).
258. Mesin, L. *et al.* Restricted Clonality and Limited Germinal Center Reentry Characterize Memory B Cell Reactivation by Boosting. *Cell* **180**, 92–106.e11 (2020).
259. Shapiro-Shelef, M. & Calame, K. C. Regulation of plasma-cell development. *Nature Reviews Immunology 2005 5:3* **5**, 230–242 (2005).
260. Seifert, M. & Küppers, R. Human memory B cells. *Leukemia 2016 30:12* **30**, 2283–2292 (2016).
261. Nutt, S. L., Hodgkin, P. D., Tarlinton, D. M. & Corcoran, L. M. The generation of antibody-secreting plasma cells. *Nature Reviews Immunology 2015 15:3* **15**, 160–171 (2015).
262. MacLennan, I. C. M. *et al.* Extrafollicular antibody responses. *Immunol Rev* **194**, 8–18 (2003).
263. Fairfax, K. A., Kallies, A., Nutt, S. L. & Tarlinton, D. M. Plasma cell development: from B-cell subsets to long-term survival niches. *Semin Immunol* **20**, 49–58 (2008).
264. Flores-Borja, F. *et al.* CD19+CD24^{hi}CD38^{hi} B cells maintain regulatory T cells while limiting TH1 and TH17 differentiation. *Sci Transl Med* **5**, (2013).

265. Wolf, S. D., Dittel, B. N., Hardardottir, F. & Janeway, C. A. Experimental Autoimmune Encephalomyelitis Induction in Genetically B Cell-deficient Mice. *J Exp Med* **184**, 2271 (1996).
266. Mizoguchi, A., Mizoguchi, E., Takedatsu, H., Blumberg, R. S. & Bhan, A. K. Chronic Intestinal Inflammatory Condition Generates IL-10-Producing Regulatory B Cell Subset Characterized by CD1d Upregulation. *Immunity* **16**, 219–230 (2002).
267. Heesters, B. A., van der Poel, C. E., Das, A. & Carroll, M. C. Antigen Presentation to B Cells. *Trends Immunol* **37**, 844–854 (2016).
268. Batista, F. D. & Harwood, N. E. The who, how and where of antigen presentation to B cells. *Nature Reviews Immunology* *2008* **9**:1 **9**, 15–27 (2009).
269. Reth, M. *et al.* The B-cell antigen receptor complex. *Immunol Today* **12**, 196–201 (1991).
270. Mattila, P. K. *et al.* The Actin and Tetraspanin Networks Organize Receptor Nanoclusters to Regulate B Cell Receptor-Mediated Signaling. *Immunity* (2013) doi:10.1016/j.immuni.2012.11.019.
271. Schamel, W. W. A. & Reth, M. Monomeric and Oligomeric Complexes of the B Cell Antigen Receptor. *Immunity* **13**, 5–14 (2000).
272. Unanue, E. R., Engers, H. D. & Karnovsky, M. J. Antigen Receptors on B Lymphocytes. <http://dx.doi.org/10.1146/annurev.iy.10.040192.000525> **32**, 44–47 (2003).
273. Schroeder, H. W., Cavacini, L., Birmingham, B. & Ala, B. Structure and function of immunoglobulins. *Journal of Allergy and Clinical Immunology* **125**, S41–S52 (2010).
274. Ohta, Y. & Flajnik, M. IgD, like IgM, is a primordial immunoglobulin class perpetuated in most jawed vertebrates. *Proc Natl Acad Sci U S A* **103**, 10723 (2006).
275. Parsons, S. J. & Parsons, J. T. Src family kinases, key regulators of signal transduction. *Oncogene* **23**, 7906–7909 (2004).
276. Williams, N. K., Lucet, I. S., Peter Klinken, S., Ingley, E. & Rossjohn, J. Crystal Structures of the Lyn Protein Tyrosine Kinase Domain in Its Apo- and Inhibitor-bound State *. *Journal of Biological Chemistry* **284**, 284–291 (2009).
277. Donella-Deana, A. *et al.* Spontaneous Autophosphorylation of Lyn Tyrosine Kinase at both Its Activation Segment and C-Terminal Tail Confers Altered Substrate Specificity †, ‡. (1998).
278. Katagiri, T., Ogimoto, M., Hasegawa, K. & Yakura, H. CD45 Negatively Regulates Lyn Activity by Dephosphorylating Both Positive and Negative Regulatory Tyrosine Residues in Immature B Cells. *The Journal of Immunology* **163**, 1321–1326 (1999).
279. Johnson, S. A. *et al.* Phosphorylated immunoreceptor signaling motifs (ITAMs) exhibit unique abilities to bind and activate Lyn and Syk tyrosine kinases. *The Journal of Immunology* **155**, (1995).
280. Dal Porto, J. M. *et al.* B cell antigen receptor signaling 101. *Mol Immunol* **41**, 599–613 (2004).
281. Mee, P. J. *et al.* Greatly reduced efficiency of both positive and negative selection of thymocytes in CD45 tyrosine phosphatase-deficient mice. doi:10.1002/(SICI)1521-4141(199909)29:09.

282. Katagiri, T., Ogimoto, M., Hasegawa, K., Mizuno, K. & Yakura, H. Selective Regulation of Lyn Tyrosine Kinase by CD45 in Immature B Cells (*). *Journal of Biological Chemistry* **270**, 27987–27990 (1995).
283. Shrivastava, P., Katagiri, T., Ogimoto, M., Mizuno, K. & Yakura, H. Dynamic regulation of Src-family kinases by CD45 in B cells. *Blood* **103**, 1425–1432 (2004).
284. Hermiston, M. L., Zikherman, J. & Zhu, J. W. CD45, CD148, and Lyp/Pep: Critical Phosphatases Regulating Src Family Kinase Signaling Networks in Immune Cells. *Immunol Rev* **228**, 288 (2009).
285. Baker, J. E., Majeti, R., Tangye, S. G. & Weiss, A. Protein Tyrosine Phosphatase CD148-Mediated Inhibition of T-Cell Receptor Signal Transduction Is Associated with Reduced LAT and Phospholipase C γ 1 Phosphorylation. *Mol Cell Biol* **21**, 2393 (2001).
286. Baker, J. E., Majeti, R., Tangye, S. G. & Weiss, A. Protein Tyrosine Phosphatase CD148-Mediated Inhibition of T-Cell Receptor Signal Transduction Is Associated with Reduced LAT and Phospholipase C γ 1 Phosphorylation. *Mol Cell Biol* **21**, 2393–2403 (2001).
287. Stepanek, O. *et al.* Regulation of Src family kinases involved in T cell receptor signaling by protein-tyrosine phosphatase CD148. *Journal of Biological Chemistry* **286**, 22101–22112 (2011).
288. Takahashi, T. *et al.* A Mutant Receptor Tyrosine Phosphatase, CD148, Causes Defects in Vascular Development. *Mol Cell Biol* **23**, 1817–1831 (2003).
289. Zhu, J. W., Brdicka, T., Katsumoto, T. R., Lin, J. & Weiss, A. Structurally Distinct Phosphatases CD45 and CD148 Both Regulate B Cell and Macrophage Immunoreceptor Signaling. *Immunity* **28**, 183–196 (2008).
290. Metzger, H. Transmembrane signaling: the joy of aggregation. *The Journal of Immunology* **149**, (1992).
291. Woodruff, M. F. A., Reid, B. & James, K. Effect of Antilymphocytic Antibody and Antibody Fragments on Human Lymphocytes in vitro. *Nature* **1967** 215:5101 **215**, 591–594 (1967).
292. Depoil, D. *et al.* CD19 is essential for B cell activation by promoting B cell receptor–antigen microcluster formation in response to membrane-bound ligand. *Nature Immunology* **2008** 9:1 **9**, 63–72 (2007).
293. Tolar, P., Sohn, H. W. & Pierce, S. K. The initiation of antigen-induced B cell antigen receptor signaling viewed in living cells by fluorescence resonance energy transfer. *Nat Immunol* **6**, 1168–1176 (2005).
294. Saphire, E. O. *et al.* Contrasting IgG Structures Reveal Extreme Asymmetry and Flexibility. *J Mol Biol* **319**, 9–18 (2002).
295. Carrasco, Y. R. & Batista, F. D. B cell recognition of membrane-bound antigen: an exquisite way of sensing ligands. *Curr Opin Immunol* **18**, 286–291 (2006).
296. Tolar, P. & Pierce, S. K. A conformation-induced oligomerization model for B cell receptor microclustering and signaling. *Curr Top Microbiol Immunol* **340**, 155 (2010).

297. Yang, J. & Reth, M. The dissociation activation model of B cell antigen receptor triggering. *FEBS Letters* vol. 584 4872–4877 Preprint at <https://doi.org/10.1016/j.febslet.2010.09.045> (2010).
298. Yang, J. & Reth, M. Oligomeric organization of the B-cell antigen receptor on resting cells. *Nature* 2010 467:7314 **467**, 465–469 (2010).
299. Lee, J., Sengupta, P., Brzostowski, J., Lippincott-Schwartz, J. & Pierce, S. K. The nanoscale spatial organization of B-cell receptors on immunoglobulin M- and G-expressing human B-cells. *Mol Biol Cell* **28**, 511–523 (2017).
300. Baumgart, F. *et al.* Varying label density allows artifact-free analysis of membrane-protein nanoclusters. *Nat Methods* **13**, 661–664 (2016).
301. Annibale, P., Vanni, S., Scarselli, M., Rothlisberger, U. & Radenovic, A. Identification of clustering artifacts in photoactivated localization microscopy. *Nature Methods* 2011 8:7 **8**, 527–528 (2011).
302. Dunne, P. D. *et al.* DySCo: Quantitating Associations of Membrane Proteins Using Two-Color Single-Molecule Tracking. *Biophys J* **97**, L5 (2009).
303. James, J. R. *et al.* The T cell receptor triggering apparatus is composed of monovalent or monomeric proteins. *Journal of Biological Chemistry* (2011) doi:10.1074/jbc.M111.219212.
304. Santos, A. M. *et al.* Capturing resting T cells: the perils of PLL. *Nat Immunol* **19**, 203–205 (2018).
305. Harwood, N. E. & Batista, F. D. New Insights into the Early Molecular Events Underlying B Cell Activation. *Immunity* vol. 28 609–619 Preprint at <https://doi.org/10.1016/j.immuni.2008.04.007> (2008).
306. Mustelin, T., Coggeshall, K. M. & Altman, A. Rapid activation of the T-cell tyrosine protein kinase pp56lck by the CD45 phosphotyrosine phosphatase. *Proc Natl Acad Sci U S A* **86**, 6302 (1989).
307. Cordoba, S. P. *et al.* The large ectodomains of CD45 and CD148 regulate their segregation from and inhibition of ligated T-cell receptor. *Blood* **121**, 4295–4302 (2013).
308. Thomas, M. L. THE LEUKOCYTE COMMON ANTIGEN FAMILY. *Ann. Rev. Immunol* **7**, 339–69 (1989).
309. Harwood, N. E. & Batista, F. D. Early Events in B Cell Activation. *Annu Rev Immunol* **28**, 185–210 (2010).
310. Treanor, B. B-cell receptor: From resting state to activate. *Immunology* **136**, 21–27 (2012).
311. Treanor, B. *et al.* The membrane skeleton controls diffusion dynamics and signaling through the B cell receptor. *Immunity* **32**, 187–199 (2010).
312. Cheng, P. C., Dykstra, M. L., Mitchell, R. N. & Pierce, S. K. A Role for Lipid Rafts in B Cell Antigen Receptor Signaling and Antigen Targeting. *J Exp Med* **190**, 1549 (1999).
313. Gupta, N. & DeFranco, A. L. Visualizing lipid raft dynamics and early signaling events during antigen receptor-mediated B-lymphocyte activation. *Mol Biol Cell* **14**, 432–444 (2003).

314. Li, J. *et al.* The coordination between B cell receptor signaling and the actin cytoskeleton during B cell activation. *Front Immunol* **10**, 3096 (2019).
315. Packard, T. A. & Cambier, J. C. B lymphocyte antigen receptor signaling: Initiation, amplification, and regulation. *F1000Prime Rep* **5**, (2013).
316. Kurosaki, T., Shinohara, H. & Baba, Y. B Cell Signaling and Fate Decision. <http://dx.doi.org/10.1146/annurev.immunol.021908.132541> **28**, 21–55 (2010).
317. Fearon, D. T. & Carroll, M. C. Regulation of B Lymphocyte Responses to Foreign and Self-Antigens by the CD19/CD21 Complex. <http://dx.doi.org/10.1146/annurev.immunol.18.1.393> **18**, 393–422 (2003).
318. Limon, J. J. & Fruman, D. A. Akt and mTOR in B Cell Activation and Differentiation. *Front Immunol* **3**, (2012).
319. Wakabayashi, C., Adachi, T., Wienands, J. & Tsubata, T. A distinct signaling pathway used by the IgG-containing B cell antigen receptor. *Science (1979)* **298**, 2392–2395 (2002).
320. Horikawa, K. *et al.* Enhancement and suppression of signaling by the conserved tail of IgG memory-type B cell antigen receptors. *Journal of Experimental Medicine* **204**, 759–769 (2007).
321. Parker, D. C. T cell-dependent B cell activation. *Annu Rev Immunol* **11**, 331–360 (1993).
322. Vos, Q., Lees, A., Wu, Z. Q., Snapper, C. M. & Mond, J. J. B-cell activation by T-cell-independent type 2 antigens as an integral part of the humoral immune response to pathogenic microorganisms. *Immunol Rev* **176**, 154–170 (2000).
323. Cochran, J. R., Cameron, T. O. & Stern, L. J. The relationship of MHC-peptide binding and T cell activation probed using chemically defined MHC class II oligomers. *Immunity* **12**, 241–250 (2000).
324. Gomes de Castro, M. A. *et al.* Differential organization of tonic and chronic B cell antigen receptors in the plasma membrane. *Nature Communications* **2019 10:1** **10**, 1–11 (2019).
325. Carbone, C. B. *et al.* In vitro reconstitution of T cell receptor-mediated segregation of the CD45 phosphatase. *Proceedings of the National Academy of Sciences* (2017) doi:10.1073/pnas.1710358114.
326. Razvag, Y., Neve-Oz, Y., Sajman, J., Reches, M. & Sherman, E. Nanoscale kinetic segregation of TCR and CD45 in engaged microvilli facilitates early T cell activation. *Nat Commun* **9**, (2018).
327. Courtney, A. H. *et al.* CD45 functions as a signaling gatekeeper in T cells. *Sci Signal* **12**, (2019).
328. Batista, F. D., Iber, D. & Neuberger, M. S. B cells acquire antigen from target cells after synapse formation. *Nature* **411**, 489–494 (2001).
329. Davis, L. S., Oppenheimer-Marks, N., Bednarczyk, J. L., McIntyre, B. W. & Lipsky, P. E. Fibronectin promotes proliferation of naive and memory T cells by signaling through both the VLA-4 and VLA-5 integrin molecules. *The Journal of Immunology* **145**, (1990).

330. Smith, A., Bracke, M., Leitinger, B., Porter, J. C. & Hogg, N. LFA-1-induced T cell migration on ICAM-1 involves regulation of MLCK-mediated attachment and ROCK-dependent detachment. *J Cell Sci* **116**, 3123–3133 (2003).
331. Ma, V. P.-Y. *et al.* The magnitude of LFA-1/ICAM-1 forces fine-tune TCR-triggered T cell activation. *Sci Adv* **8**, (2022).
332. Dustin, M. L., Starr, T., Varma, R. & Thomas, V. K. Supported Planar Bilayers for Study of the Immunological Synapse. in *Current Protocols in Immunology* vol. 76 18.13.1-18.13.35 (John Wiley & Sons, Inc., 2007).
333. McConnell, H. M., Watts, T. H., Weis, R. M. & Brian, A. A. Supported planar membranes in studies of cell-cell recognition in the immune system. *Biochimica et Biophysica Acta (BBA) - Reviews on Biomembranes* **864**, 95–106 (1986).
334. Dam, T., Junghans, V., Humphrey, J., Chouliara, M. & Jönsson, P. Calcium Signaling in T Cells Is Induced by Binding to Nickel-Chelating Lipids in Supported Lipid Bilayers. *Front Physiol* **11**, 1878 (2021).
335. Sackmann, E. Supported membranes: Scientific and practical applications. *Science (1979)* **271**, 43–48 (1996).
336. Göhring, J. *et al.* Temporal analysis of T-cell receptor-imposed forces via quantitative single molecule FRET measurements. *Nature Communications 2021 12:1* **12**, 1–14 (2021).
337. Bufi, N. *et al.* Human Primary Immune Cells Exhibit Distinct Mechanical Properties that Are Modified by Inflammation. *Biophys J* **108**, 2181 (2015).
338. Majedi, F. S. *et al.* T-cell activation is modulated by the 3D mechanical microenvironment. *Biomaterials* **252**, 120058 (2020).
339. Fisher, P. J., Bulur, P. A., Vuk-Pavlovic, S., Prendergast, F. G. & Dietz, A. B. Dendritic cell microvilli: a novel membrane structure associated with the multifocal synapse and T-cell clustering. *Blood* **112**, 5037–5045 (2008).
340. Lippert, A. H. *et al.* Soft Polydimethylsiloxane-Supported Lipid Bilayers for Studying T Cell Interactions. *Biophys J* **120**, 35 (2021).
341. Yokosuka, T. *et al.* Spatiotemporal regulation of T cell co-stimulation by TCR-CD28 microclusters through PKC θ translocation. *Immunity* **29**, 589 (2008).
342. Groves, J. T. & Dustin, M. L. Supported planar bilayers in studies on immune cell adhesion and communication. *J Immunol Methods* **278**, 19–32 (2003).
343. Zinkernagel, R. M. & Doherty, P. C. MHC-Restricted Cytotoxic T Cells: Studies on the Biological Role of Polymorphic Major Transplantation Antigens Determining T-Cell Restriction-Specificity, Function, and Responsiveness. *Adv Immunol* **27**, 51–177 (1979).
344. Schwartz, R. H. T-Lymphocyte Recognition of Antigen in Association with Gene Products of the Major Histocompatibility Complex. <https://doi.org/10.1146/annurev.iy.03.040185.001321> **3**, 237–261 (2003).
345. Benacerraf, B. & Katz, D. H. The Histocompatibility-Linked Immune Response Genes. *Adv Cancer Res* **21**, 121–173 (1975).
346. Counce, S. *et al.* Strong and Weak Histocompatibility Gene Differences in Mice and Their Role in the Rejection of Homografts of Tumors and Skin * f.

347. van der Merwe, P. A. The TCR Triggering Puzzle. *Immunity* **14**, 665–668 (2001).
348. Dustin, M. L., Sanders, M. E., Shaw, S. & Springer, T. A. Purified lymphocyte function-associated antigen 3 binds to CD2 and mediates T lymphocyte adhesion. *Journal of Experimental Medicine* **165**, 677–692 (1987).
349. Zhu, D. M., Dustin, M. L., Cairo, C. W., Thatte, H. S. & Golan, D. E. Mechanisms of Cellular Avidity Regulation in CD2-CD58-Mediated T Cell Adhesion. *ACS Chem Biol* **1**, 649–658 (2006).
350. Bachmann, M. F. *et al.* Distinct roles for LFA-1 and CD28 during activation of naive T cells: adhesion versus costimulation. *Immunity* **7**, 549–557 (1997).
351. Bromley, S. K. *et al.* The immunological synapse and CD28-CD80 interactions. *Nature Immunology 2001 2:12* **2**, 1159–1166 (2001).
352. Marlin, S. D. & Springer, T. A. Purified intercellular adhesion molecule-1 (ICAM-1) is a ligand for lymphocyte function-associated antigen 1 (LFA-1). *Cell* **51**, 813–819 (1987).
353. Lin, C. M., Li, C. S., Sheng, Y. J., Wu, D. T. & Tsao, H. K. Size-dependent properties of small unilamellar vesicles formed by model lipids. *Langmuir* **28**, 689–700 (2012).
354. Jenkins, E. *et al.* Reconstitution of immune cell interactions in free-standing membranes. *J Cell Sci* **132**, jcs.219709 (2018).
355. Gerstle, Z., Desai, R. & Veatch, S. L. Giant Plasma Membrane Vesicles: an Experimental Tool for Probing the Effects of Drugs and other Conditions on Membrane Domain Stability. *Methods Enzymol* **603**, 129 (2018).
356. Webb, D. J. & Brown, C. M. Epi-Fluorescence Microscopy. *Methods Mol Biol* **931**, 29 (2013).
357. Wang, X. & Lai, Y. Three basic types of fluorescence microscopy and recent improvement. doi:10.1051/e3sconf/202129001031.
358. Minsky, M. Memoir on inventing the confocal scanning microscope. *Scanning* **10**, 128–138 (1988).
359. Elliott, A. D. Confocal Microscopy: Principles and Modern Practices. *Curr Protoc Cytom* **92**, e68 (2020).
360. Fish, K. N. Total Internal Reflection Fluorescence (TIRF) Microscopy. *Current protocols in cytometry / editorial board, J. Paul Robinson, managing editor ... [et al.]* **0 12**, Unit12.18 (2009).
361. Stelzer, E. H. K. *et al.* Light sheet fluorescence microscopy. *Nature Reviews Methods Primers 2021 1:1* **1**, 1–25 (2021).
362. Chen, B. C. *et al.* Lattice light-sheet microscopy: Imaging molecules to embryos at high spatiotemporal resolution. *Science (1979)* **346**, (2014).
363. Schermelleh, L. *et al.* Super-resolution microscopy demystified. *Nature Cell Biology 2019 21:1* **21**, 72–84 (2019).
364. Heilemann, M. *et al.* Subdiffraction-Resolution Fluorescence Imaging with Conventional Fluorescent Probes. *Angewandte Chemie International Edition* **47**, 6172–6176 (2008).

365. Henriques, R., Griffiths, C., Rego, E. H. & Mhlanga, M. M. PALM and STORM: Unlocking live-cell super-resolution. *Biopolymers* **95**, 322–331 (2011).
366. Pittet, M. J. & Weissleder, R. Intravital imaging. *Cell* **147**, 983–991 (2011).
367. Boutrus, S. *et al.* Portable two-color in vivo flow cytometer for real-time detection of fluorescently-labeled circulating cells. <https://doi.org/10.1117/1.2722733> **12**, 020507 (2007).
368. Evans, C. L. *et al.* Chemical imaging of tissue in vivo with video-rate coherent anti-Stokes Raman scattering microscopy. *Proc Natl Acad Sci U S A* **102**, 16807–16812 (2005).
369. Schneider, U., Schwenk, H. -U & Bornkamm, G. Characterization of EBV-genome negative “null” and “T” cell lines derived from children with acute lymphoblastic leukemia and leukemic transformed non-Hodgkin lymphoma. *Int J Cancer* **19**, 621–626 (1977).
370. Abraham, R. T. & Weiss, A. Jurkat T cells and development of the T-cell receptor signalling paradigm. *Nature Reviews Immunology* *2004* **4**:4 **4**, 301–308 (2004).
371. Concordet, J. P. & Haeussler, M. CRISPOR: intuitive guide selection for CRISPR/Cas9 genome editing experiments and screens. *Nucleic Acids Res* **46**, W242–W245 (2018).
372. Schmidt, T. G. M. & Skerra, A. The Strep-tag system for one-step purification and high-affinity detection or capturing of proteins. *Nature Protocols* *2007* **2**:6 **2**, 1528–1535 (2007).
373. Edelstein, A., Amodaj, N., Hoover, K., Vale, R. & Stuurman, N. Computer Control of Microscopes Using µManager. *Curr Protoc Mol Biol* **92**, 14.20.1–14.20.17 (2010).
374. Schoene, N. W. & Kamara, K. S. Population doubling time, phosphatase activity, and hydrogen peroxide generation in Jurkat cells. *Free Radic Biol Med* **27**, 364–369 (1999).
375. Chen, J. L. *et al.* Structural and kinetic basis for heightened immunogenicity of T cell vaccines. *J Exp Med* **201**, 1243 (2005).
376. Liddy, N. Molecular engineering of high affinity T-cell receptors for bispecific therapeutics. (Cardiff University, 2013). doi:<https://orca.cardiff.ac.uk/id/eprint/47271>.
377. Robbins, P. F. *et al.* Single and Dual Amino Acid Substitutions in TCR CDRs Can Enhance Antigen-Specific T Cell Functions. *The Journal of Immunology* **180**, 6116–6131 (2008).
378. Pettmann, J. *et al.* The discriminatory power of the t cell receptor. *Elife* **10**, (2021).
379. van der Merwe, P. A. & Davis, S. J. Molecular interactions mediating T cell antigen recognition. *Annu Rev Immunol* **21**, 659–684 (2003).
380. Liddy, N. *et al.* Monoclonal TCR-redirected tumor cell killing. *Nature Medicine* *2012* **18**:6 **18**, 980–987 (2012).
381. Au-Yeung, B. B. *et al.* The structure, regulation, and function of ZAP-70. *Immunol Rev* **228**, 41–57 (2009).
382. Levin, S. E., Zhang, C., Kadlecsek, T. A., Shokat, K. M. & Weiss, A. Inhibition of ZAP-70 Kinase Activity via an Analog-sensitive Allele Blocks T Cell Receptor and CD28 Superagonist Signaling. *J Biol Chem* **283**, 15419 (2008).

383. Blanchard, N., di Bartolo, V. & Hivroz, C. In the Immune Synapse, ZAP-70 Controls T Cell Polarization and Recruitment of Signaling Proteins but Not Formation of the Synaptic Pattern. *Immunity* **17**, 389–399 (2002).
384. Jenkins, M. R. *et al.* Distinct structural and catalytic roles for Zap70 in formation of the immunological synapse in CTL. *Elife* **2014**, (2014).
385. Au-Yeung, B. B. *et al.* A genetically selective inhibitor demonstrates a function for the kinase Zap70 in regulatory T cells independent of its catalytic activity. *Nat Immunol* **11**, 1085–1092 (2010).
386. Cassioli, C. *et al.* Increasing LFA-1 Expression Enhances Immune Synapse Architecture and T Cell Receptor Signaling in Jurkat E6.1 Cells. *Front Cell Dev Biol* **9**, 1862 (2021).
387. Gaud, G., Lesourne, R. & Love, P. E. Regulatory mechanisms in T cell receptor signalling. *Nat Rev Immunol* **18**, 485–497 (2018).
388. Lee, K. H. *et al.* T cell receptor signaling precedes immunological synapse formation. *Science (1979)* **295**, 1539–1542 (2002).
389. Allen, J. R., Ross, S. T. & Davidson, M. W. Single molecule localization microscopy for superresolution. *Journal of Optics* **15**, 094001 (2013).
390. Cranfill, P. J. *et al.* Quantitative Assessment of Fluorescent Proteins. *Nat Methods* **13**, 557 (2016).
391. van der Donk, L. E. H. *et al.* Separate signaling events control TCR downregulation and T cell activation in primary human T cells. *Immun Inflamm Dis* **9**, 223–238 (2021).
392. Evans, R., Lellouch, A. C., Svensson, L., McDowall, A. & Hogg, N. The integrin LFA-1 signals through ZAP-70 to regulate expression of high-affinity LFA-1 on T lymphocytes. *Blood* **117**, 3331–3342 (2011).
393. Gioia, L., Siddique, A., Head, S. R., Salomon, D. R. & Su, A. I. A genome-wide survey of mutations in the Jurkat cell line. *BMC Genomics* **19**, 1–13 (2018).
394. Nye, J. A. & Groves, J. T. Kinetic Control of Histidine-Tagged Protein Surface Density on Supported Lipid Bilayers. *Langmuir* **24**, 4145–4149 (2008).
395. Mandl, J. N. *et al.* Quantification of lymph node transit times reveals differences in antigen surveillance strategies of naïve CD4+ and CD8+ T cells. *Proc Natl Acad Sci U S A* **109**, 18036–18041 (2012).
396. Miller, M. J., Hejazi, A. S., Wei, S. H., Cahalan, M. D. & Parker, I. T cell repertoire scanning is promoted by dynamic dendritic cell behavior and random T cell motility in the lymph node. *Proceedings of the National Academy of Sciences* **101**, 998–1003 (2004).
397. Ritter, A. T. *et al.* Actin Depletion Initiates Events Leading to Granule Secretion at the Immunological Synapse. *Immunity* **42**, 864 (2015).
398. The Python Language Reference — Python 3.10.1 documentation. <https://docs.python.org/3/reference/>.
399. Harris, C. R. *et al.* Array programming with NumPy. *Nature* **2020 585:7825** **585**, 357–362 (2020).
400. Hunter, J. D. Matplotlib: A 2D graphics environment. *Comput Sci Eng* **9**, 90–95 (2007).

401. McKinney, W. Data Structures for Statistical Computing in Python. *Proceedings of the 9th Python in Science Conference* 56–61 (2010) doi:10.25080/MAJORA-92BF1922-00A.
402. van der Walt, S. *et al.* Scikit-image: Image processing in python. *PeerJ* **2014**, e453 (2014).
403. Virtanen, P. *et al.* SciPy 1.0: fundamental algorithms for scientific computing in Python. *Nature Methods* **2020** *17*:3 **17**, 261–272 (2020).
404. Hasslen, S. R., von Andrian, U., Butcher, E. C., Nelson, R. D. & Erlandsen, S. L. Spatial distribution of L-selectin (CD62L) on human lymphocytes and transfected murine L1-2 cells. *Histochem J* **27**, 547–554 (1995).
405. Monks, C. R. F., Freiberg, B. A., Kupfer, H., Sciaky, N. & Kupfer, A. Three-dimensional segregation of supramolecular activation clusters in T cells. *Nature* **1998** *395*:6697 **395**, 82–86 (1998).
406. Saitakis, M. *et al.* Different TCR-induced T lymphocyte responses are potentiated by stiffness with variable sensitivity Different TCR-induced T lymphocyte responses are potentiated by stiffness with variable sensitivity. *Elife* **6**, (2017).
407. Ma, Y. *et al.* Clustering of the ζ -Chain Can Initiate T Cell Receptor Signaling. *Int J Mol Sci* **21**, (2020).
408. Pettmann, J., Santos, A. M., Dushek, O. & Davis, S. J. Membrane Ultrastructure and T Cell Activation. *Front Immunol* **9**, (2018).
409. Dustin, M. L. & Groves, J. T. Receptor Signaling Clusters in the Immune Synapse. <http://dx.doi.org/10.1146/annurev-biophys-042910-155238> **41**, 543–556 (2012).
410. Hashimoto-Tane, A. & Saito, T. Dynamic regulation of TCR-microclusters and the microsynapse for T cell activation. *Front Immunol* **7**, 255 (2016).
411. Neve-Oz, Y., Razvag, Y., Sajman, J. & Sherman, E. Mechanisms of localized activation of the T cell antigen receptor inside clusters. *Biochimica et Biophysica Acta (BBA) - Molecular Cell Research* **1853**, 810–821 (2015).
412. Katz, Z. B., Blount, A., Biophotonics, W. A. & Jolla, L. Amplifies and Disperses Antigenic Stimuli. **18**, 86–95 (2017).
413. Liu, H., Purbhoo, M. A., Davis, D. M. & Rudd, C. E. SH2 domain containing leukocyte phosphoprotein of 76-kDa (SLP-76) feedback regulation of ZAP-70 microclustering. *Proc Natl Acad Sci U S A* **107**, 10166–10171 (2010).
414. Jasplakinolide, a cytotoxic natural product, induces actin polymerization and competitively inhibits the binding of phalloidin to F-actin - PubMed. <https://pubmed.ncbi.nlm.nih.gov/8195116/>.
415. Flanagan, M. D. & Lins, S. Cytochalasins Block Actin Filament Elongation by Binding to High Affinity Sites Associated with F-actin*. *THE JOURNAL OF BIOLOGICAL CHEMISTRY* **255**, 835–838 (1980).
416. Morton, W. M., Ayscough, K. R. & Mclaughlin, P. J. Latrunculin alters the actin-monomer subunit interface to prevent polymerization. *Nature Cell Biology* **2000** *2*:6 **2**, 376–378 (2000).
417. O'Donoghue, G. P., Pielak, R. M., Smoligovets, A. A., Lin, J. J. & Groves, J. T. Direct single molecule measurement of TCR triggering by agonist pMHC in living primary T cells. *Elife* **2013**, 1–16 (2013).

418. Irvine, D. J., Purbhoo, M. A., Krogsgaard, M. & Davis, M. M. Direct observation of ligand recognition by T cells. *Nature* **419**, 845–849 (2002).
419. Schodin, B. A., Tsomides, T. J. & Kranz, D. M. Correlation Between the Number of T Cell Receptors Required for T Cell Activation and TCR–Ligand Affinity. *Immunity* **5**, 137–146 (1996).
420. Wooldridge, L. *et al.* MHC class I molecules with Superenhanced CD8 binding properties bypass the requirement for cognate TCR recognition and nonspecifically activate CTLs. *J Immunol* **184**, 3357–3366 (2010).
421. Dempsey, G. T., Vaughan, J. C., Chen, K. H., Bates, M. & Zhuang, X. Evaluation of fluorophores for optimal performance in localization-based super-resolution imaging. *Nat Methods* **8**, 1027 (2011).
422. Ponjavic, A. *et al.* Single-Molecule Light-Sheet Imaging of Suspended T Cells. *Biophys J* **114**, 2200 (2018).
423. Veatch, S. L. *et al.* Correlation Functions Quantify Super-Resolution Images and Estimate Apparent Clustering Due to Over-Counting. *PLoS One* **7**, e31457 (2012).
424. Ghosh, S. *et al.* CCR7 signalosomes are preassembled on tips of lymphocyte microvilli in proximity to LFA-1. *Biophys J* **120**, 4002–4012 (2021).
425. Brodovitch, A. *et al.* T lymphocytes need less than 3 min to discriminate between peptide MHCs with similar TCR-binding parameters. *Eur J Immunol* **45**, 1635 (2015).
426. Dustin, M. L. The immunological synapse. *Cancer Immunol Res* **2**, 1023 (2014).
427. Razvag, Y. *et al.* T Cell Activation through Isolated Tight Contacts. *Cell Rep* **29**, 3506–3521.e6 (2019).
428. Brodovitch, A., Bongrand, P. & Pierres, A. T Lymphocytes Sense Antigens within Seconds and Make a Decision within One Minute. *The Journal of Immunology* **191**, 2064–2071 (2013).
429. Sherman, E. *et al.* Functional Nanoscale Organization of Signaling Molecules Downstream of the T Cell Antigen Receptor. *Immunity* **35**, 705–720 (2011).
430. Fritzsche, M. *et al.* Cytoskeletal actin dynamics shape a ramifying actin network underpinning immunological synapse formation. *Sci Adv* **3**, (2017).
431. Babich, A. *et al.* F-actin polymerization and retrograde flow drive sustained PLC γ 1 signaling during T cell activation. *Journal of Cell Biology* **197**, 775–787 (2012).
432. Kumari, S. *et al.* Cytoskeletal tension actively sustains the migratory T-cell synaptic contact. *EMBO J* **39**, e102783 (2020).
433. Kumari, S. *et al.* Actin foci facilitate activation of the phospholipase C- γ in primary T lymphocytes via the WASP pathway. *Elife* **2015**, 1–31 (2015).
434. Kim, H. R. & Jun, C. D. T Cell Microvilli: Sensors or Senders? *Front Immunol* **10**, 1753 (2019).
435. Velas, L. *et al.* Three-Dimensional Single Molecule Localization Microscopy Reveals the Topography of the Immunological Synapse at Isotropic Precision below 15 nm. *Nano Lett* **21**, 9247–9255 (2021).

436. Dana, H. *et al.* High-performance calcium sensors for imaging activity in neuronal populations and microcompartments. *Nature Methods* 2019 16:7 **16**, 649–657 (2019).
437. Park, Y. il, Lee, K. T., Suh, Y. D. & Hyeon, T. Upconverting nanoparticles: a versatile platform for wide-field two-photon microscopy and multi-modal in vivo imaging. *Chem Soc Rev* **44**, 1302–1317 (2015).
438. Kalina, K., Burke, G. Contact regions of cytotoxic T lymphocyte-target cell conjugates. *Cellular immunology* **25**:1, 41-51 (1976)
439. Sanderson, CJ., Glauert, AM., The mechanism of T cell mediated cytotoxicity. V. Morphological studies by electron microscopy Proceedings of the Royal Society of London Series B Biological Sciences **198**, 315–323 (1977)
440. Sanderson, CJ., Glauert, AM. The mechanism of T-cell mediated cytotoxicity. VI. T-cell projections and their role in target cell killing *Immunology* **36**, 119–129 (1979)